LIPOPROTEIN BIOGENESIS AND DYNAMICS IN LARVAL ZEBRAFISH

by
James Henry Thierer

A dissertation submitted to Johns Hopkins University in conformity with the requirements for the degree of Doctor of Philosophy

Baltimore, Maryland
October 2019

ABSTRACT

Atherogenic lipoproteins are micelle-like particles that function in the bulk transport of lipids throughout the circulatory system. Apolipoprotein-B (APOB) is the obligate structural component of atherogenic lipoproteins, and harbors many of the key functional domains required for lipoprotein biogenesis, processing, and turnover. While lipoproteins play an essential role in lipid transport, they are also susceptible to accumulation in the vascular wall which leads to the development of atherosclerotic plaques.

While significant research has been dedicated to understanding lipoprotein homeostasis, existing techniques generally use measurements of serum cholesterol to quantify the burden of atherogenic lipoproteins. This approach has several important limitations, in that (i) it is unable to detect extra-vascular lipoproteins, (ii) it is not conducive to high-throughput studies, and (iii) it provides limited insight into the abundance or size of atherogenic lipoproteins, which are important determinants of their atherogenicity.

In an effort to overcome these limitations, I have developed a novel strategy to characterize atherogenic lipoproteins by fusing ApoB with a bright luciferase reporter (NanoLuc). By generating this reporter in optically clear larval zebrafish, I was able to image the localization of atherogenic lipoproteins throughout an intact organism and discover unexpectedly high enrichment in tendinous tissues as well as the central nervous system. Further, both the abundance and size distribution of atherogenic lipoproteins could be readily detected in individual larvae using a plate reader and native-PAGE.

Importantly, these assays are compatible with high-throughput screening, allowing me to leverage the power of the larval zebrafish model system to perform forward genetic and small-molecule screens to identify previously undiscovered modulators of the lipoprotein profile. Using an existing library of zebrafish mutants, I identified Phospholipase A2 Group 12b (Pla2g12b) as a potent regulator of the atherogenic lipoprotein profile.

The ApoB-reporter allows unprecedented insight into understudied aspects of the atherogenic lipoprotein profile, including their extravascular localization, abundance, and size. The opportunity to discover additional genetic and pharmacological modulators of the atherogenic lipoprotein profile through high-throughput screening will contribute to our fundamental understanding of lipoprotein metabolism, and could lead to new therapies to combat cardiovascular disease.

Primary Reader and Advisor: Steven A. Farber, Ph.D.

Secondary Reader: Marnie E. Halpern, Ph.D.

TABLE OF CONTENTS

LIST OF TABLES

LIST OF FIGURES

INTRODUCTION

Background

Lipids are a diverse class of molecules that play integral roles in cellular structure [1], signaling [2, 3], and metabolism [4]. Despite their diverse structures and functions, all lipids share a common property of being largely (if not completely) hydrophobic [5]. This presents a significant challenge for inter-organ transport, as lipids are not miscible in the aqueous circulatory system. Vertebrates have evolved an efficient strategy to transport lipids throughout the circulatory system by first assembling them into lipoproteins [6]. Lipoproteins resemble micelles, composed of a hydrophobic core of neutral lipid (triglycerides and cholesteryl-esters) surrounded by a monolayer of amphipathic lipids (phospholipid and cholesterol) [7]. Lipoproteins are thus able to simultaneously transport both hydrophobic and amphipathic lipids throughout the aqueous circulation.

As their name implies, lipoproteins are not only composed of lipids (lipo-), but also have a significant protein component (-proteins). Various amphipathic proteins (called apolipoproteins) are present on the surface of the lipoprotein particle [8]. Apolipoproteins regulate all the key aspects of lipoprotein homeostasis, ranging from biogenesis to lipid delivery and turnover. Apolipoproteins are also one of the markers used to differentiate between different lipoprotein classes.

The two major classes of lipoproteins are the alpha-lipoproteins and the beta-lipoproteins [9], and this thesis focuses almost exclusively on beta-lipoproteins. Alpha-lipoproteins are named for their primary structural protein apolipoprotein AI (APOAI)

[10], whereas beta-lipoproteins are named after their structural protein Apolipoprotein B (APOB) [11]. Alpha lipoproteins are significantly smaller than beta-lipoproteins, with diameters of approximately 10 nm. Owing to their small size and high protein content, alpha-lipoproteins are relatively dense and thus also referred to as high-density lipoproteins (HDL). By contrast, beta-lipoproteins are much larger (20 - 1,000 nm), and have much lower density as a result of their high lipid content [5]. Since beta-lipoproteins vary so widely in size and density, they are either generally referred to as the non-high-density lipoproteins (non-HDL) or subclassified into low-density lipoproteins (LDL) intermediate density lipoproteins (IDL), very-low-density lipoproteins (VLDL), and chylomicrons (CM) [5] (Fig. 1).

Alpha and beta-lipoproteins also play vastly different roles in lipid transport. Beta-lipoproteins serve primarily to transport lipids from their site of synthesis or absorption (the liver and intestine) to peripheral tissues [6, 8]. Chylomicrons are produced in the intestine as a means of transporting dietary lipid to peripheral tissues. Mammals express a sequence-specific cytosine deaminase in the intestine called the APOB-Editing complex 1 (APOBEC1) that introduces a stop codon in the mRNA 48% of the way through the APOB-coding sequence [12]. As a result, chylomicrons produced by the intestine have a shorter isoform of APOB called APOB-48. Chylomicrons are then secreted into the circulatory system, where they encounter numerous lipases such as Lipoprotein lipase (LPL) [13]. LPL uses an exchangeable apolipoprotein on the surface of beta-lipoproteins called Apolipoprotein C2 (APOC2) as a cofactor to digest triglycerides in the particle core and release fatty acids for absorption by nearby tissues, a process called lipolysis [14]. Lipolysis results in a gradual reduction of particle size,

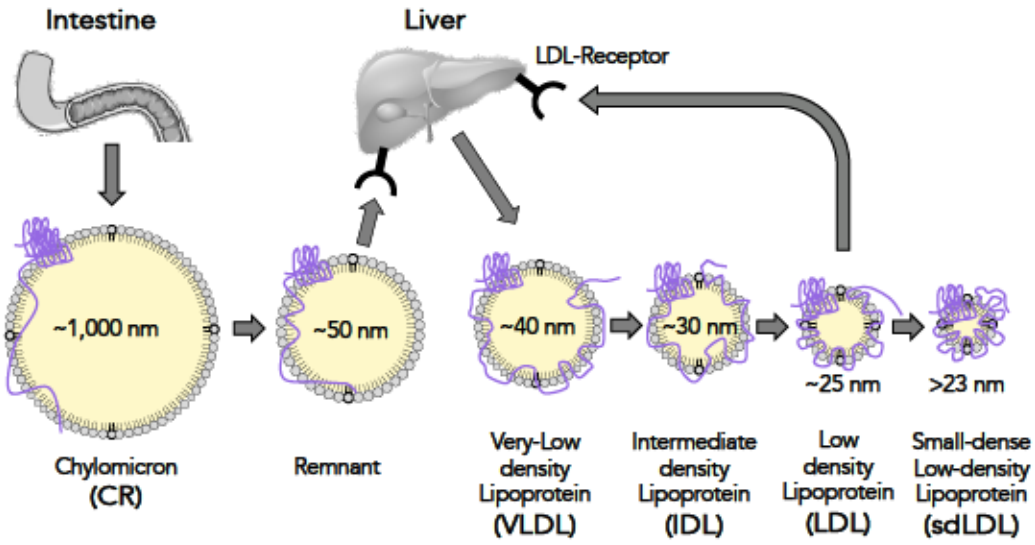

Figure 1: Overview of Beta-lipoprotein classes. Chylomicrons are the largest class of beta-lipoproteins, and transport dietary fat through the circulation using APOB-48 as their primary structural protein. In the circulation, chylomicrons are lipolyzed to form chylomicron remnants (still containing ApoB-48), and are eventually taken up by the liver. Lipids derived from remnant lipoproteins as well as *de novo* synthesis are then packaged into very-low density lipoproteins (VLDL) by the liver, which contain full-length APOB-100. VLDL is lipolyzed in the circulation into progressively smaller lipoproteins including Intermediate and low density lipoproteins (IDL and LDL), and in some cases small-dense LDL (sdLDL). These lipolyzed particles will be taken up by the LDL-receptor, which is primarily expressed in the Liver.

leading to the formation of chylomicron remnants which are eventually taken up by the liver (Fig. 1). The liver produces smaller lipoproteins called VLDL, but as APOBEC1 is rarely expressed in the liver VLDL particles are formed using the full-length APOB protein (APOB-100) [15]. Alpha-lipoproteins perform essentially the opposite function of beta-lipoproteins, scavenging lipids from peripheral tissues and returning them to the liver, intestine, or kidney for secretion [16, 17].

Significance

While lipoproteins play essential roles in lipid transport, they are also important mediators of cardiovascular disease. Beta-lipoproteins in the circulatory system are capable of crossing the vascular endothelium and accumulating in the arterial wall [18]. Sub-endothelial retention of beta-lipoproteins initiates an inflammatory response that leads to the formation of a cholesterol-rich plaques, also known as atherosclerosis [19]. Beta-lipoproteins are thus also referred to as the atherogenic lipoproteins, or colloquially as bad cholesterol. Alpha-lipoproteins again perform an opposing function, scavenging cholesterol from lesions and contributing to plaque regression, and are referred to as the atheroprotective lipoproteins or simply good cholesterol [6].

The observation that cholesterol carried by atherogenic lipoproteins contributes to atherosclerosis has spawned decades of research dedicated to controlling serum cholesterol levels, either by lowering bad cholesterol or raising good cholesterol [20, 21]. The most successful therapies to date lower bad cholesterol by inhibiting cholesterol synthesis [22] or absorption [23], promoting cholesterol secretion [24], or stabilizing the LDL-receptor (LDL-R) to increase LDL turnover [25]. Such therapies have had a

significant impact on the incidence of cardiovascular disease, often reducing disease risk 30% or more [26]. However, despite the availability of numerous therapies that modify cholesterol metabolism, cardiovascular disease still persists as the leading cause of death worldwide [27].

The high persistence of cardiovascular disease risk has created an impetus to develop alternative or complementary therapies to combat residual risk (the risk that persists despite effective cholesterol-lowering treatments). While many approaches have been proposed, one particularly promising strategy involves modulating the size and abundance of atherogenic lipoproteins, rather than pursuing additional strategies to lower bad cholesterol [28, 29]. The rationale behind this approach is that cholesterol carried by atherogenic lipoproteins will not contribute to atherosclerosis unless it enters the vascular wall, and particle size and abundance are strong determinants of rates of vascular invasion.

Several lines of evidence support that smaller beta-lipoproteins are more atherogenic [30]. Firstly, smaller particles show higher rates of intimal invasion and accumulation in the vascular wall [31]. Small particles also have lower affinity for the LDL receptor (LDL-R), which is responsible for endocytosing particles from the circulatory system [32]. Reduced uptake by the LDL-R increases the time the particle spends in the circulation, and thus increases the probability it will contact and traverse the vascular wall. Lastly, these particles are more susceptible to oxidation, and oxidized lipids are highly pro-inflammatory and are thought to accelerate the progression of atherosclerosis [33, 34]. In further support of this model, approximately 25% of the adult population have pattern-B dyslipidemia, characterized by abnormally small and dense

LDL particles (sdLDL). Pattern-B individuals experience 3-fold higher rates of cardiovascular disease relative to people with larger buoyant LDL (Fig. 2) [30, 35].

Lipoprotein abundance has also been closely linked to cardiovascular disease incidence [36, 37]. ApoB is the obligate structural component of atherogenic lipoproteins, and is present as a single copy on each particle [5]. Thus, serum levels of ApoB can be used as a marker for the abundance of atherogenic lipoproteins. While serum levels of ApoB are generally highly correlated with serum levels of bad cholesterol (more lipoproteins generally correlates with more cholesterol), there is significant variation in this relationship [38]. Discordance analysis is a strategy that seeks to isolate these confounded variables by analyzing the unusual (or discordant) cases that have high ApoB and low bad cholesterol, or vice versa. Discordance analysis has consistently shown that cardiovascular disease incidence is relatively low in individuals with low ApoB (a low number of particles), even when these individuals have high cholesterol levels. Conversely, individuals with low cholesterol levels were still at high risk if ApoB levels were high [39-41]. These observations provide strong justification to focus future efforts on lowering the abundance of atherogenic lipoproteins, rather than seeking to develop additional cholesterol-lowering therapies.

Outstanding questions

Several aspects of atherogenic lipoprotein homeostasis remain poorly understood. I will highlight four areas that are particularly relevant to this dissertation, as I describe either new discoveries or new methods that provide insight into these knowledge gaps.

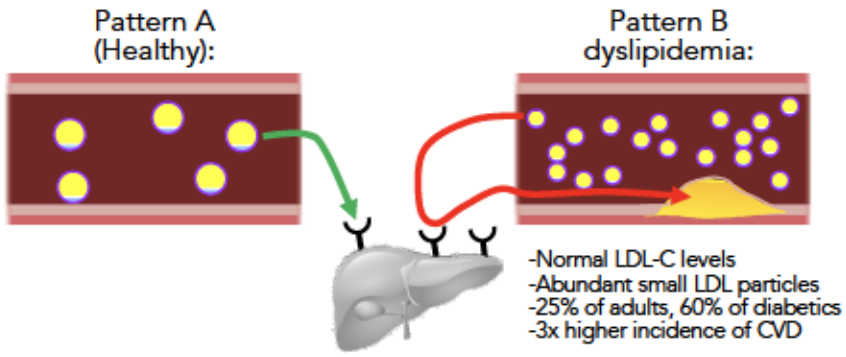

Figure 2: Schematic of the small-dense LDL phenotype. The majority of the population produces buoyant LDL particles with diameters >23 nm. Buoyant LDL has high affinity for the LDL-receptor and can be efficiently removed from the circulation. Approximately 25% of the adult population produces abnormally small lipoproteins, called pattern B dyslipidemia. Small-dense LDL has lower affinity for the LDL-receptor, and higher rates of invasion of the vascular wall. Therefore, individuals with pattern-B dyslipidemia experience approximately 3-fold higher rates of cardiovascular disease (CVD) despite having relatively normal levels of LDL-cholesterol (LDL-C).

One major knowledge gap in the field of atherogenic lipoprotein biology is the importance of extravascular lipoproteins. The current paradigm for studying atherogenic lipoproteins begins with extraction of whole-blood or lymph from the patient or model organism, and subsequent isolation of atherogenic lipoproteins [42]. However, this approach excludes all extravascular lipoproteins from analysis. A small number of kinetic studies of lipoprotein processing in humans using radiolabeled isotopes have indicated that there is a significant extravascular pool of LDL [43], but the localization and functional significance of this pool is completely unknown. Additionally, atherogenic lipoproteins have been implicated in numerous processes unrelated to lipid transport, including development [44-46], vision [47], tendon biology [48], angiogenesis [49], heart function [50], hematopoiesis [51], infection and immunity [52, 53], cancer [54], and diabetes [55]. There is thus clear evidence for both extravascular localization and function of atherogenic lipoproteins, yet this area remains vastly understudied as existing techniques almost exclusively monitor circulating lipoproteins.

A second major knowledge gap lies in our understanding of lipoprotein biogenesis (Fig. 3). The endoplasmic reticulum (ER) is the primary site of synthesis of both lipids and lipoproteins. As lipids are highly hydrophobic, the enzymes that synthesize neutral lipids are generally anchored in the ER-membrane, and deposit their products in the hydrophobic environment between the inner and outer leaflets of the ER-membrane [56]. Accumulation of neutral lipid within this bilayer is thought to form a bulge in the membrane called a lens [57]. Lipids deposited into a lens in the ER membrane are then thought to have three potential fates. First, ER-lipids may interact with perilipin (PLIN) [58, 59] proteins on the cytosolic face of the ER and bud off to

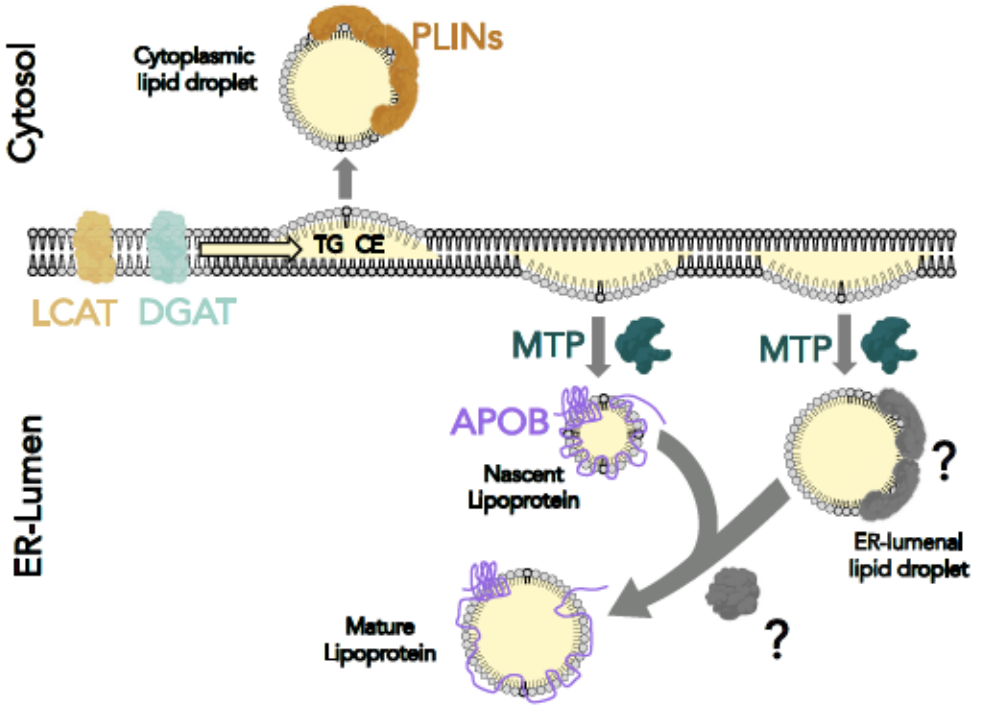

Figure 3: Biogenesis of lipid droplets and lipoproteins. Lecithin cholesterol acyl transferase (LCAT) and Diacylglycerol acyl transferase (DGAT) are transmembrane proteins that catalyze the final steps in biosynthesis cholesteryl-ester (CE) and triglycerides (TG). CE and TG accumulate between the inner and outer leaflets of the ER membrane to form lenses rich in neutral lipid. Perilipins (PLINs) are cytosolic proteins that drive the formation of cytoplasmic lipid droplets. Microsomal triglyceride transfer protein (MTP) is a lumenal protein that transfers ER-lipid to the lipid-binding pocket of APOB to form a nascent beta-lipoprotein. MTP also appears to be required for the formation of APOB-free lipid droplets within the ER lumen (ER-LDs), but no proteins have been identified that either associate with ER-LDs or promote their fusion to nascent lipoproteins (hypothetical proteins shown in gray).

form a cytoplasmic lipid droplet (LD), a micelle-like structure that specializes in intracellular storage of lipid [60, 61]. Alternatively, lipids from the lens may interact with Microsomal Triglyceride Transfer Protein (MTP), a soluble protein within the ER lumen. This protein transfers lipid from the lens to the lipid-binding pocket of APOB to form a nascent beta-lipoprotein that will eventually travel through the secretory pathway [60, 61]. The third potential fate of ER-lipids is to form a lipid droplet within the ER-lumen (ER-LD) [62]. While the process of ER-LD formation appears to be dependent on MTP, very little is known about how these lipid droplets form or how they are regulated. For example, both lipid droplets and lipoproteins are regulated and stabilized by proteins such as perilipins and apolipoproteins [60, 61], but no analogous protein has been identified that interacts with ER-LDs (Fig. 3). Also, the primary function of ER-LDs is thought to be fusion with nascent lipoproteins to form larger, more mature, lipid-rich particles [63, 64]. However, no mechanism has been proposed to account for this fusion process nor have any of the molecular players been identified. Thus, although ER-LDs are thought to play an essential role in lipoprotein biogenesis, very little is known about how they are formed or how they are able to fuse with nascent lipoproteins.

The third major knowledge gap in our understanding of lipoprotein homeostasis is how lipoprotein size is regulated. Lipoprotein size is a complex function of both their starting size and how they are processed in the circulatory system, and both of these process remain only partially understood [65]. For example, intestinal enterocytes produce chylomicrons that may have diameters over 1,000 nm, whereas the liver produces VLDL with diameters well below 100 nm [5]. It is unclear how the differences in lipoprotein biogenesis between these two tissues results in such vastly different particle

sizes, although it may relate to differences in ER-LD fusion as discussed above. There is also significant variation in particle size within the same class of atherogenic lipoproteins, as in the case of LDL. The majority of the population produces buoyant LDL particles, whereas ~30% produce abnormally small particles (sdLDL) [30, 35]. Efforts to determine the cause of sdLDL indicate that both genetic and environmental factors are involved [66], but the pattern of inheritance is highly polygenic [67]. The complexity of the genetic basis of sdLDL is particularly well illustrated by the results of genome-wide association studies showing that many loci contribute to LDL-size, but no single locus explains more than 4% of the observed population variance [68]. Despite this complex and polygenic pattern of inheritance, several genes and loci have consistently emerged as relevant regulators of LDL size. These include Cholesteryl-Ester Transfer Protein (CETP), Manganese Superoxide Dismutase (MnSOD), and Hepatic Lipase (LIPC) [67-70]. There also appears to be a strong environmental and behavioral influence on LDL size. Carbohydrate intake is positively correlated with risk for sdLDL, but the mechanism underlying this effect remains unclear [71].

The final knowledge gap relevant to the work presented here is how lipoprotein abundance is regulated. APOB levels are also governed by both genetic and environmental factors [72], but again the inheritance pattern is highly polygenic rather than governed by a small number of master regulators [68]. Serum APOB levels are determined both by the rate of production and by the rate of uptake [73]. Kinetic studies in humans have shown that beta-lipoproteins follow a first-order reappearance curve, indicating that the rate of lipoprotein production is approximately constant [74, 75], while the rate of uptake is concentration dependent [76]. While the LDL-receptor paradigm

posits that regulation of LDL-receptor expression via Sterol-Responsive Element Binding Protein (SREBP) is the master regulator of serum cholesterol levels [77], this oversimplified model fails to explain numerous aspects of ApoB homeostasis [73, 78, 79]. Thus, while many pathways have been identified that regulate lipoprotein production and uptake in isolated cell types, it remains largely unclear how these pathways are coordinated *in vivo* to determine the equilibrium concentration of atherogenic lipoproteins in vertebrate animals.

Approach

Numerous knowledge gaps persist in our understanding of atherogenic lipoprotein homeostasis, as outlined above. I reasoned that the persistence of these knowledge gaps may reflect the lack of a tractable experimental system to address these problems. While lipoproteins are studied extensively in mammalian models, these systems are not conducive to *in vivo* imaging or unbiased discovery via high-throughput screening. Conversely, cultured cells are routinely used for imaging and high-throughput screening, but cannot recapitulate the complex multi-organ physiology responsible for *in vivo* lipoprotein homeostasis. The following chapters describe my efforts to develop the larval zebrafish as a powerful new model system to study atherogenic lipoproteins. Larval zebrafish combine many of the advantages of the model systems mentioned above, as they are not only conducive to *in vivo* imaging and high-throughput screening, but are also a live vertebrate animal that recapitulates many aspects of human physiology.

Encouragingly, a handful of studies in adult zebrafish have previously demonstrated remarkable similarity between the human and zebrafish lipoprotein profile

[80, 81]. However, atherogenic lipoproteins have not been previously characterized in larval zebrafish. My initial efforts were therefore focused on developing methods capable of monitoring various properties of atherogenic lipoproteins in larval zebrafish. My general approach was to fuse a light-emitting reporter to ApoB, and use this reporter as a sensitive and specific marker of atherogenic lipoproteins. ApoB serves as an ideal scaffold for the generation of a genetically-encoded reporter of atherogenic lipoproteins, as a single ApoB polypeptide remains associated with each lipoprotein from the moment of biosynthesis until the particle is degraded. However, at the onset of this project the ApoB gene had not yet been well-characterized in zebrafish.

Chapter 1 details my efforts to characterize zebrafish ApoB as part of a collaborative project to characterize apolipoprotein gene families in zebrafish [82]. I was able to show that although the zebrafish genome contains 3 paralogs of ApoB (as opposed to 1 gene in mammalian genomes), a single paralog (*apoBb.1*) is clearly the dominant locus as is accounts for ~95% of ApoB mRNA and protein. Further, I was able to show that this gene is expressed exclusively in lipoprotein-producing tissues, including the liver, intestine, and yolk-syncytial layer (YSL).

My next goal was to evaluate whether fluorescent reporter proteins fused to ApoB could be incorporated into lipoproteins and monitored *in vivo*. Chapter 2 presents the results of these efforts, which involved transfection of cultured human cells and injection of zebrafish embryos with plasmid constructs encoding various ApoB-fusion proteins. We were able to show that lipoproteins containing the ApoB reporter were lipidated, secreted, and endocytosed, following the expected pattern of an endogenous lipoprotein particle.

Following characterization of the endogenous *apoB* genes in zebrafish and proof-of-principle experiments showing the functionality of tagged ApoB peptides, I was able to proceed to generating ApoB-fusion proteins by engineering the endogenous *apoB.1* gene within the zebrafish genome. Chapter 3 reports the precise genome editing strategy used to introduce the luciferase reporter NanoLuc as an in-frame fusion to *apoBb.1*. This reporter is referred to as LipoGlo (for glowing lipoproteins), and was used to develop three independent assays that quantify distinct aspects of the atherogenic lipoprotein profile: (i) LipoGlo-counting measures lipoprotein abundance using a plate reader to measure total NanoLuc levels, (ii) LipoGlo-electrophoresis uses native PAGE to characterize the lipoprotein size distribution, and (iii) LipoGlo-microscopy enables visualization of lipoprotein localization patterns in intact zebrafish larvae. All three of these assays were used to characterize the lipoprotein profile throughout larval development, as well as in response to various genetic, dietary, and pharmacological manipulations. This led to several interesting observations, most notably that a large fraction of lipoproteins colocalize with myosepta (tendinous junctions between muscular body segments) as well as the central nervous system.

In chapter 3, the utility of LipoGlo in discovering new modulators of atherogenic lipoproteins is further demonstrated through the identification of Phospholipase A2 Group 12B (*pla2g12b*), a gene with no known function, as a potent regulator of lipoprotein particle size. *Pla2g12b*$^{-/-}$ mutants produce abnormally small lipoproteins.

The mechanism by which *pla2g12b* promotes formation of properly-sized lipoproteins remains unknown. Chapter 4 details ongoing efforts to determine the mechanism of action of this interesting but poorly understood gene. I performed RNA *in*

situ hybridization and protein sequence analysis to show that this protein localizes to the endoplasmic reticulum of lipoprotein-producing tissues, the site of lipoprotein biogenesis. I also show that lumenal lipid droplets are retained in the ER of lipoprotein-producing tissues in *pla2g12b*$^{-/-}$ mutants. The results of these studies led me to propose two potential models whereby Pla2g12b mediates lipidation of nascent lipoproteins. I am actively testing these models by characterizing the functional domains of the protein using a mutation series, as well as characterizing the protein interactome of Pla2g12b.

In addition to facilitating discovery of novel genetic regulators of lipoprotein homeostasis, the LipoGlo reporter will promote discovery of small-molecule modulators that could eventually be developed into pharmaceuticals. Chapter 5 reports efforts to develop a high-throughput screening protocol to identify ApoB-lowering compounds using the LipoGlo reporter. Our preliminary screening data demonstrates robust statistical performance, and shows that an ApoB-lowering drug (lomitapide) used in humans is similarly effective in zebrafish. I also highlight that this drug screening approach has the potential to identify new genetic pathways involved in lipoprotein homeostasis if a library with characterized drug targets is used.

The methods and discoveries outlined here have already begun to address several glaring knowledge gaps in our understanding of lipoprotein homeostasis, such as the mechanism of lipoprotein biogenesis and their extravascular localization patterns. More importantly, however, my findings lay the foundation for numerous future studies by enabling the study of atherogenic lipoproteins in larval zebrafish, and establishing a precedent for the use of tagged ApoB reporter systems to study atherogenic lipoprotein biology.

CHAPTER 1 – ZEBRAFISH AS A MODEL OF APOLIPOPROTEIN BIOLOGY: COMPREHENSIVE EXPRESSION ANALYSIS AND A ROLE FOR APOA-IV IN REGULATING FOOD INTAKE

Jessica P. Otis[1], Erin M. Zeituni[1], **James H. Thierer**[1,2], Jennifer L. Anderson[1], Alexandria C. Brown[1], Erica D. Boehm[1,2], Derek M. Cerchione[1,2], Alexis M. Ceasrine[1,2], Inbal Avraham-Davidi[3], Hanoch Tempelhof[3], Karina Yaniv[3], and Steven A. Farber[1,2,*]

[1] Carnegie Institution for Science, Department of Embryology, Baltimore, MD, 21218
[2] Johns Hopkins University, Department of Biology, Baltimore, MD, 21218
[3] Weizmann Institute of Science, Department of Biological Regulation, Rehovot, Israel

The following chapter was published as a resource article in *Disease Models and Mechanisms*, February 2015. I performed the phylogenetic and syntenic analyses to determine the evolutionary relationships between apolipoprotein genes and gene clusters (Fig. 1). Importantly, these analyses demonstrated that there are three paralogs of the *apoB* gene in the zebrafish genome (as opposed to one in mammals; Fig. 1). I performed the *in situ* hybridization experiments to determine the expression pattern of each of the *apoB* paralogs, and showed that each was expressed in lipoprotein-producing tissues including the liver, intestine, and yolk syncytial layer (YSL, Fig. 3). I contributed to the writing of the overall manuscript, with specific emphasis on the phylogenetic and syntenic studies, as well as the localization pattern of *apoB* transcripts.

Abstract

Improved understanding of lipoproteins, particles that transport lipids throughout the circulation, is vital to developing new treatments for the dyslipidemias associated with metabolic syndrome. A key component of lipoproteins are apolipoproteins, proteins

that structure these particles and regulate lipid metabolism through control of cellular lipid exchange. Constraints of cell culture and mouse models importune for a complementary model that can replicate the complex in vivo milieu that regulates apolipoprotein and lipoprotein biology. Here, we further establish the utility of the genetically tractable and optically clear larval zebrafish as a model of apolipoprotein biology. Gene ancestry analyses were implemented to validate the nomenclature for the zebrafish apolipoprotein A-I (*apoA-I*), *apoB*, *apoE*, and *apoA-IV* genes and their expression patterns were described by whole-mount mRNA in situ hybridization (ISH) (8 cell stage through 6 days post fertilization (dpf)). The ISH results emphasized the importance of apolipoproteins in transporting yolk and dietary lipids, with universal mRNA expression in the yolk syncytial layer, and intestinal and liver expression observed from 4-6 dpf. Furthermore, real-time PCR revealed that transcription of three of the four zebrafish *apoA-IV* genes are increased by a 4-hour, high-fat feed. Therefore, we tested the hypothesis that zebrafish ApoA-IV performs a conserved role in the regulation of food intake by transiently overexpressing ApoA-IVb.1 in transgenic larvae and quantifying ingestion of a co-fed fluorescently labeled fatty acid during a high-fat meal as an indicator of food intake. Indeed, ApoA-IVb.1 overexpression decreased food intake by approximately one-third, confirming that zebrafish ApoA-IVb.1 decreases high-fat food intake. This study comprehensively describes the expression and function of eleven zebrafish apolipoproteins and serves as a springboard for future investigations to elucidate their roles in development and disease in the larval zebrafish model.

Introduction

The current epidemic of metabolic syndrome has resulted in widespread morbidity and mortality due to population increases in obesity, cardiovascular disease, type II diabetes, hypertension, and stroke [83]. Developing treatments for the dyslipidemias frequently associated with metabolic syndrome (e.g., high serum triglycerides (TG); low high-density lipoprotein (HDL) cholesterol) is a priority. It is well known that lipoprotein particles transport lipids throughout the circulation. However, the development of improved treatments for common dyslipidemias requires a deeper understanding of lipoprotein function and regulation. For instance, despite a vast scientific literature spanning over 50 years, we still lack a basic mechanistic understanding of the relationship between HDL and cardiovascular disease risk [84]. Furthermore, characterization of lipoprotein biology is impossible without a comprehensive study of apolipoproteins, the class of over a dozen secreted, lipid-binding proteins that function as structural backbones of lipoprotein particles and regulators of cellular lipid flux via cell surface receptor binding activity.

This study focuses on four major serum apolipoproteins: apolipoprotein A-I (APOA-I), apolipoprotein B (APOB), apolipoprotein E (APOE), and apolipoprotein A-IV (APOA-IV). APOA-I is the main protein component of HDL particles; in addition to its intrinsic, beneficial anti-oxidative, anti-inflammatory, and anti-bacterial properties [85-88], APOA-I regulates cholesterol efflux from cells to HDL particles, the first step in transporting peripheral cholesterol to the liver for excretion via the bile. The liver and intestine produce mammalian APOA-I and subsequently HDL. Humans have two

isoforms of the second apolipoprotein of interest, APOB, resulting from mRNA editing: the short form APOB-48 is produced by the intestine and the long form APOB-100 by the liver. ApoB48 is an essential structural component of intestinally secreted chylomicrons, while APOB100 constitutes very low-density lipoproteins (VLDL) and low-density lipoproteins (LDL) of hepatic origin. APOE, the third apolipoprotein of interest, is exchangeable, transferring between most classes of lipoproteins in the circulation. APOE binds to LDL receptors, thereby regulating lipid uptake [89]; APOE-deficient mice develop severe atherosclerosis due to increased circulating LDL cholesterol [90]. In addition to being expressed by the intestine, liver, and macrophages, APOE is synthesized in the mammalian brain and acts as the major apolipoprotein of the lipid-rich central nervous system (CNS). The final apolipoprotein examined, APOA-IV, is produced by the intestine and secreted as a component of chylomicrons following lipid-rich meals. In rats, acute administration of APOA-IV suppresses food intake [91-93].

Our choice to focus on these four apolipoproteins in this investigation was determined by their implication in a diverse range of dyslipidemias and neurodegenerative diseases. For example, there are striking positive correlations in human populations between protection from cardiovascular disease and the levels of APOA-I and HDL cholesterol, as well as the occurrence of specific APOA-I polymorphisms [94-96]. Conversely, LDL cholesterol levels, which are in part dependent on APOB due to its required structural role in these particles, are positively associated with cardiovascular disease risk [97]. Three polymorphisms in human APOE are strongly associated with the efficacy of plasma lipid clearance, and consequently with the risk of

cardiovascular disease, and risk of Alzheimer's disease [98, 99]. Finally, the action of APOA-IV in reducing food intake is blunted by chronic high-fat feeding and obesity, potentially furthering the viscous cycle of hyperphagia and weight gain [100].

Cell culture and mouse studies have provided the bulk of our understanding of the mechanistic relationships between apolipoproteins and disease. However, cell culture systems do not replicate the cross talk between multiple organs, and studies performed in whole animals often have to rely on indirect assays that measure surrogates for lipid metabolism (e.g. plasma lipid profile). As a result, the intricate details of the regulatory signals that coordinate cellular responses to lipids and production of specific lipoproteins from particular tissues remain incompletely characterized. For example, it was long believed that APOA-I and HDL prevented cardiovascular disease through reverse cholesterol transport, the transport of peripheral cholesterol to the liver, however mice lacking APOA-I have normal biliary cholesterol secretion [101] and pharmaceuticals that raise HDL-C failed to provide the protection observed with naturally high HDL cholesterol levels [102, 103]. Moreover, acute administration of APOA-IV to rats suppresses food intake [91], but chronic over-expression or deletion of APOA-IV does not affect food intake in mice [104, 105]. The seemingly conflicting findings surrounding APOA-I and APOA-IV function highlight the need for experimental model systems that support the study of global apolipoprotein dynamics in living organisms and relate these observations back to the response of a particular cell within a given organ. Remarkably, studies at this level of resolution can be performed in the larval zebrafish (*Danio rerio*). The larval zebrafish has a highly similar, yet simplified, gastrointestinal tract to that of humans [106]. Zebrafish also have a similar lipoprotein lipid transport system [107];

though the teleost genome duplication event created multiple paralogs of most zebrafish apolipoproteins. Historically an important developmental model, the zebrafish is emerging as an invaluable resource to study metabolic function in health and disease [106, 108-113]. This claim is supported by a body of research that has combined the genetic tractability and conduciveness to live imaging of larvae with novel zebrafish models of dietary manipulations (high-fat [114, 115], -cholesterol [80], and -carbohydrate diets [116, 117]), cardiovascular disease [118], type II diabetes [119, 120], hepatic steatosis [121-123], and obesity [124-126], to provide several translational insights.

Specific discoveries related to apolipoprotein function that have been gained from work in larval zebrafish include the findings that ApoB negatively regulates angiogenesis via Vegfr1 [49], ApoA-I binding protein inhibits angiogenesis via Vegfr2 [127], and ApoA-II is required for proper chromosome separation during nuclear division of in vivo larval zebrafish cells and cultured human cells [128]. Although multiple studies have described expression patterns and functions of particular zebrafish apolipoproteins [129-135], none characterized expression from the 8 cell stage comprehensively throughout larval development, included all paralogs of a given gene, or examined the effect of feeding. The establishment of the zebrafish as an effective model of lipoprotein biology has been limited by incomplete characterization of these proteins. For this reason, systematic study of the zebrafish apolipoproteins is crucial.

We undertook a study to further establish the use of the zebrafish as a model of apolipoprotein function in lipid metabolism, embryonic development, dietary nutrient processing, and disease. We first validated and clarified the zebrafish apolipoprotein nomenclature by investigating the ancestral relationships between the four human and 11

zebrafish APOA-I, APOB, APOE, and APOA-IV genes with sequence, syntenic, and phylogenic analyses. Second, we characterized zebrafish apolipoprotein spatiotemporal expression patterns throughout embryogenesis and early larval development, and determined how these metabolic proteins are transcriptionally regulated by a high-fat feed. Finally, we determined that zebrafish ApoA-IV, of which three of four paralogs are upregulated by a high-fat meal, decreases food intake when overexpressed in transgenic larvae presented with a high-fat meal. Thus indicating that zebrafish ApoA-IV has a conserved role in the regulation of high-fat food intake and further establishing the larval zebrafish as a valuable model of apolipoprotein biology.

Results

Gene Ancestry Analysis of Zebrafish Apolipoproteins

The application of a common apolipoprotein nomenclature is of paramount importance to the larger research community in order to correctly interpret, replicate, and build upon published findings. By convention, zebrafish genes are named based on their closest human orthologs, as determined by predicted amino acid sequence comparisons. To verify that each zebrafish apolipoprotein gene was correctly named, we checked not only that the 11 zebrafish *apoA-I*, *apoB*, *apoE*, and *apoA-IV* genes were most similar in amino acid sequence to their human ortholog, but also investigated shared syntenic gene regions and completed phylogenic analyses. These data were communicated to the Zebrafish Model Organism Database (ZFIN) database team to refine the nomenclature and propagate these gene names to zebrafish genome databases.

The gene ancestry analysis began with a comparison of zebrafish apolipoprotein amino acid sequences to the human reference protein sequence database via the BLASTp algorithm to verify orthology (Fig. 1a). This was followed by pairwise Needleman-Wunsch sequence alignments, which showed a range of 17.9% - 33.3% sequence identity and 29.0% - 54.2% sequence similarity between zebrafish and human orthologs (Fig. 1a). The publicly available Genomicus and Synteny DB analysis tools were used to identify syntenic blocks of genes between zebrafish and human apolipoprotein orthologs. The syntenic analysis revealed that the human and zebrafish *APOA-I* and *APOE* orthologs share clear syntenic gene regions (Fig. 1c). *apoBa* and *apoBb.1* also share

A Sequence similarity between zebrafish and human apolipoproteins orthologs.

Zebrafish Gene	Top Blast Hit	Percent Similarity
apoA-Ia	APOA-I preprotein	48.3
apoA-Ib	APOA-I preprotein	43.9
apoBa	APOB-100 precursor	54.2
apoBb.1	APOB-100 precursor	43.0
apoBb.2	APOB-100 precursor	29.0
apoEa	APOE precursor	48.6
apoEb	APOE precursor	50.9
apoA-IVa	APOA-IV precursor	34.1
apoA-IVb.1	APOA-IV precursor	38.6
apoA-IVb.2	APOA-IV precursor	37.0
apoA-IVb.3	APOA-IV precursor	38.4

B Phylogenetic tree of human, zebrafish, mouse, chicken, and coelacanth APOA-I, APOB, APOE, and APOA-IV.

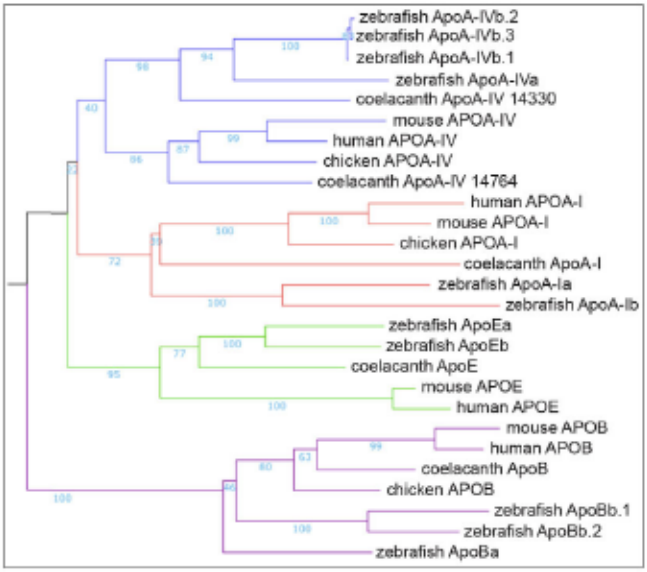

C Most zebrafish apolipoproteins share syntenic gene regions with human orthologs.

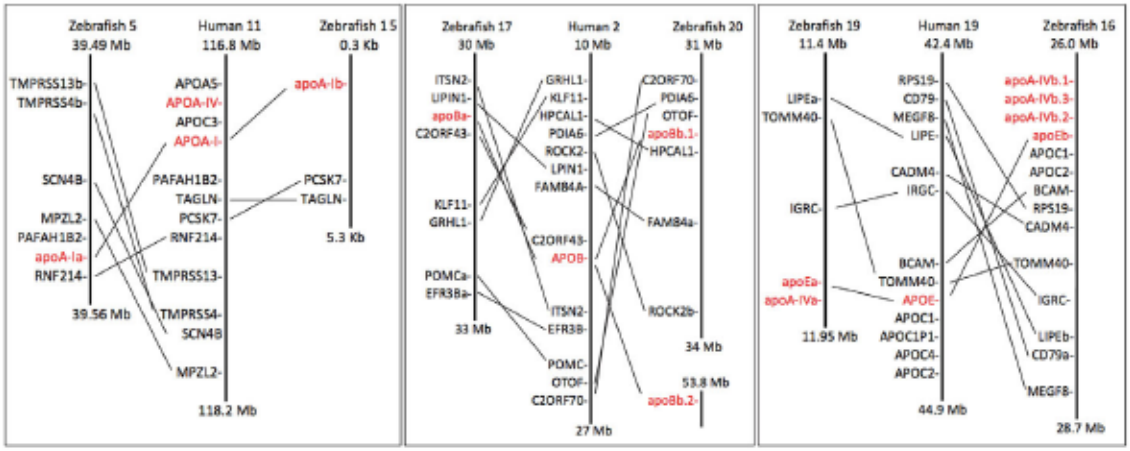

Figure 1: Apolipoprotein gene ancestry analysis. (a) There is low sequence similarity between zebrafish and human apolipoprotein orthologs. Zebrafish genes are listed next to the top BLASTp hit against the human RefSeq protein database. The percentage similarity between zebrafish and human orthologs was determined by Needleman–Wunsch amino acid pairwise sequence alignment. **(b)** Phylogenetic tree of human, zebrafish, mouse, chicken and coelacanth APOA-I, APOB, APOE and APOA-IV assembled from amino acid sequences as described in the Materials and Methods. Bootstrap support for each clade is reported in light blue (≥70 interpreted as significant). **(c)** Most zebrafish apolipoprotein genes share syntenic gene regions with their human orthologs. Schematic representation of human and zebrafish chromosomes regions with lines connecting human and zebrafish orthologs.

syntenic gene regions with human APOB, but apoBb.2 does not (Fig. 1c). The zebrafish *apoA-IV* genes share syntenic gene regions with human *APOE* (Fig. 1c).

The phylogenetic relationships between the human (*Homo sapiens*), zebrafish, mouse (*Mus musculus*), chicken (*Gallus gallus*), and coelacanth (*Latimeria chalumnae*) APOA-I, APOB, APOE, and APOA-IV genes were examined by generating a multiple sequence alignment with the iterative MAFFT multiple alignment tool. Among the suite of MAFFT iterative alignment programs, the G-INS-I strategy was selected as the most appropriate for our dataset, as it is recommended for sequences sharing global homology. The resulting alignment was funneled into the MAFFT tree server and used to build a neighbor joining tree based on all gap-free sites, using the JTT substitution model and allowing estimation of site heterogeneity (alpha). Bootstrap resampling was set to 100. The apolipoprotein gene families showed the relationships expected based on the sequence analyses and previous gene ancestry analyses [136], grouping into four distinct clades (Fig. 1b). There was strong bootstrap support (>70) grouping zebrafish apolipoprotein genes with their vertebrate orthologs in all cases except for apoA-IV. The analysis also emphasizes the close evolutionary relationship between ApoA-IVb.1, ApoA-IVb.2, and ApoA-IVb.3.

Spaciotemporal Apolipoprotein Expression Patterns

Utilization of the zebrafish to model dyslipidemias is limited by incomplete knowledge of the developmental expression patterns of each apolipoprotein. Although expression patterns of a subset of zebrafish apolipoproteins have been published, these studies generally do not indicate which apolipoprotein paralog was studied, nor

comprehensively describe how the genes are expressed throughout embryonic and larval development. Thus, we performed a comprehensive mRNA expression analysis of all 11 of the *apoA-I*, *apoB*, *apoE*, and *apoA-IV* genes from the 8-cell stage to 6 dpf.

In-situ hybridization (ISH) was carried out with antisense riboprobes specific to each apolipoprotein studied (Figs. 2-5) and control sense riboprobes (data not shown). All 11 apolipoproteins were expressed in the yolk syncytial layer (YSL) during embryogenesis (Figs. 2-5), a finding consistent with the YSL's unique role in processing yolk lipids and secreting VLDL to support embryonic and larval development [137]. Earliest apolipoprotein expression was observed with *apoEb* mRNA localization to the YSL during blastulation (30% epiboly) (Fig. 4). Gastrulation (80-100% epiboly) is associated with the earliest expression of *apoA-Ia* and *apoA-Ib* mRNA in the YSL (Fig. 2). *apoBa*, *apoBb.1* (Fig. 3a), *apoEa* (Fig. 4), and the four *apoA-IV* genes (Fig. 5) are first expressed during somitogenesis (15-20 somites). While many apolipoproteins are expressed uniformly throughout the YSL, some localize to specific YSL regions or in patterns indicative of subcellular niches. For example, at 80-100% epiboly both *apoA-Ia* and *apoA-Ib* mRNA localized to perinuclear YSL regions (Fig. 2), at 15-20 somites *apoBb.2* and *apoEa* are expressed strongly in distinct subregions of the YSL (Fig. 3a, 4), and at 1 dpf *apoA-IVa*, *apoA-IVb.2*, and *apoA-IVb.3* localize more strongly to the yolk extension than to the other areas of the YSL (Fig. 5).

As the digestive organs develop (4-6 dpf), the apolipoproteins examined begin to be expressed in the intestine and/or liver, often with gene paralogs segregated to different organs. ISH showed that *apoA-Ia* mRNA is expressed only in the intestine and that the majority of *apoA-Ib* mRNA localizes to the liver, with only weak expression in the

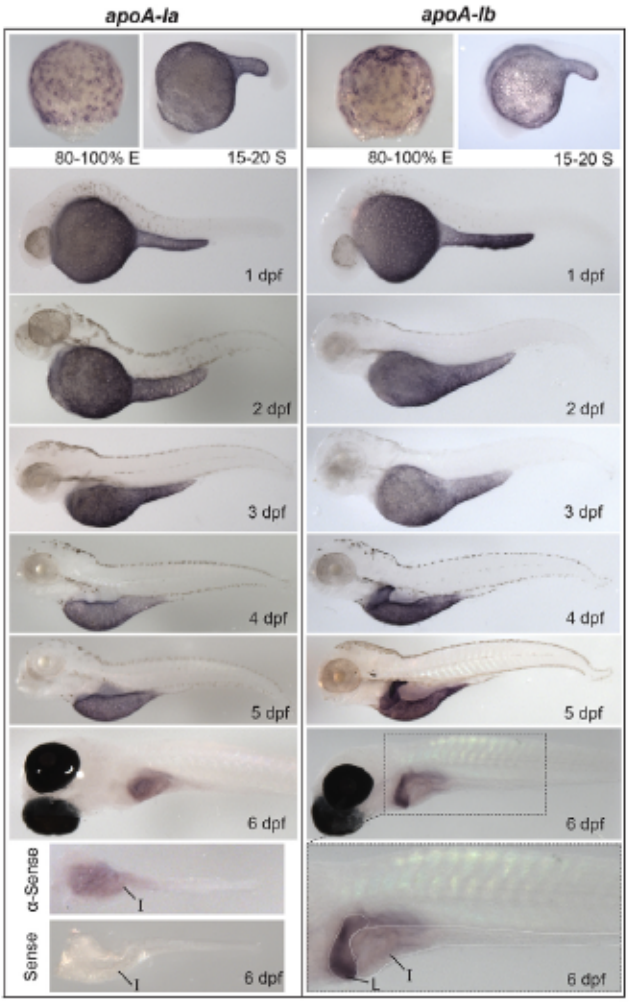

Figure 2:Developmental mRNA expression patterns of *apoA-Ia* and *apoA-Ib*. In situ hybridization of *apoA-Ia* and *apoA-Ib* during gastrulation [80–100% epiboly (E)], somitogenesis [15–20 somite (S)], and daily until 6 dpf. Both genes localize to the YSL from somitogenesis through 5 dpf, *apoA-Ia* localizes to the intestine (I) at 6 dpf, and *apoA-Ib* localizes strongly to the liver (L) and weakly to the intestine at 6 dpf. All zebrafish are wild type except 6-dpf larvae, which are nacre−/−. Larvae studied at 2–5 dpf were treated with PTU to prevent pigment formation. No signal was observed for either gene at the eight-cell stage or blastulation (supplementary material Fig. S1). Experiments were performed three times for each gene at each stage with n≥5 embryos or larvae per probe per experiment.

A. mRNA of zebrafish *apoB* genes localizes to specific regions of the YSL.

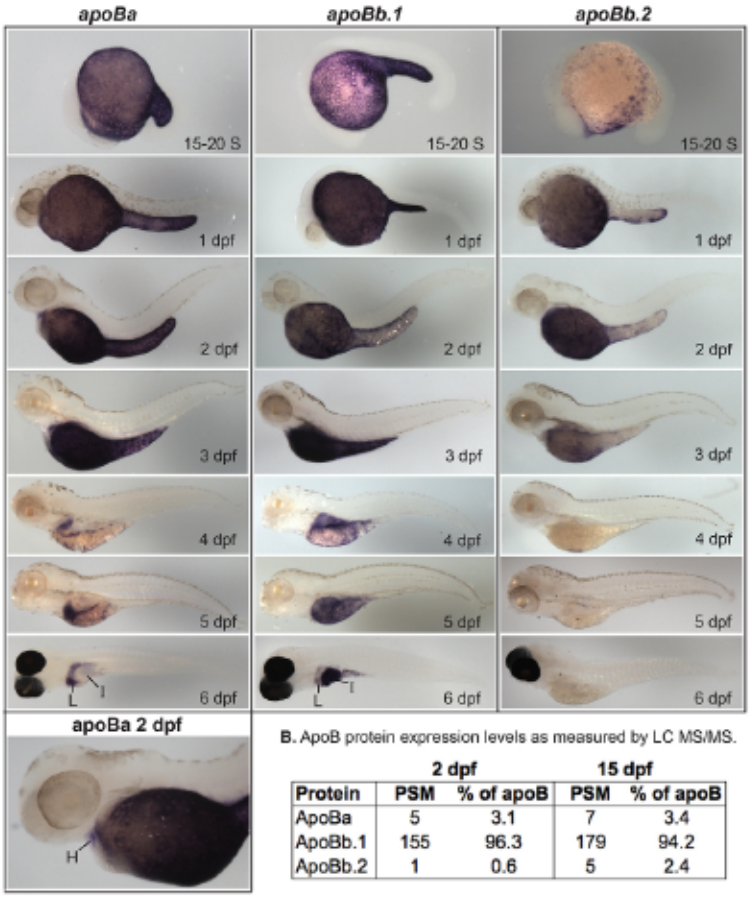

B. ApoB protein expression levels as measured by LC MS/MS.

	2 dpf		15 dpf	
Protein	**PSM**	**% of apoB**	**PSM**	**% of apoB**
ApoBa	5	3.1	7	3.4
ApoBb.1	155	96.3	179	94.2
ApoBb.2	1	0.6	5	2.4

Figure 3: Zebrafish apoB mRNA and protein expression. (a) Localization of *apoBa*, *apoBb.1* and *apoBb.2* mRNA by ISH from somitogenesis [15–20 somite (S)] to 6 dpf. All *apoB* genes are expressed in the yolk syncytial layer (YSL), but mRNAs localize to distinct subregions of the YSL at various developmental stages. *apoBa* mRNA is present in the heart (H) at 2 dpf. At 6 dpf *apoBa* mRNA is expressed strongly in the liver (L) and weakly in the intestine (I), *apoBb.1* is strongly expressed in the intestine and weakly in the liver, and apoBb.2 is not detectable by ISH. All zebrafish are wild type except 6-dpf larvae which are nacre−/−. Larvae collected at 2–5 dpf were treated with PTU to prevent pigment formation. No signal was observed at the eight-cell stage or at 30% or 80–100% epiboly (supplementary material Fig. S2). Experiments were performed three times for each gene at each stage with n≥5 embryos or larvae per probe per experiment. **(b)** Relative abundance of zebrafish ApoB paralogs as identified by peptide spectrum matches (PSM) in 2- and 15-dpf larvae (20–30 pooled larvae per experiment) as determined by LC-MS/MS of total larval proteins ≥250 kDa. Two experiments were performed for each developmental stage and both experiments yielded similar results. Data presented are from one experiment.

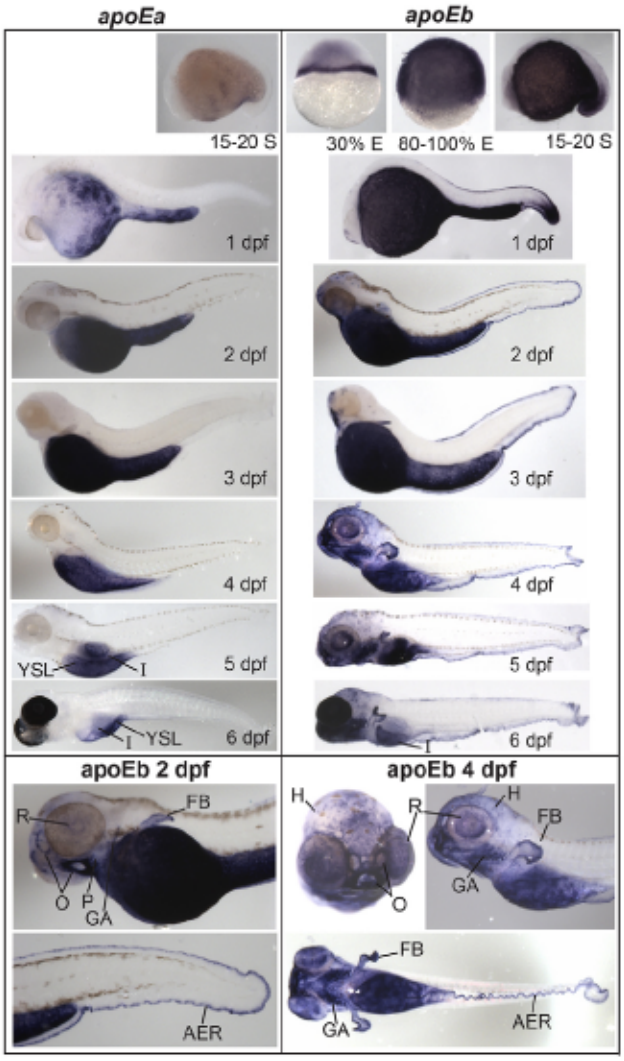

Figure 4: apoEa localization to the YSL and intestine contrasts with widespread expression of apoEb. *apoEa* and *apoEb* mRNA expression observed by ISH during blastulation [30% epiboly (E)], gastrulation (80% E), somitogenesis [15–20 somite (S)] and 1–6 dpf. *apoEa* mRNA is expressed in distinct subregions of the YSL at somitogenesis and 1 dpf, and ubiquitously throughout the YSL from 2–5 dpf. At 6 dpf (but not 5 dpf), apoEa is observed in the intestine (I). *apoEb* is expressed not only throughout the YSL (30% E to 5 dpf), but also in the tail bud (15–20 S and 1 dpf), the apical ectodermal ridge (AER) (1–6 dpf), the head (H) (1–6 dpf), mouth and nose orifices (O) (2–6 dpf), the find buds (FB) (2–6 dpf), pharynx (P) (2–6 dpf), gill arches (GA) (3–6 dpf), periderm (4–6 dpf), retina (R) (4–6 dpf), intestine (6 dpf) and swim bladder (6 dpf). No expression of *apoEa* was observed during blastulation or gastrulation, or for either gene at the eight-cell stage (supplementary material Fig. S3). Zebrafish are wild type, except for 6-dpf larvae which are nacre−/−; 1–6 dpf larvae were treated with hydrogen peroxide to remove pigmentation. ISH was performed in triplicate with n≥5 embryos or larvae per probe per experiment.

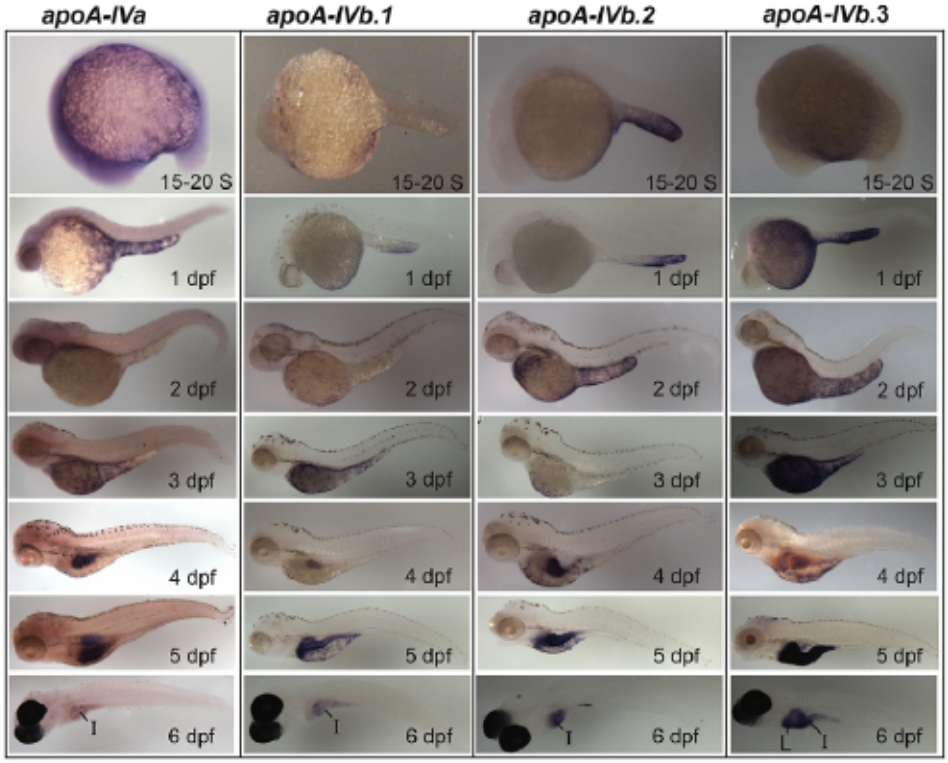

Figure 5: The zebrafish apoA-IV genes have unique expression patterns in the YSL, intestine and liver. Developmental mRNA expression dynamics of the zebrafish apoA-IV genes, as measured by ISH, during somitogenesis [15–20 somite (S)] and at 1–6 dpf. All four apoA-IV genes showed earliest mRNA expression at 15–20 S in the YSL; the mRNAs localize to distinct subregions of the YSL until 5 dpf. All four genes are expressed in the intestine (I) at 4–6 dpf, with weak intestinal expression observed for *apoA-IVa*, and *apoA-IVb.3* is expressed in the liver (L) at 4–6 dpf. No expression was observed for the *apoA-IV* genes at the eight-cell stage, 30% epiboly or 80–100% epiboly (supplementary material Fig. S4). Larvae from 15–20 S to 5 dpf are wild type (2–5 dpf treated with PTU; 6-dpf larvae are nacre−/−. Experiments were performed in triplicate with n≥5 embryos or larvae per probe in every experiment.

intestine (Fig. 2). The *apoB* genes show similar segregated mRNA localization with *apoBa* expressed strongly in the liver (4-6 dpf) and weakly in the intestine (5,6 dpf), *apoBb.1* expressed only in the intestine (5-6 dpf), and *apoBb.2* expressed solely in the liver at 5 dpf (Fig. 3a). mRNA of both *apoE* and all four *apoA-IV* genes localizes to the intestine (*apoEa* at 6 dpf, all others 4-6 dpf) (Figs. 4,5). The only *apoA-IV* paralog transcribed in both the liver and intestine is *apoA-IVb.1* (Fig. 5). The sole apolipoproteins expressed outside the YSL and digestive organs are *apoEa* and *apoEb*; *apoEb* localizes to the tail bud (15-20 somites - 1 dpf), apical ectodermal ridge (AER) (15-20 somites - 6 dpf), olfactory orifices (1-6 dpf), fin buds (2-6 dpf), esophagus/pharynx (2-6 dpf), gill arches (3-6 dpf), macrophages in the head (3-6 dpf), retina (4-6 dpf), periderm (4-6 dpf), and both *apoE* genes are expressed in the swim bladder (6 dpf) (Fig. 4).

With ISH we were able to qualitatively characterize spaciotemporal mRNA expression and localization of the zebrafish *apoB* paralogs. However, mRNA expression levels do not necessarily correlate with protein levels. Therefore, we used liquid chromatography mass spectrometry (LC-MS/MS) to determine if *apoB* mRNA expression observed by ISH is mirrored by ApoB protein levels. Total larval proteins $\geq$ 250 kDa were analyzed (all three zebrafish ApoB paralogs run in this size range on the SDS-PAGE gel; unpublished observation, I.A.D, H.T., and K.Y.). LC-MS/MS revealed that ApoBb.1 accounts for the majority of total ApoB protein in both 2 and 15 dpf larvae: 96.3% of total ApoB protein at 2 dpf and 94.2% at 15 dpf (Fig. 3b). ApoBa protein accounts for a small percentage of total ApoB at both developmental time points (3.1% of total ApoB protein at 2 dpf and 3.4% at 15 dpf) (Fig. 3b). Finally, at 2 dpf ApoBb.2

represents extremely little of the total ApoB protein (0.6% of total ApoB protein), but by 15 dpf it composes 2.4% of total larvae ApoB protein (Fig. 3b).

A High-Fat Feed Induces Apolipoprotein Transcription

The presence in the liver and/or intestine of every apolipoprotein examined, except *apoBb.2*, at 6 dpf – a developmental point that coincides with exhaustion of yolk nutrients and initiation of exogenous food intake-, suggests a crucial role for these proteins in dietary lipid transport. Despite this correlation, it is currently unknown if ingestion of dietary lipids transcriptionally regulate zebrafish apolipoprotein mRNA expression. We predicted that dietary lipids might induce apolipoprotein expression since the presence of these proteins is essential for lipid processing and transport. To address the hypothesis that ingestion of dietary lipids would induce apolipoprotein transcription, we used an established high-fat feeding paradigm in which chicken egg yolk emulsified in embryo media (5% chicken egg yolk; 4 hours) is fed to larval zebrafish [114]. Initially, we performed ISH on unfed and high-fat, 6 dpf fed larvae. While ISH is a powerful tool to localize transcripts, it can only provide a qualitative measure of expression levels since the development of the colorimetric readout is a non-linear process. Despite this limitation, we observed increased intestinal and hepatic signal of some apolipoproteins following a high-fat feed, consistent with possible increases in mRNA expression (Fig. 6a).

To quantitatively assess the effect of dietary lipids on larval apolipoprotein mRNA expression, we performed real-time PCR (RT-PCR) on the guts (intestine, liver, and pancreas) of 6 dpf unfed larvae and their fed clutch-mates 1, 2, 3, and 4 hours after

A. ISH suggests increased mRNA of several apolipoproteins in the gut after a high-fat feed.

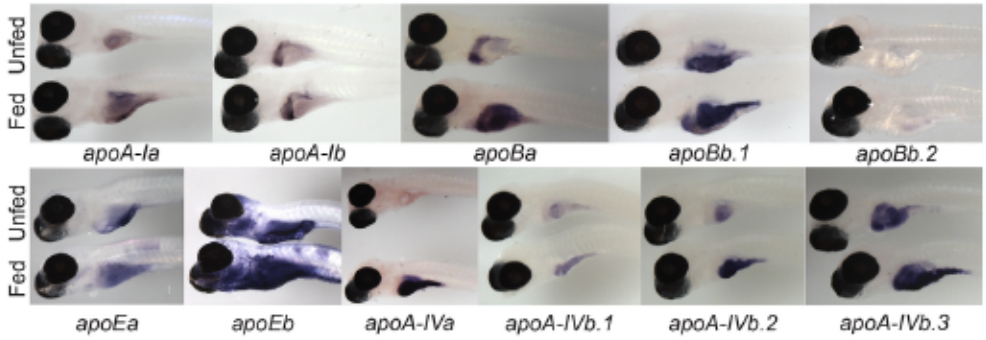

B. RT-PCR confirms mRNA expression of three *apoA-IV* paralogs is increased by a high-fat feed.

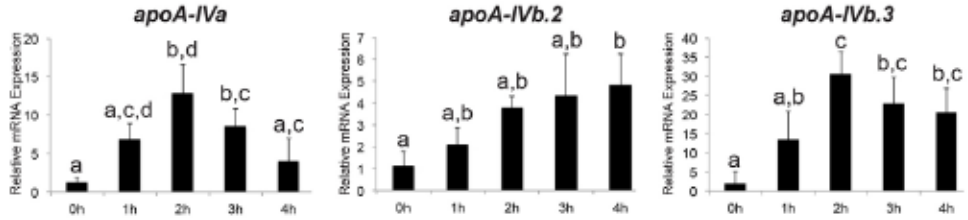

Figure 6: High-fat feed increases expression of apolipoproteins in larval gut. (a) Representative images of mRNA expression as observed by ISH of the zebrafish *apoA-I*, *apoB*, *apoE* and *apoA-IV* genes in 6-dpf nacre−/− larvae. Larvae have either never eaten exogenous food (Unfed), or have been fed a high-fat, 5% chicken egg yolk meal for 4 hours (Fed). ISH was performed in triplicate with n≥5 larvae; no staining was observed in sense probed (supplementary material Figs S1–S4). **(b)** A high-fat meal increases zebrafish apoA-IVa, apoA-IVb.2, and apoA-IVb.3 mRNA expression in the gut (intestine, liver, pancreas). Real-time PCR quantification of apolipoprotein transcriptional response in the 6-dpf zebrafish gut to 1, 2, 3 or 4 hours of a 10% chicken egg yolk feed (n=3; 10 pooled larval guts per experiment). Groups with the same letter are not significantly different (one-way ANOVA, $P<0.05$, n=3).

the onset of a high-fat feed (10% chicken egg yolk; 1 hour) (Fig. 6b). RT-PCR revealed a remarkable, ~30-fold increase in *apoA-IVb.3* mRNA at 2 hours following the onset of feeding (one-way ANOVA, $F(4,10)=9.359$, $p=0.0021$), a ~12-fold increase in *apoA-IVa* at the same time point (one-way ANOVA, $F(4,10)=9.318$, $p=0.0021$), and an ~5-fold increase in *apoA-IVb.2* by 4 hours post-feed onset (one-way ANOVA, $F(4,10)=5.433$, $p=0.0137$). The increases in gene expression appear to be specific to ingestion of dietary lipids, as no changes were observed after a high-protein, low-lipid white feed (10% egg white; 1 hour; E.M.Z. and S.A.F. unpublished observation). In contrast, although there were trends for increases in expression of the other apolipoproteins, they were not statistically significant. RT-PCR was not performed for apoBb.2 as the expression level in the gut at 6 dpf is below the detection limit of these assays.

Zebrafish ApoA-IV Overexpression Decreases Lipid-Rich Food Intake

Understanding the gut-brain signals underlying appetite regulation is critical in the context of the current obesity epidemic. Rat APOA-IV is secreted from the intestine on chylomicrons following a high-fat feed and acts as a satiety factor, signaling via vagal afferents to centrally decrease food intake [92, 138]. Therefore we hypothesized that ApoA-IV might have a conserved role in the regulation of food intake in zebrafish, predicting that it would decrease food intake during high-fat feeding. To address this question we created transgenic zebrafish that overexpress ApoA-IVb.1 and mCherry on an inducible heat shock protein 70 (hsp70) promoter (*Tg(hsp70:apoA-IVb.1:mCherry)*).

We anticipated that if ApoA-IVb.1 induces satiety, *Tg(hsp70:apoA-IVb.1:mCherry)* larvae overexpressing ApoA-IVb.1 following a heat shock would eat less

during a high-fat feed. To measure food intake, larvae were fed a high-fat meal (10% egg yolk; 4 hours) containing a fluorescently labeled lipid (BODIPY-C16), total larval lipids were extracted, and the amount of fluorescent lipids ingested was quantified via dot blot as an indication food intake (Fig. 7a). Strikingly, larvae overexpressing ApoA-IVb.1 ingested approximately one-third fewer fluorescent lipids than WT larvae (paired t-test, $p=0.004$) (Fig. 7b), demonstrating that ApoA-IV can regulate food intake in zebrafish as it does in rats.

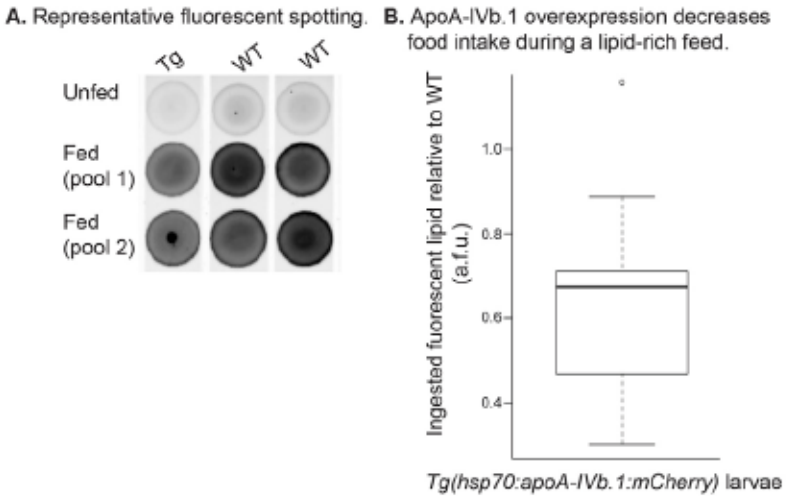

Figure 7: Overexpression of zebrafish ApoA-IVb.1 decreases food intake. (a) Representative fluorescent images of spotted lipid extracts; each spot represents the fluorescent lipids of 10 pooled larvae following lipid extraction. Tg represents Tg(*hsp70:apoA-IVb.1:mCherry*) larvae and WT represents wild-type larvae. Larvae have either never eaten exogenous food (Unfed), or have been fed a high-fat, 10% chicken egg yolk with 6.4 µM BODIPY® FL C16 for 4 hours (Fed). **(b)** Tg(*hsp70:apoA-IVb.1:mCherry*) larvae ingest fewer fluorescently labeled lipids as shown by comparison of arbitrary fluorescent units (a.f.u.) to wild type (paired Student's t-test, $P<0.001$; n=9, 20 larvae per experiment). Total larval lipids were extracted and lipid fluorescence was measured. Natural fluorescent lipid background was corrected using measurements of unfed larvae. The box represents the 25–75th percentiles, and the median is indicated. The whiskers show the 10–90th percentiles.

Discussion

Genetic Analysis of Zebrafish Apolipoproteins

This is a comprehensive study of zebrafish orthologs of four major mammalian serum apolipoproteins that are associated with disease processes. Unifying the nomenclature of zebrafish apolipoproteins is of utmost importance to enable proper interpretation of results and translation to human physiology. Historically, zebrafish gene nomenclature has been complicated by the extensive gene duplications that resulted from a whole genome duplication event in the teleost fish lineage [139-142]. Furthermore, the zebrafish community has only had the ability to start unifying gene nomenclature after the recent, more thorough annotation of the zebrafish genome. To ensure consistency between future studies and to facilitate translation to mammalian studies, we verified the ancestral relationships of the 11 zebrafish *apoA-I*, *apoB*, *apoE*, and a*poA-IV* genes with their named human orthologs through sequence, syntenic, and phylogenic analyses.

This study and others have shown that zebrafish apolipoproteins tend to have low sequence similarity to their mammalian orthologs [136]. Despite high sequence divergence, based on the results of our syntenic and phylogenetic analyses, we are confident that the zebrafish genes investigated in this study are accurately named after their human orthologs. The phylogenetic analysis showed that the apolipoproteins group into clades with their vertebrate orthologs, although the APOA-IV clade was not significantly distinct from the APOA-I clade. Babin et al. also showed that single zebrafish ApoA-I, ApoA-IV, and ApoE paralogs grouped into clades with their vertebrate orthologs, but did find a significance distinction of the APOA-IV clade [129]. One

possible explanation for these inconsistent APOA-IV clade results could be that APOA-IV evolved from a more recent duplication event than the other apolipoproteins studied. Although the APOA-IV phylogenetic clade was not significant, the close evolutionary relationship between the ApoA-IVb genes is apparent. Since ApoA-IVb.1, ApoA-IVb.2, and ApoA-IVb.3 are clustered closely together on chromosome 16, it is possible that one gene resulted from a whole genome duplication event and that the other two were relatively recently created by local, independent gene duplication events.

The zebrafish *apoA-IV* paralogs do not share syntenic gene regions with human APOA-IV, but do unexpectedly share syntenic gene regions with human *APOE*. Although the origin of this chromosomal relationship cannot be determined from this analysis, the results lead us to speculate that the *APOE* and *APOA-IV* genes may have been clustered together in a common ancestor. The lack of syntenic gene similarity between *apoBa* and human *APOB* suggest that this gene resulted from an independent, local duplication event, as opposed to the teleost whole genome duplication event.

Retention of Duplicate Apolipoproteins

It is noteworthy that zebrafish have retained multiple apolipoprotein paralogs over millions of years of evolution. The duplication-degeneration-complementation (DDC) model [143] proposes an explanation of why many duplicated genes may be retained. The DDC model predicts that, instead of being retained due to the evolution of novel functions (neofunctionalization), degenerative mutations in the regulatory elements of duplicated genes increase the likelihood of their preservation due to conservation and partitioning of their ancestral functions (subfunctionalization). The zebrafish paralogs of

pax6 and the *igf1r* are clear examples of genes that have subfunctionalized. The paralogs of these genes perform similar functions in different tissues due to differential expression patterns, likely resulting, as the DDC model predicts, from mutations in regulatory elements [144, 145]. We speculate that similar subfunctionalization has occurred in several of the zebrafish apolipoprotein paralogs. For example, while mammalian *APOA-I* is expressed both in the intestine and liver, zebrafish *apoA-Ia* is expressed in the intestine and the majority of *apoA-Ib* expression is observed the liver. Based on the DDC model, we would predict that there are mutations in the regulatory regions of these genes that restrict their expression to certain tissues while maintaining their ancestral function. Similar subfunctionalization may have occurred in the zebrafish *apoA-IV* paralogs, since all four are expressed in the larval intestine, but only *apoA-IVb.3* is expressed in the liver. Comparatively, human *APOA-IV* is expressed in the intestine, but rat *ApoA-IV* is expressed in the liver and intestine, so the ancestral gene may have had both hepatic and intestinal expression.

Zebrafish and humans have evolved unique strategies to achieve tissue specific *APOB* gene expression. In zebrafish, it is possible that the zebrafish *apoB* paralogs have subfunctionalized, with *apoBa* restricted to performing the ancestral gene's function in the liver and *apoBb.1* performing the majority of the ancestral gene's function in the intestine. Conversely, tissue specific human *APOB* expression occurs in the form of different isoforms of the same gene due to mRNA editing; a short isoform, *APOB-48*, expressed in the intestine, and a long isoform, *APOB-100*, is expressed in the liver. Although *apoBb.2* is the shortest zebrafish paralog, it is not a C-terminal truncation as is human *APOB-48* in that it contains numerous deletions throughout the protein (data not

shown) and it is not expressed in the larval intestine. Zebrafish ApoB protein analysis by LC-MS/MS indicated higher levels of ApoBb.1 as compared to ApoBa or ApoBb.2 protein, so ApoBb.1 may have a greater role in lipid transport. The mechanisms underlying the large differences in zebrafish ApoB protein levels have yet to be determined, however unpublished RNAseq data of 6 dpf larval guts (E.M.Z. and S.A.F.) similarly shows much higher mRNA levels for *apoBb.1* than for *apoBa* or *apoBb.2* at 6 dpf, suggesting that the regulation takes place at the RNA level. In addition, it is not clear whether higher expression of the ApoB.1 protein provides a functional benefit in lipid transport as compared to the other paralogs.

The zebrafish *apoE* paralogs may also have undergone subfunctionalization. Here we show *apoEa* localizing to the YSL and intestine, and both our work and that of others, finding widespread expression of *apoEb* [129, 131, 135]. Based on its spatiotemporal expression and localization patterns, we predict ApoEb likely retained the non-lipid transport, extra-digestive organ functions of the ancestral gene. Zebrafish *apoEb* has similar developmental expression to mouse *APOE* (visceral yolk sac endoderm at 8.5 days post conception (dpc), liver, lung, heart, and eye at 9.5 dpc, and cells lining the olfactory vesicle, peripheral neural cells, and the brain at 10.5 dpc [146, 147]). Since both zebrafish *apoE* paralogs are expressed in the YSL it is unclear from our data if they exhibit different lipid transport properties. Monnet et al. [131] observed similar expression of an unspecified *apoE* paralog during zebrafish development and induction during adult fin regeneration.

The segregated expression of several larval apolipoprotein paralogs between organs provides a unique opportunity to study potential differences in lipoproteins

generated from various tissues. Recent studies have emphasized the contribution of particle composition to lipoprotein function [148]. It is not known if nascent mammalian HDL particles synthesized by the liver have compositions unique from those assembled by the intestine. It is difficult to address this question with traditional mouse models since it is technically challenging to identify HDL particles of different origins. Promisingly, the nearly segregated expression patterns of the zebrafish *apoA-I* paralogs provide a system to study HDL particles of hepatic vs. intestinal origins. The apolipoprotein mRNA localization data presented in this study does not show localization to any novel organs compared to human ortholog expression, but functional studies will need to be performed in the future to rule out the possibility that any neofunctionalization has occurred.

mRNA Localization Suggests Important Roles for Apolipoproteins in YSL and Dietary Lipid Transport

Previous ISH studies support our finding that zebrafish apolipoproteins have nearly universal mRNA expression in the YSL [129, 130]. The YSL is a syncytium containing many highly dynamic nuclei that forms at the surface of the yolk cell during blastulation [137]. In addition to a multitude of key developmental functions, the YSL serves nutritive functions in the developing embryo, including the hydrolysis and export of yolk lipids via lipoproteins. Electron microscopy studies have visualized the secretion of VLDL particles from the highly developed secretary pathways of the fish YSL [149, 150] and studies in zebrafish lacking functional *mtp* (an *apoB* chaperone required for VLDL formation) have demonstrated the necessity of lipoprotein for export of yolk lipids [151]. Given these observations, it was expected that the zebrafish orthologs of

mammalian apolipoproteins known to be associated with VLDL and chylomicrons (*apoB*, *apoE*, *apoA-IV*) would be expressed in the YSL. Thus, it was surprising that both *apoA-I* paralogs were also expressed in the YSL. The presence of *apoA-I* suggests that the YSL may produce HDL particles in addition to the classically described VLDL particles, or that the previously described VLDL particles have an apolipoprotein composition unique from classical VLDL. To our knowledge, biochemical characterization of the lipoproteins produced by the YSL has never been undertaken; these studies would have the potential to reveal a wealth of information regarding lipoprotein function during embryonic development.

Mammalian embryos also have a yolk sac in early development, prior to the development of a circulatory system. Like the fish YSL, the mammalian yolk sac secretes VLDL [152, 153]. It is likely that mammalian yolk sac apolipoproteins provide required nutritive contributions during embryogenesis as *ApoB* [153] and *ApoE* [146] mRNA are expressed in the mouse yolk sac and loss of *APOB* [152] or *Mtp* [154] is embryonic lethal. Knockdown of YSL lipoproteins is similarly lethal in zebrafish [49, 151]. Taken together, these findings suggest that future studies of zebrafish YSL lipid metabolism can serve as an informative model of mammalian embryonic metabolism.

A second prominent finding from our spatiotemporal apolipoprotein mRNA expression analysis was that many of the apolipoproteins were not distributed evenly throughout the YSL, but localized to distinct subregions. A cursory analysis of publicly available YSL expression patterns on zfin.org reveals many additional examples of regional YSL gene expression, yet the significance of these YSL subregions, especially in relationship to embryonic lipid metabolism, has yet to be explored. Notably, the

apolipoproteins do not adhere to the YSL expression patterns of *gata5* and *gata6*, markers of the presumptive YSL regions that will become the liver and intestine [130]. Thereby, supporting the theory that apolipoprotein mRNA is translated into proteins that perform YSL-specific functions, and that the proteins are not simply being recruited to the nascent digestive tract.

Dietary Lipids Induce Apolipoprotein Expression

Extensive research has elucidated much of the complex, molecular network that regulates transcription of the major serum apolipoproteins [155], but it is less clear how the presence of dietary nutrients regulates apolipoprotein transcription. Dietary fats increase transcription of mammalian *ApoB* and *ApoA-IV*, two apolipoproteins involved in chylomicron assembly [156]. *ApoA-IV* is very sensitive to nutritional status; dietary lipids increase intestinal *ApoA-IV* expression via HNF-4 promoter binding [157]. Fasting [158, 159], while high-fat diets [156], diabetes [159], and hepatic steatosis increase hepatic *ApoA-IV* expression through CREBH [160]. Our results indicate that intestinal and hepatic mRNA expression of three of the four zebrafish *apoA-IV* paralogs is similarly increased in response to high-fat feeding, but whether the molecular mechanisms of this response mirrors those of mammals remains open to investigation.

In contrast to *ApoA-IV*, the effects of dietary lipids on intestinal and hepatic *ApoA-I* and *ApoE* transcription are less well studied. Additional questions regarding the effects of dietary lipids on apolipoprotein expression are raised by Yoshioka et al.'s [161] paradoxical finding that a high-fat meal decreases *ApoB* and does not change *ApoA-IV* mRNA expression in intestinal mucosa. It is possible that the inconsistent results found in

various mouse models are due in part to the nutritional status of the animals. The mice in previous studies were fasted for various lengths of time prior to refeeding with high-fat diets of varying compositions and durations. An advantage of the larval zebrafish model is that the larvae used in this study were experiencing their first exogenous meal, previously subsisting on yolk nutrients. Therefore, the larval zebrafish offers a unique opportunity to study food intake in an animal that has the homogeneity of fasted animals without the effects of fasting and refeeding. In addition, the developmental expertise established in the zebrafish presents an exceptional opportunity to explore the potential synergistic effects of developmental stage on dietary lipid regulation of apolipoprotein transcription.

Zebrafish apoA-IV Decreases High-Fat Food Intake

It has long been appreciated that APOA-IV is secreted from the intestine as a component of chylomicrons in response to long-chain dietary fatty acids [162, 163]. Over 20 years ago, Fujimoto et al. [91, 92] demonstrated that acute, peripheral administration of APOA-IV decreases food intake in rats due to reduced meal size. Recent work supports the hypothesis that peripheral APOA-IV signals via the vagal nerve [164, 165] to the CNS (where *ApoA-IV* is expressed in the hypothalamus [166]) to decrease food intake [138, 167]. Recently, Wang et al. [93] identified a specific portion of the N-terminal region of rat APOA-IV that is capable of decreasing food intake.

In this investigation we verified that zebrafish ApoA-IV performs a conserved function in the regulation of high-fat food intake. We demonstrated that acute overexpression of ApoA-IVb.1 decreases lipid ingestion during a high-fat feed. It is

possible that the additional zebrafish ApoA-IV paralogs also regulate food intake: they are highly transcriptionally responsive to dietary lipids, and ApoA-IVb.2 and ApoA-IVb.2 share a high degree of sequence similarity to ApoA-IVb.1. Although ApoA-IVa has the most divergent sequence from ApoA-IVb.1, it is also highly induced by a high-fat feed. Hence, ApoA-IVa may share a role in regulating food intake, or, since mammalian APOA-IV facilitates the production of smaller, more quickly cleared chylomicrons [168], it may be produced solely to structurally support chylomicrons.

Unexpectedly, even though ApoA-IVb.1 overexpression decreased food intake, we were not able to detect mRNA expression in the CNS, where it is thought to regulate mammalian food intake. Therefore, it is possible that the signaling pathway by which ApoA-IVb.1 reduces food intake in larvae differs from that of rats. Alternatively, *apoA-IVb.1* may be expressed at an extremely low level in the CNS that ISH to not sensitive enough to detect. An alternative explanation of our results is that ApoA-IVb.1 signaling might vary by developmental stage. In fact, neonatal swine experience a high degree of *ApoA-IV* transcriptional induction by intraduodenal lipids before, but not after, weaning [169]. Future studies should define the degree to which endogenous zebrafish ApoA-IV proteins naturally regulate high-fat food intake and explore the signaling pathways by which this occurs.

Despite the relationship between acute APOA-IV administration and decreased food intake observed in rats, mice deficient in APOA-IV, or with chronically overexpressed APOA-IV, have no changes in food intake [104, 105]. The potentially conflicting results found in the mouse models of APOA-IV overexpression or loss could result from species differences between rats and mice. Yet, evidence showing that

APOA-IV expression is decreased by chronic high-fat diet and obesity [100], suggests that long-term overexpression or loss of APOA-IV may lead to loss of function. In our study, transient overexpression of zebrafish ApoA-IVb.1 by an inducible promoter decreased food intake during a lipid-rich feed. This finding supports a model where transient vs. chronic induction of APOA-IV could have variable effects on food intake. Future studies could validate this model by chronically overexpressing ApoA-IVb.1 on a constitutively active promoter and determining if regulation of lipid-rich food intake is lost.

This study provides a framework for use in future studies of apolipoprotein biology, lipoprotein metabolism, dyslipidemias, and the roles of apolipoproteins in embryonic development in the larval zebrafish. This study presented: an analysis of the gene ancestry and genetic relationships between four major human serum apolipoproteins (APOA-I, APOB, APOE, and APOA-IV) and their 11 zebrafish orthologs; characterization of the developmental expression patterns of these apolipoproteins; and their transcriptional response to a high-fat feed. Finally, we determined that overexpression of a zebrafish ortholog of ApoA-IV, an apolipoprotein that regulates high-fat food intake in mammals, functions similarly in zebrafish. These data contribute to a growing literature establishing the larval zebrafish as a model for lipid metabolism in health and disease.

Materials and Methods

Apolipoprotein Gene Ancestry Analysis

To determine that zebrafish apolipoproteins share the same ancestral gene as their named human ortholog we performed sequence, syntenic, and phylogenic analysis. The amino acid sequences of the zebrafish apolipoproteins were obtained from the Ensembl Genome Browser (Ensembl.org). To verify that the zebrafish genes were named after the appropriate human ortholog, first the protein sequence of each zebrafish gene was used to query NCBI using BlastP (standard settings) restricted to human refseq protein database [170, 171]; the top Blast hit for each query was recorded. Optimal pairwise alignments between zebrafish and human orthologs were determined with the Needleman-Wunsch pairwise sequence alignment [172] tool available at EMBL_EBI (http://www.ebi.ac.uk/Tools/psa/emboss_needle/) [173]. Second, the syntenic relationships between the zebrafish and human apolipoproteins were established using the Genomicus [174] and SyntenyDB [175] online syntenic analysis tools by searching for orthologous apolipoproteins in the corresponding syntenic region. To examine the phylogenic relationship between zebrafish apolipoprotein paralogs and their corresponding vertebrate orthologs the amino acid sequences of human, zebrafish, mouse, chicken, and coelacanth APOA-I, APOB, APOE, and APOA-IV were aligned with using the iterative MAFFT multiple sequence alignment tool [176, 177]. Specifically, the G-INS strategy was selected, as it is recommended for sequences sharing global homology, the BLOSUM62 scoring matrix was used with a gap open penalty of 1.53. Following alignment the MAFFT tree server was used to build a neighbor joining

tree based on all gap free site, using the JTT substitution model and allowing estimation of site heterogeneity (alpha), bootstrap resampling was set to 100 with significance set at >70.

Zebrafish

All procedures were approved by the Carnegie Institution Animal Care and Use Committee (Protocol# 139) or Weizmann Institute Animal Care and Use Committee (Protocol# 01190212-3). For ISH experiments, WT (AB background) and pigment-free ($nacre^{-/-}$) (Lister 1999) embryos were collected from natural spawning, staged, and raised in zebrafish embryo media (EM) as described previously [178, 179]. WT larvae older than 1 dpf used for ISH experiments were treated with 0.003% N-phenylthiourea (PTU) (Sigma, St. Louis, MO, USA) [180] or hydrogen peroxide [181] to decrease pigmentation. Zebrafish were fixed in 4% paraformaldehyde in phosphate buffered saline overnight at 4°C, washed twice in MeOH, and stored in MeOH at -20°C. Larvae raised to 15 dpf for ApoB protein measurements were fed 3 times per day from 7-15 dpf (larval AP100, #384709-20, Zeigler, USA).

Preparation of Feeding Liposomes

Our laboratory and others have developed a high-fat feeding paradigm for larvae using chicken egg yolk [114, 115]. Briefly, 5% and 10% chicken egg yolk emulsions were prepared into liposomes from frozen aliquots of egg yolk resuspended in EM as previously described [114]. The egg yolk emulsion was vortexed (2 minutes) and pulse sonicated with a one-fourth inch tapered microtip (5 seconds total processing time, 1

second on, 1 second off, output intensity: 3W) for 40 seconds (Sonicator: Ultrasonic Processor 6000, Misonix Inc., Farmingdale, NY, USA).

Feeding Assay for ISH

Larvae (nacre$^{-/-}$, 6 dpf) were fed a high fat meal of 5% egg yolk liposomes for 4 hours at 29°C on an incubated shaker (Incu-Shaker Mini, Benchmark, Edison, NJ, USA). Fed larvae were washed three times in EM, anesthetized with tricaine (Argent Chemical Laboratories, Redmond, WA, USA), screened for the presence of food in the intestine, and fixed in 4% PFA as described above. Unfed clutch-mates were treated in tandem in EM and collected as controls.

Whole-Mount ISH

To elucidate the spaciotemporal mRNA expression patterns of the zebrafish apolipoproteins ISH was carried out as previously described [181]. Briefly, 500-800 base pairs of unique sequence of *apoA-Ia*, *apoA-Ib*, *apoBa*, *apoBb.1*, *apoBb.2*, *apoEa*, *apoEb*, *apoA-IVa*, *apoA-IVb.1*, *apoA-IVb.2*, and *apoA-IVb.3* were amplified from cDNA, topo cloned into pCRII (Invitrogen, Grand Island, NY, USA), and used to generate sense and antisense digoxigenin-labeled riboprobes (digoxigenin: Roche, Indianapolis, IN, USA). The riboprobes were hybridized against zebrafish of the following stages: 8 cell (to examine the presence of maternal mRNA transcripts), 30% epiboly (blastula), 80-100% epiboly (gastrula), 15-20 somite (somitogenesis), 1 dpf, 2 dpf, 3 dpf, 4 dpf, 5 dpf, and unfed and fed 6 dpf. ISH experiments were carried out three times on $\geq$ five larvae, for each sense and antisense probe, at each stage.

Feeding Assay for Real-Time PCR (RT-PCR) Experiments

For assays measuring the transcriptional responses of zebrafish apolipoproteins to a lipid rich feed larvae (AB, 7 dpf, pairwise crosses) were placed in a 10% egg yolk emulsion on an incubated shaker (29°C). After 1 hour of feeding larvae were washed three times in EM, anesthetized with tricaine, and examined for full intestines to verify that they had fed. Larvae representing a 1 hour time point were set aside for dissection; remaining larvae were incubated at 29°C in EM for the remainder of time course and collected for dissection at 2, 3 and 4 hours. Unfed clutch-mates were incubated in EM, anesthetized, and collected in parallel as controls. Larval guts (intestine, liver, pancreas) were dissected, pooled in groups of 10, transferred to 30 µL RNALater (Ambion, Grand Island, NY, USA), and flash frozen. Pooled experimental groups were collected in triplicate.

RT-PCR Sample Preparation and Analysis

RNA was extracted from larval guts using a RNAqueous Micro Kit (Ambion, Grand Island, NY, USA) and stored at -80°C. RNA sample purity was verified with the Agilent RNA 6000 Pico Kit (Agilent Technologies, Santa Clara, CA, USA) and the Agilent 2100 Bioanalyzer (Agilent Technologies, Santa Clara, CA, USA). cDNA was constructed using the iScript cDNA Synthesis Kit (BioRad, Hercules, CA, USA). RT-PCR samples were prepared using cDNA, SsoAdvanced Universal SYBR Green Supermix (BioRad, Hercules, CA, USA), and gene specific primers; RT-PCR was performed in triplicate for each sample.

Total Larval Protein Purification and In Gel Digestion

Relative protein expression levels of the zebrafish apoB paralogs was measured by purifying total larval protein and performing liquid chromatography-mass spectrometry (LC-MS/MS). To purify total protein, 20-30 embryos (2 and15 dpf) were anesthetized on ice, washed twice with buffer A (β-glycerophosphate 500 mM, EGTA 15 mM, orthovanadate 1 mM, EDTA 10 mM, Benzamidine 1mM, aprotinin 10 mg/ml, leupeptin 10 mg/ml, pepstatin 2 mg/ml) and suspended in 400 µl buffer H (buffer A supplemented with 1mM DTT). Embryos were homogenized with a 27-gauge syringe and sonicated twice on ice for 7 seconds at 40% power. Samples were centrifuged at 15,000 RPM at 4°C for 15 minutes, and supernatants were collected.

Total larval proteins were separated by SDS-PAGE using a 6% separating gel (4.5 ml H_2O, 1.7 ml 30% acrylamide, 2.1 ml separating buffer (3M Tris base pH 8.8, APS 1:100, TEMED 1:1000)) and a 4% stacking gel (3 ml H_2O, 0.66ml 30% acrylamide, 1.25 ml separating buffer (0.5M Tris base pH 6.9, APS 1:100, TEMED 1:1000)). GelCode Blue Stain Reagent (24590, Thermo Scientific) was used for protein detection *according to manufacturer's instructions*.

Selected areas of interest (250-550 kDa, were excised from the gel, sliced into small (1-2 mm) pieces and placed in a silicon tube (0.65 ml; PGC Scientific). Gel bands were de-stained with 25 mM NH_4HCO_3 in 50% acetonitrile and dried by centrifugation under vacuum. Protein disulfide bonds were reduced by saturating the dry gel bands with 10 mM DTT in 25 mM NH_4HCO_3 at 56°C for 1 hour, and were alkylated with 55 mM iodoacetamide in 25 mM NH_4HCO_3 in the dark for 45 minutes at room temperature. After washing in 25 mM NH_4HCO_3 in 50% acetonitrile and centrifugation under vacuum,

proteins were digested by rehydrating the gel pieces with 12.5 ng/µL trypsin in 25 mM NH_4HCO_3 at 4°C for 10 minutes followed by overnight incubation at 37°C. Peptides were extracted by addition of 50% acetonitrile/5% formic acid, *vortexing, sonicating centrifuging* and collection of the supernatant. Digestions were stopped by trifluoracetic acid (1%) addition. Extracted proteins were stored at -80°C until further analysis.

Liquid Chromatography

ULC/MS grade solvents were used for all chromatographic steps. Sample were loaded using split-less nano-Ultra Performance Liquid Chromatography (10 kpsi nanoAcquity; Waters, Milford, MA, USA). The mobile phase consisted of: A) H_2O and 0.1% formic acid and B) acetonitrile and 0.1% formic acid. Desalting of the samples was performed online using a reversed-phase C18 trapping column (180 µm internal diameter, 20 mm length, 5 µm particle size; Waters Corporation, Milford, MA, USA). Next, the peptides were separated using a T3 HSS nano-column (75 µm internal diameter, 250 mm length, 1.8 µm particle size; Waters) at 0.35 µL/minute. Peptides were eluted from the column into the mass spectrometer with the following gradient: 4% to 35% B in 105 minutes, 35% to 90% B in 5 minutes, maintained at 95% for 5 minutes and return to initial conditions.

Mass Spectrometry

The nanoUPLC was coupled online through a nanoESI emitter (10 µm tip; New Objective; Woburn, MA, USA) to a quadruple orbitrap mass spectrometer (Q Exactive Plus, Thermo Scientific) using a FlexIon nanospray apparatus (Proxeon). Data was

acquired in DDA mode, using a Top12 method. MS1 resolution was set to 60,000 (at 400m/z) and maximum injection time was set to 120 milliseconds. MS2 resolution was set to 17,500 and maximum injection time of 60 milliseconds.

Data Analysis of Mass Spectrometry Experiments

Raw data was processed using Proteome Discoverer v1.41. The MS/MS spectra were searched using Mascot 2.5 (Matrix Sciences) and Sequest HT against the zebrafish protein database UniprotKB (http://www.uniprot.org/) appended with 125 common laboratory contaminant proteins. Fixed modification was set to carbamidomethylation of cysteine and variable modification was set to oxidation of methionine. Search results were then imported back to Expressions to annotate identified peaks. Proteins were grouped based on shared peptides and identifications were filtered such that the global false discovery rate was a maximum of 1%.

Generation of Transgenic Zebrafish

Gateway cloning was used to create a construct driving zebrafish ApoA-IVb.1 and mCherry on the Heat Shock Protein 70 (HSP70) promoter and stable transgenic zebrafish lines were generated as previously reported [182]. Zebrafish *apoA-IVb.1* was amplified from cDNA (f: GGG GAC AAG TTT GTA CAA AAA AGC AGG CTC CAT GAA ACT GTA TCT GAT A r: GGG GAC CAC TTT GTA CAA GAA AGC TGG GTC TTA ATA TCT CTT GGT GA) and cloned into a Gateway middle entry vector. We then used gateway cloning to create a *hsp70:apoA4b.1:mCherry* construct flanked by tol2 sites, which was injected into the yolk of 1-2 cell embryos with tol2 transpose for genome

incorporation. Transgenic *Tg(hsp70:apoA-IVb.1:mCherry)* larvae were identified at 2 dpf by heat-shocking larvae in 15 mL EM at 37°C for 45 minutes followed by 42°C for 10 minutes and screening for fluorescence ~18 hours later. Larvae were heat-shocked a second time at 6 dpf, ~18 hours prior to feeding assays, to induce ApoA4b.1 and mCherry overexpression.

Experimental Feeding Assays for tgHSP70:ApoA-IVb.1:mCherry Larvae

As an indicator of food intake *Tg(hsp70:apoA-IVb.1:mCherry)* larvae were fed liposomes labeled with BODIPY-C16 (Invitrogen, Grand Island, NY, USA, D-3821) fatty acid analog. Labeled liposomes were made by adding BODIPY-C16 to 5 mL of 10% egg yolk emulsion immediately following sonication for a final concentration of 6.4 µM BODIPY-C16 and vortexing for 30 seconds. *Tg(hsp70:apoA-IVb.1:mCherry)* larvae (7 dpf) were placed in the fluorescent liposome solution in an incubated shaker for 4 hours at 29°C. Larvae were next washed three times in EM, anesthetized in tricaine, and screened for the presence of food in the intestine. Groups of 10 larvae were pooled, flash frozen, and stored at -80°C. Feeding assays were performed pairwise with one pool of 10 transgenic larvae and two pools to 10 WT larvae. Unfed, WT and transgenic larvae were treated in parallel and collected as controls. A total of nine paired sets of larvae were collected. All experimental and control Tg and WT larvae were treated with the same heat shock protocol at 2 and 6 dpf as described above.

Lipid Extraction and Analysis

Total lipids were extracted from the larvae fed fluorescent liposomes similarly to previous reports [151] following the Bligh and Dyer method [183]. Briefly, 100 µL of H_2O was added to the frozen pool of 10 larvae and sonicated for 4 seconds with a one-fourth-inch inch tapered microtip with an output of 3W. Next, 375 µL of Chloroform: Methanol (1:2) was added to the homogenate, it was vortexed 30 seconds, and incubated at 25°C for at least 10 minutes. 125 µL of chloroform and 125 µL 200 mM Tris, pH 7, were subsequently added, with 30 seconds of vortexing after each addition. The samples were centrifuged at 4,000 rpm for 5 minutes. The organic phase was transferred to a clean microfuge tube and stored at -80°C. For analysis, samples were dried in a speed vacuum, resuspended in 12 µL chloroform, and dotted on a channeled TLC plate (Whatman Scientific, Florham Park, NJ, USA). To detect BODIPY-C16 (as an indication of food intake) plates were scanned (Typhoon Scanner, GE Healthcare, Pittsburg, PA, USA) using a blue fluorescence laser (excitation: 488 nm; emission: 520 nm Band Pass; PMT 425). Total fluorescence of each sample was quantified using ImageQuant software (GE Healthcare, Pittsburg, PA, USA). Correction for naturally fluorescent lipid background was made with paired, unfed larval samples.

Statistics

RT-PCR gene expression results were quantified using the ΔΔCT method [184] with *18S* as the reference gene. Differences in gene expression over the course of a 4-hour feed as measured by RT-PCR were determined by one-way ANOVA followed by a Holm-Sidak test for multiple comparisons. Assays to compare difference in feeding

between WT and *Tg(hsp70:apoA-IVb.1:mCherry)* larvae were performed pairwise with one sample of transgenic larvae and two samples of WT larvae per experiment. For each experiment the fluorescence, expressed in arbitrary units, of the dot blots following correction for background fluorescence of the two WT samples was averaged together. The difference in the amount of fluorescent lipids ingested between WT and *Tg(hsp70:apoA-IVb.1:mCherry)* larvae was determined by paired t-test. All of the data was normally distributed and significance for all analyses was set at $p<0.05$.

CHAPTER 2 – ASSEMBLY AND SECRETION OF FLUORESCENTLY TAGGED APOLIPOPROTEIN B PEPTIDES

Meghan T. Walsh[1], Oni M. Celestin[2], **James H. Thierer[2]**, Steven A. Farber[2], M. Mahmood Hussain[1,3,4]

[1]Department of Cell Biology, SUNY Downstate Medical Center, Brooklyn, New York; [2]Department of Embryology, Carnegie Institution for Science, Baltimore, MD; [3]Diabetes and Obesity Research Center, New York University Winthrop Hospital, Mineola, NY; [4]VA New York Harbor Healthcare System, Brooklyn, NY

The following chapter is reprinted from a collaborative manuscript being prepared for submission to the *Journal of Lipid Research* that evaluates whether APOB-fusion proteins can be used to generate lipoproteins. I analyzed the data and wrote the results, methods, and discussion sections relating to the clonal analysis experiment performed in live zebrafish (Fig. 6). This work demonstrates that APOB tagged with fluorescent reporters can be lipidated, secreted, and endocytosed as would be expected by endogenous lipoproteins, providing a precedent for using tagged versions of APOB to monitor lipoprotein dynamics *in vivo*.

Abstract

Our understanding of intracellular and intra-organism trafficking of apolipoprotein B (APOB)-containing lipoproteins (Blps) can be greatly enhanced with the availability of tagged proteins to visualize their transport within cells and between tissues. APOB exists in two forms; APOB100, which is mainly found in hepatic very low density lipoproteins (VLDL), and APOB48, which is associated with intestinal chylomicrons. Here we report data on three plasmids expressing APOB fluorescent

fusion proteins; APOB48-GFP, APOB100-GFP and APOB48-mCherry. In Cos-7 cells, which do not naturally express APOB or microsomal triglyceride transfer protein (MTP), fluorescent APOB proteins co-localized with calnexin and were only secreted if cells were co-transfected with MTP. The secreted APOB-fusions retained the fluorescent protein and were secreted as lipoproteins with flotation properties similar to plasma high density lipoproteins (HDL) and low density lipoproteins (LDL). In a rat hepatoma McA-RH7777 cell line that naturally expresses MTP, the APOB100 fusion protein was secreted as VLDL– and LDL–sized particles, and the APOB48 fusion proteins were secreted with LDL– and HDL–size particles. To monitor lipoprotein trafficking *in vivo,* the APOB48-mCherry construct was transiently expressed in zebrafish larvae. Clonal analysis revealed that the peptide was expressed, secreted, and endocytosed into late endosomes in the liver, consistent with the expected trafficking pattern for native lipoproteins. These experiments show that the addition of fluorescent proteins to the C-terminus of APOB with does not disrupt their assembly, localization, secretion, and endocytosis. Availability of fluorescently labeled APOB proteins will facilitate exploration of assembly, degradation, and transport of Blps, and identification of novel compounds that interfere with these processes via high throughput screening.

Introduction

Lipoproteins are non-covalently held assemblies of lipid and protein that resemble micelles. They play a physiological role in the transport of hydrophobic lipids throughout the lymph and blood stream for utilization or storage by peripheral tissues [185]. Lipoproteins are composed of a core consisting of triglyceride and cholesterol esters surrounded by a monolayer composed of phospholipids, free cholesterol, and various apolipoproteins. Apolipoprotein B is a very large, amphipathic, non-exchangeable apolipoprotein that is a structural component of triglyceride rich lipoproteins, including chylomicrons (CM) and very low-density lipoproteins (VLDL) [186]. Full length APOB, APOB100, is a 512 kDa protein that is synthesized in mammalian livers and is the major apolipoprotein found in VLDL [187]. In the mammalian intestine as well as the livers of certain species, an mRNA editing enzyme (APOBEC1) converts the cytidine at position 6666 of *APOB* mRNA to uracil creating a premature stop codon [188, 189]. This edited mRNA is translated into a truncated form of APOB, APOB48, a 246 kDa protein consisting of the N-terminal 48% of APOB100 [190, 191]. APOB48 is the main apolipoprotein of CM.

During translation, the APOB peptide interacts with the endoplasmic reticulum (ER) [192, 193]. Microsomal triglyceride transfer protein (MTP) transfers lipids to a growing APOB polypeptide to form primordial lipoproteins (pre-VLDL or pre-CM) [194, 195] that are approximately the same size as plasma high-density lipoproteins (HDL). In the absence of MTP or insufficient amounts of lipids, APOB is ubiquitinated and degraded by the proteasome. In the second step, primordial lipoproteins are enlarged into

VLDL or CM [196]. These larger VLDL and CM undergo a second quality control step, post-ER presecretory proteolysis, whereby oxidized, aggregated Blps are degraded by autophagy [197] and lysosomes [198, 199]. Because of their large size, VLDL and CMs travel through the secretory pathway by noncanonical transport vesicles and are secreted via exocytosis into the circulation [200, 201]. In the circulation, CM and VLDL acquire exchangeable apolipoproteins and undergo lipolysis by lipases anchored to the endothelial cell surface. The hydrolyzed remnant Blps are cleared mainly by the liver via receptor mediated endocytosis. [202, 203].

Elevated plasma levels of Blps contribute to hyperlipidemia, coronary artery disease, atherosclerosis, obesity, diabetes, and other metabolic diseases. Plasma APOB may also be elevated due to increased secretion or decreased catabolism of Blps. Thus, much work has been done to elucidate mechanisms in the assembly, secretion, degradation, regulation, uptake, internalization, and trafficking of Blps in order to find ways to lower their plasma concentration. However, to date it has proven difficult to study these processes *in vivo*.

Fluorescently tagged proteins are invaluable tools for monitoring intracellular biological processes [204, 205]. They are frequently used in live cell imaging and intra-vital microscopy to investigate physiological processes in real time [206]. Fluorescent fusion proteins are also advantageous for high throughput screens to identify regulatory proteins in various pathways and specific antagonists. In addition, they are easier to handle and dispose of than radioactive molecules that are usually used to study lipoprotein assembly and secretion. Despite the clear value of fluorescently tagged APOB in research and drug discovery, an APOB fluorescent fusion protein has, to our

knowledge, not been previously developed and/or published. This is most likely the result of technical challenges faced in cloning the very large coding sequence of APOB, which was overcome with a combination of cloning and gene synthesis techniques. Here, we report three plasmids expressing fluorescent APOB fusion proteins. Utilizing these constructs, we were able to visualize intracellular APOB in mammalian cells. APOB fusions were secreted in an MTP-dependent fashion as full length, fluorescently-labeled lipoprotein particles. The APOB48-mCherry construct was transiently expressed in larval zebrafish to evaluate whether this approach was also effective *in vivo*. Not only could fluorescent APOB-fusion proteins be detected and visualized in living cells, but clonal analysis demonstrated that particles were both secreted and endocytosed into the liver. Taken together, these results indicate that the C-terminal fusion of fluorescent proteins to APOB does not interfere with the assembly, secretion, or uptake of Blps, and these fusion proteins can be used to study both intracellular and intra-organism transport of Blps.

Results

Subcellular localization of APOB chimeras to the ER and colocalization with MTP

Plasmids encoding tagged APOB (Fig. 1) were transfected into Cos-7 cells, and the fluorescently labeled APOB fusion proteins were visualized with a confocal microscope (Fig 2a,b). Both APOB48-GFP and APOB48-mCherry showed diffuse perinuclear labeling, which colocalized with the ER-marker calnexin. Colocalization of APOB48-GFP and APOB48-mCherry with calnexin indicates that they are present in the ER, the site of Blp assembly (Fig. 2a,b). MTP, critical for Blp assembly, is also localized mainly to the ER. In order to visualize whether MTP colocalizes with APOB, we co-expressed MTP-FLAG and APOB48-GFP in Cos-7 cells and performed immunohistochemistry. MTP-FLAG colocalized with APOB-GFP indicating that the two proteins are located in the same subcellular compartment (Fig. 3). Thus, APOB chimeras are expressed in the ER in close proximity to MTP.

Quantification of intracellular APOB chimeras

We quantified the amount of APOB present intracellularly in Cos-7 cells stably expressing MTP-FLAG. A previously characterized untagged APOB48 construct acted as a positive control. To confirm that secretion is MTP dependent, we transfected APOB expression plasmids into Cos-7 cells that do not naturally express MTP. We then performed co-transfection experiments in which cells were transfected with both APOB and MTP expression plasmids. Untagged APOB48 had the highest intracellular expression of all the APOB constructs irrespective of MTP expression (Fig. 4a).

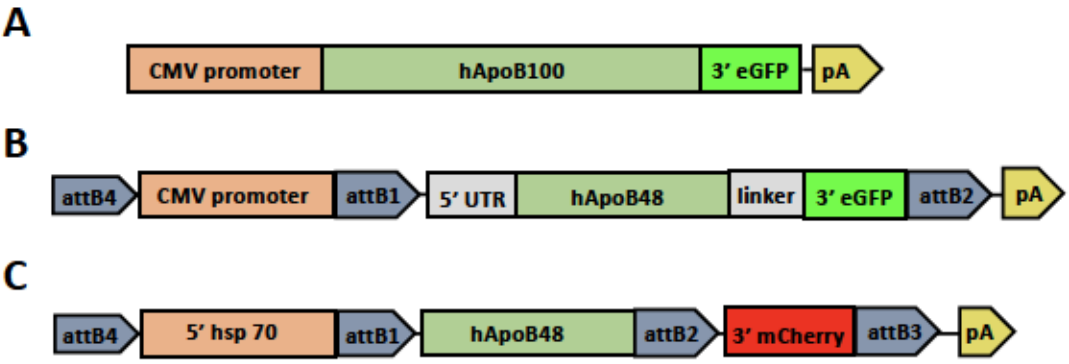

Figure 1: Plasmids expressing different apoB chimeras. (a) *APOB48-GFP* was custom designed and constructed by Cyagen Corp. The 5´-UTR and N-terminal 48% of apoB were subcloned into the pRP.ExTri-CMV vector. *APOB48-GFP* expression is driven by the CMV promoter. eGFP is added after a linker sequence at the C-terminus of the protein. **(b)** *APOB100-GFP* synthesized by Origene. The open reading frame of full length apoB is expressed under the CMV promoter. TurboGFP is added to the C-terminus of the protein. **(c)** *APOB48-mCherry* was subcloned into the pDONOR Vector and then recombined into the pDEST vector using a lambda based recombination reaction. mCherry was inserted at its C-terminus. Expression is driven by the Hsp70 promoter.

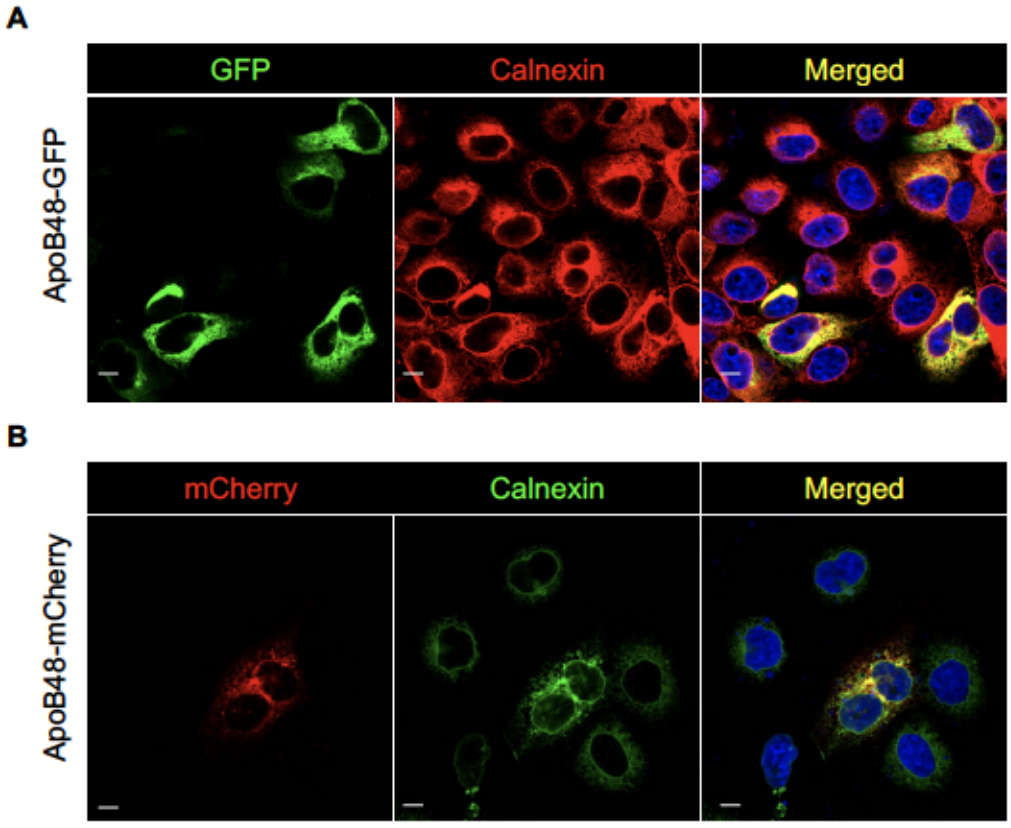

Figure 2: Fluorescently-tagged APOB is located in the endoplasmic reticulum. Cos-7 cells were plated on coverslips and transfected with plasmids expressing the various *APOB* constructs. After 48 hours, cells were fixed, blocked, and probed for calnexin. Cells expressing **(a)** APOB48-GFP (green) were incubated with secondary antibodies conjugated to Alexa-fluor 594 (calnexin, red). **(b)** Cells expressing APOB48-mCherry were incubated with secondary antibody conjugated to Alexa-fluor 488 (calnexin, green). The nucleus was stained with DAPI (blue). Cells were visualized with a confocal microscope. Images were overlaid (merged yellow) to determine colocalization. Images are representative of multiple scanned fields. Experiment was performed in duplicate and eight adjacent fields were captured per slide. Scale bars, 10 μm.

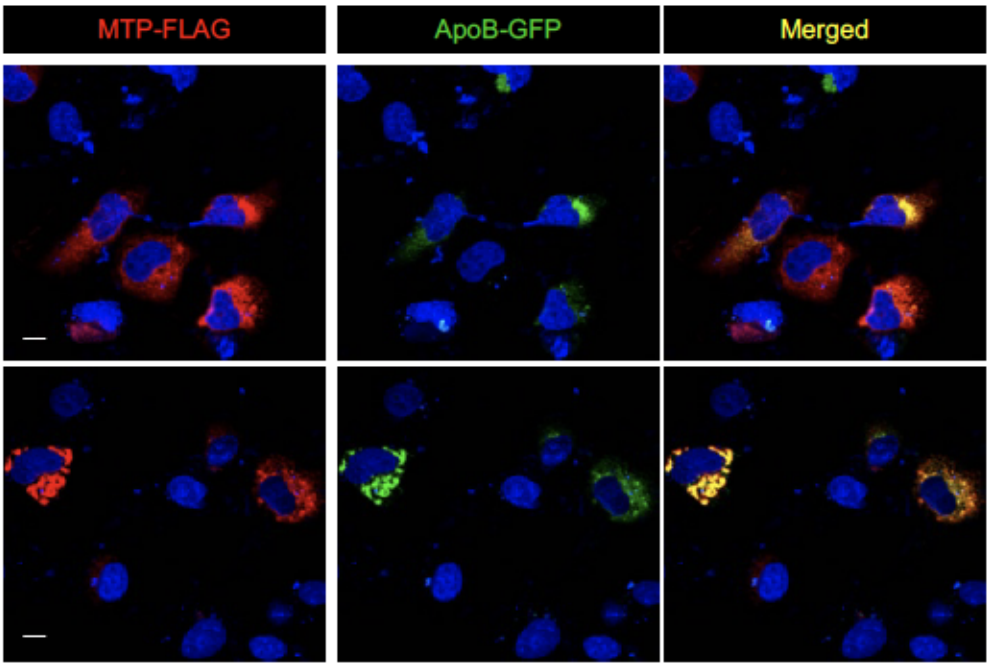

Figure 3: APOB48-GFP co-localizes with MTP. Cos-7 cells were first transfected with plasmid expressing *APOB48-GFP* followed by plasmids expressing *MTP-FLAG*. Immunofluorescent staining for APOB48-GFP (green) and MTP-FLAG (red) was visualized in an Olympus Confocal Microscope. Images were merged to determine colocalization (yellow). Experiment was performed in duplicate and eight adjacent fields were captured per slide. Scale bars, 10 μm.

APOB48-GFP and APOB48-mCherry were present at 67% and 53%, respectively, of the untagged APOB48. APOB100-GFP was also detected intracellularly, albeit at lower levels (~30% of untagged APOB48) (Fig. 4a). The expression of MTP-FLAG did not significantly affect the intracellular level of APOB expression (Fig. 4a). Thus, these studies indicate that all four APOB peptides were expressed in transfected cells, independently of the presence or absence of MTP.

APOB chimeras are secreted from cells

To evaluate whether the fluorescent tag interfered with the secretion of APOB, we measured the amount of APOB secreted into the cell culture media. Cos-7 cells are only able to secrete APOB if both MTP and APOB are co-expressed. Media from Cos-7 cells not expressing MTP had very low amounts of APOB, 0.5-5.5% of secreted APOB compared to cells expressing MTP (Fig. 4b), confirming that APOB is not secreted in appreciable amounts in the absence of MTP.

When MTP was co-transfected with the APOB-constructs, there was a significant increase in the level of APOB detected in the media irrespective of the APOB-fusion construct tested (Fig. 4b). Untagged APOB48 was the most highly secreted peptide, with media concentration reaching almost twice the levels of the tagged APOB48 constructs (APOB48-GFP or APOB48-mCherry) (Fig. 4b). Media levels of APOB100-GFP were significantly lower (~12% of untagged APOB48) (Fig. 4b), but this may be attributable to lower transfection efficiency of the larger plasmids.

To validate that the secreted peptides retained the fluorescent tag, media from cells were immunoprecipitated with an anti-APOB antibody and subjected to western blotting.

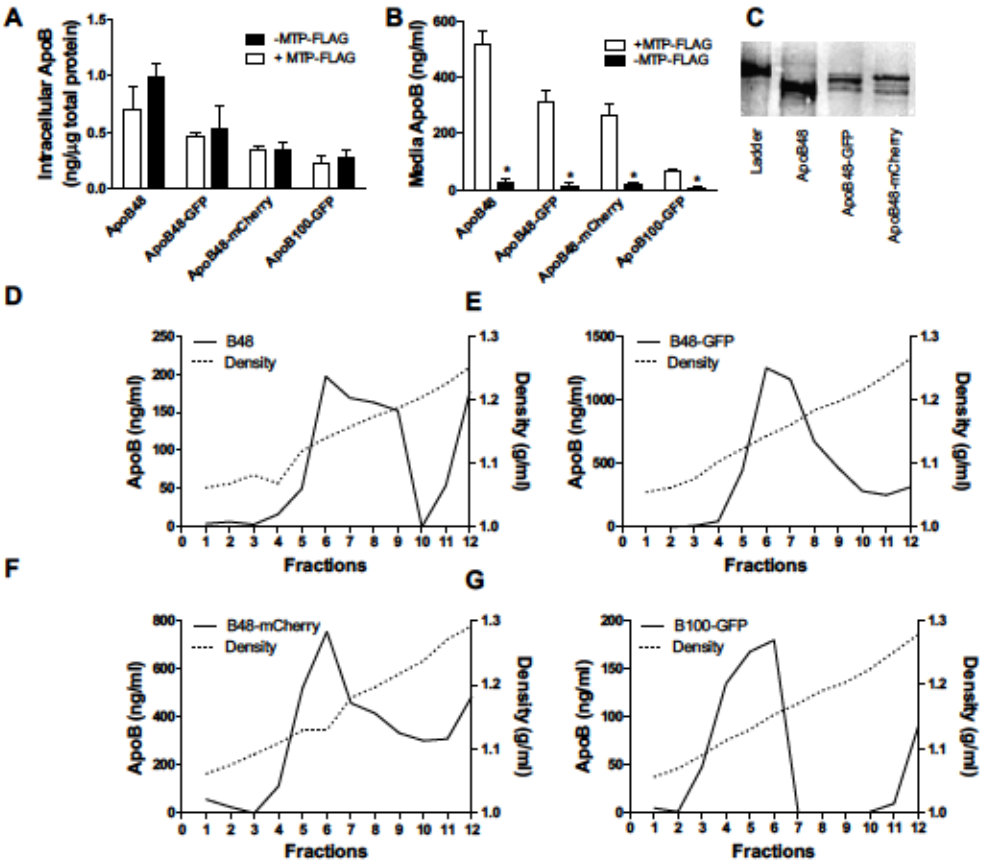

Figure 4: APOB chimeras are secreted as lipoproteins from Cos-7 cells. (a-b) *APOB* plasmids were transfected into two different Cos-7 cells. "+MTP-FLAG" are cells that were stably expressing MTP-FLAG and "-MTP-FLAG" are cells that do not express MTP. After 36 hours, cells were incubated with DMEM containing 10% FBS and 0.4 mM oleic acid complexed with BSA. Media was collected after an overnight incubation. ApoB was measured in the cell lysates **(a)** and media **(b)**. Data is representative of two experiments performed in triplicate. n=3, Student t test. **(c-g)** Cos-7 cells stably transfected with MTP-FLAG were transfected with different plasmids expressing indicated APOB peptide. ApoB was immunoprecipitated from the media **(c)**. Immunoprecipitates were run on a 6% SDS-PAGE gel, transferred to nitrocellulose, and probed for apoB. Bands were visualized in a phosphorimager. Images are representative of two experiments performed in duplicate. **(d-g)** Media from four wells for each plasmid were combined, adjusted to 1.3 g/ml with KBr, and overlaid with solutions with varying densities to create a density gradient and subjected to density gradient ultracentrifugation in a SW-41 rotor (40,000 rpm, 197568g, 14°C, 16 h) and 1 ml fractions were collected. ApoB was measured in each fraction of the media of cells expressing apoB48 **(d)**, apoB48-GFP **(e)**, apoB48-mCherry **(f)**, or apoB100-GFP **(g)** were measured via ELISA. The density in each fraction was measured with a refractometer. Data is representative of two independent experiments.

Probing the blot for APOB revealed slightly higher molecular weight bands for APOB48-GFP and APOB48-mCherry relative to untagged APOB-48, consistent with secretion of the full-length tagged APOB chimeras (Fig. 4c). Therefore, addition of C-terminal GFP or mCherry is permissive to APOB48 secretion. Although the APOB100-GFP levels could be measured by ELISA (Fig. 4b), they were not detectable by western blot analysis or immunofluorescence (not shown).

APOB peptides are secreted as lipoproteins

To determine whether fluorescently tagged APOB chimeras were secreted as buoyant lipoproteins, density gradient ultracentrifugation was used to identify the density fractions that contain the APOB-fusion proteins. Previous research has shown that Cos-7 cells, which do not naturally produce lipoproteins, secrete unusually small Blps following transfection with APOB and MTP. Consistent with previous studies, co-transfection of untagged APOB48 and MTP resulted in the secretion of particles with a density similar to high-density lipoproteins (HDL), in the range of 1.12 – 1.19 g/ml (Fig. 4d). APOB48-GFP was secreted in particles with similar densities, in the range of 1.10 – 1.19 g/ml (Fig. 4e). Like APOB48-GFP, the bulk of APOB48-mCherry was secreted as lipoproteins with a density of 1.11 – 1.20 g/ml with a peak at 1.12 g/ml (Fig. 4f). APOB100-GFP was detected in the fractions with the lowest densities, ranging from 1.08 – 1.15 g/ml (Fig. 4g). A small amount of all four APOB peptides could also be detected in the lipid-free protein fraction (fraction 12), which may be degradation products of APOB recognized by the monoclonal antibody 1D1 used for ELISA. These studies show that C-terminally tagged APOB chimeras are lipidated similarly to untagged proteins, are secreted as

buoyant lipoprotein particles, and that the fluorescent tag does not prevent assembly and secretion of Blps.

To study secretion of tagged APOB peptides in a system that naturally produces lipoproteins, we expressed the constructs in rat hepatoma cells, McA-RH7777. The monoclonal antibody used for human APOB ELISA, 1D1, does not detect rat APOB. Therefore, all assays report only the level of human APOB in the media, which is derived from the transfected plasmids. To demonstrate the specificity of the 1D1 antibody, cells were transfected with an empty plasmid and no human ApoB was detectable in the media (Fig 5a,b). APOB was detectable in the media following transfection with each of the four plasmids encoding human APOBB, although there were clear differences in the expression level between different plasmids (Fig. 5a).

Ultracentrifugation of the media from McA-RH7777 cells expressing the various APOB peptides showed that secreted lipoproteins floated at densities similar to those of plasma LDL and HDL (Fig. 5c-f). Consistent with results from previous studies [207, 208], the untagged APOB48 peptide was secreted with a peak density at 1.062 g/ml (Fig. 5c). About 20% of the untagged APOB48 peptides were secreted with a density of 1.05 g/ml (Fractions 2 and 3). There were no lipoproteins secreted in the VLDL fraction (Fraction 1). Further, all APOB peptides were secreted associated with lipids as APOB was not detected in fractions 9-12 (1.22 g/ml – 1.33 g/ml). APOB48-GFP was detected (1.03 g/ml – 1.20 g/ml) in both the HDL and LDL fractions with a peak density at 1.1 g/ml. Approximately 40% (Fractions 3 and 4) of APOB48-GFP was secreted with a density similar to LDL (1.03 g/ml – 1.061 g/ml) particles (Fig. 5d). Similar to the untagged peptide, there was no APOB48-GFP in the VLDL or lipid-free protein

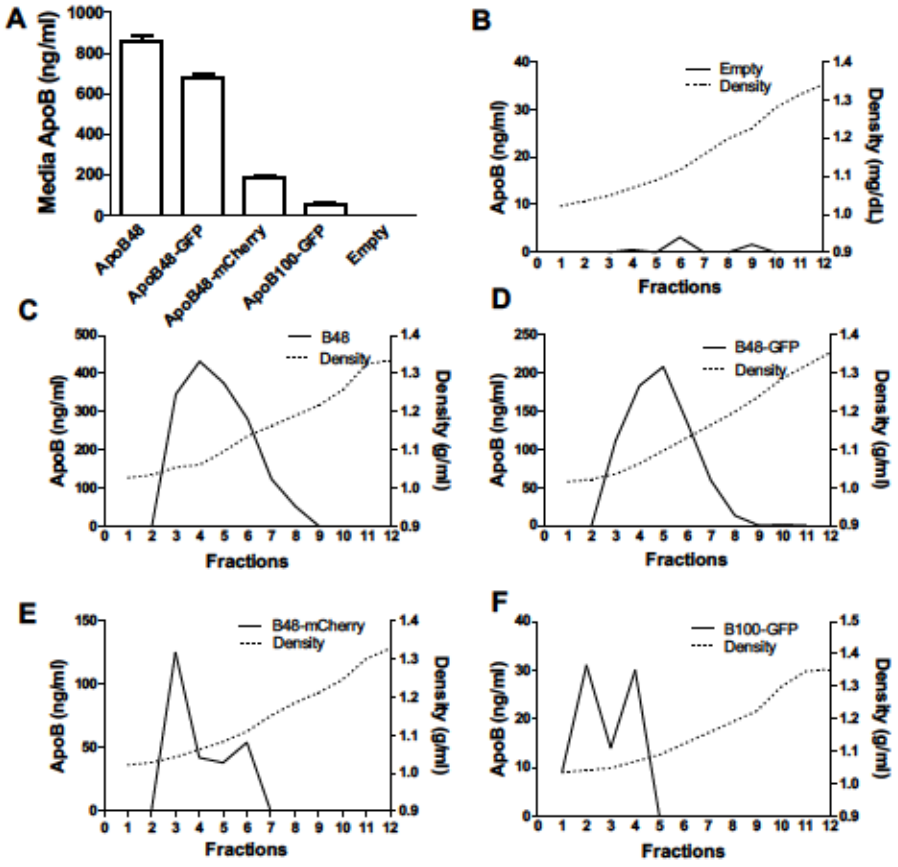

Figure 5: APOB chimeras are secreted as LDL—size particles when expressed in McA-RH7777 cells. Rat hepatoma McA-RH7777 cells were transfected with plasmids expressing various *APOB* constructs. After 36 hours, cells were incubated with DMEM containing 10% FBS and 0.4 mM oleic acid complexed with BSA. Media was collected after an overnight incubation. **(a)** APOB was measured in the media via ELISA. n=4, one-way ANOVA. **(b-f)** Media from 4 wells were combined, adjusted to 1.3 g/ml with KBr, and overlaid with KBr solutions with varying densities. Media were subjected to overnight ultracentrifugation (SW41 rotor, 40,000 rpm, 197568 x g, 15oC, 16 h) and 1 ml fractions were collected from the top. ApoB in each fraction of the media of cells expressing no human apoB **(b)**, APOB48 **(c)**, apoB48-GFP **(d)**, apoB48-mCherry **(e)**, or apoB100-GFP **(f)** were measured via ELISA. The density of each fraction was measured with a refractometer. Data is representative of two experiments.

fractions. Unlike APOB48-GFP and untagged APOB48, a majority (65%) of APOB48-mCherry was found in the LDL buoyancy fractions (1.04 – 1.06 g/ml) (Fig. 5e) with a peak at 1.04 g/ml. Longer APOB peptides form more TG-rich and less dense lipoproteins with a greater circumference[37]. Consistent with this observation, almost all the APOB100-GFP was found in the LDL fractions (1.03-1.06 g/ml) (Fig. 5f). Since some APOB100-GFP was found in Fraction 1 (1.03 g/ml), it is possible that APOB100-GFP formed VLDL-sized particles. Collectively, both studies in Cos-7 and McA-RH7777 cells suggest that APOB chimeras can form lipoproteins with similar densities to untagged APOB.

Secretion and endocytosis of APOB48-mCherry in larval zebrafish

Encouraged by the findings from cultured cells, we sought to evaluate whether these fluorescent APOB fusion proteins would enable monitoring of Blps *in vivo*. This was tested using a "clonal analysis" paradigm, whereby a subset of cells in the developing zebrafish embryo express either the APOB48-mCherry plasmid or a negative control plasmid encoding the endosomal marker Rab5c-mCherry. If the fluorescent product is detectable throughout the liver, it indicates that the peptide can be secreted and subsequently endocytosed by neighboring non-transgenic hepatocytes. By contrast, if the fluorophore is only detectable in a subset of cells, it indicates that the peptide is either not secreted or not endocytosed and therefore only labels the transgenic sub-population.

To generate these chimeric zebrafish, larvae were co-injected with 100 pg of plasmid and 100 pg of mRNA encoding Tol2 transposase, which promotes random integration of the construct into the genome of only a subset of cells, while the majority

of cells remain wild-type (non-transgenic). Bright mCherry signal was detectable in a small subset of cells injected with the Rab5c plasmid, indicating that integration of the transgene is rare and that the negative control protein product (an early endosomal marker) is not trafficked to neighboring cells (Fig. 6a). By contrast, each larva injected with the APOB48 construct had mCherry-rich puncta detectable throughout the entire liver (Fig. 6b). This indicates that although the transgene is only produced in the small subset of cells that integrated the transgene, the protein is efficiently secreted and endocytosed by neighboring cells as would be expected for endogenous Blp trafficking.

The above experiments were performed in larvae heterozygous for a transgenic marker of late endosomes, Rab7-GFP. This marker served as a convenient marker of cellular ultrastructure and enabled us to evaluate whether the APOB48 construct was taken up into the endosomal compartment *in vivo*. Consistent with the clonal appearance of Rab5-mCherry labeling at lower magnification, mCherry was detectable in few cells indicating that this protein product cannot be trafficked between hepatocytes (Fig. 6c, white outlines). By contrast, APOB48-mCherry was detectable throughout the liver including in the Rab7-GFP-labeled endosomes (Fig. 6d, white arrowheads). This indicates that the fluorescently-tagged APOB48 peptide is trafficked through the expected endosomal pathway and can be detected *in vivo* using confocal microscopy.

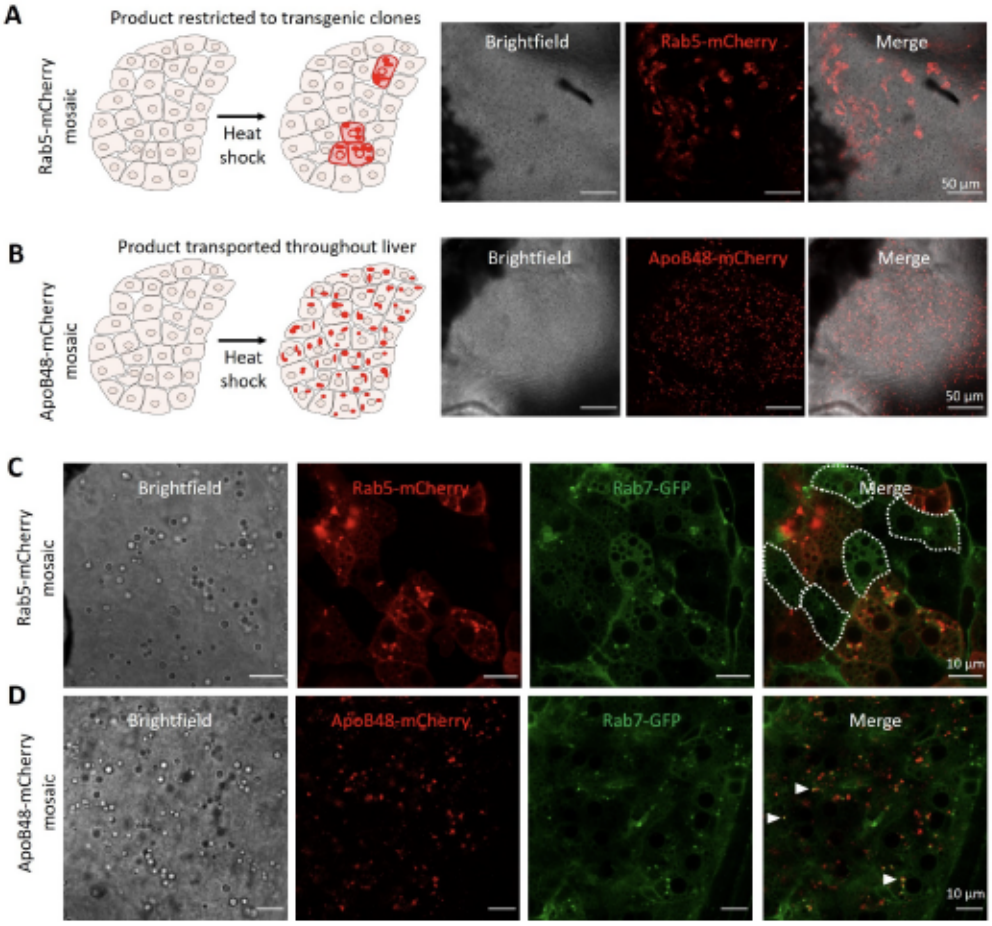

Figure 6: ApoB48-mCherry is secreted and endocytosed by zebrafish hepatocytes *in vivo*. (a) Schematic and confocal images of Rab5-mCherry clones in the zebrafish liver. As the peptide is only detectable in a subset of clones, it indicates that this product cannot be trafficked between hepatocytes. **(b)** Schematic and confocal images of APOB48-mCherry clones in the zebrafish liver. The fluorophore is detectable ubiquitously throughout the liver, indicating it can be trafficked between hepatocytes (n=13). **(c)** High-magnification confocal images of Rab5-mCherry clones in the zebrafish liver, including the stable transgenic Rab7-EGFP marker of cellular ultrastructure and early endosomes. Rab5-mCherry clones are clearly visible (dashed white lines), consistent with the conclusions from the low-magnification images (n=11). **(d)** High-magnification confocal images of apoB48-mCherry in the zebrafish liver, demonstrating not only ubiquitous dispersion of this protein product throughout the liver but also partial colocalization with late endosomes (white arrowheads).

Discussion

This study describes successful construction of several plasmids that express fluorescent APOB fusion proteins: APOB48-GFP, APOB100-GFP, and APOB48-mCherry. Importantly, these fluorescent APOB proteins exhibit several aspects of endogenous APOB homeostasis, in that they (i) localize to the ER, (ii) require MTP for secretion, and (iii) form buoyant lipid-rich lipoprotein particles. Additionally, expression in a zebrafish model indicated that the APOB was expressed, secreted, and endocytosed. Hence, the C-terminal addition of a fluorescent protein to APOB does not interfere with lipidation, secretion, and endocytosis.

One of the main motivations of a C-terminal tag was to avoid disrupting the ER-targeting signal peptide at the N-terminus. Irrespective of the APOB fusion protein studied or culture system used, fluorescent APOB localized properly to the ER. We further demonstrate that these proteins were lipidated by both human and rat MTP. Lastly, secreted fluorescent APOB was present exclusively in the buoyant density fractions of supernatant derived from rat hepatoma cells, indicating that it is lipidated and associated with a lipoprotein particle.

However, several differences were observed between the fluorescent APOB fusions and their native counterparts. APOB48-GFP and APOB48-mCherry were expressed at significantly lower levels than untagged APOB48 in Cos-7 cells. This observation could be attributable to lower transfection efficiency of the larger plasmids. However, when the same experiment was repeated in the rat hepatoma cell line, APOB48-mCherry was detectable at much lower levels than APOB48-GFP, indicating

that these different fluorescent proteins may have different effects on lipoprotein biogenesis. Additionally, the density distributions of the resulting particles were quite different between APOB48-mCherry and APOB48-GFP, with the GFP tagged version closely mirroring the native APOB48 and the mCherry fusion producing a higher number of LDL-like particles. Further work will be required to determine how specific fluorescent proteins affect the lipid composition of resulting particles.

APOB100-GFP was also secreted from cells in an MTP dependent fashion, and was associated with lipoproteins with densities comparable to LDL and HDL. However, due to its low expression, it could not be visualized by immunohistochemistry in the ER or via western blot after immunoprecipitation. The relatively low transfection efficiency of all three plasmids could be overcome by generating stably expressing cell lines or animals.

The APOB48-mCherry construct was also evaluated *in vivo* using the larval zebrafish system. Clonal analysis indicated that this peptide can both be secreted and endocytosed by larval hepatocytes and is trafficked at least partially through the endosomal pathway, confirming that the mCherry tag does not abolish interaction with the LDL-receptor. While these results support continued investigation of tagged APOB-peptides to study Blp homeostasis, there are several important limitations to this approach. In transgenic zebrafish, APOB48-mCherry was not only tagged with the fluorophore, but also (i) resulted in overexpression as an additional APOB gene incorporated into the genome, (ii) was driven by a ubiquitous heat shock promoter (hsp 70) that may have caused expression in tissues that do not normally produce lipoproteins, (iii) was encoded by a human cDNA sequence, and (iv) used the truncated APOB48

isoform that is usually associated with intestine-derived chylomicrons. Despite these departures from the biology of endogenous zebrafish APOB, human APOB48 still showed the critical hallmarks of secretion, endocytosis, and endosomal trafficking expected of native Blps.

Fluorescently-tagged proteins are valuable tools for large-scale screening in both mammalian cells and non-mammalian model systems. Here, we show that different C-terminal fluorescent proteins fused to APOB are tolerated during Blp assembly. Since APOB constructs described in this study can be visualized in mammalian cell lines, they would be valuable for live cell imaging, identifying the subcellular location of APOB, or tracking APOB intracellularly under different conditions. In addition, unlike untagged APOB, these constructs can be used in human or other mammalian cell systems that endogenously express APOB, such as liver and intestinal cells, to study both steps of lipoprotein assembly and its transport. They may also be useful for visualizing and investigating APOB in other APOB-expressing tissues that are less widely studied, such as the heart, retina, or kidney. Further, they may be valuable in high-throughput screening to identify molecules that support or interfere with APOB expression, lipoprotein assembly, and secretion pathways.

Each construct also has its own advantages and disadvantages. For example, since APOB48-mCherry is expressed under an inducible promoter, it is possible to heat shock cells and visualize the progression of APOB48 through the secretory pathway. The APOB48-GFP plasmid contains the endogenous 5′ UTR, which may help identify translational regulators. One drawback of these proteins is that they are not endogenously expressed. Overexpression of these plasmids may have unintended consequences on

other molecular pathways. Further, because the APOB48-mCherry and APOB100-GFP plasmids do not contain the 5′ UTR, they may not fully recapitulate certain aspects of translational regulation. Finally, none of the plasmids contain the 3' UTR and consequently any *cis- or trans*-acting regulatory elements will not influence their expression or mRNA degradation. The results described here and an understanding of their caveats provide justification for future efforts to insert fluorescent reporters into the endogenous APOB gene locus via precise genome editing, which may be a more valuable tool for studying APOB regulation and *in vivo* trafficking.

Larval zebrafish recapitulate the major aspects of inter-organ lipoprotein homeostasis in a transparent organism. Fluorescent APOB-fusion proteins thus create the opportunity to monitor interorgan transport of Blps *in vivo*, which can be used to expand our understanding of both normal lipoprotein homeostasis and aberrations that contribute to the progression of cardiovascular disease.

In short, we report that adding fluorescent reporter proteins at the C-terminus of APOB does not disrupt their ability to form lipoproteins. These constructs can be used to study Blp assembly, secretion, trafficking, and regulation both within cells and throughout intact organisms. Fluorescent proteins fused to APOB represent a valuable tool to investigate the cell biology of Blps as well as to identify novel molecules that interfere with lipoprotein biogenesis and transport through high-throughput screening.

Materials and Methods

Plasmids

The untagged APOB48 expression plasmid was described previously [209]. The APOB48-GFP construct was custom synthesized by Cyagen Corp (Fig. 1a). The 5′-untranslated region (UTR) and coding region of human APOB48 (7403 bp, accession # NM_000384) was subcloned into the pRP.Des2d vector via gateway cloning. ApoB48-GFP expression is driven by a cytomegalovirus (CMV) promoter. Enhanced green fluorescent protein (eGFP, 27 kDa, excitation/emission max 488/509 nM) was inserted at the C-terminus of the protein after a linker sequence (15 bp, TACAAA TTGCATTAG) and before the SV40 3′-UTR and polyA signal.

The APOB100-GFP vector (Fig. 1b) was made by Origene (Cat # RG219581). The open reading frame of full length human APOB (Accession # NM_000384) was subcloned into a PCMV6-AC-GFP plasmid via restriction digest with *sgf1* and *mlu1*. APOB100 expression is driven by the CMV promoter. At the C-terminus of the protein, a linker sequence (21 bp) followed by TurboGFP (*Pontellina plumata,* 26 kDa, excitation/emission max = 482/502 nm) was inserted before the human growth hormone polyA signal.

Multi-site gateway cloning was used to construct the APOB48-mCherry vector. The coding region of human apoB48 was amplified by PCR from APOB100 using primers that also inserted flanking sites for a recombination enzyme Att. The APOB48 coding sequence was subcloned into the pDONOR Vector and then recombined into the pDEST vector using a lambda-based recombination reaction. APOB48 expression is

driven by the zebrafish inducible heat shock protein 70 (*hsp70*) promoter. The mCherry (excitation/emission max = 587/610 nM) coding sequence was cloned as an in-frame fusion to the C-terminus of the protein (Fig. 1c).

Expression and visualization of APOB chimeras in Cos-7 cells

Cos-7 cells stably expressing MTP-FLAG[8] were plated on coverslips (70,000 cells/well of a 12 well plate) and transfected with 2 µg of plasmid expressing APOB48-GFP or APOB100-GFP using Turbofect (Thermo Scientific, #R0531; 2 µl Turbofect per 1 µg DNA) according to the manufacturer's instructions. After 48 hours, cells were fixed in 4% paraformaldehyde, rinsed, and nuclei were stained with DAPI. Coverslips were mounted with Vectashield mounting media (Vector Laboratories, # H-1000) to prevent photobleaching. Immunofluorescence was detected with an Olympus Confocal Microscope.

For the expression of APOB48-mCherry, cells were transfected as described above. After 24 hours, cells were incubated at 43°C for 30 minutes (heat shock). Eight hours later, the same cells were again subjected to one more heat shock for 30 minutes. Forty-eight hours after transfection, cells were fixed and visualized as described above.

For co-localization of APOB with the ER-marker calnexin, fixed cells were blocked with PBS supplemented with 1 mM $MgCl_2$, 0.5 mM $CaCl_2$, 3% BSA, 0.1% Triton, and 1% horse serum for one hour at room temperature and then incubated with anti-calnexin antibody (Santa Cruz, # SC-11397, 1:200 dilution) for 1 hour at room temperature. Cells expressing GFP-tagged plasmids were labeled with donkey anti-rabbit Alexa Fluor-594 (Invitrogen, # A21207, 1:250 dilution) for 1 hour at room temperature.

Cells expressing APOB48-mCherry were labeled with donkey anti-rabbit Alexa Fluor 488 (Invitrogen, #A21206, 1:250 dilution). Coverslips were mounted and visualized as described above.

Measurement of cellular and secreted APOB

Cos-7 (African green monkey kidney) cells are most commonly used to study the initiating steps of lipoprotein assembly. Although these cells do not naturally secrete lipoproteins, co-expression of APOB with MTP decreases posttranslational degradation of APOB and is sufficient for lipoprotein assembly and secretion [208]. Cos-7 cells stably expressing MTP-FLAG were plated (250,000 cells/well) in 6 well plates and transfected with 3 μg of plasmid expressing each of the four different APOB constructs (APOB48, APOB48-GFP, APOB48-mCherry, and APOB100-GFP) with Turbofect as described above. Transfections were then repeated in Cos-7 cells that do not express MTP. Cells expressing APOB48-mCherry were heat shocked twice as described above to induce apoB expression. After 36 hours, cells were incubated with DMEM containing 10% FBS and 0.4mM oleic acid complexed with 1.5% BSA for 16 hours. ApoB was measured in the media via ELISA [210].

Similar experiments were performed using a rat hepatoma cell line, McA-RH7777 cells. McA-RH7777 express endogenous rat MTP and APOB and naturally assemble APOB-containing lipoproteins. They have been extensively used to study lipoprotein assembly [211-213]. The antibodies used for ELISA are specific for human APOB and do not detect rat APOB. Therefore, it is possible to utilize this liver cell line to specifically measure the exogenously expressed human APOB constructs without

interference from the endogenous rat APOB. Plasmids expressing the chimeric APOB constructs were transfected in McA-RH7777 cells. Forty-eight hours later, media were collected from the cells after an overnight incubation with DMEM containing 20% FBS, 0.4mM oleic acid complexed to 1.5% BSA. ELISA was used to measure APOB in the media.

To measure intracellular APOB, cells were scraped in PBS. A small amount of cell lysate was used to measure total protein with the Coomassie Plus Protein Assay Kit (Thermo Scientific, #23236) according to the manufacturer's instructions. The rest of the cell lysate was pelleted by centrifugation and resuspended in cell extract buffer (100 mM Tris, pH 7.4, 150 mM NaCl, 1 mM EGTA, 1 mM EDTA, 1% Triton, 0.5% sodium deoxycholate), incubated with rotation for 1 h at 4°C to release cell contents, and centrifuged at 16,000 *g* for 5 min. The supernatant was used to measure intracellular APOB.

Immunoprecipitation

APOB plasmid constructs were transfected in Cos-7 cells stably-expressing MTP-FLAG and cells expressing mCherry were heat shocked as described for the measurement of media APOB. After 36 hours, cells were incubated overnight with DMEM containing 10% FBS and 0.4 mM oleic acid/1.5% BSA complexes. Media from three wells were combined and incubated with 2 µl of anti-APOB antibody (Academy Biomedical Company, Inc., #20S-G2) at 4°C for 1 hour. Next, 40 µl of protein A/G PLUS-agarose beads (Santa Cruz, # sc-2003) were added and rotated for 3 hours at 4°C. The beads were rinsed 3X with PBST. ApoB was eluted with SDS-PAGE loading buffer.

Immunoprecipitants were run on a 6% SDS-PAGE gel and transferred to nitrocellulose. Membranes were blocked in TBST with 5% milk powder for 1 hour and probed with a monoclonal antibody against APOB, 1D1 (University of Ottawa Heart Institute), overnight at 4°C. Next, membranes were incubated with goat anti-mouse IgG Alexa-fluor 633 (Life Technologies, #A21-052) for 1 hour at room temperature. Bands were visualized with a phosphorimager (Molecular Diagnostics, Storm 860).

Density gradient ultracentrifugation of lipoproteins

APOB plasmid constructs were transfected in Cos-7 cells stably expressing MTP FLAG or McA-RH7777 cells in 6 well plates. Cells expressing apoB48-mcherry were heat shocked as described earlier. Cells expressing the four APOB expression constructs were incubated overnight with DMEM containing 10% FBS and 0.4 mM oleic acid complexed with 1.5% BSA. Four wells were combined for density determinations. Four mls of media were brought up to 1.34 g/ml with solid KBr. Next, the media were overlaid with differing density KBr solutions in the following order: 2 mls of 1.21 g/ml, 2 mls of 1.15 g/ml, 2 mls of 1.063, 1ml of 1.019 g/ml, and 1 ml of 1.006 g/ml. Media from McA-RH7777 were adjusted to 1.34 g/ml density with solid KBr and then were overlaid with 1 ml of 1.21 g/ml, 1 ml of 1.15 g/ml, 2 mls of 1.063, 2 mls of 1.019 g/ml, and 2 mls of 1.006 g/ml. Media was centrifuged overnight (SW41 rotor, 40,000 rpm, 17h, 15°C), and 1 ml fractions were collected from the top. APOB content was measured via ELISA and the density was measured with a refractometer in each fraction.

APOB and MTP Colocalization

Cos-7 cells were plated in $10cm^2$ plates (1,000,000 cells per plate) and grown in DMEM supplemented with 10% FBS, penicillin, and L-glutamine. After 18 hours, they were transfected with 6 µg of plasmid expressing APOB48-GFP using Turbofect (Thermo Scientific, #R0531; 2 µl Turbofect per 1 µg DNA) according to the manufacturer's instructions. After 24 hours, the cells were trypsinized and plated on coverslips (70,000 cells/well of a 12 well plate) and reverse transfected with 1.5 µg of plasmid expressing FLAG-tagged WT [192, 207] or mutant MTPs. Mutant MTPs were created as described previously [214]. After 48 hours, cells were fixed in 4% paraformaldehyde, rinsed, and cells were blocked with PBS supplemented with 1 mM $MgCl_2$, 0.5 mM $CaCl_2$, 3% BSA, 0.1% Triton, and 1% horse serum for one hour at room temperature. They were then incubated with anti-FLAG antibody (Sigma, # F1804, 1:200 dilution in TBST) for 1 hour at room temperature. The GFP tag on the APOB48-GFP can be visualized without probing for APOB. Cells were then labeled with donkey anti-rabbit Alexa Fluor-594 (Invitrogen, # A21207, 1:250 dilution) for 1 hour at room temperature. The nucleus was stained with DAPI (1:5000 dilution in PBS) for 10 minutes. Cells were rinsed in PBS and mounted with Vectashield mounting media (Vector Laboratories, # H-1000) to prevent photobleaching. Immunofluorescence was detected with an Olympus Confocal Microscope. Eight adjacent fields were captured for each WT and mutant MTP. Cells expressing APOB-GFP, MTP (or mutants), both APOB-GFP and MTP (or mutants), and neither protein were manually counted. Transfection efficiency was determined by (# of cells expressing MTP, APOB48-GFP, or both from all 8 fields)/(total # of cells)*100.

Expression of APOB48-mCherry in Zebrafish

APOB48-mcherry (100 pg) or hsp70l:mcherry-rab5c (100pg) plasmids [215] were injected into zebrafish embryos at the 1-cell stage along with mRNA encoding Tol2 transposase (100 pg) in a volume of 2 nL. Transgenic fish stably expressing Tg(actin2:eGFP-Rab7) were used to facilitate visualization of cellular ultrastructure, as well as sub-cellular localization of late endosomal compartments. Injected larvae were heat-shocked at 37°C for 1 hour at 5 dpf to induce APOB48-mCherry expression, and images were captured at 6 dpf with an inverted Leica DMI6000 confocal microscope (SP5) 17-20 hours after heat shock. Live animals were mounted for imaging as previously described [216]. A total of 13 larvae from 3 independent clutches were imaged after being injected with the APOB48 plasmid, and 11 larvae were imaged following Rab5-mCherry injections.

CHAPTER 3 – LIPOGLO: A SENSITIVE AND SPECIFIC REPORTER OF ATHEROGENIC LIPOPROTEINS

James H. Thierer[1,2], Stephen C. Ekker[3] and Steven A. Farber[1,2]

[1]Carnegie Institution for Science Department of Embryology, Baltimore, MD 21218
[2]Johns Hopkins University Department of Biology, Baltimore, MD 21218
[3] Mayo Clinic Department of Biochemistry and Molecular Biology, Rochester, MN 55905

This chapter is adapted from an article published in *Nature Communications* in July 2019. I designed, performed, and quantified all experiments and wrote the manuscript, with guidance and input from the co-authors.

Abstract

Apolipoprotein-B (ApoB) is the structural component of atherogenic lipoproteins, lipid-rich particles that drive atherosclerosis by accumulating in the vascular wall. As atherosclerotic cardiovascular disease is the leading cause of death worldwide, there is an urgent need to develop new strategies to prevent lipoproteins from causing vascular damage. Here I report the LipoGlo system, which uses a luciferase enzyme (NanoLuc) fused to ApoB to monitor several key determinants of lipoprotein atherogenicity including particle abundance, size, and localization. Using LipoGlo, I was able to perform comprehensive characterization of the lipoprotein profile of individual larval zebrafish and collect the first images of atherogenic lipoprotein localization in an intact organism. I report multiple unexpected patterns of lipoprotein localization outside of the vasculature, as well as identify Phospholipase A2 group 12B (*pla2g12b)* as a potent

regulator of lipoprotein size. ApoB-fusion proteins thus represent a uniquely sensitive and specific approach to study atherogenic lipoproteins and their genetic and small molecule modifiers.

Introduction

ApoB-containing lipoproteins (ApoB-LPs) are the etiological agents of atherosclerotic cardiovascular disease [19], which is the leading cause of mortality worldwide [217]. ApoB-LPs serve to shuttle lipids throughout the circulation, but occasionally cross the vascular endothelium to form lipid-rich deposits within the vascular wall. These deposits can develop into atherosclerotic plaques, so serum levels of ApoB-LPs are routinely measured as an indicator of cardiovascular disease risk [19]. Characterization of serum ApoB-LPs is routinely performed using assays to measure triglyceride and cholesterol levels, and individuals with elevated lipid levels are considered to be at high risk for cardiovascular disease and are prescribed lipid-lowering therapies such as statins [218]. Such drugs effectively reduce cardiovascular disease risk by lowering the levels of cholesterol carried by atherogenic lipoproteins (often called "bad cholesterol").

Indirect (lipid-focused) measurements, however, provide very limited information on several properties of ApoB-LPs such as particle concentration or size distribution, both of which are key determinants of atherogenic potential. For example, serum Apolipoprotein-B (ApoB) levels directly reflect the concentration of ApoB-LP particles and show a stronger correlation with cardiovascular disease risk than lipid metrics (including cholesterol) [39, 219]. The size distribution of lipoprotein particles is also relevant to cardiovascular disease risk, as there are numerous classes of ApoB-LPs that can be differentiated by size and show varying degrees of atherogenicity [18]. Low-density lipoproteins (LDL) are the smallest and most abundant class of ApoB-LPs and are

thought to be the primary drivers of atherosclerosis [19]. There is also significant size variation within the LDL particle class, and smaller LDL particles are associated with increased atherogenicity [30]. For example, approximately 25% of the adult population produces unnaturally small LDL particles, and as a result have ~3-fold higher risk for cardiovascular disease [35]. The higher atherogenic potential of small dense LDL particles (sdLDL) has been attributed to a combination of three properties [30], including increased rates of intimal invasion, reduced receptor-mediated clearance, and increased susceptibility to oxidation.

Many of the genetic and environmental factors governing ApoB-LP size and abundance remain undiscovered or poorly characterized [65, 68, 220], and even fewer have been successfully targeted pharmaceutically [221-223]. It has proven particularly difficult to identify drugs that modulate ApoB-LP size and abundance because the simplified model systems typically used in high-throughput drug screening (such as cultured cells or invertebrate models) do not recapitulate the complex multi-organ physiology responsible for ApoB-LP homeostasis. While lipoproteins are studied extensively in mammalian models [224], these systems are not conducive to high-throughput drug discovery. By contrast, the larval zebrafish model system has proven to be a powerful system for *in vivo* drug discovery [225], as it recapitulates all major aspects of vertebrate physiology in a small, transparent, rapidly developing organism. However, existing assays are not sensitive enough to characterize ApoB-LPs in individual larval zebrafish [81, 226, 227], as each larvae contains only a few nanoliters of plasma.

Here I present the LipoGlo reporter as a remarkably sensitive and tractable new tool to study atherogenic lipoproteins. Modern genome engineering techniques were used

to fuse the endogenous ApoB gene in zebrafish with an engineered luciferase reporter (NanoLuc), such that each atherogenic lipoprotein is tagged with a light-emitting molecule. NanoLuc is an optimized luciferase reporter that generates a quantitative chemiluminescent signal through cleavage of its substrate molecule, furimazine [228]. This reporter is remarkably bright (~100 times brighter than firefly luciferase), small (19.1 kDa), stable, and provides robust signal to noise ratios that enable accurate detection even at femtomolar concentrations [228]. Using this reporter, I was able to develop several independent assays to characterize distinct aspects of the ApoB-LP profile (summarized in Fig. 1a). These include a plate-based assay to measure lipoprotein quantity (LipoGlo-Counting), a gel-based assay to measure lipoprotein size (LipoGlo-Electrophoresis), and chemiluminescent imaging to visualize lipoprotein localization (LipoGlo-Microscopy).

I also performed extensive validation of these assays *in vivo* by showing conserved responses to genetic, pharmacological, and dietary manipulations in live zebrafish larvae (summarized in Fig. 1b). Finally, I leveraged the discovery potential of these assays to identify previously uncharacterized associations between ApoB-LPs and the central nervous system [229], as well as identify the poorly characterized gene *pla2g12b* [230] as a potent regulator of lipoprotein particle size that is conserved across vertebrates.

LipoGlo was developed first in larval zebrafish as this organism is uniquely well-suited for high-throughput genetic and small molecule screening, as well as whole-organism imaging. However, LipoGlo represents a highly generalizable tool that can be expanded to function in essentially any organism with atherogenic lipoproteins, and

customized with different reporters depending on the research question. This technique has the potential to transform our understanding of atherogenic lipoprotein biology, which may have important clinical repercussions in the treatment of atherosclerotic cardiovascular disease.

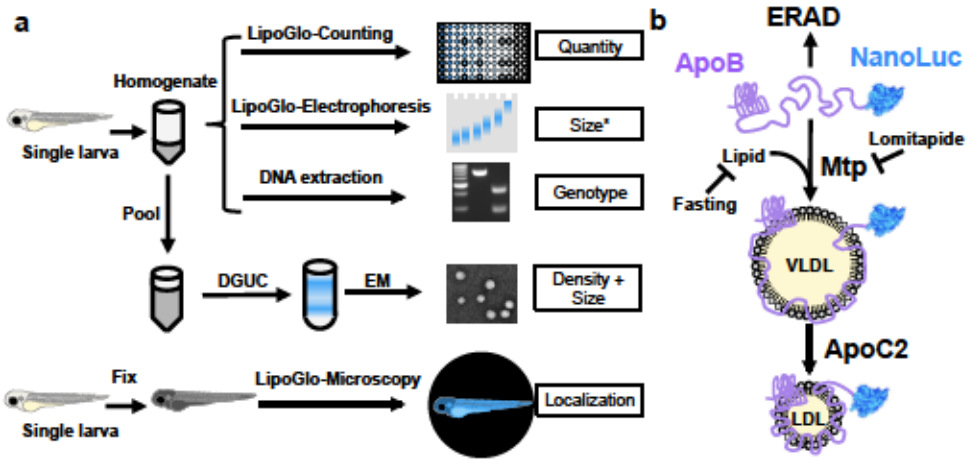

Figure 1: Overview of LipoGlo assays and experimental manipulations. (a) Individual larvae carrying the ApoB-NanoLuc reporter are first homogenized in ApoB-LP stabilization buffer. Homogenate can be used for LipoGlo-Counting (a plate-based assay for NanoLuc activity to measure the total number of ApoB-LPs), LipoGlo-Electrophoresis (a N-PAGE assay to determine the ApoB-LP size/subclass distribution), and DNA extraction for genotyping. Alternatively, lipoprotein density and size can be determined by density-gradient ultracentrifugation (DGUC) followed by electron microscopy. To determine localization of ApoB-LPs in situ, individual larvae are fixed in 4% PFA and mounted in low-melt agarose for chemiluminescent imaging (LipoGlo-Microscopy). **(b)** ApoB protein fused to NanoLuc is loaded with lipid through the activity of Mtp to form VLDL particles. In the absence of lipidation, the protein will be rapidly degraded by ERAD. VLDL is lipolyzed by serum lipases that use Apoc2 as an obligate cofactor to produce smaller lipoprotein classes such as LDL. Here we investigate the effects of (i) genetic manipulations (mutations in mtp and apoc2), (ii) dietary variation (fasting and feeding), and (iii) pharmacological treatment (inhibition of Mtp with lomitapide) on various aspects of the ApoB-LP profile.

Results

TALEN-mediated genome engineering enables creation of the LipoGlo reporter

ApoB is an ideal scaffold for creating a reporter of ApoB-LPs. It is both an obligate structural component present in single copy on each lipoprotein particle [231], and is rapidly degraded when not associated with an ApoB-LP via endoplasmic-reticulum-associated protein degradation (ERAD) [232] (Fig. 1b). In mammals there is a single *APOB* gene that can be post-transcriptionally edited into two isoforms: the full-length *APOB-100* expressed primarily in the liver, and the truncated *APOB-48* isoform expressed in the intestine [12, 233]. Although the zebrafish genome contains 3 paralogs of *APOB*, a single paralog (*apoBb.1*) is the dominant isoform, accounting for approximately 95% of the *ApoB* mRNA and protein in larval zebrafish [82]. Known functional elements of ApoB are well conserved in zebrafish, including both the microsomal triglyceride transfer protein (MTP) interacting [234] and LDL-receptor binding [235] domains (Fig. 2a). However, the APOB-48 editing site required for production of the truncated (intestine-specific) version of APOB [12] appears to be completely absent in zebrafish (Fig. 2b). Thus, ApoB-LPs intestine and liver can be simultaneously tagged with a carboxy-terminal fusion to ApoBb.1 in zebrafish.

The NanoLuc coding sequence was introduced as a carboxy-terminal fusion to the endogenous ApoBb.1 gene in zebrafish through homology directed repair of a double-stranded break [236]. Capped mRNA encoding a TALEN pair targeting the ApoBb.1 stop codon was co-injected with a donor DNA construct to induce homology-directed repair. The donor construct contains the NanoLuc coding sequence flanked on either side by

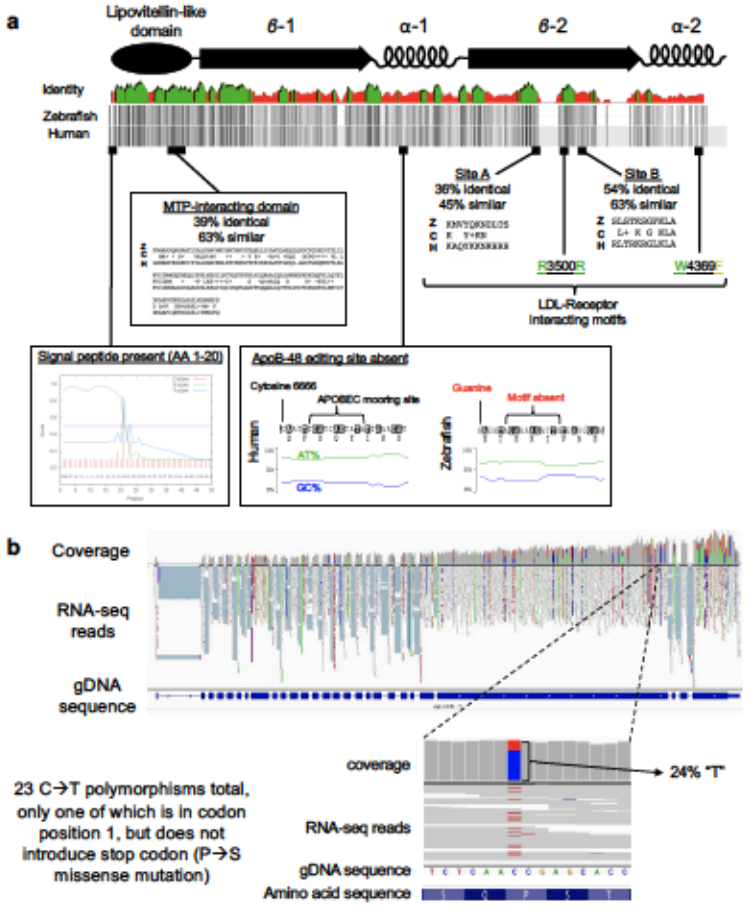

Figure 2: Conservation of functional domains in the zebrafish ApoBb.1 ortholog of Human APOB. **(a)** APOB has a penta-partite domain structure, with an amino-terminal globular domain followed by a series of beta and alpha domains. Consistent with other apolipoprotein sequences, APOB shows relatively low sequence conservation between species at the amino acid level (25% identical, 43% similar, green indicates >30% identity in identity plot). However, sequence conservation is enriched in known ApoB functional domains. For example, there is clear conservation of a signal peptide motif at the amino terminus. The MTP-interacting domain shows 39% identity and 63% similarity, and the LDL-R interacting motifs are also well-conserved. However, the ApoB-48 editing site appears completely absent, as zebrafish *apoBb.1* lacks the essential C6666 that is edited to form the premature stop, as well as the APOBEC mooring site, and shows only mild AT-richness that has been shown to be important for APOBEC binding **(b)** To further evaluate whether *apoB*-editing takes place in zebrafish, RNA reads were mapped back to this genomic locus. Post-transcriptional C→U editing would appear as a C→T polymorphism in the genomic sequence. 23 instances of C→T polymorphism were observed, but the vast majority (21) appeared in the wobble position (position 3) of the codon as would be expected for true polymorphisms (rather than post-transcriptional RNA-editing). Of the single instance that occurred in position 1, this did not result in a premature stop codon, providing further support for the absence of APOB-editing activity in zebrafish.

several hundred base pairs of sequence homologous to the genomic sequence upstream and downstream of the ApoBb.1 stop codon (Fig. 3a). Injected embryos were raised to adulthood and their progeny were screened for NanoLuc activity and subsequently for error-free integration at the target locus. The resulting tagged lipoproteins were quantified using the Nano-Glo assay (Promega Corp., N1110), which led us to name this system LipoGlo.

Fish homozygous for the LipoGlo reporter are healthy, fertile, and do not display any abnormal morphological or behavioral phenotypes. Additionally, larvae homozygous for the LipoGlo reporter show a two-fold increase in LipoGlo signal relative to their heterozygous siblings (Fig. 3c). Denaturing polyacrylamide gel electrophoresis (SDS-PAGE) followed by labeling with specific ApoB and NanoLuc antibodies reveal a single high molecular-weight band (>250 kDa) that corresponds with the expected migration pattern of an ApoB-NanoLuc fusion protein. Degradation products and/or free NanoLuc protein with lower molecular weights were undetectable (Fig. 3d). Together, these data indicate that the LipoGlo reporter signal is directly proportional to ApoB levels.

LipoGlo-Counting reveals changes in ApoB-LP abundance

The LipoGlo-Counting method uses a 96-well plate based assay to detect NanoLuc activity and quantify ApoB-LP abundance. Several genetic, pharmacological, and dietary manipulations were performed to validate that canonical aspects of lipoprotein homeostasis are conserved in zebrafish (Fig. 1b). Individual larvae carrying the LipoGlo reporter were homogenized in a standard volume of ApoB-LP stabilization buffer (100 μL) using either a pellet pestle for low throughput sample processing (Fisher

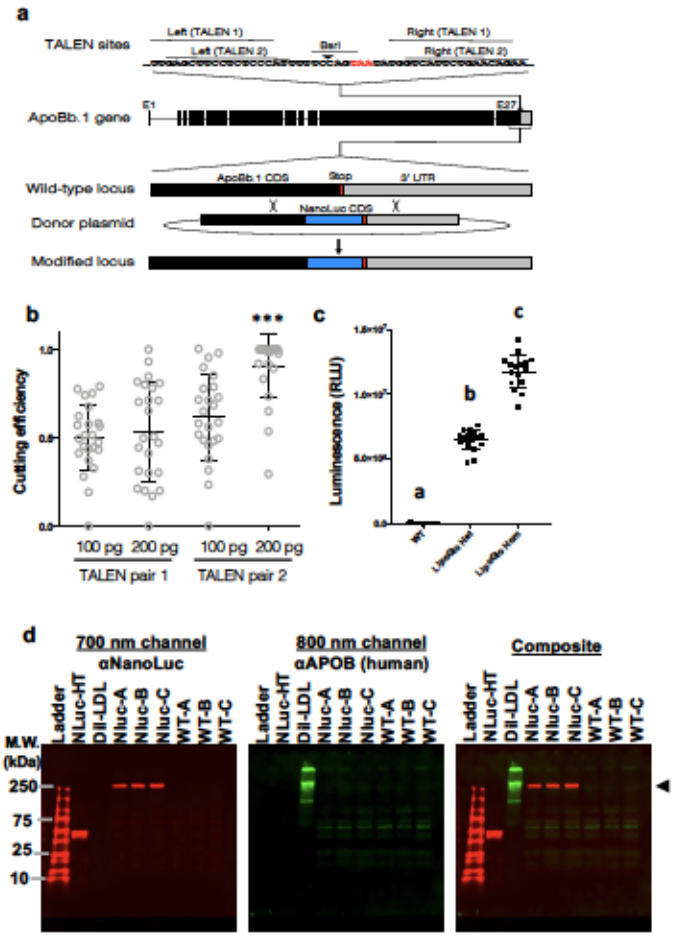

Figure 3: Introduction of an in-frame NanoLuc fusion reporter at the endogenous *apoBb.1* locus. (a) A BsrI restriction site overlaps partially with the *apoBb.1* stop codon. Two independent pairs of TALENs were designed as shown, and **(b)** tested for cutting efficiency which was quantified as a loss of susceptibility to BsrI digest. TALEN pair 2 showed significantly higher cutting efficiency, and was selected for co-injection with the DNA donor construct (DF=3, n=24, ANOVA p<0.0001, Tukey's HSD p<.0001). **(c)** An incross of adult fish heterozygous for the LipoGlo reporter revealed the expected mendelian ratio of offspring, and showed that homozygous carriers produce approximately twice the signal intensity as heterozygotes (1.2E7±1.3E6 vs 6.5E6±7.3E5) (DF=2, n≈16, ANOVA p<0.0001, Tukey's HSD p<.0001). **(d)** SDS-PAGE demonstrating that the NanoLuc reporter remains attached to ApoB. Purified halo-tagged NanoLuc protein (Nluc-HT, ~54 kDa) purchased from Promega was used to indicate the approximate migration of free NanoLuc protein, and Dil-LDL was used to mark the migration of APOB. Protein was extracted from wild-type larvae as well as those homozygous for the NanoLuc reporter, separated by SDS-PAGE, and the resulting blot was probed simultaneously for NanoLuc (Red) and Human APOB (Green). NanoLuc is exclusively detectable in a high-molecular weight band (>250 kDa, black arrowhead), corresponding to the migration of ApoB. Note that the anti-ApoB antibody does not recognize zebrafish ApoB.

scientific, 12-141-363), or a microplate horn sonicator for processing of 96 samples simultaneously in plate format (QSonica, 431MPX). The ApoB-LP stabilization buffer contains protease inhibitors, pH buffers, and cryoprotectant to ensure sample stability during processing and storage. A portion of the homogenate (40 μL) was mixed with an equal volume of Nano-Glo assay buffer and quantified in a plate reader. The remaining homogenate was either stored frozen for later use, or used for additional assays (Fig. 1a).

ApoB-LP levels were measured throughout development from 1 – 6 days post-fertilization (dpf) using zebrafish carrying the LipoGlo reporter in the wild-type (WT) genetic background (Fig. 4a). During this window of development, embryos are in the lecithotrophic (yolk-metabolizing) stage [151]. All nutrients required for development are provided by the maternally deposited yolk, until the yolk becomes depleted between 5 and 6 dpf and the larvae begin to rely on exogenous food. Yolk lipid is packaged into ApoB-LPs by the yolk syncytial layer (YSL), a specialized embryonic organ that expresses many genes involved in ApoB-LP production including *ApoBb.1* [82]. Accordingly, ApoB-LP levels are quite low early in development, but increase between 1 – 3 dpf as more yolk lipid is packaged into ApoB-LPs (Fig. 4a). As the larvae are not provided with food, ApoB-LP levels drop later in development as rates of lipoprotein metabolism and turnover exceed rates of production following yolk depletion.

LipoGlo reporter fish were then crossed with fish harboring mutations in essential components of the ApoB-LP production and breakdown pathways. Microsomal Triglyceride Transfer Protein (Mtp) is responsible for loading nascent ApoB with lipid to form ApoB-LPs [237], and Apolipoprotein-C2 (ApoC2) is a cofactor for lipoprotein lipolysis [14] (outlined in Fig. 1b). As expected, *mtp*$^{-/-}$ mutants [49] exhibit profound

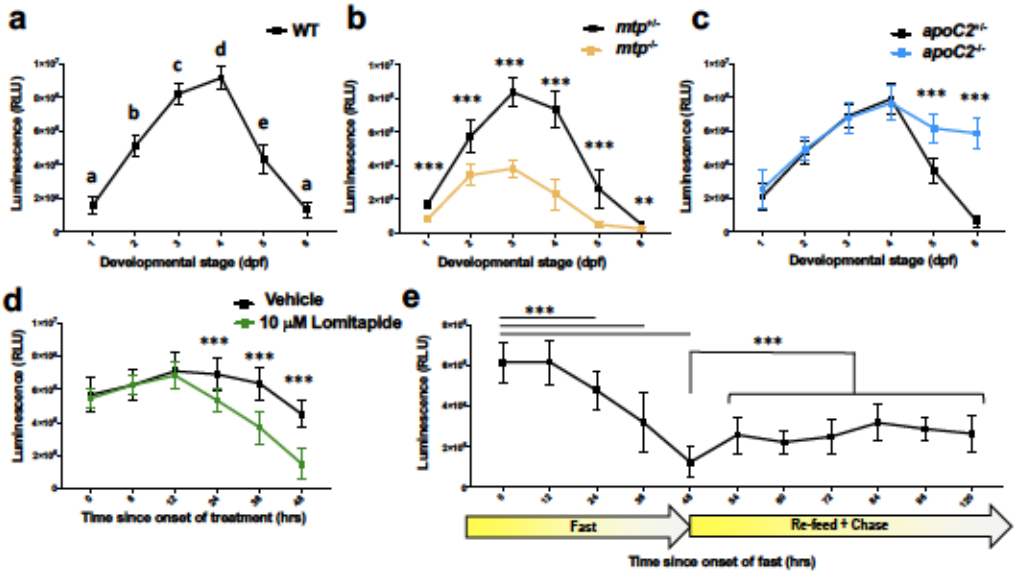

Figure 4: LipoGlo-Counting reveals conserved ApoB-LP responses to genetic, dietary, and pharmacological stimuli. (a) LipoGlo signal throughout WT larval zebrafish development (1 – 6 dpf). Time points designated with different letters are statistically significantly different (DF=5, n=24, ANOVA p<0.0001, Tukey's HSD p<.0001). **(b)** Comparison of LipoGlo signal between *mtp*$^{-/-}$ mutants (defective in lipoprotein synthesis) and *mtp*$^{+/-}$ siblings during larval development (DF=11, n≈16, Two-way robust ANOVA p<0.0001 for genotype and stage, Games-Howell p<.001). **(c)** Comparison of LipoGlo signal between *apoC2*$^{-/-}$ mutants (defective in lipoprotein breakdown) and *apoC2*$^{+/-}$ siblings during larval development (DF=11, n≈12, Two-way robust ANOVA p<0.0001 for genotype and stage, Games-Howell p<.0001). **(d)** Effect of lomitapide (10 µM, Mtp inhibitor) on LipoGlo signal (3 – 5 dpf) (DF=11, n=30, Two-way robust ANOVA p<0.0001 for treatment and time, Games-Howell p<.0001). **(e)** LipoGlo levels were measured over time throughout a fast, re-feed, and chase period. Larvae were fed a standard diet *ad libitum* from 5 to 10 dpf, and then were deprived of food for 48 hours (fast period). Larvae were then fed a high-fat (5% egg yolk) diet for 6 hours, and this meal was chased for 72 hours starting at the onset of feeding (48-120 hours) (DF=10, n=30, Welch's ANOVA p<0.0001, Games-Howell p<.0001). Results represent pooled data from three independent experiments, "n" denotes number of samples per data point.

defects in ApoB-LP production detectable from the earliest stages of development (Fig. 4b). By contrast, *apoC2*$^{-/-}$ mutants [226] produce lipoproteins normally but show significantly reduced levels of particle breakdown and turnover compared to sibling controls (Fig. 4c).

To probe the effects of transient Mtp inhibition on larval lipoprotein homeostasis, larvae were exposed to lomitapide. Lomitapide is a pharmaceutical inhibitor of Mtp used to treat familial hypercholesterolemia in humans [238]. Larvae were treated with 10 μM lomitapide or vehicle control for 48 h (3-5 dpf), and treated larvae showed a more rapid decline in NanoLuc levels than vehicle-treated controls. This observation is consistent with lomitapide inhibiting ApoB-LP production and leading to an accelerated decline of ApoB-NanoLuc levels (Fig. 4d).

To test the effect of food intake on ApoB-LP levels, larvae were subjected to a fasting and re-feeding experimental paradigm. Larvae were fed a standard diet (Gemma 75, Skretting USA) for 5 days (from 5-10 dpf) to adapt to food intake and reach a physiologically relevant baseline level of ApoB-LPs. Following the initial feeding period, larvae were fasted for 48 h (sampled every 12 h), re-fed with a high-fat meal of 5% egg-yolk [114], and sampled at various time points after the meal (the chase period). ApoB-NanoLuc levels were stable for the first 12 h of the fast, but declined rapidly for the duration of the fasting period (Fig. 4e, 0-48 h). Following the high fat meal (6 h of feeding from time point 48 h to time point 54 h), there was an immediate increase in ApoB-NanoLuc levels (Fig. 4e, 48-120 hrs). ApoB-NanoLuc levels did not recover to their pre-fasted state following the high-fat meal, but rather remained at an intermediate level for a prolonged period (the duration of the chase period, 72 h).

Determination of lipoprotein size distribution using LipoGlo-Electrophoresis

There are numerous classes of ApoB-LPs, many of which can be differentiated based on particle size [5]. Native polyacrylamide gel electrophoresis (Native-PAGE) has previously been used to separate ApoB-LPs based on size, but requires a relatively large volume of plasma (25 μL) that has been pre-stained with lipophilic dyes [239]. The LipoGlo-Electrophoresis method subjects crude larval homogenate (containing only nanoliters of plasma) to Native-PAGE to separate lipoproteins, followed by an in-gel NanoLuc assay to detect tagged lipoproteins. To analyze the ApoB-LP size distribution over development and in response to genetic, pharmacological, and dietary manipulations, representative frozen aliquots of larval homogenate from a given condition were thawed on ice. A portion of the thawed homogenate (12 μL) was mixed with 5x loading dye (3 μL) and separated via Native-PAGE (3% gel for 275 Volt-h). Following separation, the glass front plate was removed to expose the gel surface, and 1 mL of TBE containing Nano-Glo substrate solution (2 μL) was added to the plate and spread evenly using a thin plastic film. The gel was then imaged using the Odyssey Fc chemiluminescent detection system (LI-COR Biosciences). Together, this protocol is referred to as LipoGlo electrophoresis.

Smaller lipoproteins are expected to migrate further into the gel, and larger lipoproteins to show concomitantly less mobility (Fig. 5a). Following electrophoretic separation, ApoB-LPs can be divided into four different classes based on their migration distance. ApoB-LPs that remain within the loading well are classified as the "zero mobility" (ZM) fraction, which may include chylomicrons [240], remnants, aggregates

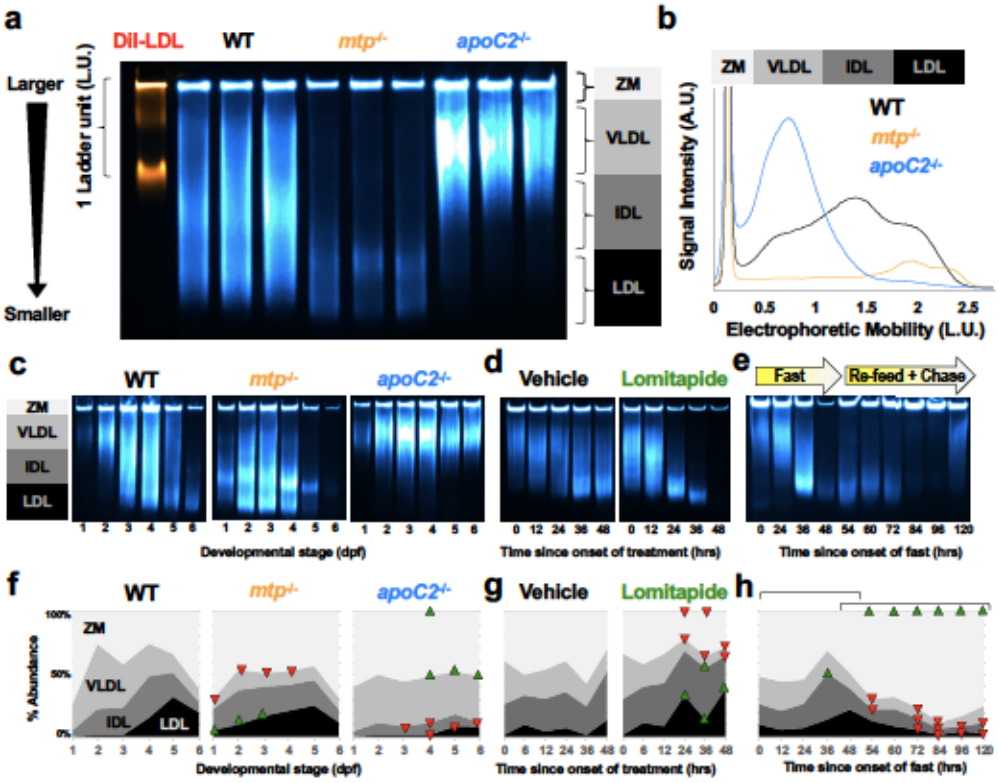

Figure 5: Changes in lipoprotein size distribution revealed through coupling native-PAGE to LipoGlo. **(a)** Representative image of the fluorescent DiI-LDL migration standard and LipoGlo emission from WT, *mtp*$^{-/-}$, and *apoC2*$^{-/-}$ genotypes (4 dpf). ApoB-LPs are divided into 4 classes based on their mobility, including ZM (zero mobility) and three classes of serum ApoB-LPs (VLDL, IDL, LDL). Image is a composite of chemiluminescent (LipoGlo, blue) and fluorescent (DiI-LDL, orange) exposures. Gel is a representative image from one of the three independent experiments performed. **(b)** Vertical plot profile generated in ImageJ from gel image displayed in **(a)**, note that the ZM peak has been appended to highlight differences in serum lipoprotein classes. **(c-e)** Representative LipoGlo PAGE gels (one of three independent experiments shown) and **(f-h)** quantification of pooled LipoGlo PAGE gel data from larval lysates used in Figure 2. Note that relative abundance was quantified, so the sum of all species will always equal 100% despite changes in total abundance over time. Relative abundance of subclasses is color-coded as shown in **(a)**. Upward-facing arrowheads (green) indicate significant enrichment of that species at that time point compared to WT, and downward-facing arrowheads (red) indicate depletion **(f)** Subclass abundance at each day of larval development in WT (DF=5, n=9, Welch's ANOVA p<0.0001 for each subclass over time), *mtp*$^{-/-}$ (DF=11, n=9, Two-way robust ANOVA p<0.001 for VLDL and LDL, Games-Howell p<.01), and *apoC2*$^{-/-}$ (DF=11, n=9, Two-way robust ANOVA p<0.01 for all classes, Games-Howell p<.005) genetic backgrounds. **(g)** Subclass abundance from 3-5 dpf in larvae treated with 10μM lomitapide or vehicle control (DF=11, n=9, Two-way robust ANOVA p<0.001 for all classes except IDL, Games-Howell p<.01). **(h)** Subclass abundance from 10-15 dpf in larvae subjected to a fasting and re-feeding paradigm. The first bracket delineates changes relative to time 0 (the onset of the fasting period), and the second bracket delineates changes relative to time point 48 (the onset of the re-feeding period) (DF=10, n=9, Welch's ANOVA p<0.0001 for each subclass over time, Games-Howell p<.01). Supplementary Figure 4 displays standard deviations for panels f-h. Results represent pooled data from three independent experiments, "n" denotes number of samples per data point.

[241], and intracellular ApoB complexed with components of the secretory pathway (such as the ER, golgi, and other secretory vesicles) [242]. Species that do migrate into the gel are classified as either Very Low-Density Lipoproteins (VLDL), Intermediate-Density Lipoproteins (IDL), or Low-Density Lipoproteins (LDL) based on their electrophoretic mobility. Di-I-labeled fluorescent LDL (L3482, ThermoFisher Scientific) is used as a migration standard to ensure consistent classification of ApoB-LP species between gels, with the migration distance of this species corresponding to one ladder unit (L.U.). Although human DiI-LDL migrates more slowly than NanoLuc-labeled LDL, which is at least partially attributable to migration retardation by DiI (Fig. 6g), this band provides a highly reproducible standard for registration and normalization across gels (Fig. 6).

In order to define physiologically relevant migration boundaries between ApoB-LP classes, ApoB-LP profiles were compared for WT, *mtp*$^{-/-}$, and *apoC2*$^{-/-}$ mutant lines at 4 dpf (Fig. 5a,b). *ApoC2*$^{-/-}$ mutants are unable to lipolyze VLDL, which allowed us to define the VLDL bin from .3 – 1 ladder units. Conversely, *mtp*$^{-/-}$ mutants display a bimodal peak of small LDL-like particles at this stage of development, which was used to define the LDL bin as 1.7 – 2.4 ladder units from the origin. Wild-type larvae have a peak of intermediate-sized lipoproteins at this stage, which corresponds to the IDL region from 1 – 1.7 ladder units. ApoB-LPs migrating less than .3 ladder units were considered to be in the zero-mobility fraction (ZM) (Fig. 5a).

Gel images were transformed into plot profiles in ImageJ for quantification (Fig. 5b). The provided Gel Quantification Template (Supplementary file 1) contains instructions and formulas for automatically calculating bin cutoffs for each ApoB-LP class based on the

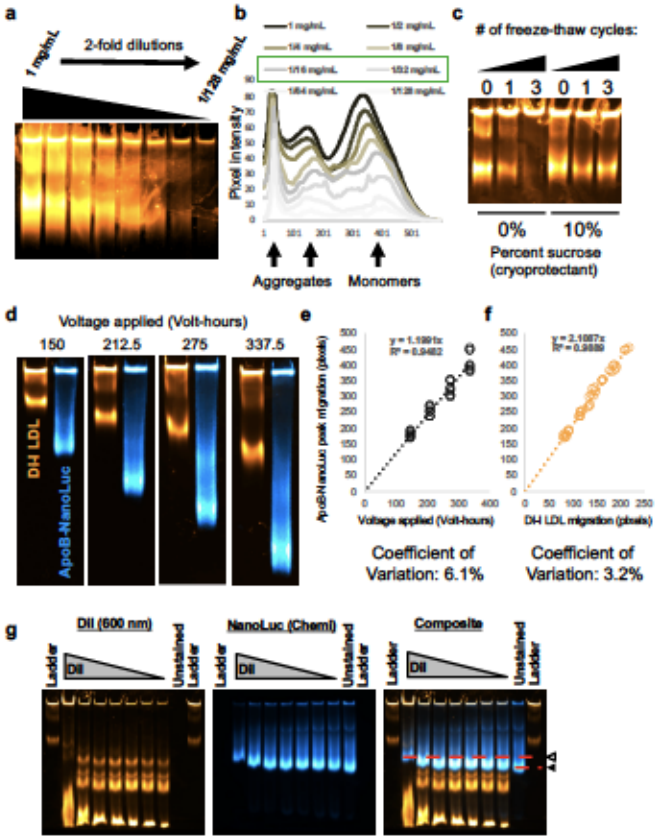

Figure 6: Development of an effective migration standard for lipoprotein gels. It is essential that lipoprotein gels include a ladder or normalization standard that has similar electrophoretic properties to ApoB-LPs. Di-I labeled human LDL serves as a commercially available option that enables standardization not only between multiple gels but also between different labs. **(a)** Di-I LDL was subjected to a series of 2-fold dilutions and separated via N-PAGE as described and imaged with the Licor-Fc to determine an appropriate dilution factor that was still readily detectable. **(b)** Plot profiles of each of the serial dilutions revealed retardation of peak mobility in the highly concentrated samples, potentially due to overcrowding. Dilution factors between 16 and 32-fold were selected as acceptable (green box), and a 24-fold dilution was used for subsequent assays. **(c)** Sucrose was included as a cryoprotectant during Di-I LDL dilution, and there is no change in peak particle mobility across at least 3 freeze-thaw cycles in the presence of 10% sucrose, whereas the ladder is almost completely aggregated without cryoprotectant. **(d)** To determine the relationship between mobility of the standard and lipoprotein samples, homogenate was prepared and pooled from *mtp -/-* (3 dpf) mutant larvae (which produce primarily LDL-like particles). Samples of homogenate were run alongside Di-I standard for either 150, 212.5, 275, or 337.5 volt-hours, and the peak migration (in pixels) was quantified for each species. **(e)** While there was a clear linear relationship between ApoB-LP migration and voltage applied (R^2=.95), **(f)** the relationship was much tighter when electrophoretic mobility was compared to the migration standard (R^2=.99), validating the utility of Di-I LDL as a migration standard. **(g)** Plasma extracted from adult female zebrafish was stained with DiI along a series of two-fold dilutions from 30 mg/mL down to approximately .5 mg/mL. Higher concentrations of DiI significantly impeded lipoprotein migration (white arrowhead) relative to unstained plasma (black arrowhead).

migration of the Di-I standard and quantifying the relative intensity of each bin. Note that LipoGlo electrophoresis is only used to determine relative abundance, rather than absolute or total abundance of lipoproteins. This is useful for highlighting differences in size distributions even when the total number of ApoB-LPs is vastly different. To illustrate this point, compare the ZM bands between 4 dpf and 6 dpf larvae. The ZM band is clearly significantly brighter at 4 dpf (higher absolute abundance), but it accounts for a smaller fraction of the total profile (lower relative abundance). To visualize the distribution of ApoB-LP classes over time, each species was color coded with darker colors corresponding to smaller lipoproteins and plotted as an 100% stacked area chart, with the thickness of each shade corresponding to the relative abundance of that species at that time (Fig. 5f-h). Upward-facing green arrowheads or downward-facing red arrowheads are used to indicate species that show significant enrichment or depletion (respectively) relative to the control group (Fig. 5f-h). Additional plots were generated that present the data grouped by ApoB-LP class (rather than genotype) (Fig. 7).

Using LipoGlo-Electrophoresis over the course of zebrafish larval development revealed that in the early embryonic stages (1-2 dpf), the wild-type ApoB-LP profile is dominated by VLDL (Fig. 5c,f), which are directly produced by the YSL. By 3 and 4 dpf, VLDL particles have been lipolyzed to generate the smaller IDL and LDL classes. When the maternal yolk has been depleted (5-6 dpf), and in the absence of exogenous food, VLDL production is significantly attenuated as indicated by enrichment of small lipolyzed lipoproteins. The ApoB-LP profile dynamics are more static in the *mtp*$^{-/-}$ and *apoC2*$^{-/-}$ mutants: *mtp*$^{-/-}$ mutants produce smaller IDL and LDL-like particles from the earliest stages of development, and *apoC2*$^{-/-}$ mutants show a VLDL peak that persists

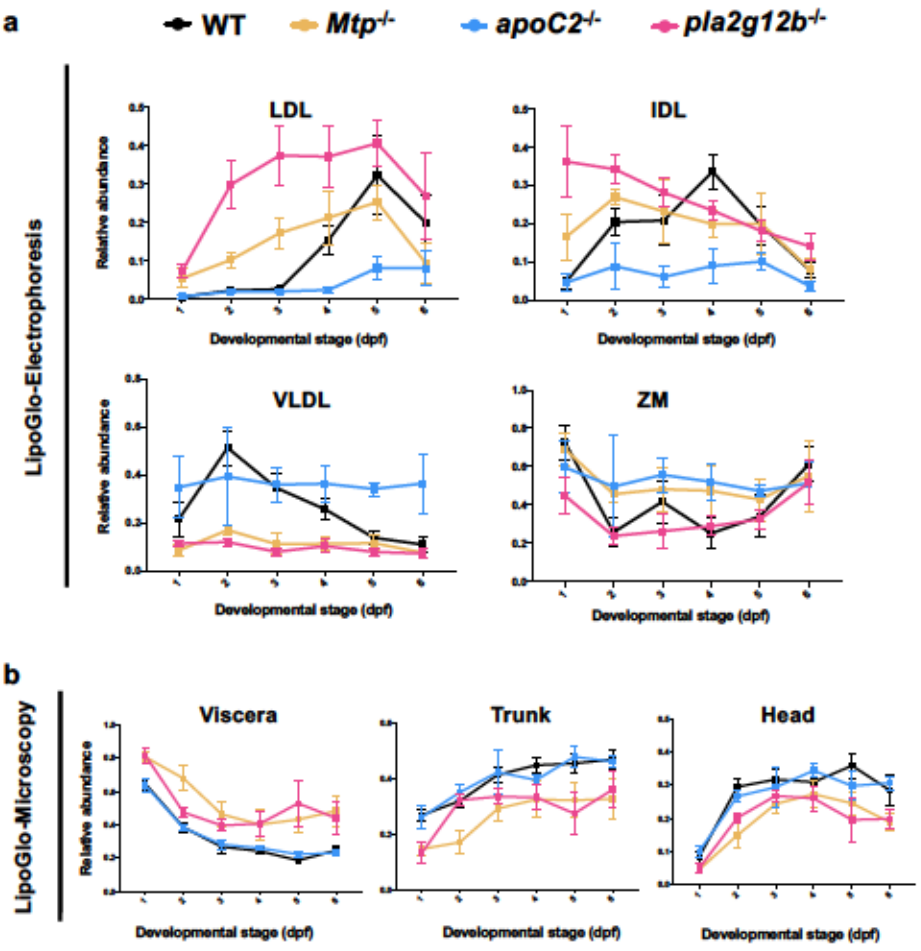

Figure 7: Side-by-side analysis of LipoGlo-Electrophoresis and Microscopy results from mutant genotypes. (a) Plots of electrophoresis and **(b)** microscopy data reported in the main text grouped by subclass rather than by genotype and showing standard deviations.

throughout development (Fig. 5c,f). Pharmacological treatment with a potent MTP inhibitor (Lomitapide) effectively blocks the production of new VLDL particles (Fig. 5d,g), leading to the accumulation of lipolyzed species such as IDL and LDL.

Consistent with the mammalian literature, there is significant depletion of VLDL and enrichment of LDL following a 48 h fast, as VLDL production is dependent on nutrient availability. A robust post prandial response was also observed in the distribution of ApoB-LP subclasses of larval zebrafish. A high lipid meal (egg yolk emulsion) produces a significant increase in the ZM band, and progressive depletion of LDL (Fig. 5e,h).

Electrophoretic mobility correlates well with lipoprotein density and size

Electrophoretic mobility in Native-PAGE is a function of both size and charge, so it is important to evaluate whether differences in migration truly reflect different sizes or if they are the result of differentially charged lipoproteins. Density gradient ultracentrifugation (DGUC) is the gold standard for discerning different subclasses of ApoB-LPs, as larger lipoprotein classes are more buoyant resulting from their large lipid core. To evaluate concordance between DGUC and the LipoGlo assays, I developed a DGUC protocol (based on the method described by Yee et al., [243]) to separate pooled larval homogenate into density fractions. I then subjected fractions to (i) LipoGlo electrophoresis to characterize their electrophoretic mobility, (ii) a plate read assay to quantify ApoB-NanoLuc levels, and (iii) negative-staining electron microscopy to visualize particle size directly [244] (Fig. 8). Importantly, denser fractions showed higher electrophoretic mobility and smaller particle sizes across all genotypes, demonstrating

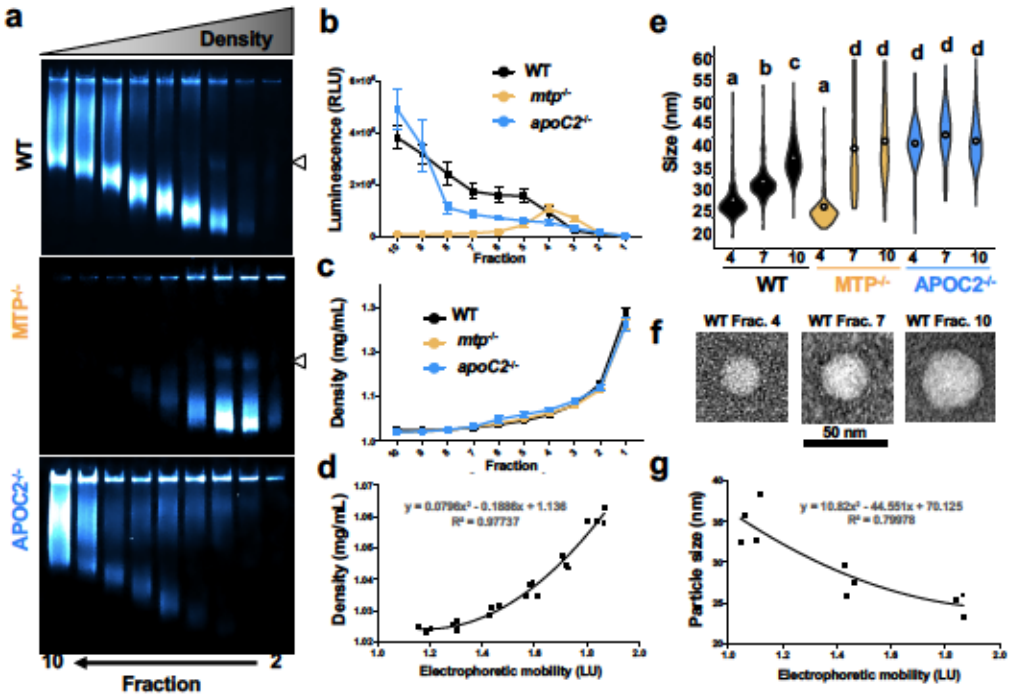

Figure 8: Concordance between LipoGlo electrophoresis and classical ApoB-LP size characterization techniques. DGUC was performed on pooled larval homogenate (4 dpf) from WT, *mtp*$^{-/-}$, and *apoC2*$^{-/-}$, and separated into 10 equal fractions of approximately 500 µL each by drip-elution (dense bottom fractions eluted first). **(a)** Fractions 2-10 were subjected to Native-PAGE, and denser fractions showed higher electrophoretic mobility. Some fractions show a faint lower mobility band (indicated at right by white arrowhead), possibly indicative of lipoprotein dimerization. **(b)** A plate-based assays of NanoLuc activity revealed the expected enrichment of VLDL in *apoC2*$^{-/-}$ mutants, and enrichment of LDL in *mtp*$^{-/-}$ mutants (confirming results reported in Fig. 3b). **(c)** A refractometer (Bausch and Lomb) was used to determine the refractive index of each fraction and density was calculated via the formula D = 3.3508 x RI - 3.4675. DGUC showed highly reproducible density profiles between replicates and genotypes. **(d)** The density of WT fractions 4 – 9 was plotted as a function of peak electrophoretic mobility for that fraction, and the second order polynomial function (y = 0.0796x2 - 0.1886x + 1.136) was able to represent this relationship with remarkable accuracy (R^2 = 0.97737) indicating that electrophoretic mobility is a useful proxy for lipoprotein density. **(e)** Fractions 4, 7, and 10 were subjected to negative-staining electron microscopy to directly visualize the size of particles in each fraction. In the wild type samples, the average particle diameter was 24.7±5.6, 29.0±4.1, and 34.9±4.7 nm for fractions 4, 7, and 10 respectively. There was no significant difference in particle size between fraction 4 of the wild-type and *mtp*$^{-/-}$ mutant samples (average diameter of 23.2 ± 6.6 nm). Particles were nearly undetectable in fractions 7 and 10 in the *mtp*$^{-/-}$ mutant sample so particle diameter shows enormous variability. ApoB-LPs in each *apocC2*$^{-/-}$ mutant fraction were significantly larger than all WT fractions, with diameters of 39.0±8.0, 40.9±7.2, and 39.1±5.9 nm respectively (DF=8, n≈170, Welch's ANOVA p<0.0001, Games-Howell p<.0001). **(f)** Representative images of lipoproteins from the three wild-type fractions are shown. **(g)** The second-order polynomial function y= 10.82x2 - 44.551x + 70.125 approximated the relationship between electrophoretic mobility and density in wild-type samples with reasonable accuracy (R^2 = 0.79978). Results represent pooled data from four independent experiments.

that electrophoretic mobility is a reliable method for differentiating ApoB-LP classes and can be used as a proxy to estimate particle size and density.

LipoGlo-Microscopy reveals the distribution of ApoB-LPs throughout an intact organism

The transparency of larval zebrafish offers the unique opportunity to perform whole-mount imaging, which has enabled us to characterize changes in ApoB-LP localization throughout an intact organism. The same developmental, genetic, dietary, and pharmacological manipulations described above (Figs. 4-5) were performed, but rather than being homogenized, larvae were fixed in 4% paraformaldehyde (PFA) for 3 h at room temperature, washed in PBS-tween, and mounted in low-melt agarose [245] supplemented with Nano-Glo substrate solution. Mounted larvae were imaged in a dark room on a Zeiss Axiozoom V16 equipped with a Zeiss AxioCam MRm set to collect a single brightfield exposure followed by multiple exposures with no illumination (chemiluminescent imaging).

The differences between WT, *mtp*$^{-/-}$, and *apoC2*$^{-/-}$ mutants were most apparent at 6 dpf (Fig. 9a). At this stage, the yolk is depleted and larvae are in a fasted state as no exogenous food has been provided. In WT larvae, signal is quite low throughout the body, but is clearly visible in the lipoprotein-producing tissues (liver and intestine). I observed a previously undescribed association of ApoB with the spinal cord (Fig. 9b, and Fig. 10) as evidenced by colocalization with the central-nervous system marker *Tg(Xla.Tubb2:mApple-CAAX)*. This reporter uses the tubulin beta-2 promoter from *X. laevis* to drive a membrane-targeted mApple fluorophore specifically in the CNS. A

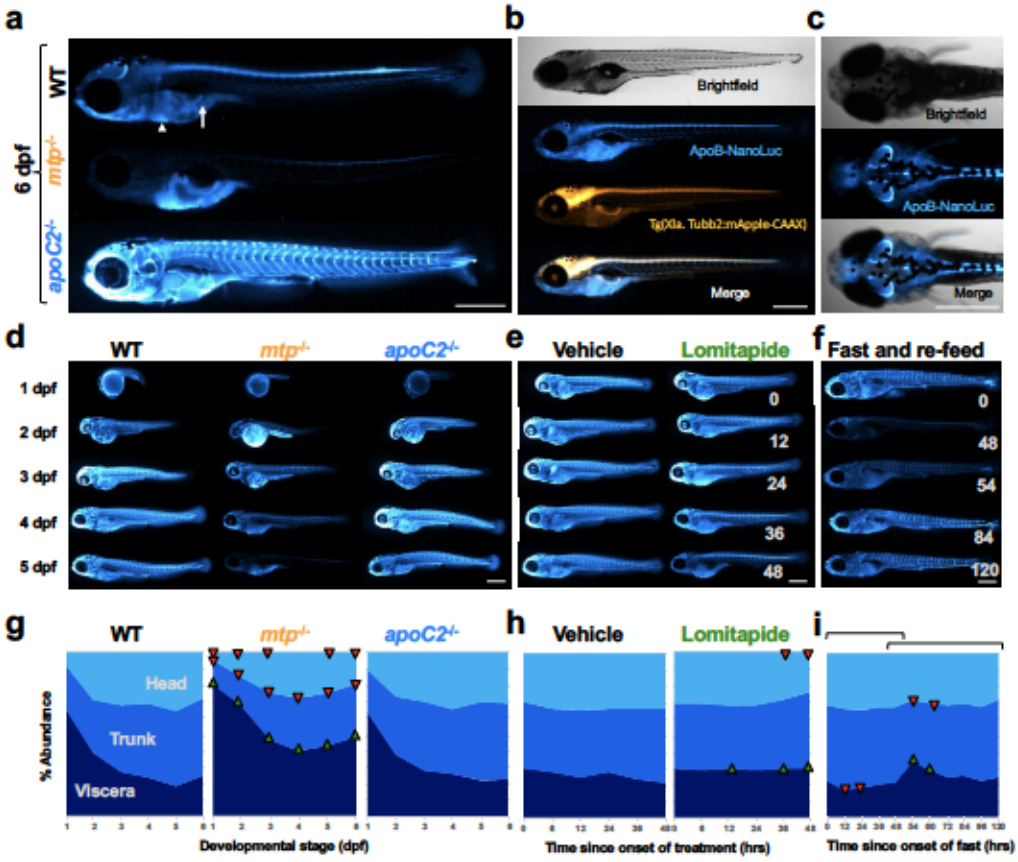

Figure 9: Whole-mount imaging of ApoB-LP localization using LipoGlo chemiluminescent microscopy. (a) Representative images of ApoB-LP localization patterns from analysis of 15 larvae per genotype from WT, *mtp*$^{-/-}$, and *apoC2*$^{-/-}$ genotypes (6 dpf). The white arrow and arrowhead mark the larval intestine and liver respectively. **(b)** LipoGlo signal colocalizes with the central nervous system marker *Tg(Xla. Tubb2-mApple-CAAX)*, quantification in Supplementary Figure 5. **(c)** LipoGlo signal localized to subregions of the CNS. **(d-f)** Representative images and **(g-i)** quantification of ApoB-LP localization across developmental, genetic, pharmacological, and dietary manipulations. **(g)** Signal localization at each day of larval development in WT (DF=5, n=15, Welch's ANOVA p<0.0001 for each region over time), *mtp*$^{-/-}$ (DF=11, n=15, Two-way robust ANOVA p<0.001 for all regions, Games-Howell p<0.001), and *apoC2*$^{-/-}$ (DF=11, n=15, Two-way robust ANOVA was not significant for any region) genetic backgrounds. **(h)** Signal localization from 3-5 dpf in larvae treated with 10μM lomitapide or vehicle control (DF=11, n=15, Two-way robust ANOVA p<0.001 for head and viscera, Games-Howell p<.0001). **(i)** Subclass abundance from 10-15 dpf in larvae subjected to a fasting and re-feeding paradigm. The first bracket delineates changes relative to time 0 (the onset of the fasting period), and the second bracket delineates changes relative to time point 48 (the onset of the re-feeding period) (DF=10, n=15, Welch's ANOVA p<0.0001 for each region, Games-Howell p<.005). Supplementary Figure 4 displays standard deviations for panels g-i. Results represent pooled data from three independent experiments, "n" denotes number of samples per data point. Body regions were defined as outlined in Supplementary Figure 5. Scale bars = 500 μm.

dorsal view revealed enrichment of NanoLuc signal in particular brain regions (Fig. 9c), which I hypothesize corresponds to the brain ventricle. In *mtp*$^{-/-}$ mutants, ApoB is very low outside of the lipoprotein-producing tissues, consistent with defects in loading ApoB with lipid to form a secretion-competent ApoB-LP. *ApoC2*$^{-/-}$ mutants show remarkably high signal throughout the body, consistent with their inability to process and turnover lipoproteins (Fig. 9a).

Images were quantified by creating separate regions of interest for the viscera, trunk, and head regions and comparing the relative levels of NanoLuc signal in each of these areas. During development, signal was initially highly enriched in the visceral region, which contains the yolk and YSL, and then gradually increased in the trunk and head regions (Fig. 9d,g). This is consistent with the vectoral transport of lipid from the YSL to the circulatory system and peripheral tissues. The distribution of ApoB between these three regions was not significantly changed in *apoC2*$^{-/-}$ mutants, whereas *mtp*$^{-/-}$ mutants showed enrichment in the viscera and depletion in the peripheral tissues at all time points (Fig. 9d,g). Results were also grouped by region to facilitate comparison of each class between genotypes (Fig. 7).

DiI-labelled LDL confirms the localization patterns observed with LipoGlo-Microscopy

ApoB-LPs have primarily been studied for their roles in the circulatory system, where they transport lipid between tissues and also contribute to the progression of atherosclerosis. However, LipoGlo-Microscopy experiments revealed two highly unexpected patterns of lipoprotein localization. Firstly, fasted larvae retain high levels of ApoB-LPs associated with the central nervous system. Secondly, a high level of ApoB-

LPs appears in a chevron pattern along the trunk of zebrafish larvae, which correspond to the myosepta (the tendinous tissue connecting body segments) and intersegmental lymphatics [246, 247]. To validate that this localization pattern was not an artifact resulting from the introduction of the NanoLuc reporter, I developed two orthogonal approaches to monitor the localization of ApoB-LPs in zebrafish larvae using a fluorescent lipophilic dye (DiI).

DiI has frequently been used to label lipoprotein particles, as its spectral properties change dramatically when it is incorporated into a phospholipid monolayer, thus reducing background fluorescence from unincorporated dye. As a means of visualizing LDL localization *in vivo,* commercially available human DiI-LDL was injected into the zebrafish bloodstream at 2 dpf and then imaged at various time points throughout development (Fig. 10c). Immediately following injection (2 dpf), bright DiI fluorescence was readily detectable throughout the vascular system, which is particularly clear in the tail vasculature including the caudal artery (CA), caudal vain plexus (CVP), and the intersegmental vessels (ISV). However, imaging at later time points (4 and 6 dpf) revealed significant accumulation in myosepta (MS) and the spinal cord (SC), closely mirroring the localization pattern observed in LipoGlo microscopy. However, in contrast to the LipoGlo microscopy experiments, significant signal accumulated in bright puncta in the ventral posterior of the trunk, which most likely corresponds to macrophages in the caudal hematopoietic tissue (CHT). This result indicates that human DiI-LDL may be immunogenic, either because not derived from zebrafish or it has become oxidized or aggregated during storage.

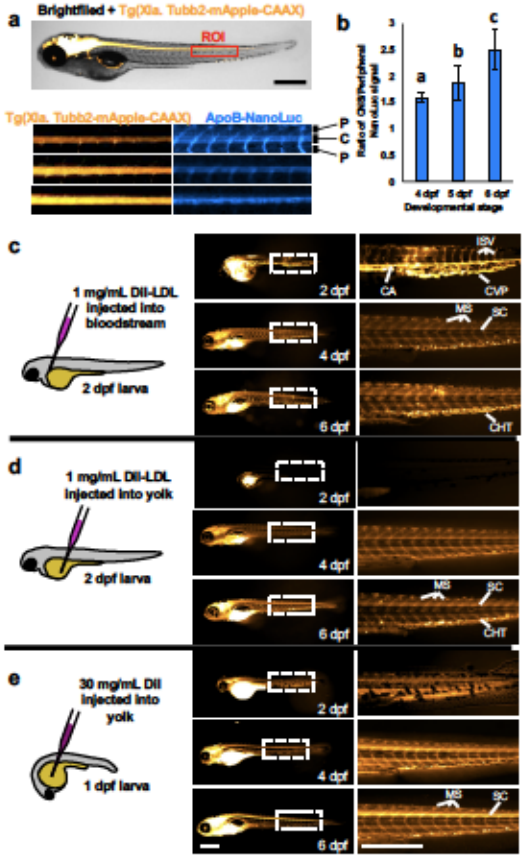

Figure 10: LipoGlo microscopy reveals ApoB-LP localization. (a) Three independent clutches of larvae carrying both the CNS marker *Tg(Xla. Tubb2-mApple-CAAX)* and ApoB-NanoLuc fusion were fixed and imaged at 4, 5, and 6 dpf as described in detailed methods. A 20x100 pixel region of interest (ROI) was drawn centered around the spinal cord (marked by mApple) just distal to the intestine. The mApple and ApoB-NanoLuc channels are displayed separately below (representative of 15 images per time point). **(b)** Quantification of the signal intensity in spinal cord (CNS) versus peripheral regions revealed a gradual enrichment of signal in the CNS relative to the periphery from 4-6 dpf (DF=2, n=15, Welch's ANOVA p<0.0001, Games-Howell p<.01). **(c)** Schematic and results of injection of DiI-labeled human LDL into the common cardinal vein of zebrafish larvae. Immediately following injection on 2 dpf, signal is primarily detectable in blood vessels such as the caudal artery (CA), caudal vein plexus (CVP), and intersegmental vessels (ISV). Later in development (4-6 dpf) signal is primarily localized to extravascular tissues such as the myosepta (MS), spinal cord (SC) and puncta in the caudal hematopoietic tissue (CHT) that likely correspond to macrophages (n=6). **(d)** When DiI-LDL is injected into the yolk, signal is undetectable in the vasculature of early-stage larvae, but in ~50% of cases (3 out of 6) will be detected in both vascular and extravascular tissues of later-stage larvae (n=6). **(e)** A solution of DiI injected into the larval yolk leads to a staining pattern that closely mirrors LipoGlo-microscopy experiments, indicating that it stains endogenous lipoproteins produced in the YSL (N=15). Results represent pooled data from three independent clutches, "n" denotes total number of samples per data point. Scale bars = 500 µm.

As a negative control, human DiI-LDL was also injected into the yolk of zebrafish larvae (Fig. 10d). Immediately after injection, signal was essentially undetectable outside of the yolk, confirming that it has not reached the vasculature. However, approximately 50% of larvae injected into the yolk accrued significant signal outside of the yolk by 6 dpf, where it appeared to mark similar structures as seen in the previous experiment, although signal in the CHT appeared less pronounced. This observation suggests that DiI injected into the yolk (even in the form of human DiI-LDL) could be transferred to endogenous lipoproteins and secreted.

To test whether DiI could be used to monitor endogenous ApoB-LPs, I injected DiI directly into the yolk of zebrafish larvae at 1 dpf (Fig. 10e). DiI signal closely mirrored the LipoGlo microscopy experiments throughout development. Importantly, this DiI-labeling paradigm showed clear enrichment in the spinal cord and myosepta by 6 dpf, validating the findings of the LipoGlo microscopy experiment.

Adult zebrafish plasma labeled with DiI confirms that LipoGlo does not disrupt the ApoB-LP profile

LipoGlo has revealed numerous aspects of the lipoprotein profile in zebrafish larvae, many of which are in line with our current understanding of lipoprotein homeostasis. However, as no alternative methods exist to study the lipoprotein profile in zebrafish larvae at this level of sensitivity or resolution with regard to particle size and number, it was not possible to compare the lipoprotein profile between wild-type and LipoGlo larval individuals. However, using plasma extracted from adult animals the hypothesis that LipoGlo labeling does not alter the plasma lipoprotein profile was tested.

Adult zebrafish plasma lipoprotein profiles determined using native-PAGE from WT animals that were labeled with DiI were essentially indistinguishable from those homozygous for the LipoGlo reporter, although there was significant variation between individuals (likely as a result of variations in activity and feeding behavior) (Fig. 11). These data indicate that the addition of NanoLuc to the carboxy-terminal of ApoB does not disrupt the lipoprotein profile.

While no differences were apparent between wild-type and LipoGlo animals, I was able to detect a significant DiI-positive (NanoLuc-negative) band that is present exclusively in female plasma, and absent in males. This most likely corresponds to vitellogenin, a large protein used to shuttle lipids through the bloodstream that will eventually be used in egg production [248, 249]. While several additional bands are present in the DiI-stained plasma, without additional molecular markers it is difficult to conclusively determine what these species may be, but high-density lipoproteins would also be expected to stain positive for DiI as well.

LipoGlo assays reveal Pla2g12b as an important regulator of ApoB-LP homeostasis

In an effort to identify novel regulators of the ApoB-LP profile using the LipoGlo system, I analyzed a collection of mutants from the zebrafish mutation project [250] that had predicted mutations in genes involved in lipid metabolic pathways. Of the six ENU alleles studied, two alleles (abca1b and pla2g12b) were particularly promising as we detected nonsense-mediated decay in the mutant transcripts [251]. Studies of abca1b using LipoGlo are underway, but I have discovered that larvae homozygous for an essential splice site mutation (sa659) in phospholipase A2 Group XII B (*pla2g12b*)

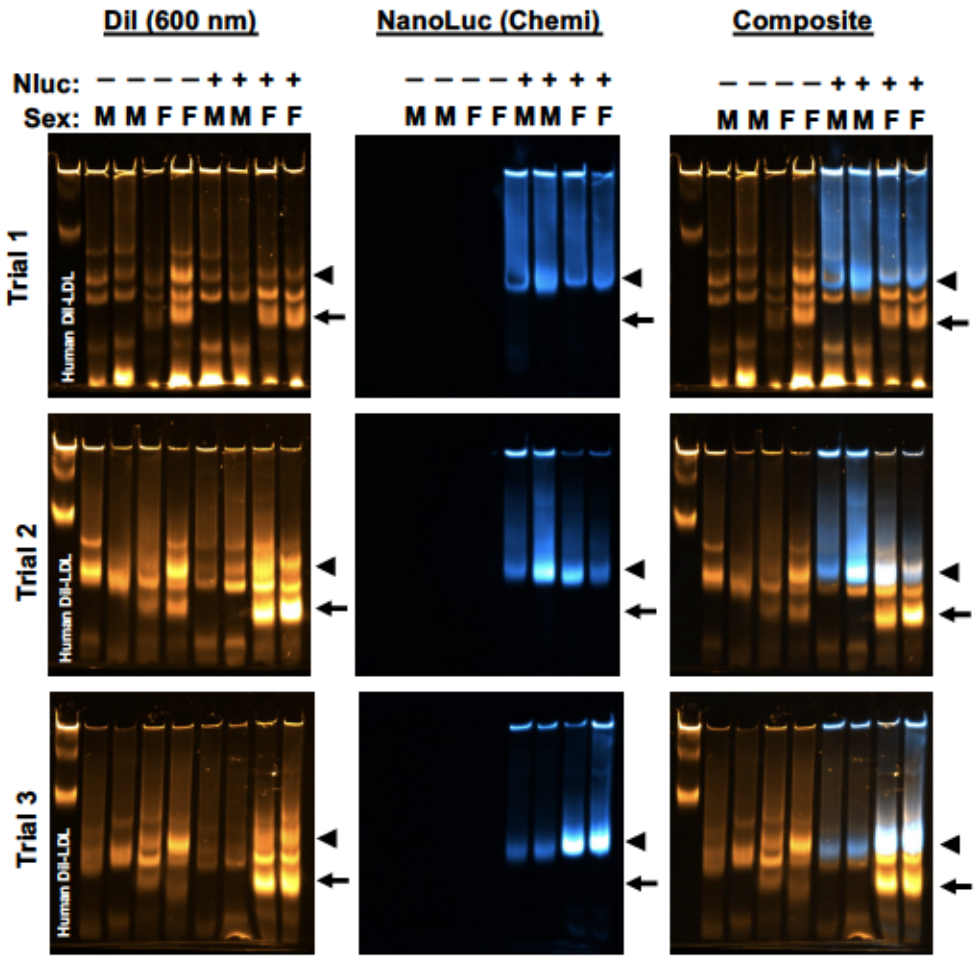

Figure 11: Characterization of the lipoprotein profile in adult zebrafish using DiI. Plasma was extracted from adult zebrafish homozygous for the LipoGlo reporter as well as wild-type controls. Plasma was then stained with DiI and then separated via native-PAGE using the LipoGlo-electrophoresis method. Numerous bands appear in the plasma profile in the DiI-channel (600 nm), but the LDL band (black arrowhead) can be identified as the smallest ApoB-positive band using the LipoGlo reporter (chemi channel). The results from three independent trials are shown, with no overt differences detectable between wild-type and LipoGlo animals, although there is significant variation between individuals. One band is present exclusively in the female plasma profile (black arrow), and likely corresponds to vitellogenin, a well-characterized lipid-transport protein that is only expressed in females.

showed perturbations in their ApoB-LP profile (Fig. 12). Homozygous mutant larvae exhibited lower levels of ApoB at multiple stages (Fig. 12a), and also appeared to have defects in lipoprotein secretion as evidenced by enrichment of visceral ApoB-NanoLuc levels (Fig. 12b,e). However, the most striking defect in *pla2g12b*$^{-/-}$ mutant larvae was a pronounced change in the ApoB-LP size distribution. Even at 1 dpf, significant accumulation of small lipoproteins in the size range of LDL, and depletion of the larger particle classes, were evident (Fig. 12c,d).

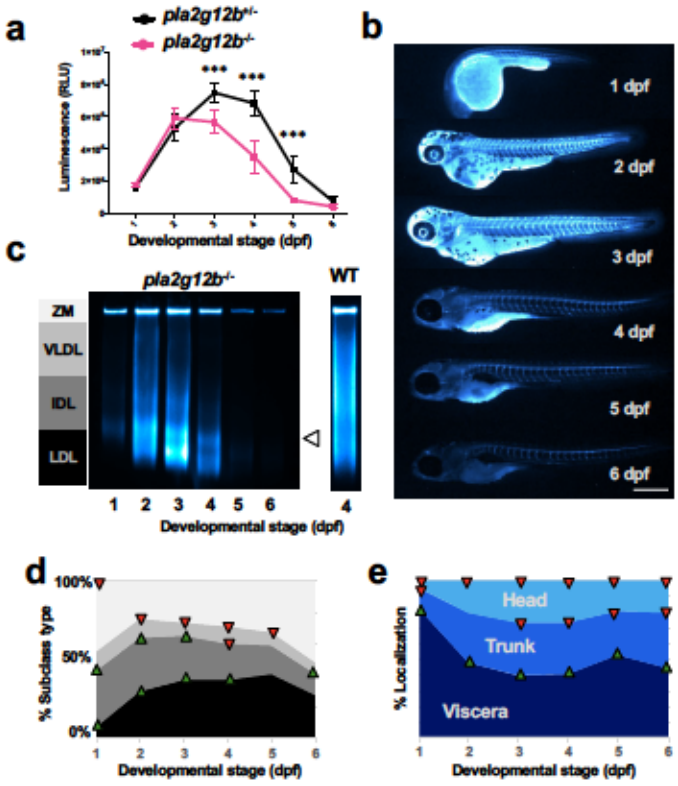

Figure 12: LipoGlo reveals profound alterations in the ApoB-LP profile in *pla2g12b*$^{-/-}$ mutant larvae. (a) Comparison of LipoGlo signal between *pla2g12b*$^{-/-}$ and *pla2g12b*$^{+/-}$ siblings during larval development (1 – 6 dpf) (DF=11, n≈11, Two-way robust ANOVA p<0.0001 for genotype and stage, Games-Howell p<.0001). **(b)** Representative images (n=15) of ApoB-LP localization collected by LipoGlo chemiluminescent imaging throughout development (1 – 6 dpf), and **(e)** quantification of percent localization into previously described subregions (DF=11, n=15, Two-way robust ANOVA p<0.001 for all regions, Games-Howell p<0.0001). **(c)** Representative gel (n=4) showing production of abnormally small lipoproteins (white arrowhead) and **(e)** quantification of LipoGlo emission pattern from native-PAGE samples in *pla2g12b*$^{-/-}$ larvae (1 – 6 dpf). Upward-facing arrowheads (green) indicate significant enrichment of that species at that time point compared to WT, and downward-facing arrowheads (red) indicate depletion (DF=11, n=9, Two-way robust ANOVA p<0.001 for all species, Games-Howell p<.01). Results represent pooled data from three independent experiments, "n" denotes number of samples per data point. Body regions were defined as outlined in Supplementary Figure 5. Scale bars = 500 μm.

Discussion

The LipoGlo reporter does not disrupt lipoprotein homeostasis

When generating a fusion protein, it is essential to evaluate whether introduction of the tag disrupts native protein function. This is particularly important in the case of tagged lipoproteins, as these particles have a complex life cycle that involves interactions with numerous cell and tissue types. The fact that fish homozygous for the LipoGlo reporter are viable, fertile, and free from any overt morphological defects served as encouraging preliminary evidence that metabolism was not greatly disrupted. To evaluate whether the NanoLuc tag disrupted lipoprotein homeostasis in a more subtle way, LipoGlo larvae were subjected to various genetic, dietary, and pharmacological manipulations known to affect the lipoprotein profile. These results validated that NanoLuc-tagged lipoproteins exhibit all of the central hallmarks of endogenous ApoB-LPs, including MTP-dependent maturation, APOC2-dependant lipolysis, responsiveness to nutrient availability, and expected density and size distributions.

Further, LipoGlo microscopy showed that ApoB-LPs are initially only detectable in lipoprotein-producing tissues, and then distribute to peripheral tissues, and finally become undetectable in peripheral tissues when larvae are fasted. These observations are constant with tagged lipoproteins being secreted into the circulatory system, processed in the peripheral circulation, and eventually endocytosed, as would be expected from untagged lipoproteins. Further, the Di-I stained plasma lipoprotein profiles from adult zebrafish homozygous for the NanoLuc reporter and wild-type controls were indistinguishable. Taken together, these observations indicate that the carboxy-terminal

fusion of NanoLuc to ApoBb.1 does not detectably alter lipoprotein homeostasis. This finding establishes a precedent for the use of ApoB-fusion proteins as a sensitive and specific approach to monitor atherogenic lipoproteins which will likely be generalizable to additional model systems. This approach can also be expanded to use alternative tags such as fluorescent reporters for high-resolution imaging or affinity tags to study the lipoprotein interactome. Potential applications of LipoGlo thus extend well beyond the study of lipoprotein abundance, size, and localization using zebrafish.

LipoGlo assays show excellent concordance with existing methods

Atherogenic lipoproteins are the primary drivers of atherosclerotic cardiovascular disease, which has made lipoprotein profiling an essential technique in both clinical and research settings. Existing methods to characterize ApoB-LPs generally rely on large amounts of starting material (microliters of plasma), use indirect measurements (e.g. lipid profiling), require expensive equipment and specialized training (e.g. an ultracentrifuge or electron microscope), have a relatively low throughput capacity, and are restricted to studying plasma lipoproteins. The LipoGlo reporter circumvents all of these issues and engenders unprecedented speed, sensitivity, and tractability to the study of the lipoprotein profile. Importantly, the described assays show excellent concordance with traditional methods, as evidenced by the tight correlation between particle size estimates measured by LipoGlo electrophoresis and both density gradient ultracentrifugation and negative-staining electron microscopy.

One limitation of the LipoGlo electrophoresis method reported here is that it is unable to resolve ApoB-LPs above a certain size threshold, which are clustered together

as the zero-mobility fraction. Further research will be required to conclusively determine which lipoprotein species are present within this band. For example, the ZM band is highly enriched in response to a high-fat meal. This observation is consistent with enrichment of intracellular ApoB and the largest lipoprotein classes (chylomicrons and remnants), both of which should increase in response to high-fat diet. It is interesting to note, however, that when lipoproteins are processed through tandem density gradient ultracentrifugation and LipoGlo-electrophoresis, there is significant signal in the ZM fraction even in the higher density fractions. The presence of higher-density species in the ZM band indicates that it is not composed exclusively of triglyceride-rich lipoproteins. I suspect this may reflect the physiological level of lipoprotein aggregation, which has been implicated as yet another determinant of cardiovascular disease risk [252].

The larval zebrafish is a powerful new system to study lipoprotein biology

The LipoGlo system is significantly more sensitive than existing lipoprotein characterization assays. To illustrate this, I have performed extensive lipoprotein characterization on individual zebrafish larvae. A single larva contains approximately one-thousand times less plasma (nanoliters rather than microliters) than is traditionally used for lipoprotein profiling, yet this is more than enough material to run multiple LipoGlo assays. The larval zebrafish has been used extensively to study metabolic diseases including cardiovascular disease [253, 254], but the inability to characterize the atherogenic lipoprotein profile presented a significant limitation. LipoGlo enabled comprehensive characterization of the atherogenic lipoprotein profile throughout larval

development, and demonstrated that the canonical aspects of mammalian lipoprotein homeostasis are conserved in the larval zebrafish.

The larval zebrafish is also an unparalleled vertebrate system for high-throughput screening. The simple plate-based LipoGlo-counting method enables processing of tens of thousands samples a day, and is thus readily conducive to high-throughput genetic and small-molecule screening. LipoGlo-electrophoresis and imaging protocols can also achieve respectable throughput capacity on the order of hundreds of samples per day, and can thus be used as tractable secondary screening assays or for stand-alone small-scale screens. The confluence of LipoGlo and the zebrafish model system present a uniquely powerful opportunity to perform unbiased screens for novel modulators of ApoB-LPs, enabling unbiased discovery approaches to be applied to the field of lipoprotein biology.

Sensitive lipoprotein profiling may provide new insights into abetalipoproteinemia

Mutations in the *mtp* gene result in a severe reduction or complete lack of ApoB-LPs, a disease called abetalipoproteinemia. The mtp^{stl} allele studied contains a single missense mutation in a highly conserved residue (L475P) [49]. Although this is thought to result in production of a non-functional protein, a true null allele would be expected to result in a complete lack of ApoB-LPs. The mtp^{stl} homozygous mutants are unequivocally able to produce and secrete ApoB-LPs (although they are smaller and less abundant) early in development. These observations suggest that the mtp^{stl} allele is either a strong hypomorph, or that ApoB-LPs can be produced without the activity of Mtp. The complete lack of ApoB-LPs later in development occurs once rates of particle turnover and uptake begin to greatly exceed rates of production. This observation highlights the LipoGlo

system as a useful tool to study allelic series of *mtp*. By studying different alleles at the earliest stages of development when rates of lipoprotein turnover are low, it may be possible to distinguish between true null alleles and hypomorphic mutations with varying degrees of severity. Such information would be useful in predicting the outcome of different abetalipoproteinemia mutations in humans.

Additionally, *mtp*$^{-/-}$ mutants produce a distinct bimodal peak of small (LDL-like) ApoB-LPs (Fig. 3a-c). This pattern warrants further investigation, but may indicate that these alleles directly produce small lipoproteins from the YSL, which are subsequently lipolyzed to produce a second peak. Further study of *mtp* alleles may provide insight into the specific functional domains of MTP that regulate the size of nascent ApoB-LPs.

Organ-level changes in the distribution of ApoB-LPs

The distribution of atherogenic lipoproteins throughout an intact organism has not previously been reported. Several observations were in line with our expectations, in that lipoproteins were clearly visible in lipoprotein-producing tissues such as the liver, intestine, and yolk-syncytial layer. Lipoproteins were also evident throughout the circulatory system as expected. However, one of the most striking patterns of lipoprotein localization is the chevron pattern outlining the somites in the trunk region. I suspect this pattern may correspond to the myosepta [247], which include tendinous structures connecting the body segments and their associated lymphatic vessels [246]. Lipoproteins have previously been shown to accumulate in tendons in cases of severe hyperlipidemia [48], but these images suggest that an unexpectedly large fraction of ApoB-LPs localize to these structures in a normal physiological state. The physiological consequences of this

association are still unknown, but suggest that the pool of non-circulating ApoB-LPs cannot be ignored in studies of whole-body energy homeostasis.

In addition to this somite pattern, surprisingly strong LipoGlo signal was also observed in the central nervous system (both within the brain and spinal cord), colocalizing with the CNS marker *Tg(Xla.Tubb2:mapple-CAAX)*. While this pattern was evident throughout development, it was most pronounced in larvae that have low levels of atherogenic lipoproteins throughout the body (such as wild-type larvae at 6 dpf, or larvae that have been fasted or treated with lomitapide for 48 hours, Fig. 9d-f). The localization pattern observed is strikingly similar to that of fluorescein (a fluorescent dye) after it is injected into the larval zebrafish ventricle [255]. Previous work has shown that LDL is present in the embryonic cerebrospinal fluid of chick embryos. There LDL can interact with SCO-spondin protein that contains multiple LDL binding domains and forms the Reissner fiber, a protein fiber found in the central canal of all chordates [51]. In zebrafish embryos this fiber contributes to proper body axis formation [45]. Prior studies in mammals found that although the blood-brain barrier expresses the LDL-receptor, levels of ApoB within the cerebrospinal fluid are extremely low [256], suggesting that a role for ApoB-LPs in the CNS may be restricted to embryonic development. However, previous studies have not analyzed cerebrospinal fluid composition in response to fasting, as our results suggest that ApoB-LPs may be preferentially retained in the ventricle as a protected source of lipid during nutrient scarcity. Although significant colocalization with the spinal cord can be observed, it should be noted that a pair of parachordal vessels is closely associated with the spinal cord.

I also developed an orthogonal approach to monitor ApoB-LP localization *in vivo* using DiI, a fluorescent lipophilic dye routinely used to label lipoproteins. Both human and endogenous lipoproteins labeled with DiI can be monitored *in vivo*, and show effectively identical localization patterns to lipoproteins labeled with NanoLuc, thus validating the unexpected localization patterns discussed above. This labeling technique serves as an additional useful tool to monitor lipoprotein dynamics in zebrafish larvae.

Although atherogenic lipoproteins are most often studied in the bloodstream as a means of evaluating cardiovascular disease risk, lipoproteins interact with essentially every tissue in the body and are involved in numerous processes such as development [46], vision [47], angiogenesis [49], heart function [50], hematopoiesis [51], infection and immunity [52, 53], and disorders such as cancer [54], and diabetes [55]. LipoGlo is an essential tool for broadening the scope of atherogenic lipoprotein biology beyond the current focus on circulating particles.

Characterization of lipoprotein abnormalities in pla2g12b$^{-/-}$ mutants

Phospholipase A2 group XII B (*pla2g12b*) encodes a catalytically inactive member of the phospholipase gene family. Although the protein lacks catalytic activity and has no other known function, its high level of evolutionary conservation suggests it may have evolved a new function. Previous studies in mice have shown that disruption of *pla2g12b* results in decreased secretion of hepatic triglyceride and ApoB [257], as well as reduced levels of HDL-cholesterol [258], indicating that this gene may play a role in lipoprotein secretion. In LipoGlo assays, *pla2g12b*$^{-/-}$ mutant larvae exhibited significantly lower levels of ApoB at multiple stages, and show enrichment of visceral ApoB-NanoLuc levels, both of which are consistent with previously reported defects in lipoprotein

secretion [257]. However, evaluation of the lipoprotein size distribution in *pla2g12b*$^{-/-}$ mutants revealed bias towards production of small LDL-like particles, which has not been reported previously. Further investigation will be required to determine whether smaller ApoB-LPs are produced directly by the YSL/liver, or if the decreased ApoB-LP secretion results in rapid lipolysis of the few lipoproteins that are successfully secreted. As Pla2g12b modulates both lipoprotein size and number, variants in the *pla2g12b* gene may modulate risk for cardiovascular disease. Ongoing work is exploring both the mechanism of action of this poorly understood protein, as well as the greater physiological repercussions of this mutation.

Overview of present and future application of LipoGlo

Overall, this study provides several key insights. First, covalent tags to ApoB enable highly sensitive and specific monitoring of ApoB-LPs without disrupting lipoprotein homeostasis. Second, the larval zebrafish represents a powerful model to study ApoB-LPs, as developmental stages provide a highly reproducible pattern of nutrient availability and larvae show human-like responses to genetic, dietary, and pharmacological stimuli. Additionally, larval zebrafish have unparalleled tractability for genetic and small-molecule screening as well as whole-organism imaging, facilitating the application of these powerful discovery techniques to the field of lipoprotein biology. ApoB-LPs also show significant patterns of enrichment outside of the circulatory system (in association with the somite junctions and central nervous system), highlighting important unexplored aspects of extravascular ApoB-LPs. Lastly, *pla2g12b* is a highly conserved regulator of lipoprotein biogenesis that plays a central role in the regulation of

the lipoprotein size/subclass distribution. The LipoGlo system thus represents an essential toolset to expand our understanding of atherogenic lipoproteins and accelerate the discovery of new drugs to combat atherosclerotic cardiovascular disease.

Materials and methods

Zebrafish husbandry and maintenance

Adult zebrafish were maintained on a 14 h light – 10 h dark cycle and fed once daily with ~3.5% body weight of Gemma Micro 500 (Skretting USA). All genotypes were bred into the wild-type AB background. All assays were performed on larvae heterozygous for the ApoB-Nanoluc reporter unless otherwise noted. To monitor the wild-type lipoprotein profile throughout larval development, pairwise crosses were set up between wild-type AB adults and adults homozygous for the ApoB-NanoLuc reporter (*apoBb.1*$^{NLuc/NLuc}$). To characterize the lipoprotein profile of *mtp* mutant larvae [49], pairwise crosses were set up between *mtp*$^{stl/+}$ and *mtp*$^{stl/+}$; *apoBb.1*$^{NLuc/NLuc}$ adults. To characterize the lipoprotein profile of *apoC2* mutant larvae [226], pairwise crosses were set up between *apoC2*$^{sd38/sd38}$ and *apoC2*$^{sd38/+}$; *apoBb.1*$^{NLuc/+}$ adults and larvae positive for the NanoLuc reporter were selected for analysis. To characterize the lipoprotein profile of *pla2g12b* mutant larvae [250], pairwise crosses were set up between *pla2g12b*$^{sa659/sa659}$ and *pla2g12b*$^{sa659/+}$; *apoBb.1*$^{NLuc/+}$ adults. To evaluate association between the ApoB-LPs and the central nervous system, adults homozygous for the ApoB-NanoLuc reporter (*apoBb.1*$^{NLuc/NLuc}$) were crossed to adults heterozygous for the central nervous system marker *Tg(Xla.Tubb2:mapple-CAAX)*, and embryos were screened for mApple prior to fixation and mounting (unpublished reagent provided by the Halpern Lab, c583). As zebrafish sex cannot be determined during the larval stages, gender can be excluded as a variable. All procedures were approved by the Carnegie Institution Animal Care and Use Committee (Protocol #139).

Genome editing

Genome integration was achieved by co-injection of 500 pg of TALEN mRNA and 30 pg of donor plasmid into 1-cell stage embryos (Fig. 3a). Two pairs of TALENs were designed and cloned that target a BsrI restriction site just upstream of the endogenous stop codon of ApoBb.1 using the Mojo Hand design tool [259] and FusX assembly system [260]. TALENs were *in-vitro* transcribed using the T3 mMessage mMachine kit (ThermoFisher Scientific, AM1348) and injected into 1-cell stage zebrafish embryos. Cutting efficiency was quantified by monitoring the loss of BsrI digestion as a result of TALEN nuclease activity, and found to be significantly higher in TALEN pair 2, so this pair was used for genome integration efforts (Fig. 3b). A donor plasmid was cloned using 3-fragment MultiSite gateway assembly (Invitrogen, 12537-023) with a 5' entry element of ~500 bp of the genomic sequence upstream of the ApoBb.1 stop codon, a middle-entry element consisting of in-frame NanoLuc coding sequence, and a 3' element of ~700 bp of genomic sequence downstream of the ApoBb.1 stop codon [261]. Injected embryos were raised to adulthood and progeny were screened for NanoLuc activity and in-frame fusion of the NanoLuc reporter at the target locus (Fig. 3c).

Preparation and storage of larval homogenate

Individual larvae are homogenized in a standard volume of ApoB-LP stabilization buffer (100 μL). The ApoB-LP stabilization buffer (see recipes) contains cOmplete Mini, EDTA-free Protease Inhibitor Cocktail (Millipore-Sigma, 11836170001), pH buffer and calcium chelator (EGTA, pH 8), and cryoprotectant [262] (Sucrose) to preserve sample integrity during homogenization (Fig. 13). The buffer is made as a 2x stock, and larvae

are anesthetized in tricaine and placed into tubes in a 50 µL volume and an equal volume of chilled 2x buffer is then added just prior to homogenization. Low-throughput homogenization can be achieved in 1.5 mL centrifuge tubes with disposable pellet-pestles (Fisher scientific, 12-141-363). For high-throughput sample processing, larvae and ApoB-LP stabilization buffer are dispensed into individual wells of a 96-well non-skirted PCR-plate (USAScientific, #1402-9589), sealed with microSeal 'B' plate sealing film (Bio-Rad, msb1001), and homogenized in a microplate-horn sonicator (Qsonica, Q700 sonicator with 431MPX microplate horn assembly). For sonication, the plate was placed in the microplate horn filled with 17 mm of chilled RO water and processed at 100% power for a total of 30 seconds, delivered as 2-second pulses interspersed with 1-second pauses. Homogenate was stored on ice for immediate use, or frozen at -20° C and thawed on ice for later use.

Quantification of ApoB-NanoLuc levels using a plate reader

To quantify ApoB-NanoLuc levels, homogenate (40 µL) was mixed with an equal volume of diluted NanoLuc buffer (for specific dilution see recipes and technical note on NanoLuc buffer) in a 96-well opaque white OptiPlate (Perkin-Elmer, 6005290). Black plates can be used as an alternative that will significantly lower absolute signal intensity, but also reduce light contamination into adjacent wells. The plate was read within 2 minutes of buffer addition using a SpectraMax M5 plate reader (Moleculardevices) set to top-read chemiluminescent detection with a 500 ms integration time. This plate-based assay has a wide linear range and long half-life (Fig. 14a-c). However, degree of

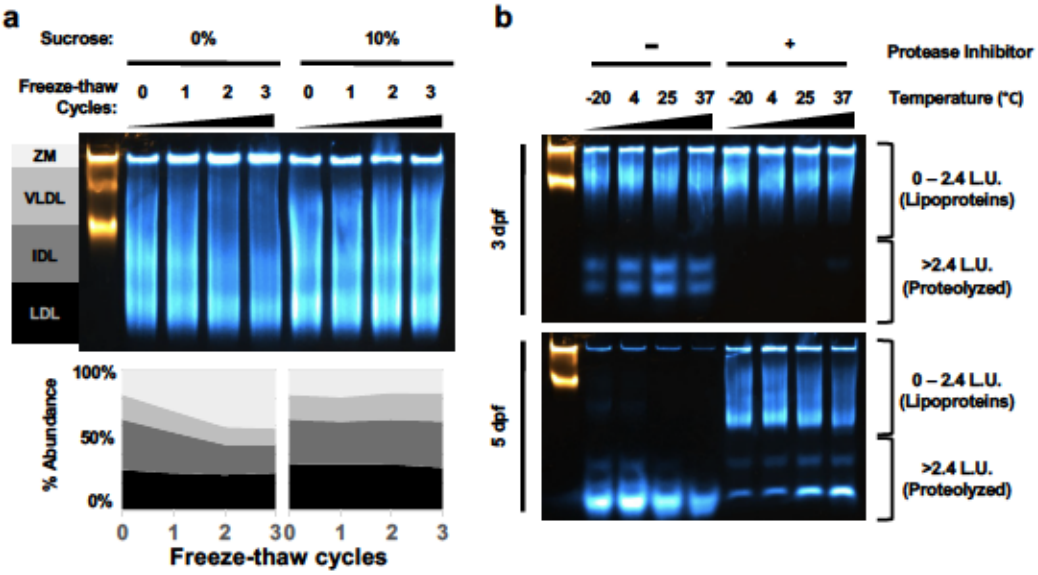

Figure 13: Cryoprotectant and protease-inhibition properties of ApoB-LP stabilization buffer. (a) 4 dpf wild-type larvae were homogenized in ApoB-LP stabilization buffer containing 0% or 10% final concentration of sucrose and subjected to between 0 and 3 freeze-thaw cycles, and then separated using native-PAGE as described in detailed methods. While the lipoprotein size distribution remained constant in samples containing sucrose as a cryoprotectant, samples without sucrose showed a gradual enrichment of ZM particles, which appears to be due to aggregation of VLDL and IDL particles. **(b)** Larvae were homogenized in ApoB-LP stabilization buffer with and without the protease inhibitor components (cOmplete mini EDTA-free tablet supplemented with 40 mM final concentration of EGTA, see recipes) and incubated at various temperatures for 2 hours. Samples were then separated by native-PAGE at 50 V for 30 minutes, and 125 V for 60 minutes. This is 125 Volt-hours less than described in detailed methods to enable visualization of proteolysis products. At 3 dpf, protease activity is quite low such that no proteolyzed products are present in the group treated with protease inhibitor, whereas degradation products are visible in a temperature-dependent manner in the absence of inhibitors. By 5 dpf, protease activity is much higher in the homogenate sample, presumably due to development of a mature intestine. Protease activity is still well-controlled in the presence of protease inhibitor at low temperatures, but in the absence of protease inhibitor degradation is so severe that there are signs of both cleavage of NanoLuc from the lipoprotein particle as well as proteolysis of the reporter itself.

pigmentation has a significant effect on signal intensity, so this variable should be accounted for with a standard curve or pigment-matched controls should be used as a baseline for comparison (Fig. 14d).

Quantification of lipoprotein size distribution with LipoGlo-electrophoresis

To quantify the electrophoretic mobility of ApoB-LPs, 3% native polyacrylamide gels were cast in Bio-rad mini-protean casting rigs using 1 mm spacer plates and 10-well combs (see recipes). Gels were allowed to polymerize overnight at 4°C and used within 24 h of casting. Each gel included a migration standard comprised of Di-I labeled human LDL (L3482, ThermoFisher Scientific) that was diluted in cryoprotectant and stored in frozen aliquots (see recipes). Gels were assembled into mini-protean electrophoresis rigs at 4°C, filled with pre-chilled 1x TBE and pre-run at 50 V for 30 minutes to equilibrate the gel prior to sample addition. 12 μL of homogenate was then combined with 3 μL of 5x load dye (see recipes), and 12.5 μL of the resulting solution was loaded per well (which corresponds to 10% of the larval homogenate per lane). Gels were then run at 50 V for 30 minutes, followed by 125 volts for 2 h.

Gels were imaged within 1 h of completion of the run. To image each gel, the thin glass short plate was carefully separated from the front of the gel with a gel releaser wedge (see technical note on hydrophobic coating of short plates). With the gel resting on the thick spacer plate, 1 mL of TBE supplemented with 2 μL of Nano-Glo substrate was gently pipetted onto the gel surface. The gel imaging solution was spread evenly across the gel surface with a thin plastic film cut to the size of the spacer plate (Staples, Sliding bar report covers). After a 5-minute equilibration, the gel was placed into an Odyssey Fc

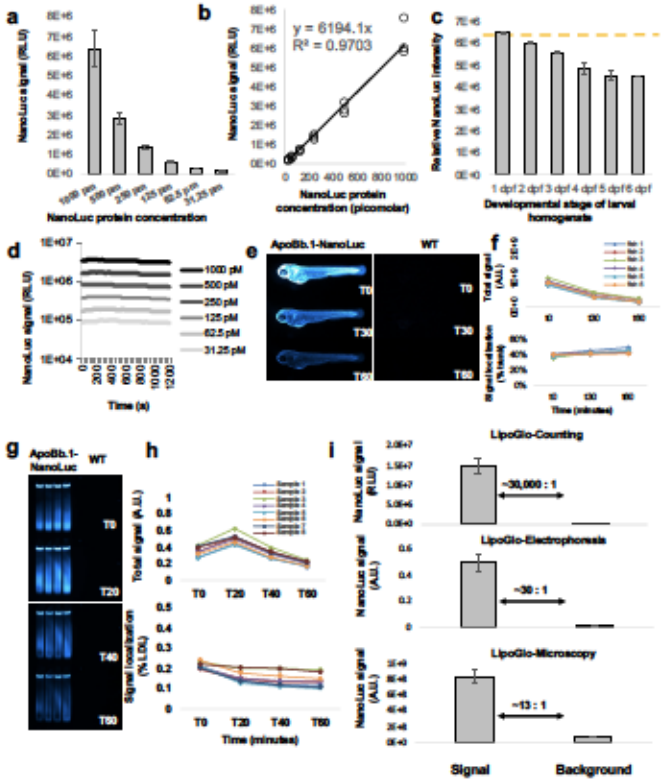

Figure 14: NanoLuc standard curves. (a) To determine the absolute concentration of ApoB-LPs in the larval homogenate, purified NanoLuc protein was ordered directly from Promega (Nluc-HT Protein, 500ug, 54.2KDa, #CS188401) and diluted to 1 nM working concentration in 1x ApoB-LP stabilization buffer. This solution was subjected to a 6-point series of 2-fold dilutions and used in a plate-based assay for NanoLuc activity, and **(b)** showed the expected log-linear relationship. **(c)** There is a marked increase in pigmentation throughout larval development, causing homogenate to become progressively more opaque. To test the effect of pigment on NanoLuc readings, wild-type larvae that lack the ApoB-NanoLuc reporter were homogenized in ApoB-LP stabilization buffer at each stage of development. This homogenate was then supplemented with a final concentration of 1 nM NanoLuc protein and subjected to a plate read assay. As expected, the relative intensity of NanoLuc signal declines from 2 – 6 dpf, indicating that absolute quantitation of NanoLuc levels should include a standard curve that accounts for larval pigmentation. **(d)** Analysis of LipoGlo counting signal over time (well values read every 40 seconds for 20 minutes) demonstrated that this assay is robust to slight fluctuations in incubation time, as signal half-lives were calculated to be greater than 60 minutes for all concentrations tested. **(e)** Analysis of LipoGlo microscopy signal over time revealed detectable signal well above background for over 60 minutes, and **(f)** although absolute signal declined over time (top panel), the signal localization remained relatively constant over short fluctuations in incubation time (bottom panel). **(g)** Analysis of LipoGlo electrophoresis signal over time **(h)** revealed that reads immediately after substrate addition (T0) were abnormally low (top panel) and biased toward detection of abundant lipoprotein species (bottom panel). However, following a brief incubation period (minimum of 5 minutes), absolute signal decays gradually over time, but changes in relative signal are much less pronounced (T20 – 60). **(i)** Quantification of the signal to background ratio of each of the LipoGlo assays.

(LI-COR Biosciences) gel imaging system (See technical note on gel imaging) and imaged in the chemiluminescence channel for 2 minutes (NanoLuc detection) and then the 600 channel for 30 seconds (Di-I LDL standard detection). Effort should be made to ensure a consistent equilibration time between substrate addition and gel imaging. While this assay is relatively robust to small variations in incubation time (Fig. 14g- h), equilibration times below 5 minutes or greater than 20 minutes are not recommended. Raw images were exported as zip files for further analysis.

The provided gel quantification template (Supplemental File 1) can be used to bin the complex lipoprotein size distribution into biologically relevant groups for analysis, and detailed instructions are provided within the supplemental file. In short, each lane was converted to a plot profile in ImageJ, and divided into LDL, IDL, VLDL, and ZM bins based on migration relative to the Di-I standard, and pixel intensity was summed within each bin for analysis.

Larvae fixation and imaging

To determine the whole-organism localization of ApoB-LPs, intact larvae are anesthetized and fixed in 4% PFA (diluted in PBS) for 3 h at room temperature. Following fixation, larvae are rinsed 3 times for 15 minutes each in PBS-tween (PBS containing 0.1% tween-20 detergent) and imaged within 12 h of fixation. Agarose for mounting is prepared by melting 0.1 grams of low-melting point agarose (BP160-100, Fisher Scientific) in 10 mLs of 1x TBE. Aliquots are maintained in the liquid state at 42°C in a heat block. Just prior to mounting, agarose aliquots were supplemented with 1% Nano-Glo substrate (furimazine). Fixed larvae are arrayed in droplets on a petri dish

lid, and the excess liquid is removed and quickly replaced with a 50 µL droplet of low-melt agarose containing Nano-Glo substrate (1%). The sample is then oriented properly with a flexible poker until the agarose solidifies sufficiently to hold the sample in place. This process was repeated for up to 15 larvae in parallel prior to imaging.
While the absolute intensity of NanoLuc signal will decay gradually over time (Supplementary Fig. 14e-f), the distribution of NanoLuc signal is relatively robust to slight variation in incubation time. Nonetheless, it is recommended that larvae be mounted and imaged with as consistent of an incubation period as possible (ideally less than 30 minutes).

To image the ApoB-LP localization, a Zeiss Axiozoom V16 microscope V16 equipped with a Zeiss AxioCam MRm was set to 30x magnification, 2x2 binning and 2x gain (to increase sensitivity), and programmed to collect a single brightfield exposure (2.4 ms, 10% light intensity) followed by two chemiluminescent imaging exposures (10 and 30 seconds, respectively) with no illumination to collect the NanoLuc signal (See technical note on NanoLuc imaging). Images were quantified in ImageJ by using the brightfield exposure to draw regions of interest (viscera, trunk, and head) and calculating the NanoLuc intensity within each of those ROIs for 30 second chemiluminescent exposure, unless saturated pixels were detected in which case the 10 second exposure was used.

Fluorescent labeling and imaging of APOB-LPs in vivo

For injection of human DiI-labelled LDL into zebrafish larvae, larvae were first anesthetized and mounted laterally in a petri dish in a 50 µL droplet of 1 % low-melt

agarose prepared in zebrafish embryo medium. After the agarose had solidified, forceps were used to remove a small portion of agarose just dorsal to the anterior portion of the yolk, providing an access window for injection. The petri dish was then filled with embryo medium to ensure that larvae did not dry out during injection and imaging. Human DiI-labelled LDL (L3482, Thermofisher Scientific) was then loaded into an microinjection needle and calibrated to an injection volume of 4 nL. Larvae were then injected into the common cardinal vein (CCV) through the agarose-free access window, or injected directly into the yolk. Larvae were imaged within 1 hour of injection, and then carefully liberated from the agarose using fine forceps.

For injection of DiI into the larval yolk, DiI (D282, ThermoFisher Scientific) was resuspended to 30 mg/mL in DMSO. This solution was then loaded into an injection needle and calibrated to 4 nL injection volume. 1 dpf was selected as an ideal time point for injection because at this stage the yolk is fully segregated from the embryo, yet the embryos are still within their chorions which eliminates the necessity for mounting in agarose prior to injection.

Larvae were then imaged on an SMZ25 microscope equipped with a Cy3 filter cube at 30x or 100x magnification. Larvae were imaged after being mounted in either 1% low-melt agarose (in the case of 2 dpf injections), or were anesthetized and imaged in 3% methylcellulose. Image brightness was adjusted arbitrarily in the display to ensure visibility of relevant structures.

DiI labeling of adult zebrafish plasma

Adult zebrafish were anesthetized and transferred to a dissection stage covered with a kimwipe moistened with anesthetic diluted in system water. Tails were then resected at the anterior of the anal fin to expose the caudal artery. An EDTA-coated capillary (ThermoFisher Scientific, 22-757-123) fitted on the end of a p20 pipette tip was used to slowly extract whole blood form the artery, and the fish was immediately euthanized in an ice bath following extraction. Blood was transferred to a 1.5 mL microcentrifuge tube and spun at 6,000 rcf for 5 minutes to pellet blood cells, and the resulting plasma was transferred to a new tube. The Plasma was then diluted ten-fold in a solution of ApoB-LP stabilization buffer containing 30 mg/mL DiI. This mixture was incubated at 37°C for two hours, and stored at 10°C overnight or used immediately for electrophoresis. 5 μL of the resulting stained lipoproteins were mixed with 45 μL of ApoB-LP buffer containing loading dye and 12.5 μL of the mixture was loaded onto a 3% native polyacrylamide gel. Native-PAGE and gel imaging were performed as described above for LipoGlo-electrophoresis.

Density-gradient ultracentrifugation

A density gradient ultracentrifugation (DGUC) protocol was developed by adapting previously published protocols using a 3-layer iodixanol gradient to function with smaller volumes of input sample [243]. Individual larvae were sonicated in 100 μL of sucrose-free ApoB-LP buffer (see recipes) to avoid disruption of the density gradient with sucrose. 15 larvae were pooled per experiment into a single 1.5 mL centrifuge tube and centrifuged for 5 minutes at 6,000 rcf to remove large cellular debris. 1 mL of the

resulting supernatant was transferred to a separate tube containing 500 µL of Optiprep Density gradient medium (D1556, Sigma-Aldrich) to yield a 20% iodixanol solution. A 9% iodixanol solution was prepared by adding 1.5 mL of Optiprep to a 15 mL conical tube containing 8.5 mL HEPES-buffered saline (HBS, see recipes), and a 12% solution was prepared by mixing 2 mL Optiprep with 8 mL HBS. A 4.9 mL Optiseal tube (formerly polyallomer, 362185, Beckman-Coulter) was then loaded with 1.5 mL of 9% iodixanol/HBS solution. This solution was carefully underlayered with 1.5 mL of the 12% iodixanol solution using a p1000 pipette fit with both the appropriate p1000 tip as well as a tapered gel loading tip which functioned as a disposable plastic cannula (USA Scientific, 1252-0610). Finally, these solutions were underlayered with 1.5 mL of the 20% iodixanol solution containing the zebrafish homogenate. The tube was then topped up with HBS (~500 uL) so that no air remained and sealed with a cap. Balanced tubes were then loaded into a VTi65.2 rotor and centrifuged at 60,000 rpm in a prechilled Beckman Optima XL 80K Ultracentrifuge set to 4°C with maximum acceleration and deceleration rates.

Following ultracentrifugation, density fractions were collected by carefully piercing the bottom of the tube with a thumbtack, and drip-eluting the samples into 10 separate fractions of approximately 500 µL each. The refractive index of each fraction was determined using a Bausch and Lomb refractometer, and used to calculate solution density using the formula density = 3.3508 x (refractive index) - 3.4675. Fractions were stored on ice or at 10°C, and used within 24 h for a plate-based NanoLuc assay, LipoGlo-electrophoresis, and negative-staining electron microscopy. Note that the high protein and

iodixanol content of fraction 1 (highest density) introduces artifacts in the native gel and was therefore excluded, which allowed lane 1 to be dedicated to the Di-I LDL standard.

Negative-staining electron microscopy

Fractions 4, 7, and 10 from the DGUC experiments outlined above were subjected to negative-staining electron microscopy [244]. 300-mesh copper grids coated with 10 nm formvar and 1 nm carbon (Electron Microscopy Sciences, FCF300-Cu) were ionized using the glow discharge filament in a Denton Vacuum dv-502 evaporator at 75 mTorr for 30 seconds. Anti-capillary forceps were then used to hold the grids in a humidified chamber, and 3 μL of the sample was carefully placed on the surface of the grid and incubated at room temperature for 10 minutes to allow the lipoproteins to adhere to the grid. The grid was then rinsed in 5 droplets of RO-water and then finally 2 droplets of 2% uranyl acetate, and touched lightly to a piece of filter paper to remove excess stain. Grids were imaged at 26,000x magnification on a Tecnai 12 transmission electron microscope.

Western Blotting

Protein extraction was performed on 10 pooled 3 dpf larvae per sample. Larvae were transferred to a 1.5 mL microcentrifuge tube, excess liquid was removed, and 100 μL of RIPA buffer containing 3x protease inhibitor cocktail was added. Larvae were immediately homogenized using a pellet pestle, and incubated at 4°C for 15 minutes with shaking. Samples were then centrifuged at 12,000 rcf for 5 minutes and the supernatant was mixed with an equal volume of 2x Laemmli buffer (BioRad, 1610737) and heated to 95°C for 5 minutes in a thermal cycler. DiI-LDL (L3482, Thermofisher Scientific) was

diluted 100-fold in RIPA buffer and extracted as above to be used as an indicator of the migration pattern of APOB, and Halo-Tagged NanoLuc protein (Promega, CS188401) was diluted 10,000-fold in RIPA buffer and used as an indicator of the migration of free NanoLuc protein. Precision Plus Protein All Blue Prestained Protein Standards (BioRad, 1610373) was used as a molecular weight marker.

25 µL of the resulting sample was loaded onto a precast 4-20% gradient gel (BioRad, 4561093) and separated at 70 V for 30 minutes and 90 V for 60 minutes. Proteins were then transferred to a PVDF membrane with the Trans-blot Turbo Transfer System (BioRad, 1704150) using a custom transfer program optimized to ensure transfer of high-molecular weight proteins (1.3 Amp constant for 15 minutes). The blot was blocked in 5% milk for 1 hour, and then probed simultaneously with primary antibodies binding NanoLuc (R&D Systems, MAB10026-100, 1:200 dilution) and human APOB (Meridian Life Sciences, K45253G, 1:200 dilution) for 4 hours at room temperature in 2.5% milk. The blot was then rinsed 3 times for 5 minutes each in TBST, and probed with fluorescent secondary antibodies (LICOR Biosciences, IRDye 800CW Donkey anti-Goat IgG, 925-32214, and IRDye 680RD Donkey anti-Mouse IgG, 925-68072, 1:5,000 dilution) for 1 hour at room temperature. The blot was then rinsed as above and imaged in the 700 and 800 nm channels for 2 minutes each using the Odyssey Fc (LI-COR Biosciences).

DNA extraction and Genotyping

Sonication of zebrafish larvae is a convenient method for highly-parallelized homogenization, as a full plate (96 samples) can be processed simultaneously. However,

this process shears DNA into significantly smaller fragments, meaning longer amplicons will amplify less efficiently or not at all. To circumvent this issue, genotyping protocols for this study were designed to use small amplicons (less than 350 bp). If intact DNA is needed for downstream applications, the pellet-pestle method can be used interchangeably with sonication.

DNA extraction of larval homogenate can be achieved with a modified version of the HotShot DNA extraction protocol [263]. 10 µL homogenate is transferred to a pcr tube/plate containing 10 µL of 100 mM NaOH, and heated at 95°C for 20 minutes. The solution was then neutralized with an equal volume (20 µL) of 100 mM Tris pH 8, and either stored frozen (-20 °C)or used immediately as a template for genotyping PCR (2 µL per reaction).

Genotyping was carried out using gene-specific primers (Table 1). The ApoBb.1-NanoLuc locus was genotyped using 3 primers with final concentrations as follows: 1µM primer 9, .2µM primer 10, and .8µM primer 11. This ratio provides similar band intensity for the 113 bp product indicating presence of the WT allele, and the 161 bp product indicating NanoLuc fusion allele (T_a = 57°C, extension time 20") in heterozygotes (only one band will amplify in homozygotes). The *mtp* genotyping locus was amplified using primers 12 and 13 (.5µM each, T_a = 60°C, extension time 30"), and digested with 3 units of AvaII restriction enzyme, which cuts the mutant (*stlI)* allele. Wild-type zebrafish should have a single 157 bp band, homozygous mutants should have a shorter 129 bp band, and heterozygotes should have both bands present (note the 28 bp fragment is not usually detectable). The *apoC2* genotyping locus was amplified using primers 14 and 15 (.5µM each, T_a = 57°C, extension time 30"), and digested with 3 units

Primer #	Purpose	Sequence
1	generate pME NanoLuc F	GGG GAC AAG TTT GTA CAA AAA AGC AGG CTT GAT GGT CTT CAC ACT CGA AGA TTT C
2	generate pME NanoLuc R	GGG GAC CAC TTT GTA CAA GAA AGC TGG GTT TAC GCC AGA ATG CGT TCG CA
3	generate left homology arm F	GGG GAC AAC TTT GTA TAG AAA AGT TGC GCT GCC TGG AAT GAA TGA AGC
4	generate left homology arm R	GGG GAC TGC TTT TTT GTA CAA ACT TGT CTG GAA AAA TGG GAG AGG AAG
5	generate right homology arm F	GGG GAC AGC TTT CTT GTA CAA AGT GGA ATA TGG TCA TTC TGA ACA GAA AGT AAA
6	generate right homology arm R	GGG GAC AAC TTT GTA TAA TAA AGT TGG GTA AGG CAG ACA TCA GTT TGT AAG
7	test TALEN cutting efficiency F	TGC AAT GAA GCA AAT CGA AAG TC
8	test TALEN cutting efficiency R	AAG ATT GGG TCG TGT TGC AT
9	genotype LipoGlo F	GCT TCC TCT CCC ATT TTT CC
10	genotype LipoGlo R1	CCC CGA GAT TCT GAA ACA AAC
11	genotype LipoGlo R2	AAG TGT CCA TTG GCT TCG AT
12	genotype mtp F	GTC TGA GGT TCA GAT GTA CCT GTT AGG AC
13	genotype mtp R	CTC TGC TGT GAT GAG CGC AGG
14	genotype apoc2 F	GAG CGG AGA GCT TTC GTG T
15	genotype apoc2 R	CTT CCA GCT TGT AGC CCT TG
16	genotype pla2g12b F	ACA AGG GAA AGC AAA CCA AA
17	genotype pla2g12b R	CAG TGT TGT ACA TGG TGT CTG C

Table 1:
Primers and plasmids used in this study.

of BtsαI restriction enzyme, which cuts the WT allele but not the sd38 mutant allele. Wild-type zebrafish should have 102 and 45 bp bands, homozygous mutants should have a single 147 bp band, and heterozygotes should have all 3 bands present. The *pla2g12b* genotyping locus was amplified using primers 16 and 17 (.5μM each, $T_a = 57°C$, extension time 30"), and digested with 3 units of BtsαI restriction enzyme, which cuts the mutant (sa659) allele. Wild-type zebrafish should have a single 150 bp band, homozygous mutants should have a shorter 111 bp band, and heterozygotes should have both bands present (note the 39 bp fragment is not usually detectable).

Technical notes and troubleshooting

NanoLuc Buffer

The NanoLuc enzyme is active in various buffers, but the key consideration is to ensure that substrate is in excess. Manufacturer's instructions dictate that 1 mL of Buffer plus 20 μL of substrate solution constitutes a 2x buffer, but we have found that this 2x buffer can be diluted 4-fold in PBS and the substrate remains in significant excess.

Hydrophobic coating of LipoGlo-electrophoresis plates

The most likely source of artifacts in the LipoGlo-electrophoresis protocol are from stretching or distortion of the fragile 3% polyacrylamide gel while removing the short plate from the gel. To circumvent this issue, the short plates were coated on both sides with Rain-X original glass water repellent (Rain-X, 3.5 oz. bottle). This hydrophobic coating greatly facilitates removal of the short plate while leaving the undistorted gel resting on the spacer plate. This coating is semi-permanent, so it is

recommended that a set of coated short plates be dedicated for this purpose and reapplied with coating as needed.

This hydrophobic coating also reduces friction between the short plate and the spacer plate, so it is important that the plates are aligned properly in the casting frames and placed very gently in the casting stands. Too much pressure from the casting stand can cause the plates to slide out of alignment and lead to leaking during casting.

Imaging of LipoGlo-electrophoresis gels

The Odyssey Fc offers sensitive signal detection as well as multi-color detection, and is therefore ideal for imaging lipoprotein gels. However, if this equipment is not available, alternative gel imaging systems or a sensitive camera are capable of imaging the gel as well, as the chemiluminescent signal should be detectable by essentially any detector although the exposure time may need to be increased to the order of minutes depending on the sensitivity of the detector. If simultaneous imaging in chemiluminescent and fluorescent channels is not available, a large aliquot of zebrafish homogenate (such as 6 dpf larvae) can be pooled, aliquoted, frozen, and used as an alternative migration normalization standard.

NanoLuc imaging

Essentially all background signal in this imaging paradigm comes from two sources: electrical noise from the camera, and light contamination from the environment. Camera noise can be attenuated by using an actively cooled camera and by enabling a blank-subtraction setting to eliminate hot pixels. To reduce contaminating light from the

environment, we recommend collecting images in a dark room and shrouding the stage and/or microscope to prevent light from reaching the imaging path. Additionally, we have found that the Zeiss Axiozoom V16 contains infrared emitters and detectors within the imaging path, which result in very high background when long exposures are used. To overcome this issue, we placed a Zeiss BG40 IR blocking filter in front of the camera which effectively filtered the contaminating infrared light.

Solutions/Recipes

ApoB-LP Stabilization Buffer (2x): For routine preparation of zebrafish homogenate

1 CoMplete mini protease inhibitor tablet

400 µL .5M EGTA (pH8)

1g Sucrose

Adjust volume to 5 mL with reverse osmosis (RO) water

Sucrose-free ApoB-LP Stabilization Buffer (2x): For preparation of zebrafish homogenate for ultracentrifugation

1 CoMplete mini protease inhibitor tablet

400 µL .5M EGTA (pH8)

Adjust volume to 5 mL with RO water

Diluted NanoLuc Buffer (2x): For plate-based measurement of NanoLuc activity

1 mL Nano-Glo buffer

3 mL PBS

20 µL NanoLuc Substrate (furimazine solution)

3% Native Polyacrylamide gels (32 mL, ~4 mini gels): For LipoGlo-electrophoresis of ApoB-LPs from larval homogenate

22.9 mL RO water

6.4 mL 5x TBE

2.4 mL 40% 19:1 polyacrylamide:bis

→De-gas under vacuum for 30 minutes

250 µL 10% APS

20 µL TEMED

→quickly mix by gentle inversion and transfer to casting plates

Di-I LDL Lipoprotein migration standard: For normalization of electrophoretic mobility in Ladder Units

200 µL DiI LDL (L3482, Thermofisher Scientific)

4 mL 1x TBE

.48 g sucrose (for 10%)

Adjust final volume to 4.8 mL with TBE

→Divide into 50 µL aliquots and store at -80°C

5x loading dye: For loading homogenate into LipoGlo-electrophoresis gels

4 g sucrose

25 mg bromophenol blue

Adjust to 10 mL with TBE

Gel imaging solution (1 gel): For in-gel chemiluminescent imaging of NanoLuc

1 mL TBE

2 μL furimazine substrate

Mounting and Imaging solution (1 mL, ~20 larvae): For imaging of ApoB-LP distribution in intact larvae

.1g low-melt agarose

10 mL 1x TBE

→heat in microwave (5-15 seconds) and swirl until dissolved

→Distribute to 1 mL aliquots in 42°C heat block

Add 10 μL furimazine to 1 mL liquid agarose just prior to mounting

HEPES-Buffered Saline: For establishing density gradient for ultracentrifugation

.85g NaCl

10 mL 1M HEPES buffer (pH 7.4)

90 mL RO water

RIPA buffer (15 mL): For homogenization of zebrafish larvae for western blotting

1.5 mL 10% NP-40

1.5 mL Sodium Deoxycholate

1.5 mL 10% SDS

2.25 mL of 1 M NaCl

1.5 mL .1 M Sodium Phosphate

.3 mL .1 M EDTA

1.8 mL PI cocktail (1 tablet dissolved per mL water)

75 µL 200 mM PMSF

150 µL 100 mM Sodium Orthovanadate

5.8 mL RO water

Quantification and statistical analyses

All datasets were initially subjected to Levene's test for homogeneity of variance. For datasets with a single factor and uniform variance, a one-way ANOVA was used to test for a main effect, and Tukey's HSD was used for *post hoc* testing. If variance was not uniform (Levene's <.05), Welch's ANOVA with a *post hoc* Games-Howell test was used as these tests are robust to the assumption of unequal variance. For two-factor datasets, the Robust Two-Factor ANOVA was used with a *post hoc* Games-Howell test. * denotes $p<.01$, ** denotes $p<.001$, and *** denotes $p<.0001$. For LipoGlo-electrophoresis experiments, statistical tests were run independently for each of the four groups of binned data (ZM, VLDL, IDL, and LDL). In this case, Bonferroni correction was used to adjust for multiple comparisons (corrected significant $p<.0125$). Bonferroni correction was also applied to the LipoGlo-Microscopy experiments which are binned into three groups, so a significant threshold was set at $p<.017$. All statistics were run using XLSTAT, with the exception of the Robust Two-Factor ANOVA which was executed in R using the

pbad2way function in the WRS2 package (https://cran.r-project.org/web/packages/WRS2/index.html).

One of the strengths of a chemiluminescent reporter is that it has excellent signal to background ratios. In our hands, the signal to background ratio varies significantly between assays, reaching approximately 300,000:1 in plate-based assays, 30:1 in gel-based assays, and 13:1 in microscopy assays (Supplementary Fig. 14i). Blank subtraction was therefore not performed for the above analyses, as it was found not to have an impact on the results. This is likely due to the fact that background signal is negligible in the plate-based assays, and the remaining assays not only have very low levels of background signal, but are also quantified in terms of relative (rather than absolute) signal and thus less susceptible to skewing from the background signal.

CHAPTER 4 –PLA2G12B MEDIATES LIPIDATION OF NASCENT LIPOPROTEINS

Abstract

Serum levels of triglyceride-rich lipoproteins (TRLs) are one of the strongest determinants of cardiometabolic disease risk. While many proteins are known to be involved in the breakdown and turnover of TRLs in the plasma, far fewer have been identified that contribute to TRL biogenesis. Nascent TRLs have long been thought to fuse with lipid droplets present in the ER lumen (ER-LDs), but no genes involved in this process have yet been identified. Here I provide evidence that Phospholipase A2 Group 12B (Pla2g12b) may serve as the molecular scaffold that mediates fusion between lumenal lipid droplets and nascent lipoproteins. I show that in the absence of functional Pla2g12b protein, abnormally small lipid-poor TRLs are secreted and high numbers of ER-LDs accumulate in lipoprotein-producing tissues. Pla2g12b has been shown not to bind or cleave phospholipid substrates *in vitro* owing to mutations in the catalytic site, suggesting it may act through phospholipase-independent mechanisms. A mutation series was used to identify essential residues within the protein, revealing two distinct functional domains that may represent the TRL and ER-LD interacting surfaces. Further efforts to characterize the interacting partners of Pla2g12b are currently underway with the intention of identifying additional proteins involved in TRL biogenesis.

Introduction

Triglyceride-rich lipoproteins (TRLs) are micelle-like particles that serve to shuttle hydrophobic lipids throughout the circulation [5]. Chylomicrons secreted by the intestine are the largest class of TRLs, and are partially digested by lipases in the circulation (lipolysis) before being taken up by the liver through receptor-mediated endocytosis [264]. The liver produces a smaller class of TRLs called very-low-density lipoproteins (VLDL), which are lipolyzed by the same circulating lipases to progressively smaller lipoproteins including low-density lipoproteins (LDL). TRLs have been extensively studied not only for their essential role in lipid transport, but also for their contribution to cardiometabolic disease [18]. Collectively, TRLs and their derivates are considered the atherogenic lipoproteins, as they contribute directly to the formation of fatty streaks in the arterial wall [19]. Accordingly, levels of cholesterol, triglycerides, and protein carried by the atherogenic lipoproteins constitute three of the strongest risk factors for developing cardiovascular disease [39, 218, 219].

The biogenesis of TRLs begins with the synthesis of an obligate structural protein called Apolipoprotein-B (ApoB) [12]. This large amphipathic protein serves as the scaffold for assembly of lipoprotein particles, and also serves as the binding domain for numerous cofactors and receptors involved in TRL processing [11]. As ApoB is translated and translocated to the ER-lumen, neutral lipids are also synthesized between the inner and outer leaflets of the ER membrane [56]. The enzyme Microsomal Triglyceride Transfer Protein (MTP) then transfers both triglyceride and phospholipid from the ER-membrane to the lipid-binding pocket of ApoB, forming a nascent TRL

[237]. In the absence of MTP activity or sufficient lipid availability, the hydrophobic domains of ApoB remain exposed and the protein is rapidly degraded by the ER-associated degradation (ERAD) pathway [232].

The steps following this initial lipidation remain poorly understood. Two competing but non-exclusive models have been proposed to explain the subsequent lipidation and expansion of nascent TRLs. One model involves the continued action of MTP to transfer lipid directly from the ER-membrane to the TRL [265]. The second model involves the fusion of nascent TRLs with lipid droplets in the lumen of the endoplasmic reticulum (ER-LDs), with each fusion event contributing a large bolus of lipid to the TRL [63, 64]. However, aspects of these models remain unclear or untested.

Firstly, there are no known markers or regulators of ER-LDs. They are thought to form when MTP uses lipid from the ER to generate an ApoB-free lipid droplet within the ER lumen [62]. However, as both cytoplasmic lipid droplets and lumenal TRLs require additional proteins (such as perilipins and apolipoproteins) [60, 61], it is likely that additional proteins are required to regulate ER-LD formation that have not yet been identified.

Additionally, it is unclear how ER-LD fusion with nascent TRLs is regulated. The consistency of TRL production within the same tissues implies there are mechanisms in place to regulate ER-LD size and catalyze fusion with nascent TRLs. By contrast, TRLs produced by the intestine are vastly different sizes than those produced by the liver [5]. This observation further supports the existence of regulatory mechanisms that are tuned differently between tissues. While there is strong evidence for fusion between nascent chylomicrons and ER-LDs in enterocytes [266, 267], evidence that this process also

occurs in hepatocytes to form VLDL is largely speculative. The ER-LD fusion pathway may therefore only be active in tissues producing extremely large lipoproteins.

Lastly, it is also unknown how lipids synthesized in the ER membrane are partitioned between their many potential fates. A generally accepted model posits that lipid droplets form by growing a lipid lens in the ER that subsequently buds off into the cytoplasm [57]. Neutral lipids can bud off of the cytoplasmic leaflet of the ER to form cytoplasmic lipid droplets, or bud off of the lumenal leaflet with the help of MTP to form either TRLs or ER-LDs. While it has been proposed that enzyme topology may play a role in channeling lipid towards the lumenal or cytoplasmic leaflets [61, 268], this mechanism cannot explain partitioning between ER-LDs and nascent TRLs, as both are thought to depend on MTP activity. Depletion of ApoB is currently the only known mechanism to promote formation of ER-LDs, but it is unclear whether ApoB depletion favors partitioning of lipid into ER-LDs, or if ER-LDs accumulate when they are not cleared by nascent TRLs.

I have discovered that Phospholipase A2 Group 12B (Pla2g12b) is required for efficient secretion of triglycerides from the zebrafish yolk-syncytial layer (YSL). An analogous phenotype has been observed in the mouse liver [258], as *Pla2g12b*$^{hlb218/hlb218}$ mutant mice develop hepatic steatosis and increased levels of hepatic ApoB, and lower levels of serum ApoB, consistent with defects in VLDL secretion [257]. The sa659 variant in zebrafish results in loss of an essential splice site and an approximately 3-fold reduction in transcript levels, likely as a result of nonsense-mediated decay. My analysis of homozygous mutant zebrafish (*pla2g12b*$^{sa659/sa659}$) revealed an almost identical phenotype, with drastic lipid accumulation and defects in lipoprotein secretion from the

yolk-syncytial layer, the embryonic structure responsible for VLDL production. Interestingly, analysis of the lipoprotein size distribution in Pla2g12b$^{sa659/sa659}$ mutants revealed significant enrichment of abnormally small lipoproteins, and an almost complete lack of VLDL particles (see chapter 3).

However, no mechanism has yet been proposed to account for the effect of Pla2g12b on VLDL metabolism. Unlike other members of the phospholipase A2 gene family, pla2g12b harbors several mutations in the phospholipase active site that would render it catalytically inactive against phospholipid substrates [230]. This observation was confirmed by Rouault et al., 2003, where PLA2G12B could not bind or cleave phospholipids *in vitro*. Despite the loss of catalytic activity, PLA2G12B is highly conserved across vertebrates, suggesting it may have evolved a new function independent of its ancestral role as a phospholipase. Studies in mouse have shown that *pla2g12b* expression is regulated by multiple transcription factors that regulate lipid metabolism, including HNF4a, FXR, and ERRγ, further implicating it as a conserved regulator of TRL metabolism [257, 269, 270].

Here I provide evidence that Pla2g12b (a protein with no previously known function) is involved in the fusion between nascent TRLs and ER-LDs. Future studies will use *pla2g12b* as a starting point to identify other proteins involved in the regulation of TRL biogenesis.

Results

Pla2g12b is highly conserved across the vertebrate lineage

Syntenic and phylogenetic analyses of the *pla2g12b* gene revealed that there is a single ortholog in every major vertebrate lineage (Fig. 1a). This high degree of evolutionary conservation implies that *pla2g12b* plays an important role in vertebrate physiology despite its loss of phospholipase activity. The closely related gene *pla2g12a* is similarly conserved, present in all major lineages except the basal hagfish group (Fig. 1a).

Alignments of the amino acid sequences between Pla2g12b and Pla2g12a revealed a strikingly high level of conservation, both between these two genes and across species (Fig. 1b). Approximately 50% of residues are identical between human and zebrafish pla2g12b despite approximately 450 million years of divergence. Interestingly, ~40% of residues are identical between Pla2g12a and Pla2g12b, indicating that a relatively small number of residue changes are responsible for the functional difference between these proteins.

Pla2g12b is expressed in lipoprotein producing tissues

Previous studies have used northern blotting to determine the tissue distribution of pla2g12b transcripts [230]. In humans, *pla2g12b* is most highly expressed in the liver and small intestine, but also shows significant expression in the kidney. In mouse, *pla2g12b* is expressed most highly in the liver and intestine, with some detectable expression in the prostate.

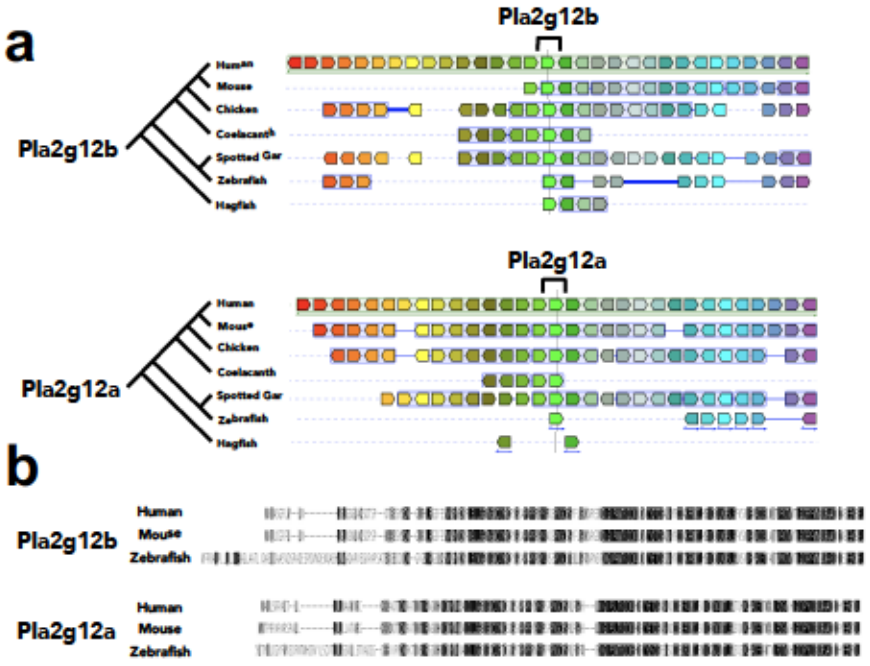

Figure 1: Evolutionary relationships between group 12 *PLA2* genes. (a) Syntenic analysis shows that a single *PLA2G12B* ortholog (bright green blocks) is present in the genomes of all vertebrates. By contrast, *PLA2G12A* is present in all vertebrates with the exception of the basal hagfish group. **(b)** Alignment of the amino acid sequences of PLA2G12A and PLA2G12B in human, mouse and zebrafish, with amino acids color-coded by similarity.

Whole-mount *in situ* hybridization with antisense riboprobes was performed to characterize the expression pattern of *pla2g12b* in larval zebrafish (Fig. 2a). Consistent with mammalian studies, strong expression was observed in the liver and intestine. Prior to development of the liver and intestine, strong signal is detectable in the YSL, which packages lipids from the maternal yolk into triglyceride-rich lipoproteins [82, 151]. Taken together, these findings suggest that pla2g12b is primarily expressed in known lipoprotein-producing tissues.

Pla2g12b protein is likely retained in the endoplasmic reticulum

Pla2g12b is a member of the secreted phospholipase A2 gene family (sPLA2) [271]. As their name implies, all members of this gene family encode proteins that are secreted into the circulatory system where they serve to cleave phospholipids in the circulation or in distal tissues, or perform other non-canonical functions such as interaction with signaling receptors [271, 272].

Analysis of the Pla2g12b amino acid sequence revealed a canonical signal peptide at the amino terminus in all species, which is a central hallmark of secreted proteins (Fig. 2b). However, the carboxy terminus of the protein also appears to harbor a KDEL signal (Fig. 2c). This amino acid motif interacts with KDEL receptors in the cis-golgi, which serve to traffic their ligands back to the ER [273]. The presence of a KDEL motif generally indicates that the protein serves as an ER-resident chaperone protein, responsible for the maturation of secreted proteins rather than being secreted itself. Zebrafish and Spotted Gar, both ray-finned fishes, have canonical KDEL motifs at the C-

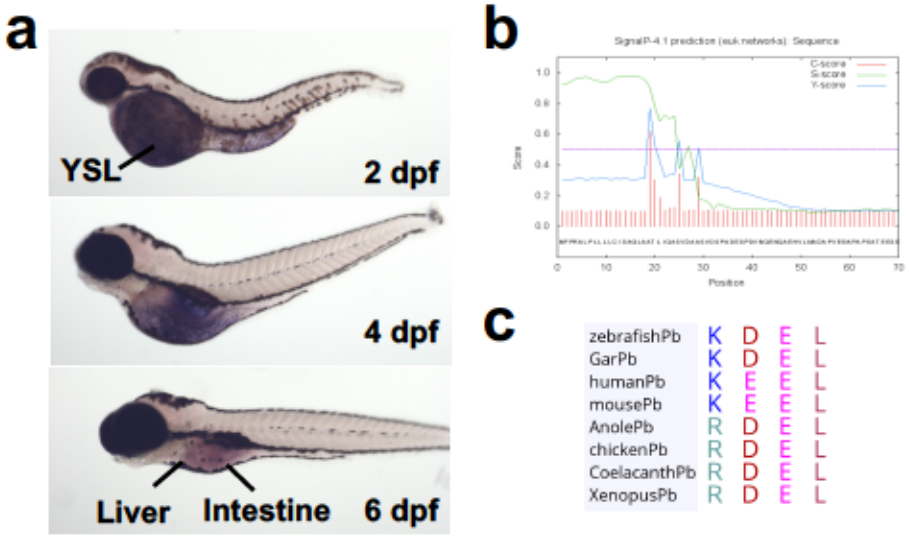

Figure 2: Localization of *pla2g12b* expression. (a) *In situ* hybridization with antisense riboprobes reveals expression in the embryonic yolk-syncytial layer (YSL), as well as the liver and intestine. **(b)** Signal peptide prediction software shows a high probability of a signal peptide at the amino terminus of Pla2g12b. **(c)** Alignment of the four terminal amino acids in various species reveals a canonical KDEL in ray-finned fishes (zebrafish and spotted gar), while many other species harbor atypical KDEL sequences with single amino acid differences.

termini of Pla2g12b. However, the additional species studied have a variety of non-canonical KDEL motifs, but each only harbors a single amino acid change.

The Protein Atlas [274] was used to determine the localization pattern of PLA2G12B in human tissues, which corresponded closely to the expression pattern of *pla2g12b* mRNA (expressed in the liver, intestine, and kidney). Further, the Human Plasma Peptide Atlas [275] was queried for the presence of PLA2G12B, and it was found to be nearly undetectable (.057 peptide spectrum matches per 100K). Western blots are currently being performed on mouse and zebrafish to evaluate the relative distribution of plasma and intracellular PLA2G12B in these species.

Pla2g12b mutants have a dark-yolk phenotype

Larval zebrafish homozygous for the *pla2g12b* sa659 allele were imaged by light microscopy from 1-6 dpf alongside wild-type controls. The mutants appear morphologically normal until approximately 3-4 dpf, when the yolk begins to appear darkened or opaque in contrast to the translucent yolk of wild-type larvae (Fig. 3a). By 6 dpf, the yolk has been completely processed and absorbed in wild-type animals. *Pla2g12b*$^{sa659/sa659}$ mutants retain a large portion of opaque, unprocessed yolk but otherwise appear overtly morphologically normal. A similar phenotype was previously observed in response to genetic mutation or pharmacological inhibition of MTP (an essential cofactor of TRL biogenesis) [49], but the etiology of this phenotype is unknown.

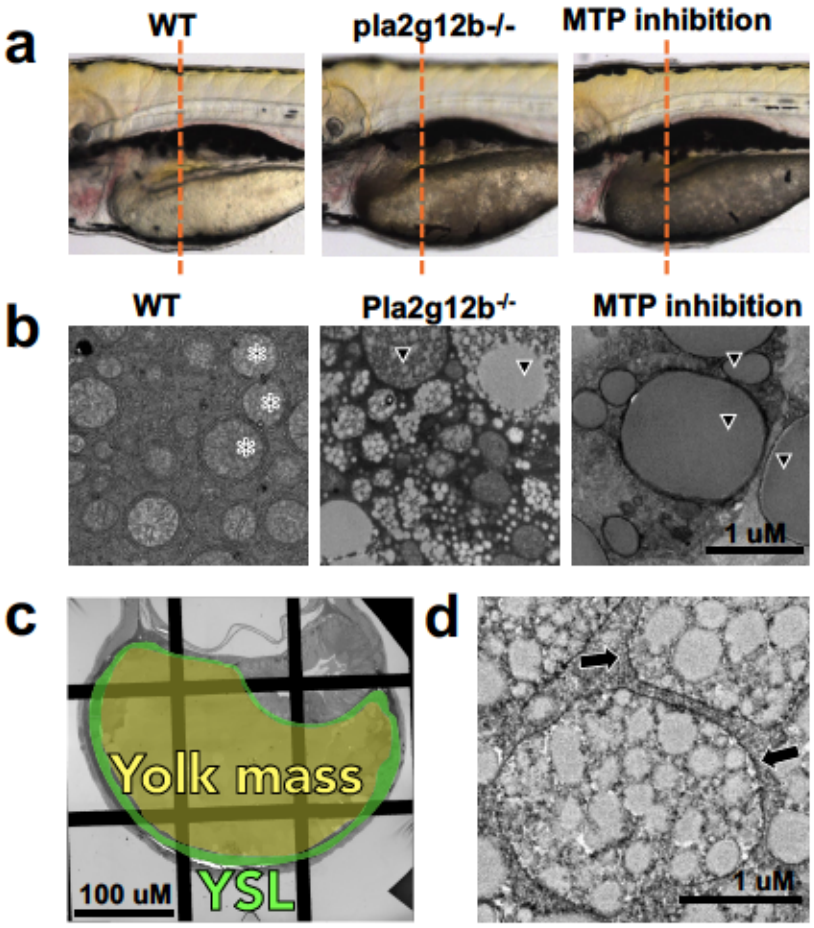

Figure 3: Characterization of abnormalities in the YSL of pla2g12b mutants. (a) Brightfield images depicting dark yolks in *pla2g12b* mutants, as well as wild-type larvae treated with lomitapide, an inhibitor of MTP. **(b)** Electron micrographs of the YSL taken from larvae depicted in panel A above, showing that the cytoplasm of the YSL in wild-type larvae is dominated by mitochondria (several are marked with asterisks). By contrast, significant lipid accumulation is apparent in the YSL of larvae with dark yolks (several lipid droplets marked with arrowheads). **(c)** Pseudo-colored low-magnification electron micrograph the larval cross sections highlighting structures of interest. **(d)** Additional micrograph of the YSL of a *pla2g12b*$^{-/-}$ mutant stained with the Kellenberger method to improve resolution of lipid membranes (marked with arrows), which can clearly be seen surrounding lipid droplets.

Pla2g12b mutants accumulate ER-lumenal lipid droplets in the YSL

Electron microscopy was used to investigate the cytological changes in the YSL underlying the dark-yolk phenotype. Four days post-fertilization was selected as an ideal stage for imaging, as this is the earliest timepoint where yolk darkening was readily apparent. Homozygous mutants (pla2g12b$^{sa659/sa659}$), wild-type controls (pla2g12b$^{+/+}$), and wild-type larvae treated with lomitapide to inhibit MTP were examined.

Larvae from each group were fixed, stained with osmium tetroxide, sectioned, and imaged on a Tecnai 12 transmission electron microscope first at low magnification, and then at high magnification focusing on the YSL (Fig. 3c). The YSL of wild-type larvae is characterized by numerous mitochondria that are frequently surrounded by an ER compartment (Fig. 3b). In larvae treated with lomitapide, the YSL accumulates large cytoplasmic lipid droplets. However, in the *pla2g12b*$^{sa659/sa659}$ mutants the YSL is dominated by a large number of small lipid droplets that appear clustered together, as if bounded by a membrane. To evaluate whether these small lipid droplets were indeed bound by a membrane, an alternative staining method optimized for visualization of lipid membranes (Kellenberger staining) was used. This protocol clearly shows that the lipid droplets are bound by a membrane (Fig. 3d arrowhead) .

An allelic series identifies at least two neo-functionalized domains in Pla2g12b

All vertebrate Pla2g12b proteins have lost the essential residues required for phospholipase activity, so it is unclear which residues or domains of pla2g12b are essential for protein function. To identify functional domains of the protein, a rescue

paradigm was designed that focused on identifying the residues and domains that had evolved new function (neo-functionalized) [276].

First, a rescue plasmid was generated that contains a YSL-specific promoter that drives expression of wild-type pla2g12b (Fig. 4a). This plasmid includes the endogenous *pla2g12b* UTRs, an in-frame FLAG-tag just downstream of the signal peptide, and a GFP marker designed to be expressed off of the same transcript using an internal ribosome entry site (IRES). Injection of this plasmid into homozygous pla2g12b mutants was able to completely rescue the dark-yolk phenotype, and fluorescence microscopy confirmed that this rescue construct was expressed exclusively in the YSL (Fig. 4b).

The protein sequence of pla2g12b was analyzed to identify potentially functional residues. We hypothesized that residues essential for the function of Pla2g12b would share two properties: first, they should be highly conserved in Pla2g12b sequences across different species, and second, that they should be different than ancestral residues found in pla2g12a. To identify residues conserved across species, the amino acid sequences of zebrafish, mouse, and human Pla2g12b were aligned, which identified 121 amino acid positions that were identical between all three species. To identify the subset of residues that were different between Pla2g12b and Pla2g12a, the pla2g12a amino acid sequences from zebrafish, mouse, and human were added to the alignment. Of the 121 residues conserved in Pla2g12b, only 44 were different from the aligned pla2g12a residues. These 44 residues were classified as the putatively neo-functionalized residues, or those that are most likely to be responsible for the novel function of pla2g12b.

The 44 putatively neofunctionalized residues were grouped into 15 blocks of adjacent residues for functional testing. Site-directed mutagenesis was then performed on

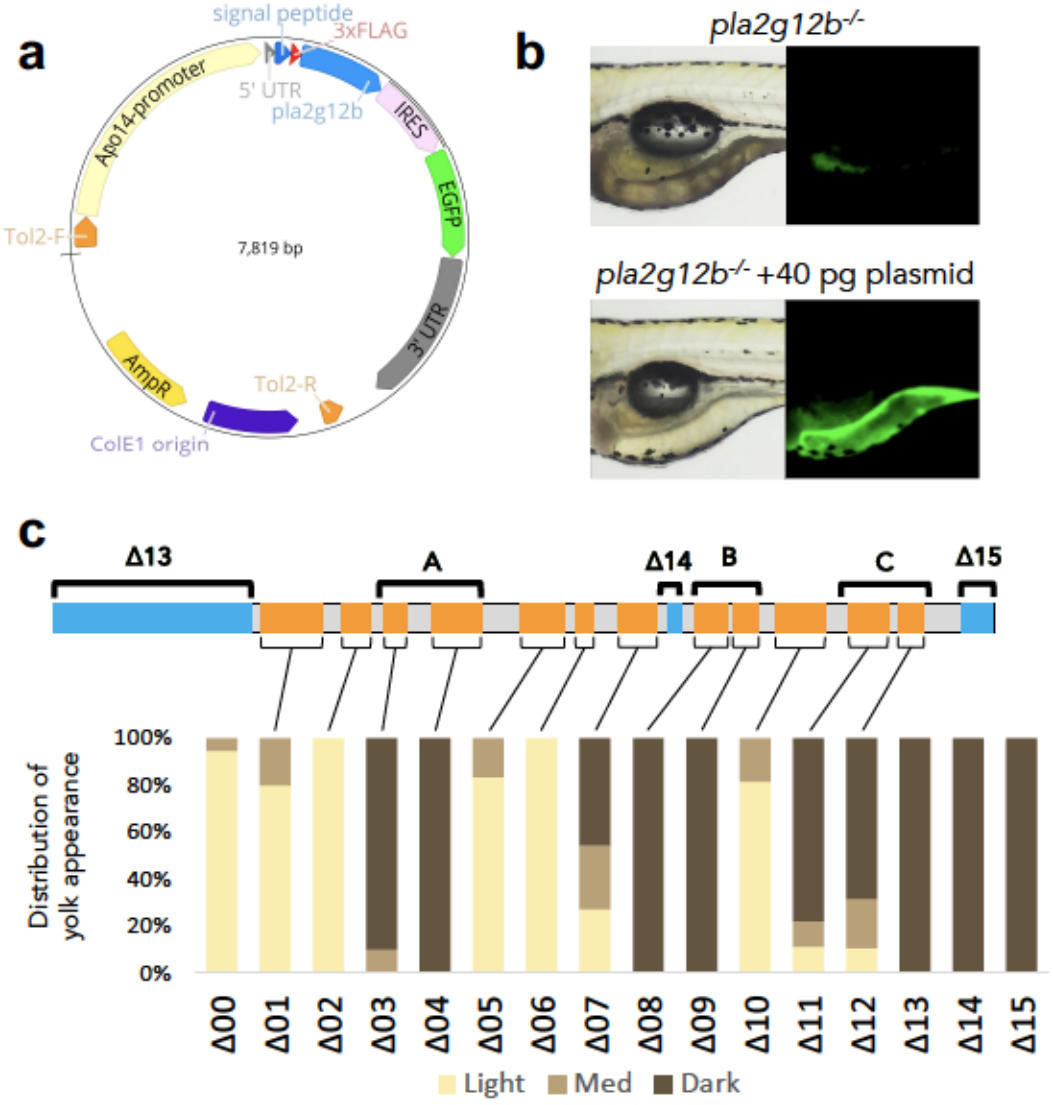

Figure 4: Identification of functional domains within pla2g12b with an allelic series. (a) Schematic of rescue plasmid using the YSL-specific Apo14 promoter to drive expression of *pla2g12b* using the endogenous UTRs, with an internal ribosome entry site (IRES) used to permit translation of EGFP from the same transcript. **(b)** Injection of the rescue plasmid is able to rescue the dark-yolk phenotype of *pla2g12b* mutants, and GFP can be used to select successfully injected larvae and confirm that expression is restricted to the YSL. **(c)** Site-directed mutagenesis was performed to generate 15 variants of the wild-type *pla2g12b* coding sequence. Each construct has between 1 and 6 amino acids changed (highlighted in orange), and in each case the residue was recoded from the *pla2g12b* sequence to the *pla2g12a* sequence. A total of 9 constructs showed severe defects in rescuing the dark yolk phenotype (Δ03-04, Δ08-09, Δ11-15). This allelic series highlights three essential functional domains which are labeled A, B, and C above. In addition to these domains, the failure of constructs Δ13-15 to rescue indicates that the signal peptide, Cysteine 159, and the KDEL are all also essential for function.

the wild-type rescue plasmid to generate 15 mutated variants of the rescue construct (named Δ1- Δ15, Table 1). In each variant, a block of putatively functional residues was mutated back to the sequence found in the pla2g12a sequence (Fig 4).

Each of these mutagenized rescue constructs was then injected into homozygous pla2g12b mutants. Larvae were screened at 2 dpf for GFP signal in the YSL, indicating a successful injection. Selected embryos were then imaged at 4dpf to determine whether the dark-yolk phenotype was rescued. Approximately half of the mutagenized rescue plasmids were able to rescue the dark-yolk phenotype, indicating that the residues therein were dispensable for function. However, several blocks of residues were unable to rescue, including Δ3-4, Δ8-9, and Δ11-15. Sites Δ3-4 span a 16 amino acid domain that will be referred to as functional domain A, sites Δ8-9 span a 15 amino acid domain that will be called functional domain B, and sites Δ11-12 span a 17 amino acid domain that will be called functional domain C. The mutations in Δ13 involved deletion of the signal peptide, providing support that expression within the ER is essential for function. The Δ14 mutation validates that cysteine 159 is essential for protein function, consistent with the mouse ENU allele published previously. The mutations in the Δ15 construct involved deletion of the KDEL, indicating that ER-retention is essential for protein function.

Plasmid name	Mutations	Primer names	Primer sequences	Ta
Δ00	none	none	none	none
Δ01	P63G, E70I, G76T	SF-JHT-537	atcgacgatgatgactggacgTTCGGCTCTATCCGAGGA	63
		SF-JHT-538	agattcttctgtggcactgccTGCAGGTTTTCCCTCAAC	
Δ02	G82S, S83G, S86R, V87I, N88D	SF-JHT-543	gcgcatagacGGCTATTTTGACTCAATACTGGAG	64
		SF-JHT-544	tgtaagccgctTCGGATAGAGCCGAACCC	
Δ03	D92N, S93M, E96D	SF-JHT-513	actggacTTGATGGGAGGCCGTGATGGT	64
		SF-JHT-514	atcatgttAAAATAGCCATTGACTGACTGTAAACTTC	
Δ04	V104Q, R108T, R110G, Y111D, K113Y, A114T	SF-JHT-515	cggcgacggttacacaCCTCAGCCTCGTCCTGGCTATCA	71
		SF-JHT-516	cacgtgtactgacactgACCATCACGGCCTCCCATCAACT	
Δ05	E125P, L134F	SF-JHT-517	agcacgtcactgtttGGCTTCCAGGTACCGAATAGT	62
		SF-JHT-518	acaaccatcaggtggTGACATCTGATAGCCAGGACG	
Δ06	V138X, P139X, S141X	SF-JHT-519	tTTTGATATGGGTGTCCCAGCCA	63
		SF-JHT-520	ttCTGGAAGCCAAGCAGTGACGT	
Δ07	A148S, L156H	SF-JHT-521	ttgcaaccagcacGATATTTGCTACGAAACCTGTGG	60
		SF-JHT-522	catttggtcatagaTGGGACACCCATATCAAAACTAT	
Δ08	N166E, Y168S, R169D, K173Q	SF-JHT-523	tgtgacacccagTTCCGCTGGTGCCTCCACAGC	69
		SF-JHT-524	gtcgctcttctcGGATCCACAGGTTTCGTAGCAAATATCT	
Δ09	R175Q, W176L, H179E, S180N	SF-JHT-525	ctcgagaacATCTGCGGTGACCTGAAGAAG	62
		SF-JHT-526	gcagagctgGAATTTGGTGTCACAGCGGTA	
Δ10	K186Q, S188T, S193Q, E196Q	SF-JHT-527	tatgcaaaaagttcaaGCATGTGAGACCTTTGCAGACA	64
		SF-JHT-528	aggcccagtgtctttttgCAGGTCACCGCAGATGCTGT	
Δ11	D203T, T204V, N207D, W210M, T211H	SF-JHT-529	tactgtgatgcacTTGGGCTGCAGACCCTTCATG	66
		SF-JHT-530	tcgtacatcacagtTGCAAAGGTCTCACATGCTTCAAC	
Δ12	R215K, F217Y, M218L, N219D	SF-JHT-531	cctggacGGCCAAAGGGCGTCCTGCTAT	70
		SF-JHT-532	tagggcttGCAGCCCAAAGTCCACACAGTGT	
Δ13	2-37X	SF-JHT-479	GATTACAAAGACCATGACG	59
		SF-JHT-480	CATGATGTCCTATTACAGTAC	
Δ14	C159Y	SF-JHT-451	GTTAGATATTtatTACGAAACCTGTGG	57
		SF-JHT-452	TGGTTGCAACATTTGGTC	
Δ15	D233P, E234D	SF-JHT-541	AGAAGAGAAGccggatCTCTGATAACGTTACTGG	59
		SF-JHT-542	CCTTCGCAATAGCAGGAC	

Table 1: List of mutations and site-directed mutagenesis primers used in allelic series. Brightfield Δ00 corresponds to the wild-type plasmid. Site-directed mutagenesis was used to generate 15 mutagenized versions (Δ01-Δ15) harboring various missense mutations as outlined above. For Δ13, 2-37X denotes deletion of amino acids 2 through 37.

Discussion

Data collected so far have led us to propose two potential models that explain why *pla2g12b* mutants secrete smaller ApoB-LPs and retain lumenal LDs in the ER (Fig. 5). In the first model, Pla2g12b channels lipids transferred by Mtp specifically to nascent lipoproteins (Fig. 5a). In our alternative model, Pla2g12b catalyzes fusion between nascent lipoproteins and lumenal lipid droplets (fig. 5b).

The localization of this protein provides initial support for these models. Not only is this gene expressed in the lipoprotein-producing tissues (liver, intestine, YSL), but the resulting protein is also retained in the ER, the subcellular compartment where lipoprotein biogenesis takes place.

Most often, lipids within a cell accumulate in the form of cytoplasmic lipid droplets (CLDs). CLDs form when lipids synthesized in the ER bud off of the cytoplasmic face of the ER, resulting in formation of a large micelle surrounded by a monolayer of phospholipids [57]. Numerous cytosolic proteins are known to associate with CLDs, including perilipins (PLINs) [58, 59]. Lipid droplets can also form within the ER by budding off of the lumenal face of the ER membrane (ERLDs) [62]. ERLDs are thought to fuse with nascent lipoproteins within the ER to form large TRLs, but have very rarely been observed [63, 64]. Although it is unclear how the balance of lumenal vs. cytoplasmic lipid droplets is mediated, MTP appears to be required for the formation of ERLDs [62]. Although both *pla2g12b* mutants and larvae treated with lomitapide show significant lipid accumulation in the YSL, this lipid is partitioned into very different

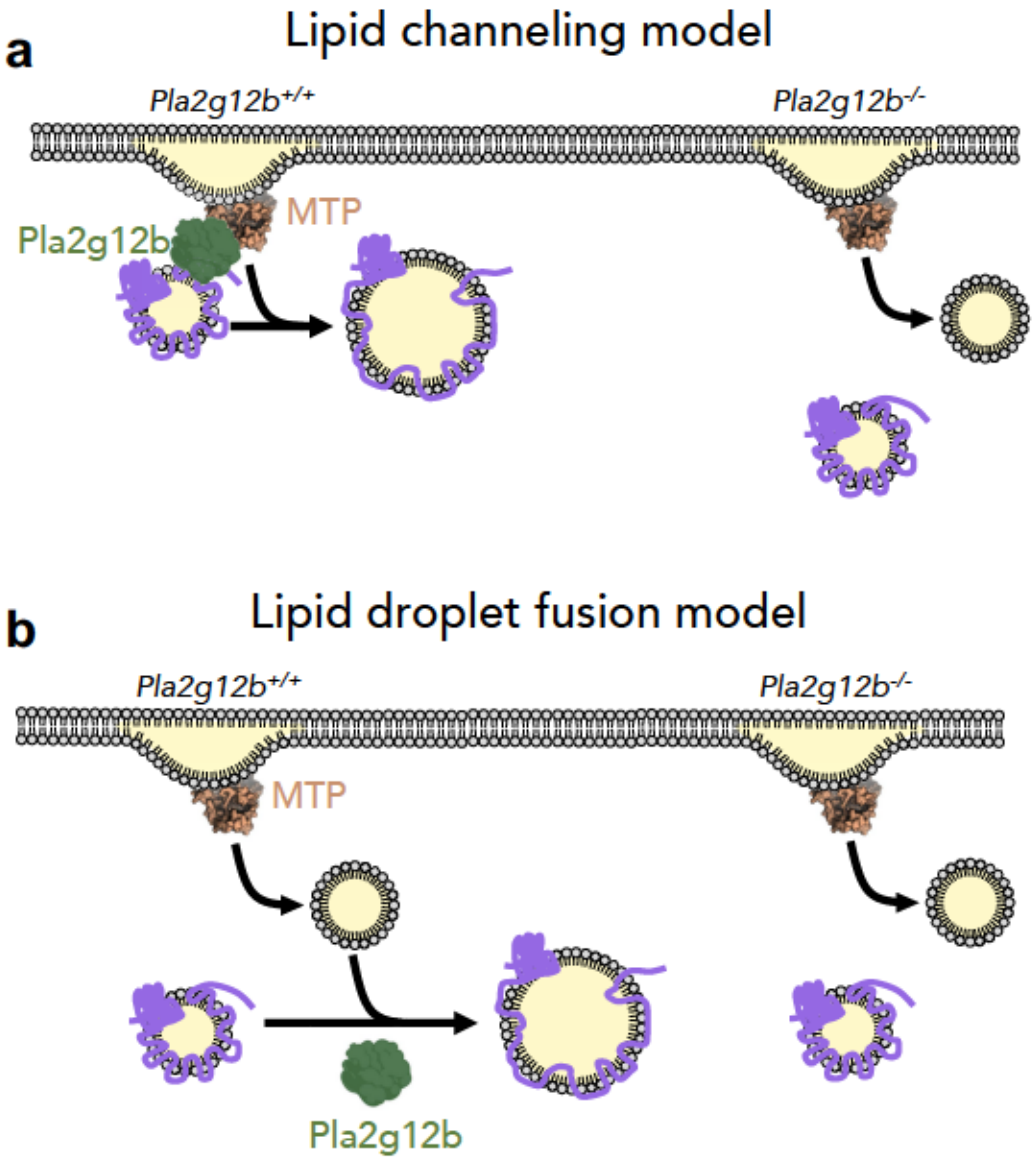

Figure 5: Proposed models. Two potential models have been proposed to explain why mutations in *pla2g12b* result in secretion of small lipoproteins and the accumulation of lipid droplets in the ER. **(a)** In the lipid channeling model, Pla2g12b interacts with Mtp and ApoB to promote efficient transfer of lipids from the ER to nascent lipoproteins. In the absence of Pla2g12b, the lipids extracted from the ER membrane are inefficiently channeled to nascent lipoproteins, and many lipids are stored as lumenal lipid droplets. **(b)** In the lipid droplet fusion model, Pla2g12b catalyzes fusion between lumenal lipid droplets and nascent lipoproteins. In the absence of Pla2g12b, lipid droplets and lipoproteins are unable to fuse.

compartments. Lomitapide induces lipid accumulation in CLDs, whereas *pla2g12b* mutants accumulate lipid in the form of ERLDs.

As further support of the models proposed in Fig. 5, *pla2g12b* mutant zebrafish produce abnormally small TRLs, indicating that they are lipidated less efficiently. Mutants also show significant accumulation of ERLDs in the YSL, suggesting that lipid droplets are either created more often (Fig. 5a) or are left behind (Fig. 5b) in the absence of Pla2g12b.

Finally, the mutagenesis series designed to highlight functional domains revealed not only the necessity for ER retention (KDEL signal), but also indicated the presence of at least three functional domains, designated A-C. The functional domains may represent the interacting surfaces that bind to ApoB, MTP, or ERLDs. These proposed models, combined with the identification of protein functional domains, provide a framework for designing future experiments to test the specific mechanism of action of Pla2g12b.

Materials and Methods

Sequence analysis

Genomicus (http://www.genomicus.biologie.ens.fr) online synteny analysis software was used to identify syntenic blocks across species. Species included in the alignment were manually selected to represent all major vertebrate lineages. Amino Acid sequences for zebrafish, human, and mouse PLA2G12B were downloaded from the Ensembl database (http://useast.ensembl.org/index.html) and aligned using MUSCLE multiple-sequence alignment software using standard settings. Alignments were color-coded based on similarity using the BLOSUM 62 similarity matrix. The online signal peptide prediction tool from the center for biological sequence analysis was used (http://www.cbs.dtu.dk/services/SignalP/) to test for the presence of a signal peptide.

In situ hybridization

Whole-mount *in situ* hybridization was carried out as previously described [181]. Briefly, a portion of the *pla2g12b* coding sequence sharing low homology to *pla2g12a* was amplified from cDNA, topo cloned into pCRII (Invitrogen, Grand Island, NY, USA), and used to generate sense and antisense digoxigenin-labeled riboprobes (digoxigenin: Roche, Indianapolis, IN, USA). The riboprobes were hybridized against zebrafish at 2, 4, and 6 dpf. Experiments were repeated using sense riboprobes to estimate the level of background signal (data not shown).

Electron microscopy

Larvae from each group were fixed, stained with osmium tetroxide, sectioned, and imaged on a Tecnai 12 transmission electron microscope first at low magnification, and then at high magnification focusing on the YSL. A subset of experiments were repeated using the Kellenberger staining method to highlight lipid membranes.

Drug treatment

Larvae were treated with 5 micromolar lomitapide for 48 hours (2-4 dpf) to induce the dark-yolk phenotype in wild-type larvae. 5 millimolar stock solution was prepared in 100% DMSO as a 1000x stock solution (0.1% final concentration of DMSO), and inhibitor was carefully dissolved in embryo medium prior to larval exposure.

Cloning

The backbone of the rescue plasmid was custom synthesized by Gene Universal (http://www.geneuniversal.com), and contained the *pla2g12b* coding sequence with endogenous UTRs, as well as the T3 initiation site for *in vitro* transcription. Traditional cloning using restriction enzymes and DNA ligase was used to introduce the Apo14 promoter and IRES-EGFP sequences into the plasmid. The Q5 site directed mutagenesis kit (New England Biolabs) was used to introduce the FLAG-tag into the construct several amino acids downstream of the predicted signal sequence cleavage site. The Q5 kit was also used to create each of the 15 mutagenized versions of the rescue plasmid that were used for rescue experiments using the primer pairs described in Table 1.

Rescue injections

Adult zebrafish with homozygous mutations in *pla2g12b* were inbred to generate progeny that were 100% homozygous mutants for *pla2g12b*. Larvae were then injected with 40 pg of DNA from one of the rescue constructs, as well as 50 pg of transposase mRNA. Larvae were then screened for GFP expression in the YSL at 2 dpf. GFP-positive larvae were then imaged using brightfield microscopy at 4 dpf using transmission illumination. Larvae were then scored as either completely dark, partially dark, or clear/light.

CHAPTER 5 – PILOT STUDIES FOR USE OF THE LIPOGLO REPORTER IN AN AUTOMATED HIGH-THROUGHPUT SCREEN

Abstract

Apolipoprotein-B (ApoB) is both a biomarker and a causal risk factor for multiple metabolic diseases. Within the liver, elevated ApoB promotes insulin resistance, ER-stress, and fatty liver disease. In the circulatory system, ApoB contributes to atherosclerosis and chronic inflammation. ApoB levels are consequently one of the strongest predictors of diabetes, metabolic syndrome, and cardiovascular disease in humans. Compounds that lower ApoB levels could therefore ameliorate several of the most prevalent and metabolic diseases worldwide. Several therapies are available that lower ApoB, which function by potently inhibiting the transcription or maturation of ApoB. As ApoB is a central mediator of lipid transport and metabolism, disruption of ApoB biogenesis leads to numerous detrimental side effects resulting from ectopic lipid accumulation in digestive tissues. There is thus significant need for alternative strategies to lower ApoB that do not block ApoB biogenesis. Here we seek to develop a strategy to identify ApoB-lowering compounds through unbiased high-throughput screening using a live vertebrate model system, the larval zebrafish. It is essential that screening take place in a live vertebrate organism, as screens using cultured cells are unable to recapitulate the complex inter-organ signaling and physiology responsible for determining ApoB levels. The LipoGlo reporter system couples ApoB levels to a quantifiable chemiluminescent signal that can be quantified in transparent larval zebrafish. We provide evidence that LipoGlo can be used for a high-throughput *in vivo* drug screen by demonstrating

conserved pharmacological responses to an ApoB-lowering compound (lomitapide), establishing a screening assay with strong statistical performance, and outlining a series of secondary-screening assays that can be used to prioritize hits from the primary screen.

Introduction

ApoB plays an essential role in lipid transport as the structural protein for ApoB-containing lipoproteins (ApoB-LPs). ApoB-LPs transport lipid from sites of absorption and synthesis (the liver and intestine) through the bloodstream to peripheral tissues (muscle, adipose, etc.) [5]. ApoB is synthesized by ER-resident ribosomes and co-translationally loaded with lipid by microsomal triglyceride transfer protein (MTP) [237]. In the absence of either sufficient lipid availability or MTP activity, nascent ApoB polypeptides are quickly degraded by the ER-associated protein degradation (ERAD) pathway [277]. Thus, ApoB production is largely regulated at the post-translational level, as rates of transcription and translation remain relatively constant, whereas the amount of mature protein produced depends heavily on lipid availability [278]. Once secreted, ApoB-LPs are taken up from the circulatory system primarily by LDL-receptors (LDL-R) expressed on the surface of the liver [77].

In addition to its central role in lipid transport, ApoB also plays a causal role in the etiology of numerous metabolic diseases including cardiovascular disease, diabetes, and fatty liver disease. ApoB is a strong predictor of cardiovascular disease risk, as ApoB-LPs are the primary drivers of atherosclerosis [279]. Elevated ApoB engenders higher cardiovascular disease risk independently of serum levels of cholesterol and triglyceride [280], which is particularly apparent in the case of pattern-B dyslipidemia, where patients have normal cholesterol levels but elevated ApoB and experience 3-fold higher rates of cardiovascular disease relative to the general population [30, 35].

ApoB also plays a causal role in mediating insulin resistance through the induction of ER-stress [281, 282] and inflammation [283]. In both in vitro and mammalian model systems, excess lipid availability led to increases in ER-stress and insulin resistance that were exacerbated by ApoB over-expression and attenuated by ApoB knockdown [281], indicating that ApoB is the molecular link between excess lipid accumulation and ER-stress induced insulin resistance [284]. Elevated ApoB is one of the strongest predictors of the onset of diabetes [285] and metabolic syndrome [286, 287], and its reduction is the strongest indicator of restored insulin sensitivity [288].

ApoB levels also correlate with hepatic triglyceride content [289], the primary diagnostic for fatty liver disease [290]. Interestingly, humans with genetic deficiencies in ApoB production have elevated hepatic lipid content but rarely develop fibrotic liver diseases [291], implicating ApoB as a causal mediator of disease etiology.

Despite significant research dedicated to understanding and treating metabolic diseases, they remain the leading causes of morbidity and mortality worldwide. Metabolic syndrome affects about 25% of the world's population [292], diabetes affects 9% [27], non-alcoholic fatty-liver disease (NAFLD) affects 25% [293], and cardiovascular disease is responsible for 31% of all mortalities [27]. Therapies to treat these metabolic diseases could thus improve the longevity and quality of life of billions of people.

ApoB-lowering therapies represent a uniquely promising approach to combat metabolic disease, as there are direct mechanistic links between increased ApoB and the progression of cardiovascular disease, diabetes, and fatty liver disease. While several ApoB-lowering therapies have been developed, existing drugs cause severe side-effects

and are thus only approved for treatment of familial hypercholesterolemia [294, 295], a genetic condition characterized by extremely high levels of ApoB-LPs [296]. Mipomersen is one ApoB-lowering compound that acts as an anti-sense oligonucleotide (ASO) and interferes with ApoB transcription [297]. Lomitapide is a pharmacological inhibitor of MTP that serves to lower ApoB levels by preventing lipid transfer to ApoB-LPs, resulting in increased degradation of ApoB [298]. Both Lomitapide and Mipomersen induce severe hepatic steatosis (lipid accumulation in the liver) as a result of potent inhibition of lipid secretion via ApoB-LPs.

ApoB levels can also be reduced with cholesterol-lowering therapies such as statins (which inhibit cholesterol biosynthesis) and ezetimibe (which inhibits cholesterol absorption) [299, 300]. However, these compounds are more effective at lowering the cholesterol content of ApoB-LPs, and have a slightly less pronounced effect on ApoB levels [26, 40, 222]. Also, although statins and ezetimibe inhibit different enzymes, they both modulate the same downstream pathway and upregulate expression of the LDL-receptor via sterol-responsive element binding proteins (SREBPs) [301].

In summary, there are clear metabolic benefits associated with lowering ApoB levels. However, existing ApoB-lowering therapies target a relatively small number of pathways, and have either limited potential for lowering ApoB or intolerable side effects. We therefore seek to expand the collection of therapeutic targets and pharmaceuticals available to modulate ApoB levels, and prioritize these compounds based on their potential to treat metabolic disease.

There are numerous pathways known to modulate ApoB, with each pathway serving as a potential therapeutic target to develop ApoB-lowering compounds. Several

promising therapeutic targets have been highlighted by recent genetic studies in humans, but have not yet been inhibited pharmaceutically. For example, mutations in Proprotein convertase subtilisin/kexin type 9 (PCSK9), Sortilin (SORT1) and Asialoglycoprotein-1 (ASGR1) act through diverse mechanisms but consistently result in reduced levels of serum ApoB and a significant reduction in cardiovascular disease risk [302-304]. There are numerous other proteins and pathways known to modulate ApoB [68, 72], and likely many more that have not been characterized, that represent similarly promising therapeutic targets for lowering ApoB levels.

Rather than screen for inhibitors of each pathway individually (target-based screening), I have developed an approach to screen for inhibitors of many ApoB-lowering pathways in parallel using *in vivo* phenotypic screening. Phenotypic screening uses a single phenotype (in this case, ApoB levels) as a readout, and seeks to identify compounds that modulate this phenotype [305, 306]. It is important to note that this screen is not focused on identifying compounds that interact or interfere with the ApoB protein itself, but rather seeks to target pathways that regulate ApoB homeostasis. For example, hits from this screen could include inhibitors of MTP, PCSK9, ASGR1, or any number of previously uncharacterized pathways that serve to regulate ApoB levels. As ApoB is regulated by a complex homeostatic network that spans numerous cell types, performing phenotypic screening in cultured cells would fail to capture much of the inter-organ physiology responsible for controlling ApoB levels [307]. While unbiased screening in a live vertebrate affords the opportunity to identify ApoB modulators that act in any cell and tissue type, it is not practical to perform such screens in the mammalian model systems classically used to study lipoprotein biology.

The larval zebrafish has emerged as the premiere model system for high-throughput screening *in vivo*, as it is easy to produce a large number of organisms that can be maintained and exposed to test compounds in 96-well plate format. Importantly, phenotypic screens, like the one proposed here, have had high success rates in first-in-class compound discovery in recent decades [305, 306], validating the utility of this approach. There are also plentiful examples of human therapeutics showing similar activity in zebrafish, including anti-diabetic, cardiovascular, anti-angiogenic, anti-cancer [308], cardiotoxic, atheroprotective [309], and psychoactive compounds [310, 311]. Additionally, zebrafish proteins are highly conserved with humans and 82% of human disease proteins have annotated zebrafish orthologs [312]. The high genetic and pharmacological conservation with humans and the success of previous HTS efforts provide strong justification for the continued use of zebrafish as a tool for human drug discovery.

While the larval zebrafish is an established system for drug discovery, it has only recently been developed as a model to study ApoB levels (see Chapter 3). As larval zebrafish are too small to perform routine extraction of plasma and isolation of lipoproteins, I created a transgenic reporter line that couples ApoB levels to a quantitative light-emitting readout called LipoGlo. I created LipoGlo by introducing a bright chemiluminescent reporter (Nanoluc) as an in-frame fusion to ApoB in the zebrafish genome.

Here I show that the LipoGlo reporter system enables high-throughput quantification of ApoB-levels in zebrafish larvae. I also demonstrate conservation of numerous important genes involved in ApoB homeostasis in zebrafish, and develop a

screening paradigm with robust statistical performance that uses lomitapide as a positive control to evaluate ApoB levels in zebrafish. I go on to show that an internal counterscreen can be used to eliminate false-positives, and outline a suite of secondary screens that can be used to prioritize compounds based on their metabolic benefit. These findings establish a paradigm for coupling the LipoGlo system to *in vivo* HTS for the discovery of diverse new classes of ApoB-lowering compounds.

Results

Larval zebrafish recapitulate all major aspects of ApoB homeostasis-

Larval zebrafish show remarkable conservation of pathways related to ApoB metabolism compared to humans. By 5 dpf, zebrafish have developed all major digestive organs (Fig. 1b), and possess all the cell and tissue types that contribute to ApoB regulation. I have previously shown that although there are multiple duplications of the ApoB gene in zebrafish, a single isoform (*apoBb.1*; focus of this study) is responsible for producing over 95% of the ApoB mRNA and protein from both the liver and intestine [82], and that the ApoB amino acid sequence is well conserved compared to humans [82, 313, 314], with particularly high conservation in all the essential functional domains such as the MTP-interacting domain, the LDL-receptor binding site, a proline-rich region, and the conserved residue that causes familial hypercholesterolemia when mutated in humans (Fig. 1a, green boxes) [314-316]. Although two of the proline-rich repeats are absent in zebrafish ApoB, they are thought to have arisen from partial gene-duplication and likely have little functional importance (Fig. 1a, red boxes) [316]. In humans, a full-length ApoB-100 protein is expressed in the liver and the transcript is post-transcriptionally modified in the intestine to form a truncated (ApoB-48) isoform. Zebrafish have neither the cytosine deaminase enzyme nor the conserved modification site (Fig. 1a, red box) that mediate post-transcriptional processing in mammals [317], indicating that zebrafish produce exclusively full-length ApoB. The physiological relevance of the truncated ApoB-48 is not well understood, but might permit more efficient production of lipoproteins following a high-fat meal [318]. Importantly, as beta-lipoproteins of both

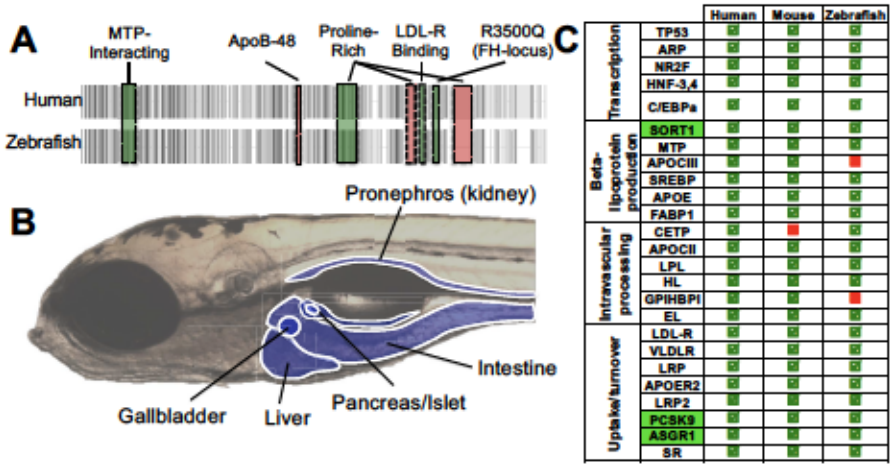

Figure 1: Larval zebrafish recapitulate the major aspects of ApoB homeostasis. (a) Amino acid alignments between human and zebrafish APOB reflect a high degree of identity (dark gray) and similarity (medium gray). Green boxes denote well-conserved functional domains, while red denotes poorly conserved or absent domains, showing that zebrafish do not produce APOB48 nor do they contain multiple proline- rich repeats in the protein sequence, but do have highly conserved key functional domains such as the MTP and LDL-receptor interacting domains. **(b)** Larval zebrafish have all the major digestive organs by 5 dpf. **(c)** Zebrafish express the majority of genes involved in *APOB* transcription, production, intravascular processing, and uptake (green checked boxes).

liver and intestinal origin are risk factors for cardiometabolic disease [319], the lack of a truncated isoform in zebrafish allows us to tag all ApoB proteins with a single carboxy-terminal tag. This single reporter fusion protein is therefore sensitive to modulators of both gut and liver derived beta-lipoproteins. In addition, zebrafish also have conserved orthologs of the majority of genes involved in ApoB cell biology and physiology (Fig. 1c, with several promising drug targets highlighted in green), and mutations in these genes recapitulate phenotypes seen in corresponding human disease (Fig. 2f) [226, 320].

Luciferase-tagged ApoB permits sensitive characterization of lipoprotein phenotypes-

To quantify ApoB-levels in individual zebrafish, we used TALEN-mediated precise genome engineering to introduce the NanoLuc reporter as a carboxy-terminal tag on ApoB (Fig. 2a). NanoLuc luciferase is half the size (14 kDa) and ~100-fold brighter than firefly luciferase, shows essentially no background signal, and allows for independent parallel quantification of a second reporter (firefly luciferase), thus engendering unparalleled sensitivity for our assay [321]. We provide substantial preliminary data to validate that the NanoLuc tag does not disrupt ApoB function, NanoLuc signal accumulates in the expected lipoprotein density fractions (Fig. 2b), lipoproteins present in each fraction are the expected sizes (20-60 nm) (Fig. 2c), and the particles show the expected electrophoretic mobility on a 3% polyacrylamide gel (Fig. 2d).

We then set out to verify that specific dietary, genetic, and pharmacological manipulations known to modulate ApoB in humans had similar effects in zebrafish. Specifically, a high-fat meal increases lipid availability and concomitantly raises ApoB

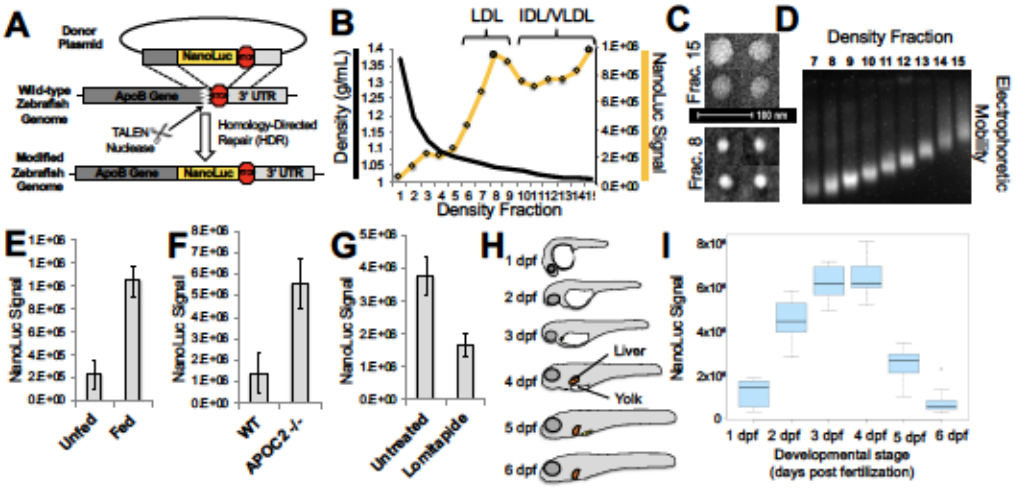

Figure 2: The ApoB-NanoLuc fusion protein enables sensitive detection of ApoB phenotypes. (a) TALEN-mediated genome engineering results in precise fusion of the NanoLuc tag to the ApoB gene in zebrafish. (b) NanoLuc signal accumulates in the expected density fractions following density gradient ultracentrifugation, and these density fractions contain beta-lipoproteins of the expected (c) size and (d) electrophoretic mobility. (e) Feeding with high-fat diet or (f) knockout of the *apoc2* gene required for ApoB processing and uptake results in strong induction of ApoB-NanoLuc signal, whereas (g) inhibition of Mtp with lomitapide results in reduced signal. (h) Cartoon showing the size of the liver and yolk throughout development, and (i) the corresponding NanoLuc levels during development as yolk is absorbed (1-4 dpf) and depleted (4-6 dpf).

levels [80], and the ApoB-NanoLuc reporter shows the expected induction in response to high-fat feeding (Fig. 2e). Humans lacking Apolipoprotein-CII (ApoC2) have profoundly increased ApoB levels (hyperlipoproteinemia type IB) as a result of defects in processing and turnover of ApoB- containing lipoproteins [322]. We have used CRISPR to target the apoc2 gene in zebrafish, and found the expected hallmarks of hyperlipoproteinemia type IB including elevated ApoB levels (Fig. 2f) and accumulation of large lipoprotein particles (data not shown). Pharmaceutical treatment using lomitapide (an MTP inhibitor) results in significant reduction of ApoB levels in humans [294], and significantly lowered ApoB-NanoLuc levels in zebrafish larvae (Fig. 2g). Finally, we performed a developmental time-course to determine the optimal treatment window for compound screening. Larvae are nourished by maternal yolk at this stage, which is absorbed and packaged into beta-lipoproteins at a stereotypic rate throughout development thus providing predictable reference levels to identify modulators of ApoB (Fig. 2h,i). In conclusion, the ApoB-NanoLuc reporter perfectly reflects ApoB dynamics, allowing us to capture modulators of ApoB production, stability, and turnover.

Lomitapide treatment results in a robust and reproducible reduction of ApoB levels

Lomitapide has previously been used in larval zebrafish to inhibit production of ApoB-LPs. Lomitapide was thus used as a positive control to evaluate the statistical performance of the LipoGlo assay. A standard metric for HTS assay quality is the Z'-factor (Z'), which has an arbitrary threshold of .5 for an HTS-ready assay [323]. Z' calculations for this assay reveal its excellent performance (>.5) based on genetic positive and negative controls (Fig. 3a, ApoB-NanoLuc vs. wild-type, reflecting very high signal

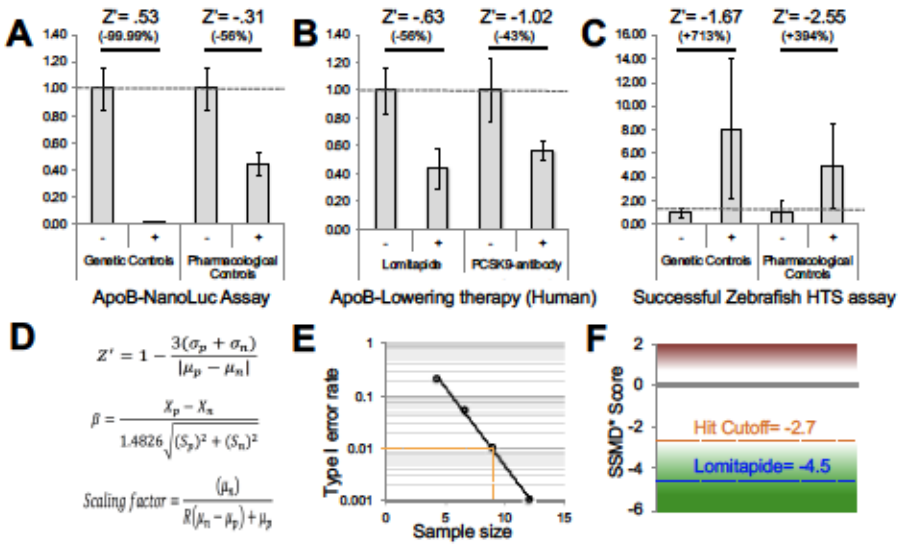

Figure 3: Assay performance statistics. (a) Z-factor calculations for the ApoB-NanoLuc assay using genetic and pharmacological controls show excellent and better than expected statistical performance respectively, as **(b)** aggressive ApoB-lowering therapy in humans is insufficient to generate a strong Z-factor. **(c)** Previous HTS in zebrafish were unable to demonstrate good assay performance using the Z' cutoff of >.5, but adopted **(d)** the SSMD score as an appropriate statistical parameter, formulas for Z-factor, SSMD-score (beta) and scaling factor shown. **(e)** Power calculations indicate that a sample size of 9 (yellow line) would be sufficient to detect hits with 50% of the efficacy of positive control compounds with type I and type II error rates of ~1%. **(f)** Visualization of SSMD score cutoff criteria. Lomitapide lowers ApoB and has a strong negative SSMD score (dark green) and was used to calculate the hit cutoff score of -2.7 (light green, weak hits).

to background ratios), but poorer performance based on lomitapide, the best pharmacological positive control available (Fig. 3a). Poorer assay performance in the latter experiment is a result of both the inherent variability of live vertebrate systems, as well as the lack of availability of a sufficiently potent ApoB-lowering therapy to use as a positive control. To contextualize these calculations, humans treated with the strongest ApoB-lowering therapies available (lomitapide and a PCSK9 antibody) show similar magnitudes of reduction in ApoB with higher levels of variability [238, 324] (Fig. 3b), and have poorer Z'-factors (-0.63 and -1.02). The lower variability in the zebrafish model is likely due to the highly consistent diet of maternal yolk used to nourish zebrafish during the screen. The inability of the strongest pharmaceuticals available to achieve a Z' greater than .5 in humans or zebrafish indicates that this may not be a realistic threshold to screen for modulators of ApoB in live vertebrates.

Previous screening efforts using live zebrafish to study different processes were also unable to reach the Z' threshold of 0.5 (Fig. 3c, note screen was for compounds that increase signal), and promote adoption of an alternative analytical framework based on the strictly standardized mean difference (SSMD) statistic. SSMD scores are (i) frequently used for *in vivo* screening (such as RNAi-screens), (ii) account for the inherent variability in live vertebrate systems, and (iii) are better suited to assays where an extremely strong positive control is not available or appropriate [325, 326]. The LipoGlo assay described here has significantly higher statistical performance than previously published HTS assays using live zebrafish [327] as measured by both the Z'-factor and power calculations (Fig. 3a-c). In summary, the proposed assay shows excellent statistical performance based on genetic controls (Z' >.5), better performance than expected using

pharmaceutical controls as compared to ApoB-lowering treatments in humans, and superior assay quality to the previous successful HTS in zebrafish, suggesting a high probability of success in the primary screen.

Sample size, error rate, and hit selection calculations-

Statistical resampling of positive control treatments can be used to estimate the appropriate sample size for HTS assays given type I and type II error rate thresholds and a desired cutoff for effect size [225]. Assuming a type II error rate of .01 and setting the hit selection cutoff to 50% the magnitude of positive control treatment generates a log-linear relationship between sample size and type I error rate (Fig. 3e). A sample size of 9 corresponds to an error rate of .01, suggesting that a relatively small number of biological replicates can be used to perform a robust primary screen (previous assays required a sample size of 16). Besides serving as a metric for assay quality, the SSMD score can also be used to determine hit cutoff criteria. This statistical test compares the averages between the negative control and each experimental sample, and then adjusts this difference based on the median absolute deviation (MAD) of each sample, such that samples with high variability will be penalized and produce a poor SSMD score even if there is a large difference between the means. In positive control treatments, lomitapide produced an SSMD score of -4.5, reflecting a very strong control assay. The scaling factor formula (Fig. 3d) can be used to determine the SSMD hit-selection cutoff based on the desired magnitude relative to the positive control. A compound with a 50% effect size relative to MTP was chosen as a physiologically relevant effect size, which sets an SSMD hit cutoff score of -2.7 (Fig. 3f).

Development of an internal counterscreen for cytotoxicity

The NanoLuc reporter uses a different substrate than firefly luciferase, allowing a second luciferase reporter to be measured in parallel as an internal control. We chose to use a transgenic line expressing Firefly Luciferase (Fluc) reporter in every cell (driven by the ubiquitin promoter) for this purpose [328]. By monitoring levels of Firefly luciferase, the screening assay will be able to detect if any treatments result in developmental delay, cytotoxicity/death, or general disruptions in transcription, translation, or protein turnover/stability. The internal control line was bred with the ApoB-NanoLuc reporter line, and the progeny were incrossed and to create a breeding stock homozygous for both reporters.

Results of pilot screen using selected compounds from LOPAC 1280 library

We have validated the proposed approach on a collection of compounds implicated in lipid and lipoprotein metabolism (Fig. 4c). Consistent with our understanding that very few known compounds modulate ApoB metabolism, none of the compounds tested resulted in a significant change in ApoB except for the positive control compound, lomitapide. The screening assay includes firefly luciferase as an internal control reporter to detect off-target or cytotoxic effects, and the majority of compounds tested resulted in almost no effect on firefly luciferase levels, as evidenced by the tight distribution of SSMD scores for firefly luciferase around zero (Fig. 4a). Cutoff values for firefly luciferase were set to positive (increase in signal) and negative (decrease in signal) 2.4, corresponding to 6 standard deviations away from the average SSMD score.

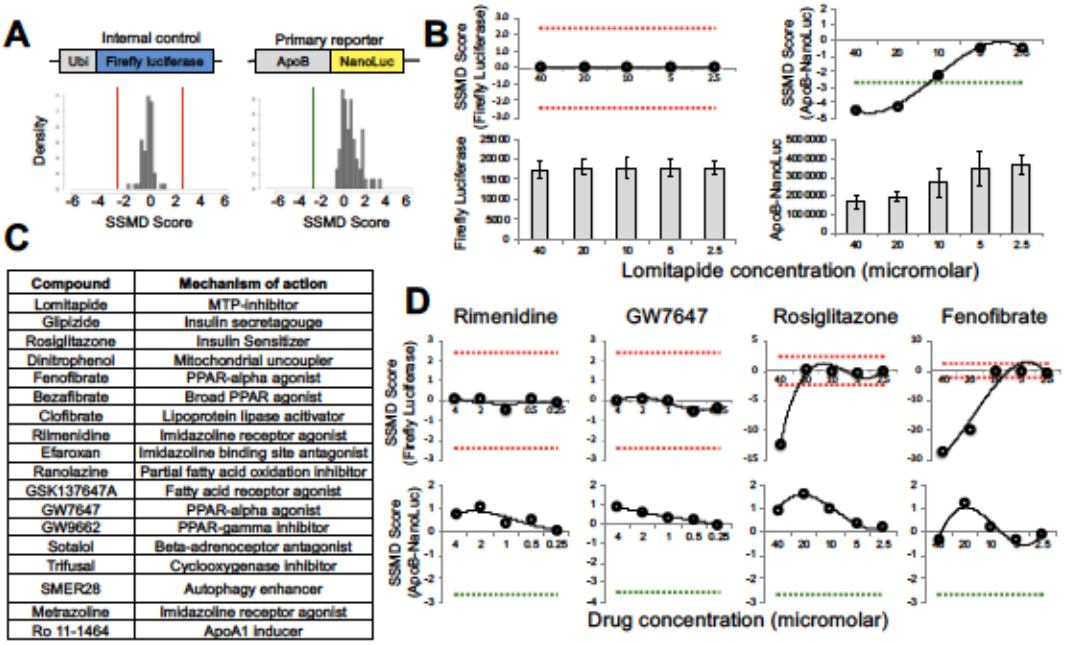

C

Compound	Mechanism of action
Lomitapide	MTP-inhibitor
Glipizide	Insulin secretagouge
Rosiglitazone	Insulin Sensitizer
Dinitrophenol	Mitochondrial uncoupler
Fenofibrate	PPAR-alpha agonist
Bezafibrate	Broad PPAR agonist
Clofibrate	Lipoprotein lipase acitivator
Rilmenidine	Imidazoline receptor agonist
Efaroxan	Imidazoline binding site antagonist
Ranolazine	Partial fatty acid oxidation inhibitor
GSK137647A	Fatty acid receptor agonist
GW7647	PPAR-alpha agonist
GW9662	PPAR-gamma inhibitor
Sotalol	Beta-adrenoceptor antagonist
Trifusal	Cyclooxygenase inhibitor
SMER28	Autophagy enhancer
Metrazoline	Imidazoline receptor agonist
Ro 11-1464	ApoA1 inducer

Figure 4: Data from preliminary screen. (a) Distribution of SSMD scores is centered around zero for both the internal control firefly luciferase and ApoB-NanoLuc reporter when positive control and cytotoxic compounds are removed from analysis. SSMD cutoffs were set to +/- 2.4 for firefly luciferase (6 standard deviations, red dotted lines), and -2.7 for ApoB-NanoLuc as discussed earlier (green dotted line). **(b)** lomitapide treatment results in a dose-dependent decrease in ApoB-NanoLuc signal with no effect on firefly luciferase (lower panels) that translates to an SSMD score of zero for firefly luciferase and strong nega- tive SSMD scores for the effective lomitapide concentrations. **(c)** Drugs from the Lopac-1280 collection and Sigma used in a preliminary screen, and **(d)** selected results from the screen demonstrating that certain compounds show dose-responsive increases in ApoB-NanoLuc most likely mediated by developmental delay (bottom panels), and lethal concentrations of certain drugs result in very strong negative SSMD scores (<-10, upper panels).

Any SSMD scores outside of this range (denoted by red lines) will be discarded as they result in severe off-target effects such as developmental delay or toxicity. Several concentrations of test compounds were lethal to zebrafish larvae and, as expected, returned very strong negative SSMD scores (<-10) that clearly signal for exclusion from analysis (Fig. 4d, Rosiglitazone and Fenofibrate).

ApoB-NanoLuc will be the primary readout, and the hit selection cutoff was set to -2.7 (Fig. 4a,b,d, indicated by dashed green line) as previously discussed (Fig. 3f). Positive control treatment with lomitapide resulted in a dose-dependent decrease in NanoLuc levels that exceeds threshold cutoff requirements without affecting the internal control reporter (Fig. 4b). Interestingly, several compounds resulted in a mild but dose-dependent increase in ApoB levels, most likely an indication of developmental delay (Fig. 4d). ApoB levels are declining in the period from 4 to 5 dpf (Fig. 2i), so any compound that delays development would be expected to result in a higher level of ApoB. Compounds inducing developmental delay or increases in ApoB levels are of no interest to this screen, and there is therefore no upper/positive 'hit' threshold. Results from the preliminary screen support that (i) the screening process is robust and free of false positives, (ii) cytotoxic/lethal compounds can be readily detected and discarded, and (iii) the positive control treatment results in strong, dose-responsive effects that meet all hit selection criteria.

Outline of a secondary screening pipeline to prioritize hits from primary screen

Secondary assays are an essential component of HTS, as hits identified in the primary screen may act through extremely diverse mechanisms or result in undesirable

off-target effects and are unlikely to be adopted for further development without some degree of additional categorization and prioritization. High content screening (HCS) using automated microscopy and image analysis provides a useful follow-up to HTS, as it can provide much more detailed and high-dimensional datasets to complement a primary screen. I outline use of the Vertebrate Automated Screening Technology (VAST) imaging platform to expedite secondary screening [329] (Union Biometrica) and monitor effects of lead compounds on disease progression using a diet-induced zebrafish model of metabolic disease and a collection of transgenic zebrafish carrying reporters of central metabolic disease phenotypes. (Fig. 5)

Automated imaging and analysis platform-

The VAST automated imaging platform provides unparalleled consistency and throughput capacity for in-vivo HCS. This instrument uses microfluidics to precisely position larval zebrafish in an optically transparent capillary on a high-resolution microscope stage and collect images at user-defined exposure settings. We have purchased this instrument and shown that it is capable of collecting high-resolution fluorescent images of live zebrafish tissue. The VAST is capable of imaging approximately 100 larvae per hour, which will provide sufficient throughput capacity to keep pace with hits identified by the primary screen.

Fluorescent assay for secretory pathway activity:

ApoB relies on several core components of the secretory pathway to be trafficked and exported properly. Compounds that disrupt the secretory pathway may therefore

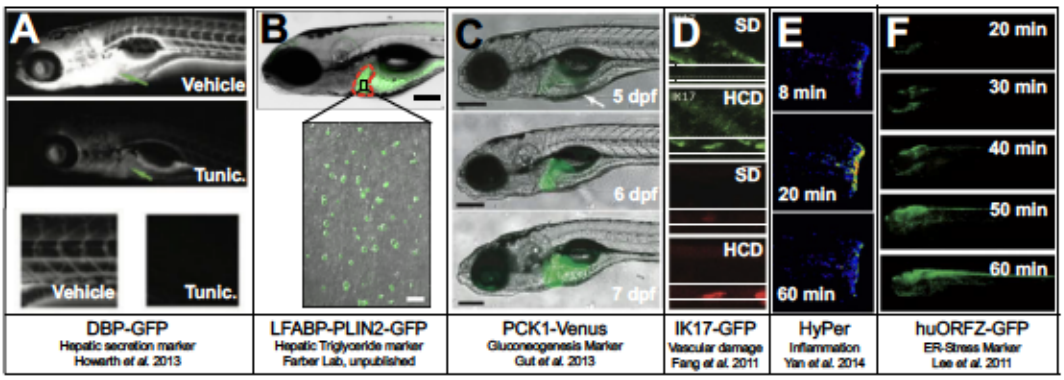

Figure 5: Representative images of transgenic lines to be used in secondary screening. **(a)** Under normal conditions, the DBP-GFP reporter is secreted from the liver and visible throughput the vasculature (top image, and detail bottom left). However treatment with tunicamycin (glycosylation inhibitor) results in ER-stress and defects in protein secretion, which results in stark reduction of reporter signal. **(b)** GFP-tagged Plin2 serves as an excellent marker of lipid accumulation, as it is degraded unless it is able to associate with the surface of a lipid droplet, as shown by the confocal detail image (scale bars 200 and 10 uM respectively). **(c)** PCK1 is the rate limiting enzyme in gluconeogenesis and is potently upregulated in the fasted and insulin resistant states, as shown by increasing fluorescence at the onset of the fasted state following yolk depletion (6-7 dpf). **(d)** A genetically encoded fluorescent antibody to oxidized LDL (IK17, top green panels) and fluorescent cholesterol analogs (red, bottom panels) both mark atherosclerotic lesions in the zebrafish caudal vein (outlined in white dotted lines) in response to high-cholesterol diet (HCD) that are absent in the standard diet (SD). **(e)** The HyPer reporter is an intracellular hydrogen peroxide sensor, and has been used to monitor the acute inflammatory response following tail transection (peak ~20 minutes post-transection). **(f)** The huORFZ-GFP reporter contains the 5' translational control element of the CHOP gene, such that fluorescence is repressed except under conditions of ER-stress, which can be induced in zebrafish by heat-shock at 40 C (time-course shown).

result in a significant reduction in ApoB levels, but will be unlikely to engender therapeutic value due to off target effects. Vitamin-D binding protein (DBP) is constitutively secreted from the liver and has been used as a marker of hepatic secretory activity by creating a DBP-GFP fusion protein (Fig. 5a) [330]. Hits that restrict GFP fluorescence to the liver will be discarded as general inhibitors of the secretory pathway.

Fluorescent assay for hepatic triglyceride content:

Hepatic triglyceride accumulation is an important risk factor for metabolic disease, but tools capable of screening this phenotype in vivo have not been previously developed. The Farber lab has developed a transgenic zebrafish line to address this issue that expresses the perilipin-2 (Plin2) gene fused to EGFP on a liver specific promoter. Plin2 was selected as an ideal marker for lipid accumulation, as the protein is rapidly degraded unless associated with a cytoplasmic lipid droplet [331]. The line shows bright fluorescent signal while hepatic lipid droplets are present, and confocal microscopy confirms that this signal is indeed localized to the periphery of cytoplasmic lipid droplets (Fig. 5b).

Fluorescent assay for changes in insulin signaling:

A fluorescent and bioluminescent reporter of phosphoenolpyruvate carboxykinase (pck1) has already been developed as a means of studying insulin signaling in larval zebrafish [332]. Pck1 is a hepatic enzyme involved in gluconeogenesis, and is activated in the starved or insulin resistant state (Fig. 5c). As ApoB has been implicated as both a

marker and causal risk factor of insulin resistance, many hits are likely to have an effect on insulin signaling as well.

Fluorescent assay for atherogenic plaque formation:

The zebrafish is an established model of atherogenic plaque formation with multiple approaches to assess plaque formation in-vivo. We will assess both the use of fluorescent lipid analogs and a genetically encoded fluorescent antibody to oxidized LDL (IK17) [309] as means of monitoring atherogenesis in real time (Fig. 5d).

Fluorescent assay for inflammation:

A hallmark of inflammation is the generation of hydrogen peroxide through the combined actions of NADPH Oxidase (NOX) and superoxide dismutase (SOD). The HyPer sensor [333] relays the increase in hydrogen peroxide production into a fluorescent readout through fusion of a modified yellow fluorescent protein (cpYFP) to a split version of the prokaryotic hydrogen peroxide sensing protein OxyR. Hydrogen peroxide cross-links the split OxyR domains and results in a conformational change in the cpYFP to produce a red-shifted signal. Ratiometric measurement of the native and cross-linked fluorescent signals provides a localized readout of inflammation in larval zebrafish (Fig. 5e) [334].

Fluorescent assay for ER-stress:

The CCAAT/enhancer-binding protein homologous protein (CHOP) is rapidly upregulated in response to ER-stress, and although it is constitutively transcribed, CHOP

mRNA is under strong translational inhibition due to an upstream open reading frame (uORF) present in the 5' UTR, which is de-repressed in states of ER-stress. An in vivo reporter of ER-stress has been developed using zebrafish that ubiquitously express GFP mRNA with the 5' uORF sequence from CHOP appended to the 5' end of the coding sequence (Fig. 5f) [335], such that translation is repressed under normal conditions but de-repressed in response to ER-stress to provide a tissue localized fluorescent readout for ER stress.

Discussion

Metabolic disease remain a major global health concern, with diabetes, fatty liver disease, and cardiovascular disease each affecting large fractions of the global population [27, 293]. APOB-lowering therapies represent a powerful therapeutic approach to combat numerous metabolic diseases, as APOB is directly involved in the etiology of diabetes, cardiovascular disease, and fatty liver disease [279, 284, 291]. However, existing APOB-lowering therapies block production of APOB-LPs, resulting in severe side effects. Identification of additional APOB-lowering compounds could therefore transform our treatment of metabolic disease.

APOB is regulated by a complex homeostatic network that includes numerous cell and tissue types, which creates countless opportunities for therapeutic intervention. While several promising therapeutic targets have been identified (but not yet targeted pharmaceutically), heritability studies suggest that many additional genes are involved in APOB homeostasis which have not yet been characterized. It is therefore impractical to use target-based screening to identify APOB-lowering compounds, as significant effort would be required to identify regulators of APOB homeostasis, and then an independent screen would need to be developed and executed for each target. By contrast, phenotypic screening presents the opportunity to screen for ApoB-lowering drugs without *a priori* information on drug targets. Thus, it would be possible to identify inhibitors to both characterized and undiscovered modulators of APOB simultaneously.

The larval zebrafish is an unparalleled vertebrate system for *in vivo* phenotypic screening. The recent development of the LipoGlo reporter in zebrafish couples ApoB

levels to a quantitative chemiluminescent signal, which created the opportunity to monitor ApoB levels in a high-throughput compatible assay. Here we show that larval zebrafish recapitulate all the major aspects of vertebrate lipoprotein biology, including expression of several promising therapeutic targets (PCSK9, ASGR1, and SORT1).

A key advantage of the larval zebrafish is that it develops externally from the mother, and is nourished by a maternally deposited yolk. This creates a highly reproducible pattern of nutrient availability, with excess lipid available at 1 dpf and virtually none remaining by 6 dpf. This stereotypic pattern provides a naturally occurring system with low variation that is likely one of the key reasons behind the strong statistical performance of the screening assay. Similar efforts in mammalian systems would require precise regulation of the timing and quantity of food intake as well as monitoring of activity level, all of which represent potential sources of variation that are virtually absent in the larval zebrafish.

Statistical performance is a critically important factor of an HTS assay, as poor performance requires a larger sample size and will not be as sensitive to smaller effect sizes. I have shown that the NanoLuc reporter system has excellent statistical performance using genetic controls, and that the poorer performance using pharmacological controls is due to the variability inherent in living systems. Importantly, this assay shows superior statistical performance relative to both APOB-lowering therapies used in humans, as well as previous assays used for HTS in zebrafish.

An additional advantage of phenotypic screening is that it can be used for simultaneous discovery of both genes and inhibitors using a library with previously characterized drug targets. Following execution of the screen, the drug target information

for each hit is extracted and subjected to pathway analysis. Pathway analysis identifies the common genetic pathways that are targeted by multiple hits from the screen, and the entire pathway can then be implicated in the regulation of APOB. Thus, a carefully designed drug screen has the potential to function as a genetic screen in parallel.

A key aspect of the proposed screen is that it is designed to quickly prioritize compounds based on their therapeutic potential. For example, inhibition of the secretory pathway would be expected to potently decrease APOB levels, but would fundamentally disrupt numerous additional cellular processes in parallel. This led us to identify the DBP-GFP reporter line as a useful marker of secretory activity that can screen. Similarly, direct inhibition of APOB production is of limited therapeutic value as it promotes steatosis. A secondary screen has thus been designed to filter out compounds that promote lipid accumulation in the liver. Thus, we have identified multiple categories of hits that could result in lower APOB without the associated therapeutic value, and identified assays to eliminate these hits.

By combining the numerous advantages of the larval zebrafish system, the LipoGlo reporter, and phenotypic drug screening, I have generated a robust high-throughput screening platform for the identification of APOB-lowering compounds. Additional classes of APOB-lowering compounds would have significant therapeutic value, providing numerous metabolic benefits without the associated side-effects.

Materials and Methods

Sequence analysis

Amino Acid sequences for human and zebrafish APOB were downloaded from ensembl (http://useast.ensembl.org/index.html) and aligned using MUSCLE multiple-sequence alignment software using standard settings. Alignments were color-coded based on similarity using the BLOSUM 62 similarity matrix. Sequences were manually annotated with functional domains based on review of the literature. The ensembl database was also queried for annotated orthologs of many of the genes central to lipoprotein processing.

Quantification of ApoB-NanoLuc levels using a plate reader

ApoB-NanoLuc levels were quantified as previously described (see Chapter 3). Briefly, homogenate (40 μL) was mixed with an equal volume of diluted NanoLuc buffer (for specific dilution see recipes and technical note on NanoLuc buffer) in a 96-well opaque white OptiPlate (Perkin-Elmer, 6005290). The plate was read within 2 minutes of buffer addition using a SpectraMax M5 plate reader (Moleculardevices) set to top-read chemiluminescent detection with a 500 ms integration time. The Nano-Glo Dual Luciferase Reporter Assay (Nano-DLR, N1610) was used for dual-luciferase assays, following manufacturer's instructions.

Drug treatment

All experiments use a treatment window of 48 hours (from 3-5 dpf) unless otherwise noted. A titration series was used to test each compound at various concentrations. LOPAC stocks solutions were stored at 4 micromolar, and diluted across a 5-point titration series to .25 micromolar. Lomitapide, Rosiglitazone, and Fenofibrate (SIGMA), were stored at 40 micromolar stock concentrations and titrated from 40 to 2.5 micromolar concentrations.

CONCLUSIONS AND FUTURE DIRECTIONS

ApoB-containing lipoproteins have been studied extensively in the past, as these complex structures not only play an essential role in lipid metabolism, but also are directly involved in the progression of cardiovascular disease. The overwhelming majority of previous research in this field has focused on measuring and modulating levels of "bad cholesterol", or LDL-C. These efforts have been remarkably successful, leading to the discovery of numerous pathways and pharmaceuticals to control cholesterol absorption, biosynthesis, trafficking, and excretion. However, this longstanding emphasis on lowering serum cholesterol has left several other aspects of lipoprotein metabolism relatively understudied. The work reported here seeks to highlight the importance of several understudied aspects of lipoprotein metabolism, generate new tools to facilitate their study, and use these tools to address outstanding gaps in our knowledge.

Developing new tools to study ApoB-LPs

Three understudied aspects of the lipoprotein profile in particular: lipoprotein size, lipoprotein abundance, and lipoprotein localization, are the focus of this thesis. Lipoprotein size and abundance have both emerged as critically important determinants of cardiovascular disease risk [29], with several lines of evidence suggesting that they may be more relevant therapeutic targets than LDL-C [39, 40]. Studies of lipoprotein localization, by contrast, are exceedingly rare. While lipoproteins are routinely monitored

in the circulation and in the vascular wall, extremely few studies have ever attempted to detect lipoproteins outside of vascular tissues [44].

The dearth of knowledge in these areas may stem from the lack of a suitable experimental system to conveniently study these processes. Krogh's principle states that "for such a large number of problems there will be some animal of choice, or a few such animals, on which it can be most conveniently studied." Thus I sought to apply Krogh's principle to the topic of lipoprotein biology, and a promising solution emerged in the form of the larval zebrafish, which offers numerous unique advantages. Firstly, larval zebrafish recapitulate all the major aspects of human lipoprotein metabolism. Secondly, larval zebrafish are transparent and thus suitable for *in vivo* imaging studies. Third, a wide variety of genetic tools are available to introduce, manipulate, or knock-out genes. Lastly, larvae can be produced in large numbers and develop rapidly. This not only expedites hypothesis-driven research, but also engenders unprecedented capacity to high-throughput screening for potential therapeutic drugs.

Several additional advantages of the larval zebrafish system emerged throughout the course of my studies that proved to be critically important to the success of this model system. Firstly, larvae are nourished by a maternally deposited yolk, which provides a remarkably consistent lipid-rich nutrient source that is eventually packaged into lipoproteins. The stereotypic processing of this yolk provides a reproducible framework to study perturbations in lipoprotein metabolism without the inherent variability introduced by variation in the timing and quantity of food intake. Additionally, the zebrafish genome encodes a functional copy of cholesteryl ester transfer protein (CETP) [81]. CETP is one of the master regulators of lipoprotein particle size, and mediates the

balance between HDL and LDL cholesterol [5]. Interestingly, CETP is not conserved in the rodent lineage, resulting in remarkably different lipoprotein profiles in mice and rats, which show significant depletion of LDL-C relative to humans and zebrafish [224]. Thus, while neither rodents nor zebrafish perfectly recapitulate the human lipoprotein profile, zebrafish do express the majority of genes known to be involved in lipoprotein processing including CETP, a master regulator of ApoB-LPs.

However, the clear advantages of the larval zebrafish were diminished by the fact that very little was known about atherogenic lipoprotein processing in zebrafish. Initial efforts were thus dedicated to observational studies, as well as method development to facilitate the study of atherogenic lipoproteins in zebrafish larvae. Characterization of the apolipoprotein genes in zebrafish highlighted the importance of the yolk syncytial layer in biogenesis of atherogenic lipoproteins. This tissue arises in the very early stages of embryonic development, and quickly initiates expression of numerous apolipoprotein genes essential to lipoprotein homeostasis.

The main goal of my initial observational studies was to understand the expression pattern of ApoB. ApoB is a classical marker of atherogenic lipoproteins, central to particle biogenesis, processing, and turnover. Interestingly, I was able to identify three paralogous *apoB* genes in zebrafish, as opposed to mammals which have a single *apoB* gene. While a single paralog (*apoBb.1*) emerged as an unambiguously dominant isoform accounting for ~95% of the mRNA and protein at multiple stages of development, the remaining paralogs were still expressed at detectable levels at certain time points. It remains unclear what role the additional paralogs may be playing. The simplest hypothesis is that these genes may have undergone sub-functionalization by

developing distinct spatial and temporal expression patterns. While this observation is supported by *in situ* mRNA expression patterns, the overwhelmingly higher expression of a single paralog in all lipoprotein-producing tissues does not provide strong support for this model. An alternative explanation is that, in some contexts, it may be beneficial to have an increased copy number of *apoB* genes to rapidly respond to high levels of dietary (or potentially yolk-derived) lipid. It is also possible that the duplicated genes play more specialized functional roles, but this warrants additional investigation. Based on these data, I can confidently state that the majority of bulk-lipid transport is performed by the *apoBb.1* paralog, and this gene was thus the focus of additional investigation.

I next sought to evaluate whether ApoB-fusion proteins could be used to track ApoB-LPs *in vivo*, which would greatly facilitate future studies in transparent zebrafish larvae. Several experiments using transient transfection of ApoB transgenes fused with various fluorescent reporters were used to evaluate whether the resultant proteins could form lipoproteins and be detected *in vivo*. The results of these experiments were quite promising, as they indicated that tagged lipoproteins could be lipidated, secreted, and endocytosed just like their untagged counterparts. However, the experiments carried numerous caveats. Most importantly, slight differences were observed depending on the fluorophore used (i.e. APOB-GFP provided slightly different results than APOB-mCherry). Also, the lipoproteins formed were somewhat atypical, exhibiting unusually high density in most cases. However, many of these observations could be explained by the fact that the transgenes were (i) being transiently transfected, leading to non-physiological levels of expression, and (ii) introduced into cultured cells, some of which do not naturally produce lipoproteins. Thus, inconsistencies in lipoproteins production

may not result from the addition of the fluorophore reporters, but rather differences in transfection efficiency or absence of other essential cofactors involved in lipoprotein biogenesis. To address these caveats, the next logical experiment would be to tag endogenous *apoB* genes with reporters, and evaluate whether such reporters impact lipoprotein homeostasis.

The LipoGlo system was thus developed using a chemiluminescent reporter (NanoLuc) fused to ApoB (*apoB.1*) in the zebrafish genome. Importantly, this reporter enabled rapid and sensitive quantification of the abundance of atherogenic lipoproteins, their size distribution, and their localization.

Novel insights into extravascular ApoB-LPs

One of the most powerful advantages of the LipoGlo system is that it enables imaging of the localization of lipoproteins in an intact animal which, to our knowledge, has not been possible in any other system. Observation of localization patterns across larval development revealed several unexpected extravascular localization patterns, including enrichment in the central nervous system and myosepta.

While the initial observation of ApoB-LPs in the central nervous system was surprising, closer evaluation of the literature revealed additional evidence to support this localization pattern. Lipoproteins have been detected in the embryonic cerebrospinal fluid of chicken embryos [44], where they are thought to interact with the protein SCO-SPONDIN to form a threadlike structure called the Reissner fiber [45], which is involved in body axis formation [45]. The detection of ApoB-LPs in the larval zebrafish CNS provides additional evidence that this is a conserved process, and also opens several questions. For example, the ability to monitor CNS localization over time revealed that it

persists (and is in fact most apparent) in states of nutrient shortage. It is unclear how lipoproteins are preferentially retained in the CNS (presumptively in the embryonic cerebrospinal fluid) despite clearance of lipoproteins from essentially all other tissues in the body. Further, it remains unclear (i) how lipoproteins are transported to the CNS, (ii) whether ApoB-LPs are also present in the CNS of adult animals, and (iii) what functional role lipoproteins play in body axis formation. The LipoGlo system represents a useful strategy to continue to investigate these outstanding questions.

ApoB-LPs were also apparent in the larval zebrafish myosepta, tendon-like structures connecting the segments along the zebrafish body axis [247] that are associated with lymphatic vessels [246, 247]. While lipoproteins are known to circulate through the lymphatic system, their apparent association with tendinous tissues relates to a poorly understood phenomenon in humans. Humans with homozygous familial hypercholesterolemia develop cholesterol-rich xanthomas on tendons [336], suggesting that lipoproteins may also localize to tendons in humans. However, similar to the case of the central nervous system, it is unclear how lipoproteins are recruited, maintained, or are involved in signaling in this tissue.

The LipoGlo system offers several unique opportunities to study the localization of ApoB-LPs in more detail. Firstly, NanoLuc serves as a specific epitope for affinity purification, and could thus be used to study the ApoB-LP interactome through co-immunoprecipitation (Co-IP). Co-IP coupled to mass spectrometry could identify the binding partners involved in recruiting or retaining ApoB-LPs in tendons and cerebrospinal fluid, or identify the receptors involved in mediating downstream signaling.

Identification of new molecular players in lipoprotein biogenesis

LipoGlo was used to screen for perturbations in the lipoprotein profile in a collection of ENU-mutagenized zebrafish. I was able to detect drastic changes in lipoprotein abundance, size, and localization in *pla2g12b*$^{-/-}$ mutants. Phospholipase A2 Group 12B (Pla2g12b) is an unexpected regulator of the lipoprotein profile, as it catalytically inactive (unable to bind or cleave phospholipids) [230]. Further review of the literature revealed that this gene is conserved throughout the vertebrate lineage, yet has no known function.

Further investigation of the functional role of Pla2g12b revealed that it may promote expansion of nascent lipoproteins by mediating fusion with ER-lumenal lipid droplets. I show that mutants produce abnormally small ApoB-LPs, and that large lumenal lipid droplets are left behind in the ER of lipoprotein-producing tissues. I suspect that this protein may interact directly with ApoB, and may also interact with proteins on the surface of ER-lipid droplets. If this model is correct, Pla2g12b may serve as the gateway to the identification of additional proteins involved in the regulation of ERLDs.

ERLDs are very poorly understood. Structurally, they are likely very similar to cytoplasmic lipid droplets or lipoproteins, adopting a micellar structure with a neutral lipid core surrounded by a phospholipid monolayer. However, both lipoproteins and lipid droplets require structural proteins to form (apolipoproteins and perilipins, respectively), but no protein has been identified that associates with lumenal lipid droplets. If Pla2g12b interacts (directly or indirectly) with ERLDs, then co-IP and mass spectrometry experiments will be able to identify the as of yet unidentified proteins involved in regulating ERLDs.

Genetic and dietary modulators of lipoprotein size

Lipoprotein size is a clinically important phenotype, reflecting the subclass distribution and atherogenic potential of ApoB-LPs. Throughout the course of this study, I have identified numerous factors that modulate lipoprotein particle size.

Unsurprisingly, *apoC2*$^{-/-}$ mutants are unable to lipolyze lipoproteins, and thus are unable to produce small (LDL-sized) particles. However, characterization of the lipoprotein profile in *mtp*$^{-/-}$ mutants revealed production of unexpectedly small ApoB-LPs. This was thought to be a null mutation, which should result in a complete lack of ApoB-LPs. The observation that lipoproteins were clearly produced and secreted in *mtp*$^{-/-}$ mutants indicates that although this allele is clearly defective, it is still permissive to lipoprotein biogenesis. Most interestingly, mutants appear to produce small (IDL-sized) lipoproteins as early as 1 dpf. This observation implicates polymorphism in MTP as a potent regulator of LDL size, which may in turn have implications for cardiometabolic disease risk.

I also identified *pla2g12b*$^{-/-}$ as a novel regulator of lipoprotein particle size. Similar to *mtp*$^{-/-}$ mutants, *pla2g12b*$^{-/-}$ mutants produce abnormally small lipoproteins. However, both LipoGlo assays and electron microscopy of the YSL suggest that Pla2g12b and Mtp act through different mechanisms to regulate particle size. As discussed above, I have proposed a model whereby Pla2g12b may be involved in lipoprotein expansion by promoting fusion with ERLDs. These results indicate that proteins involved in lipoprotein biogenesis have an important impact on determining the lipoprotein size distribution. The larval zebrafish enables monitoring of the lipoprotein

profile at the very earliest time points in development, which reveals dynamics that may be masked by the complex lipoprotein profile in adult organisms.

In addition to identifying genetic modulators of the lipoprotein profile, I also studied the effect of feeding on the lipoprotein size. I showed that in response to fasting, there was a gradual depletion in large lipoproteins and enrichment of their smaller lipolyzed counterparts. Conversely, following feeding with a high-fat meal I noticed a significant increase in the abundance of zero-mobility (ZM) species. Although it is difficult to conclude what specific class of lipoprotein is within the zero mobility band, the ZM particles induced by high-fat feeding are most likely chylomicrons. It was surprising to note how long the ZM particles persisted following the high fat meal (~72 hours), which may reflect slower overall lipoprotein processing in larval zebrafish, or a unique property of the egg-yolk emulsion used, or some combination of these factors. In either case, the LipoGlo assay provides a convenient opportunity to evaluate the effect of specific diets on lipoprotein dynamics, and may reveal unexpected relationships between diet and the lipoprotein size distribution.

Unbiased discovery of factors regulating abundance of ApoB-LPs

One of the principal motivations behind developing LipoGlo in zebrafish was its application in high-throughput screens to identify novel genetic and pharmacological modulators of the atherogenic lipoprotein profile. The LipoGlo counting method is performed in 96-well plate format, and is thus readily conducive to high-throughput assays.

Chapter 5 provides detailed discussion of the importance of identifying new pharmacological modulators of the atherogenic lipoprotein profile, as well as preliminary data demonstrating robust assay performance. The high statistical performance of the HTS assay described stems from a confluence of factors, including an excellent signal to noise ratio for the reporter protein, highly reproducible patterns of yolk utilization in zebrafish larvae, and conserved responses to pharmaceuticals between zebrafish and humans. Execution of the proposed high-throughput screen, followed by hit prioritization through secondary screening, will enable identification of ApoB-lowering compounds that are effective *in vivo*. The ability to reduce ApoB levels pharmacologically will provide promising new therapies for the treatment of several of the worlds' most prevalent metabolic diseases, including diabetes, fatty liver disease, and cardiovascular disease.

LipoGlo also provides the opportunity for unbiased identification of genetic pathways involved in lipoprotein homeostasis. Larval zebrafish are a powerful system for forward genetics, and the ability to assay the lipoprotein profile in individual larvae using LipoGlo creates the opportunity to apply the advantages of the zebrafish system to further our understanding of lipoprotein biology. The identification of *pla2g12b* as a novel regulator of the lipoprotein profile provides proof of concept for the continued discovery of genetic modulators of atherogenic lipoproteins using larval zebrafish.

In summary, the LipoGlo reporter represents a powerful new approach to study atherogenic lipoproteins that escapes the biases of existing paradigms, which focus on serum cholesterol. In-depth characterization of the lipoprotein profile across larval development revealed several unexpected dynamics, including production of unusually

small lipoproteins in *mtp* mutants and association of ApoB-LPs with the central nervous system and myosepta. LipoGlo is also a useful tool for unbiased discovery, and has facilitated discovery of Pla2g12b as the first putative mediator of ERLD fusion with nascent lipoproteins. Further, I have demonstrated robust performance of LipoGlo in a high-throughput drug screen for the discovery of ApoB-lowering compounds, which could have a significant impact on the global burden of metabolic disease.

REFERENCES

1. Harayama, T. and H. Riezman, *Understanding the diversity of membrane lipid composition.* Nat Rev Mol Cell Biol, 2018. **19**(5): p. 281-296.
2. Fernandis, A.Z. and M.R. Wenk, *Membrane lipids as signaling molecules.* Curr Opin Lipidol, 2007. **18**(2): p. 121-8.
3. Wymann, M.P. and R. Schneiter, *Lipid signalling in disease.* Nat Rev Mol Cell Biol, 2008. **9**(2): p. 162-76.
4. Alves-Bezerra, M. and D.E. Cohen, *Triglyceride Metabolism in the Liver.* Compr Physiol, 2017. **8**(1): p. 1-8.
5. Feingold, K.R. and C. Grunfeld, *Introduction to Lipids and Lipoproteins*, in *Endotext*, K.R. Feingold, et al., Editors. 2000: South Dartmouth (MA).
6. Kwiterovich, P.O., Jr., *The metabolic pathways of high-density lipoprotein, low-density lipoprotein, and triglycerides: a current review.* Am J Cardiol, 2000. **86**(12A): p. 5L-10L.
7. Jonas, A. and M.C. Phillips, *Lipoprotein structure*, in *Biochemistry of lipids, lipoproteins and membranes*. 2008, Elsevier. p. 485-506.
8. Dominiczak, M.H. and M.J. Caslake, *Apolipoproteins: metabolic role and clinical biochemistry applications.* Ann Clin Biochem, 2011. **48**(Pt 6): p. 498-515.
9. Siri-Tarino, P.W. and R.M. Krauss, *The early years of lipoprotein research: from discovery to clinical application.* J Lipid Res, 2016. **57**(10): p. 1771-1777.

10. Silva, R.A., et al., *Structure of apolipoprotein A-I in spherical high density lipoproteins of different sizes.* Proc Natl Acad Sci U S A, 2008. **105**(34): p. 12176-81.

11. Segrest, J.P., et al., *Structure of apolipoprotein B-100 in low density lipoproteins.* J Lipid Res, 2001. **42**(9): p. 1346-67.

12. Davidson, N.O. and G.S. Shelness, *APOLIPOPROTEIN B: mRNA editing, lipoprotein assembly, and presecretory degradation.* Annu Rev Nutr, 2000. **20**: p. 169-93.

13. Goldberg, I.J., *Lipoprotein lipase and lipolysis: central roles in lipoprotein metabolism and atherogenesis.* J Lipid Res, 1996. **37**(4): p. 693-707.

14. Jong, M.C., M.H. Hofker, and L.M. Havekes, *Role of ApoCs in lipoprotein metabolism: functional differences between ApoC1, ApoC2, and ApoC3.* Arterioscler Thromb Vasc Biol, 1999. **19**(3): p. 472-84.

15. Blanc, V. and N.O. Davidson, *APOBEC-1-mediated RNA editing.* Wiley Interdiscip Rev Syst Biol Med, 2010. **2**(5): p. 594-602.

16. von Eckardstein, A., Y. Huang, and G. Assmann, *Physiological role and clinical relevance of high-density lipoprotein subclasses.* Curr Opin Lipidol, 1994. **5**(6): p. 404-16.

17. Florentin, M., et al., *Multiple actions of high-density lipoprotein.* Curr Opin Cardiol, 2008. **23**(4): p. 370-8.

18. Lawler, P.R., et al., *Atherogenic Lipoprotein Determinants of Cardiovascular Disease and Residual Risk Among Individuals With Low Low-Density Lipoprotein Cholesterol.* J Am Heart Assoc, 2017. **6**(7).

19. Tabas, I., K.J. Williams, and J. Boren, *Subendothelial lipoprotein retention as the initiating process in atherosclerosis: update and therapeutic implications.* Circulation, 2007. **116**(16): p. 1832-44.

20. Grundy, S.M. and N.J. Stone, *2018 American Heart Association/American College of Cardiology/Multisociety Guideline on the Management of Blood Cholesterol-Secondary Prevention.* JAMA Cardiol, 2019.

21. Endo, A., *A historical perspective on the discovery of statins.* Proc Jpn Acad Ser B Phys Biol Sci, 2010. **86**(5): p. 484-93.

22. Hajar, R., *Statins: past and present.* Heart Views, 2011. **12**(3): p. 121-7.

23. Vavlukis, M. and A. Vavlukis, *Adding ezetimibe to statin therapy: latest evidence and clinical implications.* Drugs Context, 2018. **7**: p. 212534.

24. Mazidi, M., et al., *The effects of bile acid sequestrants on lipid profile and blood glucose concentrations: A systematic review and meta-analysis of randomized controlled trials.* Int J Cardiol, 2017. **227**: p. 850-857.

25. Chaudhary, R., et al., *PCSK9 inhibitors: A new era of lipid lowering therapy.* World J Cardiol, 2017. **9**(2): p. 76-91.

26. Silverman, M.G., et al., *Association Between Lowering LDL-C and Cardiovascular Risk Reduction Among Different Therapeutic Interventions: A Systematic Review and Meta-analysis.* JAMA, 2016. **316**(12): p. 1289-97.

27. *"World Health Organization" The top 10 causes of death* http://www.who.int/mediacentre/factsheets/fs310/en/ *Accessed:* . 2016.

28. Superko, H.R. and R.R. Gadesam, *Is it LDL particle size or number that correlates with risk for cardiovascular disease?* Curr Atheroscler Rep, 2008. **10**(5): p. 377-85.

29. Allaire, J., et al., *LDL particle number and size and cardiovascular risk: anything new under the sun?* Curr Opin Lipidol, 2017. **28**(3): p. 261-266.

30. Rizzo, M. and K. Berneis, *Low-density lipoprotein size and cardiovascular risk assessment.* QJM, 2006. **99**(1): p. 1-14.

31. Bjornheden, T., et al., *Accumulation of lipoprotein fractions and subfractions in the arterial wall, determined in an in vitro perfusion system.* Atherosclerosis, 1996. **123**(1-2): p. 43-56.

32. Galeano, N.F., et al., *Apoprotein B structure and receptor recognition of triglyceride-rich low density lipoprotein (LDL) is modified in small LDL but not in triglyceride-rich LDL of normal size.* J Biol Chem, 1994. **269**(1): p. 511-9.

33. Tribble, D.L., et al., *Variations in oxidative susceptibility among six low density lipoprotein subfractions of differing density and particle size.* Atherosclerosis, 1992. **93**(3): p. 189-99.

34. Tribble, D.L., et al., *Oxidative susceptibility of low density lipoprotein subfractions is related to their ubiquinol-10 and alpha-tocopherol content.* Proc Natl Acad Sci U S A, 1994. **91**(3): p. 1183-7.

35. Austin, M.A., et al., *Low-density lipoprotein subclass patterns and risk of myocardial infarction.* JAMA, 1988. **260**(13): p. 1917-21.

36. Brown, G., et al., *Regression of coronary artery disease as a result of intensive lipid-lowering therapy in men with high levels of apolipoprotein B.* N Engl J Med, 1990. **323**(19): p. 1289-98.

37. Gotto, A.M., Jr., et al., *Relation between baseline and on-treatment lipid parameters and first acute major coronary events in the Air Force/Texas Coronary Atherosclerosis Prevention Study (AFCAPS/TexCAPS).* Circulation, 2000. **101**(5): p. 477-84.

38. Kim, B.J., et al., *Comparison of the relationships between serum apolipoprotein B and serum lipid distributions.* Clin Chem, 2005. **51**(12): p. 2257-63.

39. Sniderman, A.D., et al., *Discordance analysis of apolipoprotein B and non-high density lipoprotein cholesterol as markers of cardiovascular risk in the INTERHEART study.* Atherosclerosis, 2012. **225**(2): p. 444-9.

40. Otvos, J.D., et al., *Clinical implications of discordance between low-density lipoprotein cholesterol and particle number.* J Clin Lipidol, 2011. **5**(2): p. 105-13.

41. Lawler, P.R., et al., *Discordance between Circulating Atherogenic Cholesterol Mass and Lipoprotein Particle Concentration in Relation to Future Coronary Events in Women.* Clin Chem, 2017. **63**(4): p. 870-879.

42. Fukuyama, N., et al., *Validation of the Friedewald Equation for Evaluation of Plasma LDL-Cholesterol.* J Clin Biochem Nutr, 2008. **43**(1): p. 1-5.

43. Packard, C.J., et al., *Apolipoprotein B metabolism and the distribution of VLDL and LDL subfractions.* J Lipid Res, 2000. **41**(2): p. 305-18.

44. Vera, A., et al., *Interaction between SCO-spondin and low density lipoproteins from embryonic cerebrospinal fluid modulates their roles in early neurogenesis.* Front Neuroanat, 2015. **9**: p. 72.

45. Cantaut-Belarif, Y., et al., *The Reissner Fiber in the Cerebrospinal Fluid Controls Morphogenesis of the Body Axis.* Curr Biol, 2018. **28**(15): p. 2479-2486 e4.

46. Neumann, S., et al., *Mammalian Wnt3a is released on lipoprotein particles.* Traffic, 2009. **10**(3): p. 334-43.

47. Pikuleva, I.A. and C.A. Curcio, *Cholesterol in the retina: the best is yet to come.* Prog Retin Eye Res, 2014. **41**: p. 64-89.

48. Tsouli, S.G., et al., *Regression of Achilles tendon thickness after statin treatment in patients with familial hypercholesterolemia: an ultrasonographic study.* Atherosclerosis, 2009. **205**(1): p. 151-5.

49. Avraham-Davidi, I., et al., *ApoB-containing lipoproteins regulate angiogenesis by modulating expression of VEGF receptor 1.* Nat Med, 2012. **18**(6): p. 967-73.

50. Yu, X., et al., *Inhibition of cardiac lipoprotein utilization by transgenic overexpression of Angptl4 in the heart.* Proc Natl Acad Sci U S A, 2005. **102**(5): p. 1767-72.

51. Liu, C., et al., *Lipoprotein lipase regulates hematopoietic stem progenitor cell maintenance through DHA supply.* Nat Commun, 2018. **9**(1): p. 1310.

52. Manifold-Wheeler, B.C., et al., *Serum Lipoproteins Are Critical for Pulmonary Innate Defense against Staphylococcus aureus Quorum Sensing.* J Immunol, 2016. **196**(1): p. 328-35.

53. Bashmakov, Y.K., et al., *ApoB-containing lipoproteins promote infectivity of chlamydial species in human hepatoma cell line.* World J Hepatol, 2010. **2**(2): p. 74-80.

54. Borgquist, S., et al., *Apolipoproteins, lipids and risk of cancer.* Int J Cancer, 2016. **138**(11): p. 2648-56.

55. Ley, S.H., et al., *Association of apolipoprotein B with incident type 2 diabetes in an aboriginal Canadian population.* Clin Chem, 2010. **56**(4): p. 666-70.

56. Jacquemyn, J., A. Cascalho, and R.E. Goodchild, *The ins and outs of endoplasmic reticulum-controlled lipid biosynthesis.* EMBO Rep, 2017. **18**(11): p. 1905-1921.

57. Martin, S. and R.G. Parton, *Lipid droplets: a unified view of a dynamic organelle.* Nat Rev Mol Cell Biol, 2006. **7**(5): p. 373-8.

58. Itabe, H., et al., *Perilipins: a diversity of intracellular lipid droplet proteins.* Lipids Health Dis, 2017. **16**(1): p. 83.

59. Kimmel, A.R. and C. Sztalryd, *The Perilipins: Major Cytosolic Lipid Droplet-Associated Proteins and Their Roles in Cellular Lipid Storage, Mobilization, and Systemic Homeostasis.* Annu Rev Nutr, 2016. **36**: p. 471-509.

60. Murphy, D.J. and J. Vance, *Mechanisms of lipid-body formation.* Trends Biochem Sci, 1999. **24**(3): p. 109-15.

61. Sturley, S.L. and M.M. Hussain, *Lipid droplet formation on opposing sides of the endoplasmic reticulum.* J Lipid Res, 2012. **53**(9): p. 1800-10.

62. Kulinski, A., S. Rustaeus, and J.E. Vance, *Microsomal triacylglycerol transfer protein is required for lumenal accretion of triacylglycerol not associated with ApoB, as well as for ApoB lipidation.* J Biol Chem, 2002. **277**(35): p. 31516-25.

63. Alexander, C.A., R.L. Hamilton, and R.J. Havel, *Subcellular localization of B apoprotein of plasma lipoproteins in rat liver.* J Cell Biol, 1976. **69**(2): p. 241-63.

64. Demignot, S., F. Beilstein, and E. Morel, *Triglyceride-rich lipoproteins and cytosolic lipid droplets in enterocytes: key players in intestinal physiology and metabolic disorders.* Biochimie, 2014. **96**: p. 48-55.

65. Berneis, K.K. and R.M. Krauss, *Metabolic origins and clinical significance of LDL heterogeneity.* J Lipid Res, 2002. **43**(9): p. 1363-79.

66. Austin, M.A., *Genetic epidemiology of low-density lipoprotein subclass phenotypes.* Ann Med, 1992. **24**(6): p. 477-81.

67. Vakkilainen, J., et al., *Genetic influences contributing to LDL particle size in familial combined hyperlipidaemia.* Eur J Hum Genet, 2002. **10**(9): p. 547-52.

68. Chasman, D.I., et al., *Forty-three loci associated with plasma lipoprotein size, concentration, and cholesterol content in genome-wide analysis.* PLoS Genet, 2009. **5**(11): p. e1000730.

69. Allayee, H., et al., *Families with familial combined hyperlipidemia and families enriched for coronary artery disease share genetic determinants for the atherogenic lipoprotein phenotype.* Am J Hum Genet, 1998. **63**(2): p. 577-85.

70. Rotter, J.I., et al., *Multilocus genetic determinants of LDL particle size in coronary artery disease families.* Am J Hum Genet, 1996. **58**(3): p. 585-94.

71. Krauss, R.M., et al., *Separate effects of reduced carbohydrate intake and weight loss on atherogenic dyslipidemia.* Am J Clin Nutr, 2006. **83**(5): p. 1025-31; quiz 1205.

72. Snieder, H., L.J. van Doornen, and D.I. Boomsma, *The age dependency of gene expression for plasma lipids, lipoproteins, and apolipoproteins.* Am J Hum Genet, 1997. **60**(3): p. 638-50.

73. Sniderman, A.D., et al., *Regulation of plasma LDL: the apoB paradigm.* Clin Sci (Lond), 2009. **118**(5): p. 333-9.

74. Soutar, A.K., N.B. Myant, and G.R. Thompson, *Metabolism of apolipoprotein B-containing lipoproteins in familial hypercholesterolaemia: effects of plasma exchange.* Atherosclerosis, 1979. **32**(3): p. 315-25.

75. Apstein, C.S., et al., *Effect of intessive plasmapheresis on the plasma cholesterol concentration with familial hypercholesterolemia.* Atherosclerosis, 1978. **31**(2): p. 105-15.

76. Kroon, A.A., et al., *The rebound of lipoproteins after LDL-apheresis. Kinetics and estimation of mean lipoprotein levels.* Atherosclerosis, 2000. **152**(2): p. 519-26.

77. Brown, M.S. and J.L. Goldstein, *A receptor-mediated pathway for cholesterol homeostasis.* Science, 1986. **232**(4746): p. 34-47.

78. Fisher, W.R., L.A. Zech, and P.W. Stacpoole, *ApoB metabolism in familial hypercholesterolemia. Inconsistencies with the LDL receptor paradigm.* Arterioscler Thromb, 1994. **14**(4): p. 501-10.

79. Sniderman, A.D., X.J. Zhang, and K. Cianflone, *Governance of the concentration of plasma LDL: a reevaluation of the LDL receptor paradigm.* Atherosclerosis, 2000. **148**(2): p. 215-29.

80. Stoletov, K., et al., *Vascular lipid accumulation, lipoprotein oxidation, and macrophage lipid uptake in hypercholesterolemic zebrafish.* Circ Res, 2009. **104**(8): p. 952-60.

81. Schlegel, A., *Zebrafish Models for Dyslipidemia and Atherosclerosis Research.* Front Endocrinol (Lausanne), 2016. **7**: p. 159.

82. Otis, J.P., et al., *Zebrafish as a model for apolipoprotein biology: comprehensive expression analysis and a role for ApoA-IV in regulating food intake.* Dis Model Mech, 2015. **8**(3): p. 295-309.

83. Grundy, S.M., et al., *Diagnosis and management of the metabolic syndrome: an American Heart Association/National Heart, Lung, and Blood Institute scientific statement: Executive Summary.* Crit Pathw Cardiol, 2005. **4**(4): p. 198-203.

84. Voight, B.F., et al., *Plasma HDL cholesterol and risk of myocardial infarction: a mendelian randomisation study.* Lancet, 2012. **380**(9841): p. 572-80.

85. Feingold, K.R. and C. Grunfeld, *The role of HDL in innate immunity.* J Lipid Res, 2011. **52**(1): p. 1-3.

86. Navab, M., et al., *Normal high density lipoprotein inhibits three steps in the formation of mildly oxidized low density lipoprotein: steps 2 and 3.* J Lipid Res, 2000. **41**(9): p. 1495-508.

87. Navab, M., et al., *Normal high density lipoprotein inhibits three steps in the formation of mildly oxidized low density lipoprotein: step 1.* J Lipid Res, 2000. **41**(9): p. 1481-94.

88. Garner, B., et al., *Oxidation of high density lipoproteins. II. Evidence for direct reduction of lipid hydroperoxides by methionine residues of apolipoproteins AI and AII.* J Biol Chem, 1998. **273**(11): p. 6088-95.

89. Mahley, R.W., *Apolipoprotein E: cholesterol transport protein with expanding role in cell biology.* Science, 1988. **240**(4852): p. 622-30.

90. Nakashima, Y., et al., *ApoE-deficient mice develop lesions of all phases of atherosclerosis throughout the arterial tree.* Arterioscler Thromb, 1994. **14**(1): p. 133-40.

91. Fujimoto, K., et al., *Effect of intravenous administration of apolipoprotein A-IV on patterns of feeding, drinking and ambulatory activity of rats.* Brain Res, 1993. **608**(2): p. 233-7.

92. Fujimoto, K., J.A. Cardelli, and P. Tso, *Increased apolipoprotein A-IV in rat mesenteric lymph after lipid meal acts as a physiological signal for satiation.* Am J Physiol, 1992. **262**(6 Pt 1): p. G1002-6.

93. Wang, F., et al., *Specific sequences in N termini of apolipoprotein A-IV modulate its anorectic effect.* Physiol Behav, 2013. **120**: p. 136-42.

94. Kannel, W.B., et al., *Risk Factors in Coronary Heart Disease. An Evaluation of Several Serum Lipids as Predictors of Coronary Heart Disease; the Framingham Study.* Ann Intern Med, 1964. **61**: p. 888-99.

95. Toth PP, B.P., Rosenson RS, Boden WE, Chapman MJ, Cuchel M, D'Agostino RB Sr, Davidson MH, Davidson WS, Heinecke JW, Karas RH, Kontush A, Krauss RM, Miller M, Rader DJ., *High-density lipoproteins: a consensus statement from the National Lipid Association.* J Clin Lipidol, 2013. **7**(5): p. 484-525.

96. Franceschini, G., et al., *A-IMilano apoprotein. Decreased high density lipoprotein cholesterol levels with significant lipoprotein modifications and without clinical atherosclerosis in an Italian family.* J Clin Invest, 1980. **66**(5): p. 892-900.

97. Wilson, P.W., et al., *Prediction of coronary heart disease using risk factor categories.* Circulation, 1998. **97**(18): p. 1837-47.

98. Utermann, G., M. Hees, and A. Steinmetz, *Polymorphism of apolipoprotein E and occurrence of dysbetalipoproteinaemia in man.* Nature, 1977. **269**(5629): p. 604-7.

99. Corder, E.H., et al., *Gene dose of apolipoprotein E type 4 allele and the risk of Alzheimer's disease in late onset families.* Science, 1993. **261**(5123): p. 921-3.

100. Tso, P. and M. Liu, *Apolipoprotein A-IV, food intake, and obesity.* Physiol Behav, 2004. **83**(4): p. 631-43.

101. Amigo, L., et al., *Apolipoprotein A-I deficiency does not affect biliary lipid secretion and gallstone formation in mice.* Liver Int, 2011. **31**(2): p. 263-71.

102. Investigators, A.-H., et al., *Niacin in patients with low HDL cholesterol levels receiving intensive statin therapy.* N Engl J Med, 2011. **365**(24): p. 2255-67.

103. Barter, P.J., et al., *Effects of torcetrapib in patients at high risk for coronary events.* N Engl J Med, 2007. **357**(21): p. 2109-22.

104. Weinstock, P.H., et al., *Decreased HDL cholesterol levels but normal lipid absorption, growth, and feeding behavior in apolipoprotein A-IV knockout mice.* J Lipid Res, 1997. **38**(9): p. 1782-94.

105. Aalto-Setala, K., et al., *Intestinal expression of human apolipoprotein A-IV in transgenic mice fails to influence dietary lipid absorption or feeding behavior.* J Clin Invest, 1994. **93**(4): p. 1776-86.

106. Carten, J.D. and S.A. Farber, *A new model system swims into focus: using the zebrafish to visualize intestinal metabolism in vivo.* Clin Lipidol, 2009. **4**(4): p. 501.

107. Babin, P.J. and J.M. Vernier, *Plasma lipoproteins in fish.* J Lipid Res, 1989. **30**(4): p. 467-89.

108. Fang, L. and Y.I. Miller, *Emerging applications for zebrafish as a model organism to study oxidative mechanisms and their roles in inflammation and vascular accumulation of oxidized lipids.* Free Radic Biol Med, 2012. **53**(7): p. 1411-20.

109. Schlegel, A. and D.Y. Stainier, *Lessons from "lower" organisms: what worms, flies, and zebrafish can teach us about human energy metabolism.* PLoS Genet, 2007. **3**(11): p. e199.

110. Asaoka, Y., et al., *The expanding role of fish models in understanding non-alcoholic fatty liver disease.* Dis Model Mech, 2013. **6**(4): p. 905-14.

111. Seth, A., D.L. Stemple, and I. Barroso, *The emerging use of zebrafish to model metabolic disease.* Dis Model Mech, 2013. **6**(5): p. 1080-8.

112. Otis, J.P. and S.A. Farber, *Imaging vertebrate digestive function and lipid metabolism.* Drug Discov Today Dis Models, 2013. **10**(1).

113. Anderson, J.L., J.D. Carten, and S.A. Farber, *Zebrafish lipid metabolism: from mediating early patterning to the metabolism of dietary fat and cholesterol.* Methods in cell biology, 2011. **101**: p. 111-41.

114. Carten, J.D., M.K. Bradford, and S.A. Farber, *Visualizing digestive organ morphology and function using differential fatty acid metabolism in live zebrafish.* Dev Biol, 2011. **360**(2): p. 276-85.

115. Marza, E., et al., *Developmental expression and nutritional regulation of a zebrafish gene homologous to mammalian microsomal triglyceride transfer protein large subunit.* Dev Dyn, 2005. **232**(2): p. 506-18.

116. Fang, L., et al., *Programming effects of high-carbohydrate feeding of larvae on adult glucose metabolism in zebrafish, Danio rerio.* Br J Nutr, 2014. **111**(5): p. 808-18.

117. Wang, Z., et al., *Impact of a combined high cholesterol diet and high glucose environment on vasculature.* PLoS One, 2013. **8**(12): p. e81485.

118. Fang, L., et al., *In vivo visualization and attenuation of oxidized lipid accumulation in hypercholesterolemic zebrafish.* The Journal of clinical investigation, 2011. **121**(12): p. 4861-9.

119. Curado, S., et al., *Conditional targeted cell ablation in zebrafish: a new tool for regeneration studies.* Dev Dyn, 2007. **236**(4): p. 1025-35.

120. Pisharath, H., et al., *Targeted ablation of beta cells in the embryonic zebrafish pancreas using E. coli nitroreductase.* Mech Dev, 2007. **124**(3): p. 218-29.

121. Passeri, M.J., et al., *Hepatic steatosis in response to acute alcohol exposure in zebrafish requires sterol regulatory element binding protein activation.* Hepatology, 2009. **49**(2): p. 443-52.

122. Sadler, K.C., et al., *A genetic screen in zebrafish identifies the mutants vps18, nf2 and foie gras as models of liver disease.* Development, 2005. **132**(15): p. 3561-72.

123. Matthews, R.P., et al., *TNFalpha-dependent hepatic steatosis and liver degeneration caused by mutation of zebrafish S-adenosylhomocysteine hydrolase.* Development, 2009. **136**(5): p. 865-75.

124. Oka, T., et al., *Diet-induced obesity in zebrafish shares common pathophysiological pathways with mammalian obesity.* BMC Physiol, 2010. **10**: p. 21.

125. Chu, C.Y., et al., *Overexpression of Akt1 enhances adipogenesis and leads to lipoma formation in zebrafish.* PLoS One, 2012. **7**(5): p. e36474.

126. Song, Y. and R.D. Cone, *Creation of a genetic model of obesity in a teleost.* FASEB J, 2007. **21**(9): p. 2042-9.

127. Fang, L., et al., *Control of angiogenesis by AIBP-mediated cholesterol efflux.* Nature, 2013. **498**(7452): p. 118-22.

128. Zhang, T., et al., *ApoA-II directs morphogenetic movements of zebrafish embryo by preventing chromosome fusion during nuclear division in yolk syncytial layer.* J Biol Chem, 2011. **286**(11): p. 9514-25.

129. Babin, P.J., et al., *Both apolipoprotein E and A-I genes are present in a nonmammalian vertebrate and are highly expressed during embryonic development.* Proceedings of the National Academy of Sciences of the United States of America, 1997. **94**(16): p. 8622-7.

130. Thisse, B., Pflumio, S., Fürthauer, M., Loppin, B., Heyer, V., Degrave, A., Woehl, R., Lux, A., Steffan, T., Charbonnier, X.Q. and Thisse, C. , *Expression of the zebrafish genome during embryogenesis (NIH R01 RR15402).* . ZFIN Direct Data Submission, 2001.

131. Monnot, M.J., et al., *Epidermal expression of apolipoprotein E gene during fin and scale development and fin regeneration in zebrafish.* Dev Dyn, 1999. **214**(3): p. 207-15.

132. Poupard, G., et al., *Apolipoprotein E gene expression correlates with endogenous lipid nutrition and yolk syncytial layer lipoprotein synthesis during fish development.* Cell Tissue Res, 2000. **300**(2): p. 251-61.

133. Thisse, C., and Thisse, B. , ***High Throughput Expression Analysis of ZF-Models Consortium Clones.*** ZFIN Direct Data Submission, 2005.

134. Tingaud-Sequeira, A., et al., *Epidermal transient down-regulation of retinol-binding protein 4 and mirror expression of apolipoprotein Eb and estrogen receptor 2a during zebrafish fin and scale development.* Dev Dyn, 2006. **235**(11): p. 3071-9.

135. Herbomel, P., B. Thisse, and C. Thisse, *Zebrafish early macrophages colonize cephalic mesenchyme and developing brain, retina, and epidermis through a M-CSF receptor-dependent invasive process.* Dev Biol, 2001. **238**(2): p. 274-88.

136. Durliat, M., M. Andre, and P.J. Babin, *Conserved protein motifs and structural organization of a fish gene homologous to mammalian apolipoprotein E.* European Journal of Biochemistry, 2000. **267**(2): p. 549-59.

137. Carvalho, L. and C.P. Heisenberg, *The yolk syncytial layer in early zebrafish development.* Trends Cell Biol, 2010. **20**(10): p. 586-92.

138. Fujimoto, K., et al., *Suppression of food intake by apolipoprotein A-IV is mediated through the central nervous system in rats.* J Clin Invest, 1993. **91**(4): p. 1830-3.

139. Postlethwait, J.H., et al., *Vertebrate genome evolution and the zebrafish gene map [see comments].* Nat Genet,, 1998. **18**(4): p. 345-9.

140. Taylor, J.S., et al., *Comparative genomics provides evidence for an ancient genome duplication event in fish.* Philos Trans R Soc Lond B Biol Sci, 2001. **356**(1414): p. 1661-79.

141. Gates, M.A., et al., *A genetic linkage map for zebrafish: comparative analysis and localization of genes and expressed sequences.* Genome Res, 1999. **9**(4): p. 334-47.

142. Amores, A., et al., *Zebrafish hox clusters and vertebrate genome evolution.* Science, 1998. **282**(5394): p. 1711-4.

143. Force, A., et al., *Preservation of duplicate genes by complementary, degenerative mutations.* Genetics, 1999. **151**(4): p. 1531-45.

144. Kleinjan, D.A., et al., *Subfunctionalization of duplicated zebrafish pax6 genes by cis-regulatory divergence.* PLoS Genet, 2008. **4**(2): p. e29.

145. Schlueter, P.J., et al., *Gene duplication and functional divergence of the zebrafish insulin-like growth factor 1 receptors.* FASEB J, 2006. **20**(8): p. 1230-2.

146. Harrison, S.M., et al., *Isolation of novel tissue-specific genes from cDNA libraries representing the individual tissue constituents of the gastrulating mouse embryo.* Development, 1995. **121**(8): p. 2479-89.

147. Bachner, D., et al., *Apolipoprotein E (ApoE), a Bmp-2 (bone morphogenetic protein) upregulated gene in mesenchymal progenitors (C3H10T1/2), is highly expressed in murine embryonic development.* Biofactors, 1999. **9**(1): p. 11-7.

148. Khera, A.V., et al., *Cholesterol efflux capacity, high-density lipoprotein function, and atherosclerosis.* N Engl J Med, 2011. **364**(2): p. 127-35.

149. Walzer, C. and N. Schonenberger, *Ultrastructure and cytochemistry study of the yolk syncytial layer in the alevin of trout (Salmo fario trutta L.) after hatching. I. The vitellolysis zone.* Cell Tissue Res, 1979. **196**(1): p. 59-73.

150. L. Mani-Ponset, E.G., J. P. Diaz, R. Connes *Utilization of yolk reserves during post-embryonic development in three teleostean species: the sea bream Sparus aurata, the sea bass Dicentrarchus labrax, and the pike-perch Stizostedion lucioperca.* Marine Biology, 1996. **126**: p. 539-547.

151. Miyares, R.L., V.B. de Rezende, and S.A. Farber, *Zebrafish yolk lipid processing: a tractable tool for the study of vertebrate lipid transport and metabolism.* Dis Model Mech, 2014. **7**(7): p. 915-27.

152. Farese, R.V., Jr., et al., *Knockout of the mouse apolipoprotein B gene results in embryonic lethality in homozygotes and protection against diet-induced hypercholesterolemia in heterozygotes.* Proc Natl Acad Sci U S A, 1995. **92**(5): p. 1774-8.

153. Terasawa, Y., et al., *Apolipoprotein B-related gene expression and ultrastructural characteristics of lipoprotein secretion in mouse yolk sac during embryonic development.* J Lipid Res, 1999. **40**(11): p. 1967-77.

154. Raabe, M., et al., *Knockout of the abetalipoproteinemia gene in mice: reduced lipoprotein secretion in heterozygotes and embryonic lethality in homozygotes.* Proc Natl Acad Sci U S A, 1998. **95**(15): p. 8686-91.

155. Zannis, V.I., et al., *Transcriptional regulatory mechanisms of the human apolipoprotein genes in vitro and in vivo.* Curr Opin Lipidol, 2001. **12**(2): p. 181-207.

156. Hernandez Vallejo, S.J., et al., *Short-term adaptation of postprandial lipoprotein secretion and intestinal gene expression to a high-fat diet.* Am J Physiol Gastrointest Liver Physiol, 2009. **296**(4): p. G782-92.

157. Carriere, V., et al., *HNF-4-dependent induction of apolipoprotein A-IV gene transcription by an apical supply of lipid micelles in intestinal cells.* J Biol Chem, 2005. **280**(7): p. 5406-13.

158. LeBoeuf, R.C., M. Caldwell, and E. Kirk, *Regulation by nutritional status of lipids and apolipoproteins A-I, A-II, and A-IV in inbred mice.* J Lipid Res, 1994. **35**(1): p. 121-33.

159. Hanniman, E.A., et al., *Apolipoprotein A-IV is regulated by nutritional and metabolic stress: involvement of glucocorticoids, HNF-4 alpha, and PGC-1 alpha.* J Lipid Res, 2006. **47**(11): p. 2503-14.

160. Xu, X., et al., *Transcriptional regulation of apolipoprotein A-IV by the transcription factor CREBH.* J Lipid Res, 2014. **55**(5): p. 850-9.

161. Yoshioka, M., et al., *High-fat meal-induced changes in the duodenum mucosa transcriptome.* Obesity (Silver Spring), 2008. **16**(10): p. 2302-7.

162. Hayashi, H., et al., *Transport of lipid and apolipoproteins A-I and A-IV in intestinal lymph of the rat.* J Lipid Res, 1990. **31**(9): p. 1613-25.

163. Kalogeris, T.J., et al., *Intestinal synthesis and lymphatic secretion of apolipoprotein A-IV vary with chain length of intestinally infused fatty acids in rats.* J Nutr, 1996. **126**(11): p. 2720-9.

164. Kalogeris, T.J., V.R. Holden, and P. Tso, *Stimulation of jejunal synthesis of apolipoprotein A-IV by ileal lipid infusion is blocked by vagotomy.* Am J Physiol, 1999. **277**(5 Pt 1): p. G1081-7.

165. Lo, C.C., et al., *Apolipoprotein AIV requires cholecystokinin and vagal nerves to suppress food intake.* Endocrinology, 2012. **153**(12): p. 5857-65.

166. Liu, M., et al., *Intestinal satiety protein apolipoprotein AIV is synthesized and regulated in rat hypothalamus.* Am J Physiol Regul Integr Comp Physiol, 2001. **280**(5): p. R1382-7.

167. Shen, L., et al., *Characterization of apolipoprotein A-IV in brain areas involved in energy homeostasis.* Physiol Behav, 2008. **95**(1-2): p. 161-7.

168. Kohan, A.B., et al., *Apolipoprotein A-IV regulates chylomicron metabolism-mechanism and function.* Am J Physiol Gastrointest Liver Physiol, 2012. **302**(6): p. G628-36.

169. Black, D.D., P.L. Rohwer-Nutter, and N.O. Davidson, *Intestinal apolipoprotein A-IV gene expression in the piglet.* J Lipid Res, 1990. **31**(3): p. 497-505.

170. Altschul, S.F., et al., *Protein database searches using compositionally adjusted substitution matrices.* FEBS J, 2005. **272**(20): p. 5101-9.

171. Altschul, S.F., et al., *Gapped BLAST and PSI-BLAST: a new generation of protein database search programs.* Nucleic Acids Res, 1997. **25**(17): p. 3389-402.

172. Needleman, S.B. and C.D. Wunsch, *A general method applicable to the search for similarities in the amino acid sequence of two proteins.* J Mol Biol, 1970. **48**(3): p. 443-53.

173. McWilliam, H., et al., *Analysis Tool Web Services from the EMBL-EBI.* Nucleic Acids Res, 2013. **41**(Web Server issue): p. W597-600.

174. Louis, A., M. Muffato, and H. Roest Crollius, *Genomicus: five genome browsers for comparative genomics in eukaryota.* Nucleic Acids Res, 2013. **41**(Database issue): p. D700-5.

175. Catchen, J.M., J.S. Conery, and J.H. Postlethwait, *Automated identification of conserved synteny after whole-genome duplication.* Genome Res, 2009. **19**(8): p. 1497-505.

176. Thompson, J.D., et al., *A comprehensive benchmark study of multiple sequence alignment methods: current challenges and future perspectives.* PLoS One, 2011. **6**(3): p. e18093.

177. Kuraku, S., et al., *aLeaves facilitates on-demand exploration of metazoan gene family trees on MAFFT sequence alignment server with enhanced interactivity.* Nucleic Acids Res, 2013. **41**(Web Server issue): p. W22-8.

178. Kimmel, C., et al., *Stages of embryonic development of the zebrafish.* Dev Dyn, 1995. **203**(3): p. 253-310.

179. Westerfield, M., *The Zebrafish Book*. 3rd ed. 1995, Eugene: University of Oregon.

180. Karlsson, J., J. von Hofsten, and P.E. Olsson, *Generating transparent zebrafish: a refined method to improve detection of gene expression during embryonic development.* Mar Biotechnol (NY), 2001. **3**(6): p. 522-7.

181. Thisse, C. and B. Thisse, *High-resolution in situ hybridization to whole-mount zebrafish embryos.* Nat Protoc, 2008. **3**(1): p. 59-69.

182. Kwan, K.M., et al., *The Tol2kit: a multisite gateway-based construction kit for Tol2 transposon transgenesis constructs.* Dev Dyn, 2007. **236**(11): p. 3088-99.

183. Bligh, E. and W. Dyer, *A rapid method of total lipid extraction and purification.* Can. J. Biochem. Physiol., 1959. **37**: p. 911-918.

184. Livak, K.J. and T.D. Schmittgen, *Analysis of relative gene expression data using real-time quantitative PCR and the 2(-Delta Delta C(T)) Method.* Methods, 2001. **25**(4): p. 402-8.

185. Hussain, M.M., et al., *Chylomicron assembly and catabolism: role of apolipoproteins and receptors.* Biochim Biophys Acta, 1996. **1300**: p. 151-170.

186. Segrest, J.P., et al., *Structure of apolipoprotein B-100 in low density lipoproteins.* Journal of lipid research, 2001. **42**: p. 1346-1367.

187. Bell-Quint, J., T. Forte, and P. Graham, *Synthesis of two forms of apolipoprotein B by cultured rat hepatocytes.* Biochemical and Biophysical Research Communications, 1981. **99**: p. 700-706.

188. Nakamuta, M., et al., *Alternative mRNA splicing and differential promoter utilization determine tissue-specific expression of the apolipoprotein B mRNA-editing protein (Apobec1) gene in mice.: structure and evolution of apobec1 and related nucleoside/nucleotide deaminase.* Journal of Biological Chemistry, 1995. **270**: p. 13042-13056.

189. Laut, P.P., et al., *Dimeric structure of a human apolipoprotein B mRNA editing protein and cloning and chromosomal localization of its gene.* Proceedings of the National Academy of Sciences of the United States of America, 1994. **91**: p. 8522-8526.

190. Chen, S.H., et al., *Apolipoprotein B-48 is the product of a messenger RNA with an organ-specific in-frame stop codon.* Science (New York, N.Y.), 1987. **238**: p. 363-366.

191. Powell, L.M., et al., *A novel form of tissue-specific RNA processing produces apolipoprotein-B48 in intestine.* Cell, 1987. **50**: p. 831-840.

192. Khatun, I., M.T. Walsh, and M.M. Hussain, *Loss of both phospholipid and triglyceride transfer activities of microsomal triglyceride transfer protein in abetalipoproteinemia.* Journal of Lipid Research, 2013. **54**.

193. Walsh, M.T. and M.M. Hussain, *Targeting microsomal triglyceride transfer protein and lipoprotein assembly to treat homozygous familial hypercholesterolemia.* Critical Reviews in Clinical Laboratory Sciences, 2017. **54**.

194. Hussain, M.M., J. Shi, and P. Dreizen, *Microsomal triglyceride transfer protein and its role in apoB-lipoprotein assembly.* The Journal of Lipid Research, 2003. **44**: p. 22-32.

195. Iqbal, J., et al., *Microsomal triglyceride transfer protein transfers and determines plasma concentrations of ceramide and sphingomyelin but not glycosylceramide.* Journal of Biological Chemistry, 2015. **290**.

196. Hussain, M.M., *A proposed model for the assembly of chylomicrons.* Atherosclerosis, 2000. **148**: p. 1-15.

197. Pan, M., et al., *Presecretory oxidation, aggregation, and autophagic destruction of apoprotein-B: a pathway for late-stage quality control.* Proceedings of the National Academy of Sciences of the United States of America, 2008. **105**: p. 5862-5867.

198. Kjolby, M., et al., *Sort1, encoded by the cardiovascular risk locus 1p13.3, is a regulator of hepatic lipoprotein export.* Cell Metabolism, 2010. **12**: p. 213-223.

199. Strong, A., et al., *Hepatic sortilin regulates both apolipoprotein B secretion and LDL catabolism.* J Clin Invest, 2012. **122**(8): p. 2807-16.

200. Tiwari, S. and S.a. Siddiqi, *Intracellular trafficking and secretion of VLDL.* Arteriosclerosis, thrombosis, and vascular biology, 2012. **32**: p. 1079-1086.

201. Mansbach, C.M. and S.A. Siddiqi, *The biogenesis of chylomicrons.* Annual Review of Physiology, 2010: p. 315-333.

202. Hussain, M.M., D.K. Strickland, and A. Bakillah, *The mammalian low-density lipoprotein receptor family.* Annual review of nutrition, 1999. **19**: p. 141-172.

203. Harrington, L.S., et al., *Regulation of multiple angiogenic pathways by Dll4 and Notch in human umbilical vein endothelial cells.* Microvasc Res, 2008. **75**(2): p. 144-54.

204. Rodriguez, E.A., et al., *The growing and glowing toolbox of fluorescent and photoactive proteins.* Trends in biochemical sciences, 2017. **42**: p. 111-129.

205. Giepmans, B.N.G., et al., *The fluorescent toolbox for assessing protein location and function.* Science (New York, N.Y.), 2006. **312**: p. 217-224.

206. Chudakov, D.M., S. Lukyanov, and K.A. Lukyanov, *Fluorescent proteins as a toolkit for in vivo imaging.* Trends in Biotechnology, 2005. **23**: p. 605-613.

207. Rava, P., et al., *Phospholipid transfer activity of microsomal triacylglycerol transfer protein is sufficient for the assembly and secretion of apolipoprotein B lipoproteins.* J Biol Chem, 2006. **281**(16): p. 11019-27.

208. Wang, S., et al., *The microsomal triglyceride transfer protein facilitates assembly and secretion of apolipoprotein B-containing lipoproteins and decreases cotranslational degradation of apolipoprotein B in transfected COS-7 cells.* Journal of Biological Chemistry, 1996. **271**: p. 14124-14133.

209. Hussain, M.M., et al., *Characterization of recombinant human apoB-48-containing lipoproteins in rat hepatoma McA-RH7777 cells transfected with apoB-48 cDNA. Overexpression of apoB-48 decreases synthesis of endogenous apoB-100.* Arteriosclerosis, thrombosis, and vascular biology, 1995. **15**: p. 485-494.

210. Bakillah, A., et al., *Measurement of apolipoprotein B in various cell lines: Correlation between intracellular levels and rates of secretion.* Lipids, 1997. **32**: p. 1113-1118.

211. Blackhart, B.D., Z.M. Yao, and B.J. McCarthy, *An expression system for human apolipoprotein B100 in a rat hepatoma cell line.* The Journal of biological chemistry, 1990. **265**: p. 8358-8360.

212. Boren, J., S. Rustaeus, and S.O. Olofsson, *Studies on the assembly of apolipoprotein B-100- and B-48-containing very low density lipoproteins in McA-RH7777 cells.* J Biol Chem, 1994. **269**(41): p. 25879-88.

213. Yao, Z. and R.S. McLeod, *Synthesis and secretion of hepatic apolipoprotein B-containing lipoproteins.* Biochimica et Biophysica Acta (BBA) - Lipids and Lipid Metabolism, 1994. **1212**: p. 152-166.

214. Walsh, M.T., et al., *A novel abetalipoproteinemia missense mutation highlights the importance of N-terminal β-barrel in microsomal triglyceride transfer protein function.* Circulation: Cardiovascular Genetics, 2015. **8**: p. 677-687.

215. Otis Meng-Chieh, C., Blake A., J P Shen, O.E. Reyes Gaido, and S.A. Farber, *Dietary cholesterol and apolipoprotein A-1 are trafficked in endosomes and*

lysosomes in live zebrafish intestine. American Journal of Physiology - Gastrointestinal and Liver Physiology, 2019.

216. Otis, J.P. and S.A. Farber, *High-fat feeding paradigm for larval zebrafish: Feeding, live imaging, and quantification of food intake.* Journal of Visualized Experiments, 2016. **2016**: p. 2-8.

217. WHO. *The top 10 causes of death*. Fact Sheets [Web Page] 2018 05/24/2018 [cited 2018 09/25/2018]; Available from: http://www.who.int/news-room/fact-sheets/detail/the-top-10-causes-of-death.

218. Stone, N.J., et al., *2013 ACC/AHA guideline on the treatment of blood cholesterol to reduce atherosclerotic cardiovascular risk in adults: a report of the American College of Cardiology/American Heart Association Task Force on Practice Guidelines.* Circulation, 2014. **129**(25 Suppl 2): p. S1-45.

219. McQueen, M.J., et al., *Lipids, lipoproteins, and apolipoproteins as risk markers of myocardial infarction in 52 countries (the INTERHEART study): a case-control study.* Lancet, 2008. **372**(9634): p. 224-33.

220. Shim, H., et al., *A multivariate genome-wide association analysis of 10 LDL subfractions, and their response to statin treatment, in 1868 Caucasians.* PLoS One, 2015. **10**(4): p. e0120758.

221. Rajman, I., et al., *LDL particle size: an important drug target?* Br J Clin Pharmacol, 1999. **48**(2): p. 125-33.

222. Jacobson, T.A., *Opening a new lipid "apo-thecary": incorporating apolipoproteins as potential risk factors and treatment targets to reduce cardiovascular risk.* Mayo Clin Proc, 2011. **86**(8): p. 762-80.

223. Xiao, C., et al., *Pharmacological Targeting of the Atherogenic Dyslipidemia Complex: The Next Frontier in CVD Prevention Beyond Lowering LDL Cholesterol.* Diabetes, 2016. **65**(7): p. 1767-78.

224. Yin, W., et al., *Plasma lipid profiling across species for the identification of optimal animal models of human dyslipidemia.* J Lipid Res, 2012. **53**(1): p. 51-65.

225. White, D.T., et al., *ARQiv-HTS, a versatile whole-organism screening platform enabling in vivo drug discovery at high-throughput rates.* Nat Protoc, 2016. **11**(12): p. 2432-2453.

226. Liu, C., et al., *Apoc2 loss-of-function zebrafish mutant as a genetic model of hyperlipidemia.* Dis Model Mech, 2015. **8**(8): p. 989-98.

227. O'Hare, E.A., et al., *Disruption of ldlr causes increased LDL-c and vascular lipid accumulation in a zebrafish model of hypercholesterolemia.* J Lipid Res, 2014. **55**(11): p. 2242-53.

228. Hall, M.P., et al., *Engineered luciferase reporter from a deep sea shrimp utilizing a novel imidazopyrazinone substrate.* ACS Chem Biol, 2012. **7**(11): p. 1848-57.

229. Mahley, R.W., *Central Nervous System Lipoproteins: ApoE and Regulation of Cholesterol Metabolism.* Arterioscler Thromb Vasc Biol, 2016. **36**(7): p. 1305-15.

230. Rouault, M., et al., *Novel mammalian group XII secreted phospholipase A2 lacking enzymatic activity.* Biochemistry, 2003. **42**(39): p. 11494-503.

231. Elovson, J., et al., *Plasma very low density lipoproteins contain a single molecule of apolipoprotein B.* J Lipid Res, 1988. **29**(11): p. 1461-73.

232. Fisher, E., E. Lake, and R.S. McLeod, *Apolipoprotein B100 quality control and the regulation of hepatic very low density lipoprotein secretion.* J Biomed Res, 2014. **28**(3): p. 178-93.

233. Kane, J.P., D.A. Hardman, and H.E. Paulus, *Heterogeneity of apolipoprotein B: isolation of a new species from human chylomicrons.* Proc Natl Acad Sci U S A, 1980. **77**(5): p. 2465-9.

234. Hussain, M.M., et al., *Amino acids 430-570 in apolipoprotein B are critical for its binding to microsomal triglyceride transfer protein.* J Biol Chem, 1998. **273**(40): p. 25612-5.

235. Boren, J., et al., *The molecular mechanism for the genetic disorder familial defective apolipoprotein B100.* J Biol Chem, 2001. **276**(12): p. 9214-8.

236. Shin, J., J. Chen, and L. Solnica-Krezel, *Efficient homologous recombination-mediated genome engineering in zebrafish using TALE nucleases.* Development, 2014. **141**(19): p. 3807-18.

237. Hussain, M.M., J. Shi, and P. Dreizen, *Microsomal triglyceride transfer protein and its role in apoB-lipoprotein assembly.* J Lipid Res, 2003. **44**(1): p. 22-32.

238. Cuchel, M., et al., *Inhibition of microsomal triglyceride transfer protein in familial hypercholesterolemia.* N Engl J Med, 2007. **356**(2): p. 148-56.

239. Singh, Y., et al., *A rapid 3% polyacrylamide slab gel electrophoresis method for high through put screening of LDL phenotype.* Lipids Health Dis, 2008. **7**: p. 47.

240. Hoefner, D.M., et al., *Development of a rapid, quantitative method for LDL subfractionation with use of the Quantimetrix Lipoprint LDL System.* Clin Chem, 2001. **47**(2): p. 266-74.

241. Sato, A., et al., *Angiotensin II induces the aggregation of native and oxidized low-density lipoprotein.* Eur Biophys J, 2018. **47**(1): p. 1-9.

242. Tiwari, S. and S.A. Siddiqi, *Intracellular trafficking and secretion of VLDL.* Arterioscler Thromb Vasc Biol, 2012. **32**(5): p. 1079-86.

243. Yee, M.S., et al., *Lipoprotein separation in a novel iodixanol density gradient, for composition, density, and phenotype analysis.* J Lipid Res, 2008. **49**(6): p. 1364-71.

244. Garewal, M., L. Zhang, and G. Ren, *Optimized negative-staining protocol for examining lipid-protein interactions by electron microscopy.* Methods Mol Biol, 2013. **974**: p. 111-8.

245. Westerfield, M., *The zebrafish book: a guide for the laboratory use of zebrafish (Danio rerio)*. 2007: University of Oregon press.

246. Jung, H.M., et al., *Development of the larval lymphatic system in zebrafish.* Development, 2017. **144**(11): p. 2070-2081.

247. Charvet, B., et al., *Development of the zebrafish myoseptum with emphasis on the myotendinous junction.* Cell Tissue Res, 2011. **346**(3): p. 439-49.

248. Sullivan, C.V. and O. Yilmaz, *Vitellogenesis and Yolk Proteins, Fish*, in *Encyclopedia of Reproduction*. 2018. p. 266-277.

249. Babaei, F., et al., *Novel blood collection method allows plasma proteome analysis from single zebrafish.* J Proteome Res, 2013. **12**(4): p. 1580-90.

250. Kettleborough, R.N., et al., *A systematic genome-wide analysis of zebrafish protein-coding gene function.* Nature, 2013. **496**(7446): p. 494-7.

251. Anderson, J.L., et al., *mRNA processing in mutant zebrafish lines generated by chemical and CRISPR-mediated mutagenesis produces unexpected transcripts that escape nonsense-mediated decay.* PLoS Genet, 2017. **13**(11): p. e1007105.

252. Ruuth, M., et al., *Susceptibility of low-density lipoprotein particles to aggregate depends on particle lipidome, is modifiable, and associates with future cardiovascular deaths.* Eur Heart J, 2018. **39**(27): p. 2562-2573.

253. Chico, T.J., P.W. Ingham, and D.C. Crossman, *Modeling cardiovascular disease in the zebrafish.* Trends Cardiovasc Med, 2008. **18**(4): p. 150-5.

254. Salmi, T.M., V.W.T. Tan, and A.G. Cox, *Dissecting metabolism using zebrafish models of disease.* Biochem Soc Trans, 2019. **47**(1): p. 305-315.

255. Henson, H.E., et al., *Functional and genetic analysis of choroid plexus development in zebrafish.* Front Neurosci, 2014. **8**: p. 364.

256. Dehouck, B., et al., *A new function for the LDL receptor: transcytosis of LDL across the blood-brain barrier.* J Cell Biol, 1997. **138**(4): p. 877-89.

257. Guan, M., et al., *Hepatocyte nuclear factor-4 alpha regulates liver triglyceride metabolism in part through secreted phospholipase A(2) GXIIB.* Hepatology, 2011. **53**(2): p. 458-66.

258. Aljakna, A., et al., *Pla2g12b and Hpn are genes identified by mouse ENU mutagenesis that affect HDL cholesterol.* PLoS One, 2012. **7**(8): p. e43139.

259. Neff, K.L., et al., *Mojo Hand, a TALEN design tool for genome editing applications.* BMC Bioinformatics, 2013. **14**: p. 1.

260. Ma, A.C., et al., *FusX: A Rapid One-Step Transcription Activator-Like Effector Assembly System for Genome Science.* Hum Gene Ther, 2016. **27**(6): p. 451-63.

261. Petersen, L.K. and R.S. Stowers, *A Gateway MultiSite recombination cloning toolkit.* PLoS One, 2011. **6**(9): p. e24531.

262. Rumsey, S.C., et al., *Cryopreservation with sucrose maintains normal physical and biological properties of human plasma low density lipoproteins.* J Lipid Res, 1992. **33**(10): p. 1551-61.

263. Meeker, N.D., et al., *Method for isolation of PCR-ready genomic DNA from zebrafish tissues.* Biotechniques, 2007. **43**(5): p. 610, 612, 614.

264. Hussain, M.M., et al., *Chylomicron assembly and catabolism: role of apolipoproteins and receptors.* Biochim Biophys Acta, 1996. **1300**(3): p. 151-70.

265. Bakillah, A., et al., *Decreased secretion of ApoB follows inhibition of ApoB-MTP binding by a novel antagonist.* Biochemistry, 2000. **39**(16): p. 4892-9.

266. Cartwright, I.J. and J.A. Higgins, *Direct evidence for a two-step assembly of ApoB48-containing lipoproteins in the lumen of the smooth endoplasmic reticulum of rabbit enterocytes.* J Biol Chem, 2001. **276**(51): p. 48048-57.

267. Hamilton, R.L., et al., *Chylomicron-sized lipid particles are formed in the setting of apolipoprotein B deficiency.* J Lipid Res, 1998. **39**(8): p. 1543-57.

268. Wurie, H.R., L. Buckett, and V.A. Zammit, *Evidence that diacylglycerol acyltransferase 1 (DGAT1) has dual membrane topology in the endoplasmic reticulum of HepG2 cells.* J Biol Chem, 2011. **286**(42): p. 36238-47.

269. Liu, Q., et al., *Activation of farnesoid X receptor promotes triglycerides lowering by suppressing phospholipase A2 G12B expression.* Mol Cell Endocrinol, 2016. **436**: p. 93-101.

270. Chen, L., et al., *Estrogen-related receptor gamma regulates hepatic triglyceride metabolism through phospholipase A2 G12B.* FASEB J, 2019: p. fj201802704R.

271. Murakami, M., et al., *Emerging roles of secreted phospholipase A2 enzymes: the 3rd edition.* Biochimie, 2014. **107 Pt A**: p. 105-13.

272. Murakami, M., et al., *A new era of secreted phospholipase A(2).* J Lipid Res, 2015. **56**(7): p. 1248-61.

273. Raykhel, I., et al., *A molecular specificity code for the three mammalian KDEL receptors.* J Cell Biol, 2007. **179**(6): p. 1193-204.

274. Uhlen, M., et al., *Proteomics. Tissue-based map of the human proteome.* Science, 2015. **347**(6220): p. 1260419.

275. Desiere, F., et al., *The PeptideAtlas project.* Nucleic Acids Res, 2006. **34**(Database issue): p. D655-8.

276. Force, A., et al., *Preservation of duplicate genes by complementary, degenerative mutations.* Genetics, 1999. **151**(4): p. 1531-45.

277. Fisher, E.A., N.A. Khanna, and R.S. McLeod, *Ubiquitination regulates the assembly of VLDL in HepG2 cells and is the committing step of the apoB-100 ERAD pathway.* J Lipid Res, 2011. **52**(6): p. 1170-80.

278. Avramoglu, R.K., K. Cianflone, and A.D. Sniderman, *Role of the neutral lipid accessible pool in the regulation of secretion of apoB-100 lipoprotein particles by HepG2 cells.* J Lipid Res, 1995. **36**(12): p. 2513-28.

279. Walldius, G. and I. Jungner, *Apolipoprotein B and apolipoprotein A-I: risk indicators of coronary heart disease and targets for lipid-modifying therapy.* J Intern Med, 2004. **255**(2): p. 188-205.

280. Sniderman, A.D., et al., *Is the superiority of apoB over non–HDL-C as a marker of cardiovascular risk in the INTERHEART study due to confounding by related variables?* Journal of Clinical Lipidology, 2013. **7**(6): p. 626-631.

281. Su, Q., et al., *Apolipoprotein B100 acts as a molecular link between lipid-induced endoplasmic reticulum stress and hepatic insulin resistance.* Hepatology, 2009. **50**(1): p. 77–84

282. Liao, W., *Blocking microsomal triglyceride transfer protein interferes with apoB secretion without causing retention or stress in the ER.* The Journal of Lipid Research, 2003. **44**(5): p. 978-985

283. Williams, K., et al., *Comparison of the associations of apolipoprotein B and low-density lipoprotein cholesterol with other cardiovascular risk factors in the Insulin Resistance Atherosclerosis Study (IRAS).* Circulation, 2003. **108**(19): p. 2312-6.

284. Su, Q., et al., *Apolipoprotein B: not just a biomarker but a causal factor in hepatic endoplasmic reticulum stress and insulin resistance.* Clinical Lipidology, 2010. **5**(2): p. 267-276.

285. Salomaa, V., et al., *Thirty-one novel biomarkers as predictors for clinically incident diabetes.* PLoS One, 2010. **5**(4): p. e10100.

286. Ryoo, J.-H. and S.K. Park, *Association of apolipoprotein B and incidence of metabolic syndrome in Korean men: a 5-years' follow-up study.* Atherosclerosis, 2013. **226**(2): p. 496-501.

287. Onat, A., et al., *Serum apolipoprotein B predicts dyslipidemia, metabolic syndrome and, in women, hypertension and diabetes, independent of markers of central obesity and inflammation.* Int J Obes (Lond), 2007. **31**(7): p. 1119-25.

288. Faraj, M., et al., *Reduction in serum apoB is associated with reduced inflammation and insulin resistance in post-menopausal women: A MONET study.* Atherosclerosis, 2010. **211**(2): p. 682-688

289. Adiels, M., et al., *Overproduction of large VLDL particles is driven by increased liver fat content in man.* Diabetologia, 2006. **49**(4): p. 755-65.

290. Samuel, V.T., et al., *Mechanism of hepatic insulin resistance in non-alcoholic fatty liver disease.* J Biol Chem, 2004. **279**(31): p. 32345-53.

291. Visser, M.E., et al., *Hepatic steatosis does not cause insulin resistance in people with familial hypobetalipoproteinaemia.* Diabetologia, 2011. **54**(8): p. 2113-21.

292. Kaur, J., *A comprehensive review on metabolic syndrome.* Cardiol Res Pract, 2014. **2014**: p. 943162.

293. Younossi, Z.M., et al., *Global epidemiology of nonalcoholic fatty liver disease-Meta-analytic assessment of prevalence, incidence, and outcomes.* Hepatology, 2016. **64**(1): p. 73-84.

294. Dixon, D.L., et al., *Lomitapide and mipomersen: novel lipid-lowering agents for the management of familial hypercholesterolemia.* J Cardiovasc Nurs, 2014. **29**(5): p. E7-E12.

295. Gouni-Berthold, I. and H.K. Berthold, *Mipomersen and lomitapide: Two new drugs for the treatment of homozygous familial hypercholesterolemia.* Atheroscler Suppl, 2015. **18**: p. 28-34.

296. Hobbs, H.H., M.S. Brown, and J.L. Goldstein, *Molecular genetics of the LDL receptor gene in familial hypercholesterolemia.* Hum Mutat, 1992. **1**(6): p. 445-66.

297. Raal, F.J., et al., *Mipomersen, an apolipoprotein B synthesis inhibitor, for lowering of LDL cholesterol concentrations in patients with homozygous familial hypercholesterolaemia: a randomised, double-blind, placebo-controlled trial.* Lancet, 2010. **375**(9719): p. 998-1006.

298. Rizzo, M., *Lomitapide, a microsomal triglyceride transfer protein inhibitor for the treatment of hypercholesterolemia.* IDrugs, 2010. **13**(2): p. 103-11.

299. Ballantyne, C.M., J.S. Raichlen, and V.A. Cain, *Statin therapy alters the relationship between apolipoprotein B and low-density lipoprotein cholesterol and non-high-density lipoprotein cholesterol targets in high-risk patients: the*

MERCURY II (Measuring Effective Reductions in Cholesterol Using Rosuvastatin) trial. J Am Coll Cardiol, 2008. **52**(8): p. 626-32.

300. Telford, D.E., et al., *The molecular mechanisms underlying the reduction of LDL apoB-100 by ezetimibe plus simvastatin.* J Lipid Res, 2007. **48**(3): p. 699-708.

301. Miao, J., et al., *Hepatic insulin receptor deficiency impairs the SREBP-2 response to feeding and statins.* J Lipid Res, 2014. **55**(4): p. 659-67.

302. Cohen , J.C., et al., *Sequence Variations in PCSK9, Low LDL, and Protection against Coronary Heart Disease.* New England Journal of Medicine, 2006. **354**(12): p. 1264-1272.

303. Musunuru, K., et al., *From noncoding variant to phenotype via SORT1 at the 1p13 cholesterol locus.* Nature, 2010. **466**: p. 714.

304. Nioi, P., et al., *Variant ASGR1 Associated with a Reduced Risk of Coronary Artery Disease.* New England Journal of Medicine, 2016. **374**(22): p. 2131-2141.

305. Swinney, D.C. and J. Anthony, *How were new medicines discovered?* Nature Reviews Drug Discovery, 2011. **10**(7): p. 507-519

306. MacRae, C.A. and R.T. Peterson, *Zebrafish as tools for drug discovery.* Nat Rev Drug Discov, 2015. **14**(10): p. 721-31.

307. Kraehling, J.R., et al., *Genome-wide RNAi screen reveals ALK1 mediates LDL uptake and transcytosis in endothelial cells.* Nat Commun, 2016. **7**: p. 13516.

308. Langheinrich, U., *Zebrafish: a new model on the pharmaceutical catwalk.* Bioessays, 2003. **25**(9): p. 904-12.

309. Fang, L., et al., *In vivo visualization and attenuation of oxidized lipid accumulation in hypercholesterolemic zebrafish.* J Clin Invest, 2011. **121**(12): p. 4861-9.

310. Rihel, J., et al., *Zebrafish behavioral profiling links drugs to biological targets and rest/wake regulation.* Science, 2010. **327**(5963): p. 348-51.

311. Winter, M.J., et al., *Validation of a larval zebrafish locomotor assay for assessing the seizure liability of early-stage development drugs.* J Pharmacol Toxicol Methods, 2008. **57**(3): p. 176-87.

312. Howe, K., et al., *The zebrafish reference genome sequence and its relationship to the human genome.* Nature, 2013. **496**(7446): p. 498-503.

313. Babin, P.J., et al., *Both apolipoprotein E and A-I genes are present in a nonmammalian vertebrate and are highly expressed during embryonic development.* Proc Natl Acad Sci U S A, 1997. **94**(16): p. 8622-7.

314. Koch, M., et al., *Detection of the apolipoprotein B-100 arg(3500) > gl mutation in familial defective apoB-100 by temperature-gradient gel electrophoresis.* Z Gastroenterol, 1996. **34 Suppl 3**: p. 16-8.

315. De Loof, H., et al., *Human apolipoprotein B: analysis of internal repeats and homology with other apolipoproteins.* J Lipid Res, 1987. **28**(12): p. 1455-65.

316. Segrest, J.P., et al., *apoB-100 has a pentapartite structure composed of three amphipathic alpha-helical domains alternating with two amphipathic beta-strand domains. Detection by the computer program LOCATE.* Arterioscler Thromb, 1994. **14**(10): p. 1674-85.

317. Davidson, N.O. and G.S. Shelness, *Apolipoprotein B: mRNA editing, lipoprotein assembly, and presecretory degradation.* Annual review of nutrition, 2000. **20**(1): p. 169-193.

318. Lo, C.M., et al., *Why does the gut choose apolipoprotein B48 but not B100 for chylomicron formation?* Am J Physiol Gastrointest Liver Physiol, 2008. **294**(1): p. G344-52.

319. Alaupovic, P., et al., *The role of triglyceride-rich lipoprotein families in the progression of atherosclerotic lesions as determined by sequential coronary angiography from a controlled clinical trial.* Arterioscler Thromb Vasc Biol, 1997. **17**(4): p. 715-22.

320. Zu, Y., et al., *TALEN-mediated precise genome modification by homologous recombination in zebrafish.* Nat Methods, 2013. **10**(4): p. 329-31.

321. Stacer, A.C., et al., *NanoLuc reporter for dual luciferase imaging in living animals.* Mol Imaging, 2013. **12**(7): p. 1-13.

322. Miller, N.E., et al., *Familial apolipoprotein CII deficiency: plasma lipoproteins and apolipoproteins in heterozygous and homozygous subjects and the effects of plasma infusion.* Eur J Clin Invest, 1981. **11**(1): p. 69-76.

323. Zhang, J.-H., T.D. Chung, and K.R. Oldenburg, *A simple statistical parameter for use in evaluation and validation of high throughput screening assays.* Journal of biomolecular screening, 1999. **4**(2): p. 67-73.

324. Sullivan, D., et al., *Effect of a monoclonal antibody to PCSK9 on low-density lipoprotein cholesterol levels in statin-intolerant patients: the GAUSS randomized trial.* JAMA, 2012. **308**(23): p. 2497-506.

325. Zhang, X.D., *Illustration of SSMD, z score, SSMD*, z* score, and t statistic for hit selection in RNAi high-throughput screens.* J Biomol Screen, 2011. **16**(7): p. 775-85.

326. Zhang, X.D., *Novel analytic criteria and effective plate designs for quality control in genome-scale RNAi screens.* J Biomol Screen, 2008. **13**(5): p. 363-77.

327. Wang, G., et al., *First quantitative high-throughput screen in zebrafish identifies novel pathways for increasing pancreatic beta-cell mass.* Elife, 2015. **4**: p. e08261.

328. Chen, C.H., et al., *zebraflash transgenic lines for in vivo bioluminescence imaging of stem cells and regeneration in adult zebrafish.* Development, 2013. **140**(24): p. 4988-97.

329. Pardo-Martin, C., et al., *High-throughput in vivo vertebrate screening.* Nat Methods, 2010. **7**(8): p. 634-6.

330. Howarth, D.L., et al., *Defining hepatic dysfunction parameters in two models of fatty liver disease in zebrafish larvae.* Zebrafish, 2013. **10**(2): p. 199-210.

331. Xu, G., et al., *Post-translational regulation of adipose differentiation-related protein by the ubiquitin/proteasome pathway.* J Biol Chem, 2005. **280**(52): p. 42841-7.

332. Gut, P., et al., *Whole-organism screening for gluconeogenesis identifies activators of fasting metabolism.* Nat Chem Biol, 2013. **9**(2): p. 97-104.

333. Belousov, V.V., et al., *Genetically encoded fluorescent indicator for intracellular hydrogen peroxide.* Nat Methods, 2006. **3**(4): p. 281-6.

334. Yan, B., et al., *IL-1beta and reactive oxygen species differentially regulate neutrophil directional migration and Basal random motility in a zebrafish injury-induced inflammation model.* J Immunol, 2014. **192**(12): p. 5998-6008.

335. Lee, H.C., et al., *Transgenic zebrafish model to study translational control mediated by upstream open reading frame of human chop gene.* Nucleic Acids Res, 2011. **39**(20): p. e139.

336. Civeira, F., et al., *Tendon xanthomas in familial hypercholesterolemia are associated with cardiovascular risk independently of the low-density lipoprotein receptor gene mutation.* Arterioscler Thromb Vasc Biol, 2005. **25**(9): p. 1960-5.

BIOGRAPHICAL STATEMENT

James Henry Thierer was born in Baltimore on July 25th, 1990. He attended public school in the Towson area, and attained his B.S. degree in General Biology from the University of Maryland, College Park, in December 2011. During his first summer at University of Maryland, James performed research in infectious disease epidemiology in the laboratory of Dr. O. C. Stine at the University of Maryland School of Medicine. For the remainder of his undergraduate education, he worked part-time in the laboratories of Drs. Charles Delwiche and Caren Chang investigating the evolutionary history of plant hormone signaling pathways. James then worked as a lab technician for approximately 6 months following graduation while applying to graduate programs. James then committed to the CMDB program at Johns Hopkins University and joined the laboratory of Dr. Steven Farber in August 2013. James performed his thesis research studying lipoprotein biology using the larval zebrafish model system and completed his degree in the Fall of 2019.